University of Perpignan Via Domitia - UPVD

Doctoral School E^2
Energy and Environment

P H D T H E S I S

to obtain the title of

PhD of Science

Specialty : Engineering Sciences

Defended by

Daoud Baalbaki

Simulation and modeling of turbulent non isothermal vapor-droplet dispersed flow

Thesis Advisor: Françoise Bataille

prepared at PROMES-CNRS Perpignan & IRSN Cadarche

defended on December 15, 2011

Jury :

Reviewers :	Jocelyn Bonjour	-	Insa - Lyon
	Michel Gradeck	-	LEMTA - Nancy
President :	Najib laraqi	-	Université Paris Ouest
Examinators :	Françoise Bataille	-	PROMES-CNRS
	Pierre Ruyer	-	IRSN
	Adrien Toutant	-	PROMES-CNRS
Invited :	Georges Repetto	-	IRSN
	Nicolas Tregoures	-	IRSN

Contents

1 General introduction **1**
- 1.1 Context of the study . . . 2
- 1.2 Process and plan of the study . . . 6

2 Governing equations for two-phase flow **8**
- 2.1 Introduction . . . 8
- 2.2 Numerical methods . . . 9
- 2.3 Dynamic equations for single-phase and two-phase flows classical derivation . . . 12
  - 2.3.1 Instantaneous single-phase equations . . . 12
  - 2.3.2 Instantaneous local equations for the two-phase flow . . . 13
  - 2.3.3 Averaged local equations . . . 15
- 2.4 Derivation of dispersed phase Eulerian modeling from particles point of view . . . 23
  - 2.4.1 Probability density function . . . 23
  - 2.4.2 Discrete particle momentum conservation equation . . . 24
  - 2.4.3 Dispersed phase averaging . . . 25
  - 2.4.4 Mass balance ($\psi = 1$) . . . 26
  - 2.4.5 Momentum balance ($\psi = u_{2,i}$) . . . 27
- 2.5 Interfacial momentum transfer . . . 35
- 2.6 Turbulence modeling . . . 39
- 2.7 Conclusion . . . 39

3 Main forces involved in droplets dispersion **41**
- 3.1 Introduction . . . 41
- 3.2 Calculation tool . . . 42
- 3.3 Geometry and mesh . . . 42
- 3.4 General study case flow description . . . 44
- 3.5 Discussion about the model of each force . . . 48
- 3.6 Conclusion . . . 51

4 Turbulence modeling **53**
- 4.1 Introduction . . . 53

4.2 Turbulence modeling of the continuous phase 54
4.2.1 $k-\varepsilon$ turbulence model 55
4.2.2 $R_{ij}-\varepsilon$ turbulence model 57
4.2.3 Adequacy of the models $k-\varepsilon$ and $R_{ij}-\varepsilon$ in the studied case 60
4.3 Turbulence of the dispersed phase 60
4.4 Interpretation of the effect of the prediction of the particles' agitation in channel flow 75
4.5 Turbulent coupling 81
4.5.1 Bibliographical review 81
4.5.2 Closure Models of Π_{q1} and Π_{q2} in Q2Q12 83
4.5.3 Models' limitations from bibliography 85
4.5.4 Turbulence coupling model based on multi turbulent scales 88
4.6 Numerical simulation in a long vertical tube 91
4.6.1 Effect of the turbulence modeling of the continuous phase 92
4.6.2 Effect of the turbulence modeling for the dispersed phase 98
4.7 Conclusion 102

5 Lift force 105
5.1 Problem Description 108
5.2 Impact of the lift force modeling on the study case 117
5.3 Conclusion 119

6 Application on the cooling of a damaged PWR reactor core 121

7 General conclusion 126

8 Résumé en français 132

I Introduction générale 133
I.1. Contexte de l'étude 133

II Modélisation des écoulements diphasiques 137
II.1. Les équations de conservation locales moyennées 138
II.1.1. Equation de bilan locale moyennée de masse 138
II.1.2. Equation de conservation locale moyennée de Quantité De Mouvement 139
II.1.3. Equation de bilan locale moyennée de l'énergie 143
II.2. Modélisation de la turbulence 145
II.3. Conclusion 145

III Simulation 146

IV Turbulence **149**
IV.1. Introduction 149
IV.2. Modèle de turbulence de la phase continue 149
IV.2.1. $R_{ij} - \varepsilon$ modele 151
IV.2.2. Compatibilité des modèles $k - \varepsilon$ et $R_{ij} - \varepsilon$ dans le cas étudié 152
IV.3. Turbulence des phases dispersées 152
IV.3.1. Tchen-Hinze 153
IV.3.2. Q2-Q12 153
IV.4. Comparaison avec les données expérimentales dans un écoulement canal 155
IV.4.1. Modèle d'échange interfacial de turbulence basé sur l'hypothèse de une turbulence multi échelle 159
IV.4.2. L'impact de la modélisation de la turbulence sur la distribution des gouttelettes 161
IV.5. Conclusion 163

V Force de Portance **165**
V.1. Impact de la modélisation de la force de portance sur la distribution des gouttelettes 171
V.2. Conclusion 171

VI Application sur le refroidissement du coeur accidenté d'un réacteur PWR **173**

VII Conclusion **177**

Acknowledgments

It is a pleasure to thank the many people who made this thesis possible.
First and foremost I would like to express my heartfelt thanks to my supervisor Pierre Ruyer, with whom it has been a pleasure to work. I am also sincerely grateful to my director Francoise Daumas and my supervisor Adrien Toutant for their continued interest and guidance. Throughout my thesis period, they provided encouragement, sound advice, good teaching, good company, and lots of good ideas. I would have been lost without them.
I would like to acknowledge the financial and technical support of the IRSN (Institut de Radioprotection et de Sûreté Nucléaire) that provided the necessary financial support for this research. I also thank the university of Perpignan and the PROMES (PROcédés, Matériaux et Energie Solaire) Laboratory for their support and assistance.
I am most grateful to France the country that gave the chance to achieve this part of my dreams.
Lastly, and most importantly, I wish to thank my parents. They bore me, raised me, supported me, taught me, and loved me. To them I dedicate this thesis.

Nomenclature

Roman symbols

a^I	volumic interfacial area
C_β	crossing trajectories coefficient
C^D	drag force coefficient
C^{Ma}	virtual mass force coefficient
C^L	lift force coefficient
d_p	droplet diameter
d_h	hydraulic diameter
$D^t_{12,ij}$	turbulent dispersion tensor
E_k	total energy of the phase k
$F_{r,i}$	sum of interfacial forces
F^D	averaged drag force
F^{Ma}	averaged virtual mass force
F^L	averaged lift force
g_i	gravitational acceleration constant
h_k	internal enthalpy of the phase k
h_k^{Im}	averaged enthalpy at the interface
H_k	total enthalpy of the phase k
k_1	turbulent kinetic energy of the vapor phase
k_1^L	turbulent kinetic energy of the vapor phase contained in the large eddies
k_1^S	turbulent kinetic energy of the vapor phase contained in the small eddies
k_2	turbulent kinetic energy of the droplets phase
k_{12}	vapor-droplets fluctuating velocity covariance
K_2^{kin}	coefficient of eddy-diffusivity
$\dot{m}_k$	mass flux
M_k	deferent forms of the averaged interfacial momentum transfer rate
M_k'	
M_k''	
n_{ki}	unit vector normal to the interface of the phase k
$\overline{p_k}$	averaged pressure
p_k'	fluctuating pressure
p_k^{Im}	averaged pressure at the interface
Pr^T	Prandtl turbulent number
$\overline{q_k}^T$	turbulent heat flux
Re_p	Reynolds particular number
Re_s	shear Reynolds number
$\Re_{2,ii}$	Lagrangian auto correlation
$\overline{R_{ij,k}}$	Reynolds stress tensor for the phase k
S_r	non dimensional shear rate
t	time
T_{sat}	saturation temperature
T_k	averaged temperature of the phase k

$\overline{u_{ki}}$	averaged velocity of the phase k
u'_{ki}	fluctuating velocity
u_{ki}^{Im}	averaged velocity at the interface
u_σ	averaged velocity of the mass flux
v_r	relative velocity
V_d	drift velocity
V_p	particle volume
w_i	velocity of the interface
W_k	power of the interface stresses
Z	mass load

Greek symbols

α_k	volumetric fraction of phase k
δ_{ij}	Dirac distribution
ε_k	turbulent dissipation rate of the phase k
η_r	inverse of turbulent stokes number
μ_1	dynamic molecular viscosity of the vapor
ν_1	kinetic molecular viscosity of the vapor
ν_2^{kin}	kinetic viscosity of the droplets
ν_{12}^T	vapor-droplets turbulent viscosity
Π_{qk}	the averaged turbulent energy transfer
$\tilde{\Pi}_{q2}$	the averaged turbulent energy gained by the droplets when they cross large eddies
Π_w	the averaged turbulent energy lost by the particles in the wake
χ_k	the characteristic function of the phase k
σ	interfacial surface tension
$\sigma_{k,ij}$	the stress tensor of the phase k
ρ_k	averaged density of the phase k
$\overline{\tau_{ij,k}}$	viscous stress tensor
τ_1^T	turbulent time scale of the continuous phase turbulence
τ_p	the characteristic time scale of the droplet
τ_{12}^F	characteristic time scale of the momentum transfer between the two phases
τ_{12}^t	time scale of the continuous phase turbulence viewed by the droplets
Γ_k	the averaged interfacial mass transfer rate
$\xi_{2,ij}$	the Lagrangian spectrum

Operators

$<>_2$	statistical average over the dispersed phase
$\overline{k}$	average over the phase k
$\frac{D}{Dt}$	the material derivative following the velocity of the undisturbed fluid
$\frac{d}{dt}$	the material derivative following the velocity of a particle

$\frac{\bar{d}}{\bar{d}t}$	the material derivative following the averaged velocity of the dispersed phase

Subscripts

1	vapor
2	liquid
r	relative
i, j, m	vector components

Superscripts

˜	noting the undisturbed characteristics of the vapor

Chapter 1

General introduction

The two-phase flows, gas-droplets or vapor-droplets, may occur in natural and industrial situations. These flows are subject of challenging research in many industrial sectors such as production of electrical energy (steam generators of power plants, condensers, heat exchangers), the petroleum industry (extraction and transport of petroleum products), gasoline and air combustion in an automobile engine etc. Here we will focus our attention on vapor-droplet flow but most of the presented methods are applicable to gas-solid and gas-liquid flows as well.
The estimation of global characteristics of the heat transfer in a unit geometry, as the sub channel[1] in nuclear applications and combustion chamber in the automobile engine, is of high interest for many industrial applications. But actually an accurate estimation depends on the local spatial flow structures inside the unit geometry. For example, the estimation of the local spatial distribution of the droplets through the unit geometry is essential for a better understanding of the main phenomena occurring, as the combustion or the heat transfer. Then the development of computer calculation tools to simulate this type of flow and complex geometries is helpful. In particular, the improvement of local physical modeling of turbulent two-phase is of great relevance. The coexistence of the two-phase phenomena and the turbulent structures, makes the simulation of these local characteristics very complicated. Since the direct numerical simulation methods are too expensive for the industrial applications, the simulation of averaged values over sub grids inside these geometries appears to be the optimum solution. On the contrary, the simulation of averaged values requires high modeling effort to reproduce the local physics with a satisfying accuracy. The simulation of the spatial distribution of droplets, models are required to reproduce the macroscopic scale phenomena lost during the averaging process. For example, the interaction between the vapor and the droplet at the level of the interface as the friction and interfacial forces and the fluctuation of the ve-

[1] The flow area between the fuel bars in the core of a nuclear reactor

locities of the vapor and the droplets, are the main phenomena that should be modeled.
In the present study, we consider a specific physical problem in the context of nuclear safety. Actually, the vapor-droplet flows play a major role in the heat transfer problematic for the study of the accidental events in the nuclear reactors.

1.1 Context of the study

One of the reference accident that may occur in PWR (Pressurized Water Reactor) is LOCA (Loss of Coolant Accident). The LOCA is studied to design some emergency systems implemented in the basic nuclear installations. The LOCA corresponds to the break of a pipe in the primary loop. This accident is associated with a loss of pressure which leads to the vaporization of the water in the reactor core and then to the rise of the temperature of the assemblies. In the following sequence of events of the LOCA, the backup systems inject liquid water into the core in order to cool the fuel assemblies, this is called the reflooding phase. Although the reactor by this time is subcritical so that little power is produced from fission, a large amount of decay power exists and causes the fuel rod to have a temperature in the region of 800 °C. Then the injected water rises up along the rods and evaporates due to contact with the heated rods. This is followed by a violent evaporation of water at the level of the interface between water and vapor, which is called the quench front. The violent evaporation increases the vapor flow downstream of the quench front and causes the tear of water drops at the front. These droplets have first an inertial departure then they will be entrained by the vapor. Going up in the flow, these drops evaporate until they disappear. Thus along an assembly during the reflooding phase, the regime of heat exchange between the fluid and the wall varies from bottom to top, passing from purely convection water, to nucleate boiling, then vapor carrying droplets and then vapor single phase. In this study, we focus on the area of vapor-droplet flow, where the cooling effectiveness of such a mixture is a major concern. The droplets act as heat sinks for the vapor and control the vapor temperature profile which, in turn, determines the wall heat transfer rate.
For the thermal-hydraulic analysis in nuclear applications three main simulation scales exists: The system scale, dedicated to the overall description of the reactor circuits; the component scale, at which the reactor core is studied using the 'porosity' concept and the CFD in open medium scale, which allows one to go for a finer description of the flows and detect local phenomena. The present work lays in the later category, where the simulation part of this study deals with the adaptation of the CFD code Neptune_CFD (mainly devoted to bubbly and separated-phase flows) to the simulations of dispersed

droplets two-phase flow. Therefore, we focus our work on the droplets dispersed flow inside a subchannel representing the flow domain between four rods. Figure 1.1 shows a representative figure of the vapor-droplet turbulent flow, initiated at the level of the quench front,between two hot fuel rods in a damaged PWR reactor core.

The mechanisms of heat transfer in such a dispersed flow is illustrated

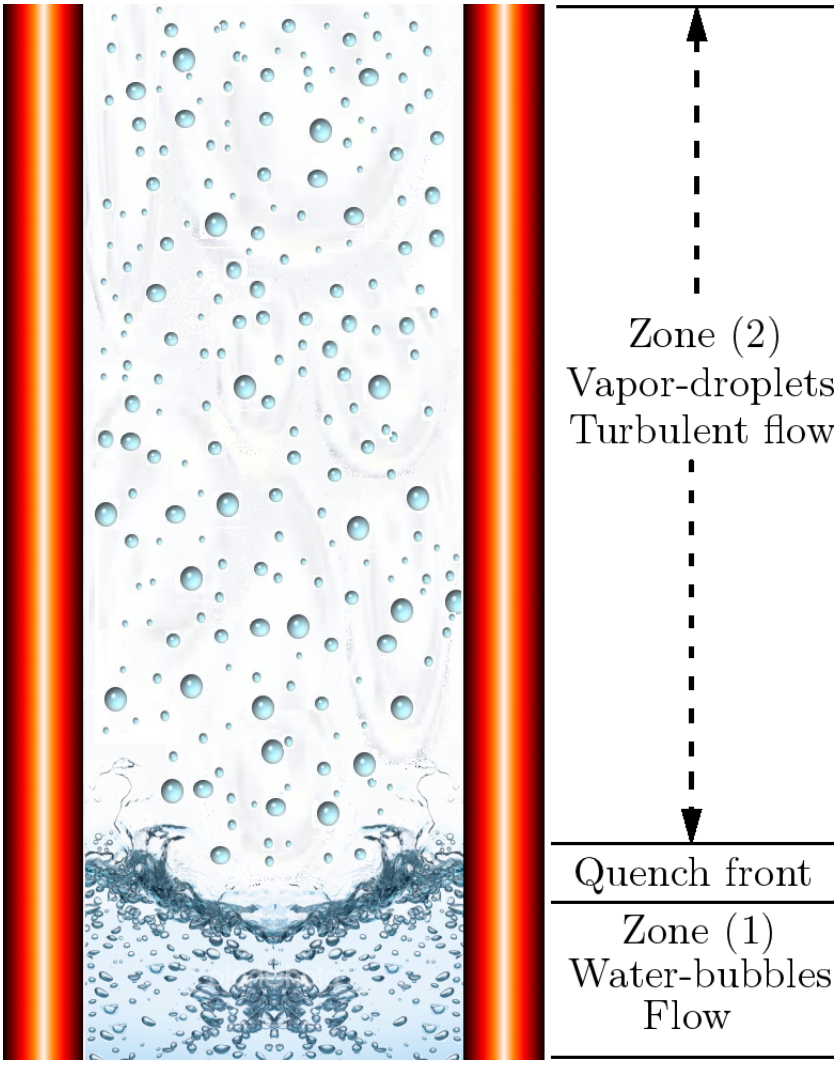

Figure 1.1: Representative figure of the vapor-droplet turbulent flow between two hot fuel rods in a damaged PWR reactor core.

in figure 1.2. These effects are distinguished by Andreani and Yadigaroglu (1997) as follows:

- Convective heat transfer from wall to vapor

- Convective heat transfer between vapor and droplets
- Direct contact wall-to-droplet heat transfer
- Radiative heat transfer from the wall to the droplets and the vapor
- Radiative heat transfer from the vapor to the droplets
- Transfer by droplets evaporation or vapor condensation

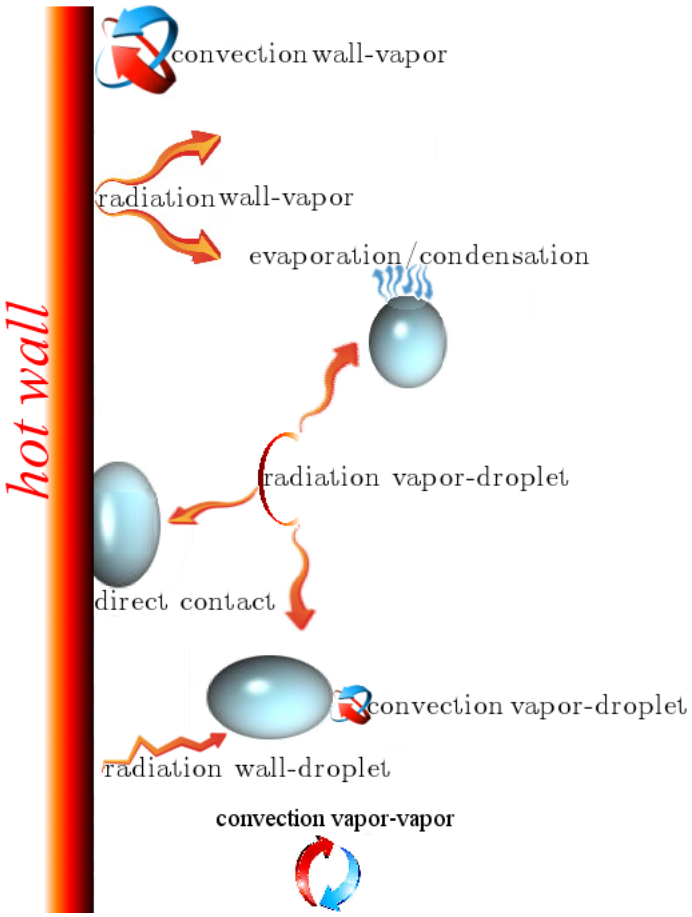

Figure 1.2: Representative figure of the heat transfer mechanisms between a hot wall and a vapor-droplet flow

Each one of these mechanisms is a separate phenomenon that needs to be modeled but it can be noticed that the distribution of the droplets is an important factor that impacts the modeling of most of these mechanisms. For example, the vapor-droplet convection depends on the distribution of the droplets in the vapor while the radiation from the wall to the droplets and the direct contact of the droplets with the wall depend directly on

the distance separating between the droplet and the wall. Andreani and Yadigaroglu (1997) noted that the droplets concentration and droplets diameters are not uniformally distributed across the channel. Then, they concluded that the 1-D models are not suitable in this case and even the 2-D models, that consider an uniform droplets radial distribution (Webb and Chen (1982)) are not suitable as well. The first model that combines the 2-D analysis of the vapor field with the radial migration of the droplets was proposed by Kirillov et al. (1987). It takes into account the forces acting on the droplets (drag, lift and virtual mass) Andreani and Yadigaroglu (1997) proposed a Eulerian-Lagrangian 3-D model that treats in detail the features of the droplets, vapor velocity and temperature fields under typical dispersed field flow. Although this model defines most of the physical phenomena that may occur, it uses the common closure models of these phenomena without extending the research about the compatibility of these models.

After many years of intense research into the reflood process, high fidelity simulation of core reflood remains elusive. Basic phenomena associated with reflood have been studied extensively with many separate effects and integral experiments. Very basic analysis by researchers such as Andreani and Yadigaroglu (1997) has also increased our understanding. However, attempts to integrate this knowledge in the models, used by safety analysis tools such as CATHARE (system scale tool), have still results with large uncertainties and can not take into account many phenomena (ex: the influence of the rod deformation). Typical shortcomings are noticed, including poor predictions of vapor temperature downstream the quench front.

Accurate prediction of droplets concentration is essential, since the void fraction distribution affects the heat transfer rate in the reactor core. The modeling of the droplets distribution is a composed problem since it depends on several phenomena. The main phenomena that affect the droplets distribution are the forces between the vapor and the droplets; and the turbulence of the vapor and the droplets. The direct numerical simulation (DNS) of these flows is so expensive, due to the coexistence of the two-phase and the turbulence phenomena. Therefore, subgrid models should be used. They have to model accurately the effect of the turbulent dispersion and of each force on the droplet distribution. **Our general objective is to ameliorate the modeling of the vapor-droplet flow (i.e. at CFD scale). Particularly the estimation of the radial distribution of the droplets**.

1.2 Process and plan of the study

The volume fraction distribution of the two phases depends on the size and dispersion of the droplets in the flow. The size of the droplets is controlled by the rupture and coalescence mechanisms and the interfacial mass transfer (evaporation/condensation). The distribution of the droplets is controlled by the transfer of momentum between the two phases. Our study focuses particularly on the latter point. We are restricted to flows where the liquid water flows under the form of non-deformable spherical droplets that do not interact with each other. Both phases are treated by a two-fluid approach Euler-Euler.

In chapter 2, a description of two-phase flow model is presented, using separate mass, momentum, and energy equations for the two phases. These separate balance equations are obtained in an averaging process starting from the local instantaneous conservation equations of the individual phases. During the averaging process, important information on local flow processes are lost and, consequently, additional correlations are needed in order to close the system of equations. The terms that need closure models are then identified, such as the terms of turbulence of the two phases and the terms of the interfacial transfer of mass, momentum, and energy. Then the momentum balance equation of the dispersed phase is derived via a statistical approach starting from a Lagrangian point of view. This derivation is required for the closure of the momentum interfacial transfer. Then we limit our interest on the terms that impact the spatial distribution of the droplets in context of our case of interest. A brief presentation of the different forces allows to understand the role of each force on the motion of the droplets. **Consequently, our objective becomes to identify the terms that are not well modeled for the droplets flow case**.

In order to identify the terms that need a refined research, a parametric study is proposed, in Chapter 3, to show the effect of the modeling of the various terms specified in chapter 2. We first present the calculation software and the geometry of the study case with the choice of the mesh. A study case with basic models is done and the results are presented. This test case helps us to draw a general description of the droplets distribution, and to specify the role of each term. After that we discuss briefly the modeling of each term regarding the basic models used in the test. **At the end of this chapter we specify the basic models which affect the radial distribution of the droplets,which requires more research**.

Chapter 4 discusses in details the models of turbulence of the both phases. Two models of different levels of numerical complexity and physical accuracy are considered for each phase. For the continuous phase the choice between an isotropic model $k-\varepsilon$ and a non-isotropic model $R_{ij}-\varepsilon$ is studied, to check if the modeling of the anisotropy of the vapor turbulence has an important impact on the droplets distribution. For the droplets turbulence, two mod-

els have been studied: the simple algebraic model called Tchen-Hinze (Tchen (1947)) is compared with a more elaborated model called Q2Q12 (Simonin (2000)). The results of different combinations of these models are verified with the help of the experimental data realized in a similar case by Kulick et al. (1994). Moreover the interfacial turbulence coupling between the two phases is analyzed and the modification of the modeling of this term in the Q2Q12 model is proposed. The proposed modeling is then verified based on the experimental results of Kulick et al. (1994).
Due to its critical role in the prediction of the droplets distribution, the modeling of the lift force is studied separately in chapter 5. A detailed bibliographical study is presented about the classical analytical modelings of this force (e.g. Auton (1987) and Saffman (1965)). Then a parametric study is presented about the compatibility of these models to the present case. Due to recent DNS results achieved in this domain, as the results of Sugioka and Komori (2006) and Zeng et al. (2009), we succeeded to propose two new modelings. The first one is based on the model of Saffman (1965) by extending the correction proposed by McLaughlin (1991) to cover a wide range of Reynolds number and the second is a proposed numerical correlation that fits the results from DNS.
Back to the context of the study, chapter 6 is dedicated to check the impact of the modeling proposed in this study on the thermal transfer through the flow. For this purpose, a series of simulations are achieved for a case with hot walls. From the seven transfer mechanisms presented in figure 1.2, only the convection models are considered because the other models are still under construction in parallel projects. The models are evaluated by quantifying the heat extracted by flow from the wall and results are presented.
Finally, a general conclusion and a perspectives will be drawn.

Chapter 2

Governing equations for two-phase flow

2.1 Introduction

As described in the introduction, the simulation of the two-phase flow vapor-droplet, where vapor is considered as the continuous phase and droplets are presented as dispersed inclusions, is required. A two-phase mixture can generally be divided into two purely monophasic regions, where physical quantities obey the classical local balance equations, separated by interfaces infinitely thin and massless. The simulation problem of this flow is extremely complex due to the coexistence of the local two-phase structures and the physical quantities of the turbulent flow. Detailed knowledge of local and instantaneous characteristics of the two-phase turbulent flow is inaccessible due to the complexity of these structures. Therefore the numerical calculation of this type of flows should pass through developed models, that use simplifying hypotheses that permit to avoid the knowledge of the local and instantaneous characteristics.
Several numerical approaches exist to simulate two phase flows. The choice between these approaches is usually a matter of balance between their physical accuracy and their numerical cost. In our case, Euler/Euler method is chosen due to its light numerical effort. The Eulerian approach consists in applying a statistical averaging on the variables and equations, in order to define average quantities that can be treated by the usual methods of numerical analysis. In contrast to this simplicity in the treatment, the averaged formulation is accompanied by a loss of information on turbulence and interfacial exchanges and the appearance of new unknown terms. The closure of these terms requires to develop mathematical expressions, what we will call sub models. These sub models are responsible to reproduce the physical effects lost in the averaging process. These physical effects are in general, the turbulence of the two phases an the interfacial transfer of mass,

momentum and energy. In our work we identify all these phenomena, but we will focus our research on the models that have important impact on the droplet's distribution inside the flow domain.
In the following we justify our choice of Euler/Euler approach after a general comparison between the different numerical methods that can be proposed for this kind of flow. Then, the averaged equations of the two phases are derived from instantaneous equations in a classical Eulerian approach. The closure of the interfacial forces requires to know about the local instantaneous forces exerted by the vapor on a droplet. Therefore we present the Lagrangian approach to derive the RANS (Reynolds Averaged Navier Stokes) equations for the dispersed phase. Finally the two approaches are coupled to close the interfacial momentum term.

2.2 Numerical methods

For single-phase flow there are two different approaches to describe a fluid flow:

- The first approach, Eulerian, provides variations of different characteristics of the fluid at each instant at any point in the domain. The Eulerian variables are functions of the time and position and will form characteristic fields. In figure 2.1, the physical quantity G is attached to the point A with coordinates x, y, z. At instant t_1 this physical quantity is equal to that of particle P_1 which passed in A at instant t_1. While at instant t_2, this physical quantity is equal to that of particle P_2 which passed in A at instant t_2.

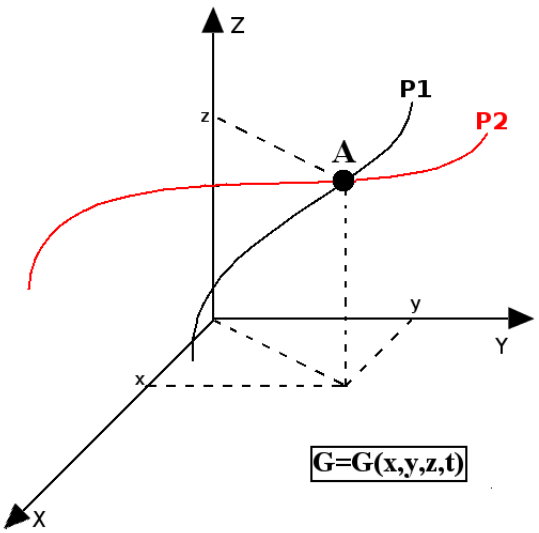

Figure 2.1: Eulerian system

- The second, Lagrangian approach, which follows each particle as it moves through space with time. We focus on the trajectories of fluid particles where each particle has its own velocity. The different physical quantities are then functions of time. The identification is usually done by the three coordinates of the positions occupied by the particles initially at t_0. In (figure 2.2), the particle P whose coordinates are $x(t)$, $y(t)$, $z(t)$, is the one found at the point P_0 whose coordinates are $x_0 = x(t_0)$, $y_0 = y(t_0)$, $z_0 = z(t_0)$ at the time t_0. Then the physical quantity G which is attached to the particle P is a function of time t and x_0, y_0, z_0.

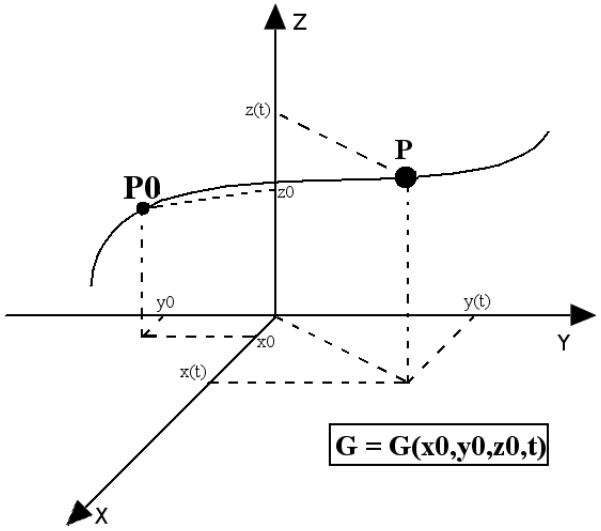

Figure 2.2: Lagrangian system

In two-phase flows, it is obvious to use the Eulerian approach for the continuous phase. In contrast, the two approaches are possible for the dispersed phase. The Lagrangian approach provides more accurate representation of the local dynamics of the particles. But this approach is expensive, when the calculation of large number of particle trajectories is required. So there are two approaches for the computation of dispersed two-phase flows: (1) Eulerian-Lagrangian, also known as particle-tracking, and (2) Eulerian-Eulerian, also known as two-fluid. In the first approach, the continuous-phase is solved using the Navier-Stokes equations, and the individual particles are tracked. In the second approach, the dispersed phase is described by the averaged characteristics of the population defined as fields. Their evolution obeys balance equations, which are quite similar to the Reynolds Averaged Navier-Stokes (RANS) equations of single-phase flows, with some extra coupling-terms.
Navier-Stokes equations can be solved numerically by three main methods:

(1) Direct Numerical Simulations (DNS), in which Navier-Stokes equations are solved directly and no averaging or modeling is applied. DNS needs resolution for all the scales of the flow structures (turbulence structures), thus very dense grids are used in order to reach the smallest scale, where turbulence dissipation occurs. DNS requires a huge amount of computer capacity. (2) Large Eddy Simulation (LES) where the main flow field is solved from the Navier-Stokes equations and the smallest eddies are modeled. This method also depends on the grid density (or filter width). This means that when we use a denser grid in LES we approach direct numerical simulations. The choice of the density of the grid in LES depends on the level of the required accuracy. But this choice in two phase flow becomes more difficult because it becomes dependent on the size of the turbulent structure and on the size of the particles of the dispersed phase. Also large eddy simulation requires a huge amount of computer capacity. (3) RANS equations where the averaging process leads to the appearance of new terms that should be modeled. RANS does not require high computational effort but it demands modeling.

Eulerian-Lagrangian DNS/LES is a high cost computational method so it is used mostly as a research tool, in order to improve the models used in the RANS simulations. Also Eulerian-Lagrangian RANS can become too costly due to the large number of particles that need to be tracked to reach the minimum level of accuracy. The Eulerian-Eulerian approach is somehow comparable to the RANS approach of single-phase flows and the computational effort is quite similar to it. Industrial applications, as the concerned context case, require practical calculation tool with low numerical cost and an acceptable level of accuracy. Therefore this approach will be considered here. The major inconvenience of the Eulerian-Eulerian approach is that it requires more levels of modeling to reproduce the main phenomena lost during the averaging process. The present study aims to adapt the closure models to the case of vapor-droplet flow.

The derivation of the system of averaged equations of the two phases can be based on a Lagrangian or on an Eulerian point of view. The most popular simple way is to start from an Eulerian point of view by averaging the separate local instantaneous phase equations accounted for the interfacial jump conditions. This method is compatible with the nature of the continuous phase, but such an averaging approach is very restrictive for the dispersed phase because particle sizes and particle distances have to be smaller than the smallest length scale of the turbulence. This approach is not able to model some important phenomena as the turbulence correction of the interfacial forces and the derivation of the transport equations of the kinetic energy of the particles.

The other approach is to start from a Lagrangian point of view in which the mixture (fluid-particles) is treated as an ensemble of fluid and discrete particles. This is an statistical approach in the framework of kinetic theory

by defining a point probability density function (pdf). The discretization of the continuous medium (the vapor in our case) into particles is not a natural step. Here we should consider that the fluid particle can be seen as a small element of fluid whose characteristic length scale is much larger than the molecular mean free path and much smaller than the Kolmogorov length scale. In contrast for the dispersed phase, when the interactions between particles are negligible, the Lagrangian approach permits to study the dynamics of isolated particles and their interaction with the surrounding fluid. Then we can obtain a realistic description of the dispersed phase flow and its influence on the continuous phase by summation over a large number of particles. The statistical treatment of the Lagrangian equations permits to derive simple formulations for the interfacial transfer laws and reflects the influence of the turbulence.
In the following we derive the averaged balance equations for the two phase by the classical method (Eulerian), from the local instantaneous phase equations with the interfacial jump conditions. Then we derive the equations of the dispersed phase by the probabilistic method (Lagrangian) in order to close the interfacial terms.

2.3 Dynamic equations for single-phase and two-phase flows classical derivation

2.3.1 Instantaneous single-phase equations

The instantaneous single-phase equations, or the transport equations, are the following:.

- Mass balance equation:

$$\frac{\partial(\rho)}{\partial t} + \frac{\partial(\rho u_i)}{\partial x_i} = 0 \tag{2.1}$$

  where ρ is the density, u_i is the instantaneous velocity in the x_i direction, x_i is ith component of the position vector, and t is the time.

- Momentum balance equation:

$$\frac{\partial(\rho u_i)}{\partial t} + \frac{\partial(\rho u_i u_j)}{\partial x_j} = \rho g_i + \frac{\partial(\sigma_{ij})}{\partial x_j} \tag{2.2}$$

  where g_i is the gravity and σ_{ij} is the stress tensor which can be written in terms of the pressure p and the viscous stress tensor τ_{ij}:

$$\sigma_{ij} = -p\delta_{ij} + \tau_{ij} \tag{2.3}$$

In the case of Newtonian fluids the viscous stress tensor τ_{ij} can be written in the following form, (which means that the stress to rate-of-strain relation is linearly isotropic)

$$\tau_{ij} = \rho\nu(\frac{\partial u_i}{\partial x_j} + \frac{\partial u_j}{\partial x_j}) - \frac{2}{3}\rho\nu\frac{\partial u_m}{\partial x_m}\delta_{ij} \tag{2.4}$$

where ν represents the kinetic viscosity.

- Total energy balance equation:

$$\frac{\partial(\rho E)}{\partial t} + \frac{\partial(\rho E u_i)}{\partial x_j} = \frac{\partial(u_j\sigma_{ij})}{\partial x_i} - \frac{\partial q_i}{\partial x_i} + \rho g_i u_i + Q \tag{2.5}$$

with

$$E = e + \frac{1}{2}u_i u_i \tag{2.6}$$

$$q_i = -\lambda\frac{\partial T}{\partial x_i} \tag{2.7}$$

where E is the specific total energy, e is the specific internal energy, q is the thermal conduction heat flux, λ is the thermal conductivity and Q is the volumetric heat source.

2.3.2 Instantaneous local equations for the two-phase flow

For two-phase flows, the two phases are separated by discontinuity surfaces (interfaces). These interfaces are supposed infinitely thin and massless. Then, the conservation equations are not continuous and differentiable all over the domain. So we should define a space where we can derive these quantities, which permits us to write the conservation equations for the two-phase flows. These equations should be defined all over the space of distribution and valid at every instant.
The distribution function introduces for every local and instantaneous quantity ϕ_k, a new quantity $\phi_k\ \chi_k$ defined on the whole two phase flow domain.

Phase characteristic function

$\chi_k(M,t)$ is the phase characteristic function or presence function which indicates the presence of the phase k at point M and instant t. The phase index k takes the values 1 for the continuous phase (vapor) and 2 for the dispersed phase (droplets).
If at instant t, the point M is located in the phase k then

$$\chi_k(M,t) = 1 \tag{2.8}$$

else:

$$\chi_k(M,t) = 0 \tag{2.9}$$

The derivatives of the function χ_k read

$$\frac{\partial \chi_k}{\partial t} = \omega_i n_{k,i} \delta \tag{2.10}$$

$$\frac{\partial \chi_k}{\partial x_i} = -n_{k,i} \delta \tag{2.11}$$

where $\overrightarrow{n_k}$ is the unit vector normal to the interface and oriented outward of the phase k, $\overrightarrow{\omega}$ is the velocity of the interface, and δ is the Dirac distribution function on the interface (figure 2.3).

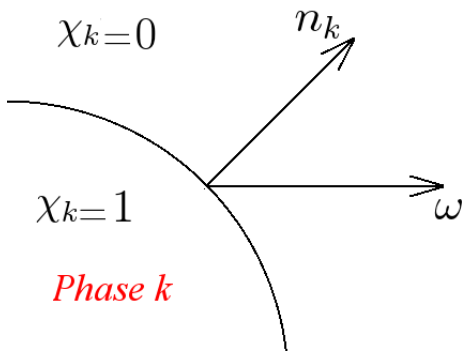

Figure 2.3: Interface jump

Two-phase equations

Two-phase local instantaneous equations are established by multiplying the local instantaneous equation of the single-phase flow by the phase indicator function χ_k. After integrating χ_k in the different derivative operations, by using the derivation properties of χ_k, we got the following equations for each phase:

- Mass balance equation for the phase k:

$$\frac{\partial(\chi_k \rho_k)}{\partial t} + \frac{\partial(\chi_k \rho_k u_{ki})}{\partial x_i} = \rho_k(\omega_i - u_{ki}) n_{ki} \delta \tag{2.12}$$

- Momentum balance equation for the phase k:

$$\begin{aligned} \frac{\partial(\chi_k \rho_k u_{ki})}{\partial t} + \frac{\partial(\chi_k \rho_k u_{ki} u_{kj})}{\partial x_j} &= \chi_k \rho_k g_i + \frac{\partial(\chi_k \sigma_{kij})}{\partial x_j} \\ &+ [\sigma_{kij} - \rho_k u_{ki}(u_{kj} - \omega_j)] n_{kj} \delta \end{aligned} \tag{2.13}$$

- Total energy balance equation for the phase k:

$$\begin{aligned}\frac{\partial(\chi_k\rho_k E_k)}{\partial t}+\frac{\partial(\chi_k\rho_k E_k u_{ki})}{\partial x_i} &= \frac{\partial(\chi_k\sigma_{kij}u_{kj})}{\partial x_i}-\frac{\partial\chi_k q_{ki}}{\partial x_i}\\ &+ \chi_k\rho_k g_i u_{ki}+\chi_k Q_k\\ &+ [\sigma_{kij}u_{kj}-q_{ki}-\rho_k E_k(u_{ki}-\omega_i)]n_{ki}\delta\end{aligned} \tag{2.14}$$

We consider that the interface has no mass and no internal energy in the surface unit, but it carries surface tension forces. Thus the interfacial conditions of mass, momentum and total energy are added to these:

$$\sum_{k=1,2}\rho_k(\omega_i-u_{ki})n_{ki}\delta = 0 \tag{2.15}$$

$$\sum_{k=1,2}[\sigma_{kij}-\rho_k u_{ki}(u_{kj}-\omega_j)]n_{kj}\delta = F_{si}\delta \tag{2.16}$$

$$\sum_{k=1,2}[-\sigma_{kij}u_{kj}+q_{ki}+\rho_k E_k(u_{ki}-\omega_i)]n_{ki}\delta+F_{si}\omega_i = 0 \tag{2.17}$$

F_{si} is the i^{th} component of the surface tension force, in section 2.5 we present a detailed closure of this term.

2.3.3 Averaged local equations

Several types of averaging can be defined and applied.

Averaging operator: Properties and definition

The averaged formulation are related to the definition of an average operator, which must verify a number of essential properties known as Axioms of Reynolds, which are:

- linearity

$$\overline{\phi+\theta}=\overline{\phi}+\overline{\theta} \quad ; \quad \overline{\lambda\theta}=\lambda\overline{\theta} \tag{2.18}$$

  where ϕ and θ are random variables and λ is a constant.

- idempotence

$$\overline{\phi\overline{\theta}}=\overline{\phi}\,\overline{\theta} \tag{2.19}$$

- commutativity with derivation operations

$$\overline{\frac{\partial \phi}{\partial x_j}} = \frac{\partial \overline{\phi}}{\partial x_j} \quad ; \quad \overline{\frac{\partial \phi}{\partial t}} = \frac{\partial \overline{\phi}}{\partial t} \tag{2.20}$$

Then any local instantaneous variable can be decomposed into a mean and a fluctuating value which verify:

$$\phi = \overline{\phi} + \phi' \qquad \overline{\phi'} = 0 \tag{2.21}$$

Principally because of the random attitude of the turbulent flow characteristics, this operator can be defined as the limit of arithmetic mean of a number N of phenomenon realizations, where N tends to infinity.

$$\overline{\phi} = \lim_{N \to \infty} \sum_{0}^{N} \phi \tag{2.22}$$

Normally the time and spatial averaging are used. These averages satisfy the properties of the Reynolds axiom only when the flow is steady and homogeneous.

$$\overline{\phi} = \frac{1}{\Omega} \int_{\Omega} \phi d\omega \quad ; \quad \overline{\phi} = \frac{1}{\Delta t} \int_{t}^{t+\Delta t} \phi d\tau \tag{2.23}$$

All these kinds of averages are equivalent if they verify the Reynolds axioms. Then it is not necessary to precise what kind of average is used to establish the mean value equations.
In two-phase flows, the common averages are:
- The classical Eulerian phase average

$$\underline{\phi} = \frac{\overline{\phi \chi_k}}{\alpha_k} \tag{2.24}$$

where $\alpha_k = \overline{\chi_k}$ is the volume fraction of phase k. It is possible to define a fluctuation associated to this average.

$$\underline{\phi}'' \equiv \phi - \underline{\phi} \tag{2.25}$$

Then the averaged density of the phase k is defined by:

$$\underline{\rho_k} = \frac{\overline{\rho_k \chi_k}}{\alpha_k} \tag{2.26}$$

- For the local balance equations, it is more practical for problems with variable density to define a Favre type average weighted by the density which is written

$$\overline{\theta}^k \equiv \frac{\overline{\rho_k \theta \chi_k}}{\overline{\rho_k \chi_k}} = \frac{\overline{\rho_k \theta \chi_k}}{\alpha_k \widetilde{\rho_k}} \tag{2.27}$$

The main interest of this average is to take into account the variations in phase densities. The fluctuation associated to this average is

$$\theta' \equiv \theta - \overline{\theta}^k \quad ; \quad \overline{\rho_k \theta' \chi_k} = 0 \tag{2.28}$$

Important remark: Practically the averaged density will be calculated by using classical Eulerian average and will be noted later as ρ_k for purpose of simplifying the notations. Other quantities will be averaged using Favre average. We will use the following simplified notation

$$\overline{\theta}_k^k = \overline{\theta}_k \tag{2.29}$$

Mass balance equations

After averaging the mass balance equations 2.12, we got:

$$\boxed{\frac{\partial(\alpha_k \rho_k)}{\partial t} + \frac{\partial(\alpha_k \rho_k \overline{u_{ki}})}{\partial x_i} = \Gamma_k \qquad k = 1, 2} \tag{2.30}$$

where $\overline{u_{ki}}$ is the Favre averaged velocity of phase k.
The right hand side of the equation, Γ_k, is the new term which appears after the averaging process. This term accounts for the averaged interfacial mass flow rate. It represents the local balance of evaporation/condensation at the vapor/droplet interface. It is defined by

$$\Gamma_k = \overline{\rho_k(\omega_i - u_{ki}) n_{ki} \delta} \tag{2.31}$$

This term can not be calculated easily as a function of the main (solved) variables then it should be modeled. The closure of this term will be presented in the next paragraph.

Momentum balance equations

After averaging the momentum balance equations 2.13 we obtain:

$$\begin{aligned} \frac{\partial(\alpha_k \rho_k \overline{u_{ki}})}{\partial t} + \frac{\partial(\alpha_k \rho_k \overline{u_{ki}}\ \overline{u_{kj}})}{\partial x_j} &= \alpha_k \rho_k g_i - \frac{\partial \alpha_k \overline{p_k}}{\partial x_j} \\ + \frac{\partial}{\partial x_j}[\alpha_k(\overline{\tau_{ij,k}} - \rho_k \overline{R_{ij,k}})] &+ \overline{[(-p_k \delta_{ij} + \tau_{ij,k}) - \rho_k u_{ki}(u_{kj} - \omega_j)] n_{kj} \delta} \end{aligned} \tag{2.32}$$

Two new terms appear after the averaging of the momentum equation:

- The Reynolds stress tensor $\overline{R_{ij,k}}$, which accounts for the turbulence of the flow is the average of

$$\alpha_k \rho_k \overline{R_{ij,k}} = \overline{\rho_k u'_{ki} u'_{kj} \chi_k} \tag{2.33}$$

where u'_{ki} is the fluctuation velocity of the phase k. $\overline{R_{ij,k}}$ is not solved directly; and it should be closed by mean of a turbulence model.

- The interfacial momentum transfer term

$$\overline{[(-p_k\delta_{ij}+\tau_{ij,k})-\rho_k u_{ki}(u_{kj}-\omega_j)]n_{kj}\delta}$$

The term transfer of momentum at the interface has been the subject of several modelings. According to the authors, this term can be divided in different ways into several contributions in order to separate the different physical phenomena. Therefore the contribution accounting for the classical forces acting on a particle (i.e. drag force, added mass, lift ...) is different from one author to another. In the following we will pass over different decompositions of this term before choosing a form to be used.

  - First it is proposed to isolate a term M_k which accounts for the perturbation of the stress tensor near the interfaces, then M_k contains the local effects of the drag and the wake as noted by Simonin (1991a). We write the right hand side (RHS) of the momentum balance equation

$$\begin{aligned} RHS &= \alpha_k\rho_k g_i - \frac{\partial\alpha_k\overline{p_k}}{\partial x_j} + \frac{\partial}{\partial x_j}[(\alpha_k\overline{\tau_{kij}}) - \alpha_k\rho_k\overline{R_{ij,k}}] \\ &+ \overline{[-p_k\delta_{ij}+\tau_{kij}-\rho_k u_{ki}(u_{kj}-\omega_j)]n_{kj}\delta} \end{aligned} \tag{2.34}$$

    we start by decomposing the pressure terms in RHS as follows

$$\frac{\partial\alpha_k\overline{p_k}}{\partial x_j} = \alpha_k\frac{\partial\overline{p_k}}{\partial x_j} + \overline{p_k}\frac{\partial\alpha_k}{\partial x_j} \tag{2.35}$$

$$\overline{[p_k\delta_{ij}]n_{kj}\delta} = \overline{[p'_k\delta_{ij}]n_{kj}\delta} - \overline{p_k}\frac{\partial\alpha_k}{\partial x_j} \tag{2.36}$$

$$\tag{2.37}$$

    as well as separating the term of the interfacial momentum flow into a mean and a fluctuating part

$$\overline{-\rho_k u_{ki}(u_{ki}-\omega_j)n_{kj}\delta} = \overline{-\rho_k u'_{ki}(u_{ki}-\omega_j)n_{kj}\delta} + \Gamma_k\overline{u}_{ki} \tag{2.38}$$

    now we can write the right hand side of the momentum balance equation as follows

$$RHS = \alpha_k\rho_k g_i - \alpha_k\frac{\partial\overline{p_k}}{\partial x_j} + \frac{\partial}{\partial x_j}[(\alpha_k\overline{\tau_{kij}}) - \alpha_k\rho_k\overline{R_{ij,k}}] + M_k + \Gamma_k\overline{u}_{ki} \tag{2.39}$$

where

$$\begin{aligned} M_k &= \overline{[-p'_k\delta_{ij} + \tau_{kij} - \rho_k u'_{ki}(u_{kj} - \omega_j)]n_{kj}\delta} \\ &= \overline{[-p_k\delta_{ij} + \tau_{kij} - \rho_k u_{ki}(u_{kj} - \omega_j)]n_{kj}\delta} - \Gamma_k\overline{u}_{ki} - \overline{p_k}\frac{\partial\alpha_k}{\partial x_j} \end{aligned} \tag{2.40}$$

– However, other authors express differently the interfacial forces (which are related to the classical forces of drag,lift...). Thus, Drew (1992) preferred to write separately the force induced by the mass transfer from the other interfacial contributions:

$$RHS = \frac{\partial}{\partial x_j}[\alpha_k\overline{\sigma_{kij}} - \alpha_k\rho_k\overline{R_{ij,k}}] + \alpha_k\rho_k g_i + \Gamma_k u_{ki}^{Im} + M'_{ki} \tag{2.41}$$

where u_{ki}^{Im} is the averaged velocity at the interface and it is defined by using an average weighted by the mass flux going out from the phase k through the interface

$$u_{ki}^{Im} = \frac{\overline{u_{ki}\dot{m}_k\delta}}{\overline{\dot{m}_k\delta}} = -\frac{\overline{u_{ki}\dot{m}_k\delta}}{\Gamma_k} \tag{2.42}$$

which is equivalent to

$$\Gamma_k u_{ki}^{Im} = -\overline{\rho_k u_{ki}(u_{kj} - \omega_j)n_{kj}\delta} \tag{2.43}$$

M'_k represent the impact of the stresses (pressure and viscous stresses) on the interface:

$$M'_k = \overline{\sigma_{kij}n_{kj}\delta} \tag{2.44}$$

– Ishii (1975) used the term M'_k after subtracting a term related to the averaged pressure on the interface, noted p_k^I:

$$M''_{ki} = \overline{[-(p_k - p_k^I)\delta_{ij} + \tau_{kij}]n_{kj}\delta} = M'_{ki} - p_k^I\frac{\partial\alpha_k}{\partial x_i} \tag{2.45}$$

where the averaged pressure at the interface reads

$$p_k^I = \frac{1}{a^I}(\overline{p_k\frac{\partial\chi_k}{\partial n_k}}) = \frac{1}{a^I}(\overline{p_k\delta}) \tag{2.46}$$

with a^I is the volumic interfacial area

$$a^I = \overline{\frac{\partial\chi_k}{\partial n_k}} = \overline{\delta} \tag{2.47}$$

which permits to write the right hand side of the equation (RHS) under the form:

$$\begin{aligned} RHS &= \alpha_k\rho_k g_i - \alpha_k\frac{\partial\overline{p_k}}{\partial x_i} + \frac{\partial}{\partial x_j}[(\alpha_k\overline{\tau_{kij}}) - \alpha_k\rho_k\overline{R_{ij,k}}] \\ &+ \Gamma_k u_{ki}^{Im} + M_{ki}'' + (p_k^I - \overline{p_k})\frac{\partial\alpha_k}{\partial x_i} \end{aligned} \tag{2.48}$$

So M_k'' takes into account the local variation of the pressure field near the interfaces.

– Finally, similar to what has been done for the pressure, Hewitt et al. (1990) and Ishii and Mishima (1984) proposed to separate the contribution of the averaged viscous stress at the interface from the term of the interfacial momentum transfer. Then RHS can be written as follows:

$$\begin{aligned} RHS &= \alpha_k\rho_k g_i - \alpha_k\frac{\partial\overline{p_k}}{\partial x_i} + \frac{\partial}{\partial x_j}[(\alpha_k\overline{\tau_{kij}}) - \alpha_k\rho_k\overline{R_{ij,k}}] \\ &+ \Gamma_k u_{ki}^{Im} + M_{ki}''' + (p_k^I - \overline{p_k})\frac{\partial\alpha_k}{\partial x_i} - \tau_{kij}^I\frac{\partial\alpha_k}{\partial x_i} \end{aligned} \tag{2.49}$$

where

$$M_{ki}''' = \overline{[-(p_k - p_k^I)\delta_{ij} + (\tau_{kij} - \tau_{kij}^I]n_{kj}\delta} = M_{ki}' - p_k^I\frac{\partial\alpha_k}{\partial x_i} - \tau_{kij}^I\frac{\partial\alpha_k}{\partial x_i} \tag{2.50}$$

In this work, we neglected the effect of the local variation of the pressure and the viscous stresses near the interface, and the decomposition of Drew (1992) is considered. Therefore the interfacial momentum transfer is decomposed into two terms

1. $\Gamma_k u_{ki}^{Im}$ accounts for the momentum transfer due to the mass transfer and it is the average of

$$\boxed{\Gamma_k u_{ki}^{Im} = \overline{-\rho_k u_{ki}(u_{kj} - \omega_j)n_{kj}\delta}} \tag{2.51}$$

The contribution depending on the mass transfer is small in comparison with the other contributions. Therefore the interfacial velocity u_{ki}^{Im} is closed in a simple way as follows

$$u_{ki}^{Im} = \begin{cases} \overline{u_{2i}}, & \text{Mass transfer from } 2 \to 1 \text{ (evaporation)} \\ \overline{u_{1i}}, & \text{Mass transfer from } 1 \to 2 \text{ (condensation)} \end{cases} \tag{2.52}$$

2. M_k' presents the interfacial momentum transfer that remains after substitution of the mass transfer contribution,

$$\boxed{M_k' = \overline{\sigma_{ij,k}n_{kj}\delta}} \tag{2.53}$$

At this step, the form of the momentum balance equation is written as follows

$$\frac{\partial(\alpha_k\rho_k\overline{u_{ki}})}{\partial t}+\frac{\partial(\alpha_k\rho_k\overline{u_{ki}}\ \overline{u_{kj}})}{\partial x_j}=\alpha_k\rho_k g_i-\frac{\partial\alpha_k\overline{p_k}}{\partial x_j}$$
$$+\frac{\partial}{\partial x_j}[\alpha_k(\overline{\tau_{ij,k}}-\rho_k\overline{R_{ij,k}})]+M'_{ki}+\Gamma_k u^{Im}_{ki} \tag{2.54}$$

The final form of the momentum balance equation used in our simulations will be presented in section 2.5 with slight modifications.
M'_k accounts for the interfacial forces between the two phases. This term should be modeled precisely because it plays a major role in the comprehension and the simulation of the two-phase flow. The modeling of this term is not possible via the Eulerian approach. In order to close this term we should consider the dispersed phase as a population of particles. Then we study the dynamics of the isolated particles and their transfer with the surrounding fluid, via a Lagrangian approach. This approach permits to treat the forces exerted by the fluid on each particle separately then to average them over the ensemble of particles. These steps are presented in details the next section of this chapter.
The distribution of the droplets and the vapor over the domain is mainly controlled by the momentum balance equations. Therefore the closure of these terms and their impact on the simulation are the main object of our study.

Total enthalpy balance equations

The averaged total energy equation is written in terms of total enthalpy variable:

$$H_k=E_k+\frac{\overline{p_k}}{\rho_k}\quad;\quad H_k=h_k+\frac{\overline{u_{ki}}^2}{2} \tag{2.55}$$

where H_k is the total specific enthalpy, h_k is the specific enthalpy, and E_k is the total energy of the phase k.
Then, the total enthalpy balance equation can be written as follows:

$$\begin{aligned}\frac{\partial}{\partial t}(\alpha_k\rho_k\overline{H_k})+\frac{\partial}{\partial x_i}(\alpha_k\rho_k\overline{H_k}\overline{u}_{ki}) &= \alpha_k\frac{\partial\overline{p_k}}{\partial t}-\frac{\partial}{\partial x_i}[\alpha_k(\overline{q_{ki}}+\overline{q_{ki}}^T)]\\ &+ \frac{\partial(\alpha_k\overline{\tau_{ij,k}u_{kj}})}{\partial x_i}+\alpha_k\rho_k g_i\overline{u_{ki}}+\alpha_k\overline{Q_k}^k\\ &+ W_k+\Pi'_k+\Gamma_k(\frac{1}{2}(u^{Im}_{ki})^2+h^{Im}_k)\end{aligned} \tag{2.56}$$

The turbulent heat flux $\overline{q_k}^T$ is defined as:

$$-\alpha_k\overline{q_k}^T=-\alpha_k\rho_k\overline{H'_k u'_{ki}}+\overline{\chi_k\tau_{ij,k}u'_{kj}} \tag{2.57}$$

For the interfacial energy transfer we will introduce the following terms:

- Power of interfacial stresses:

$$W_k = \overline{\sigma_{kij} u_{kj} n_{ki} \delta} \tag{2.58}$$

- Interfacial heat transfer by thermal conductivity:

$$\Pi'_k = \overline{-q_{ki} n_{ki} \delta} \tag{2.59}$$

- Kinetic energy transfer due to mass transfer:

$$\frac{1}{2}(u_{ki}^{Im})^2 \Gamma_k = -\frac{1}{2}\overline{\rho_k u_k^2 (u_{ki} - \omega_i) n_{ki} \delta} \tag{2.60}$$

- Enthalpy transfer due to mass transfer:

$$h_k^{Im} \Gamma_k = -\overline{\rho_k h_k (u_{ki} - \omega_i) n_{ki} \delta} \tag{2.61}$$

  The interfacial enthalpy that appears in this equation is the enthalpy h_k^{Im} averaged in the same way we averaged the velocity in equation (2.42) and closed in the same way of the equation (2.52).

The flow of water droplets in the hot vapor, involves heat and mass transfer between the two phases. The droplets act as heat sinks for the vapor and affect the vapor temperature which, in turn, determines the wall heat transfer rate.
The thermal exchanges between the two phases are considered as source terms in the energy and the mass balance equation of both the phases. In order to model these terms we use the interfacial energy jump condition defined in equation (2.17). After averaging the jump condition we can write

$$\sum_{k=1,2} \left[W_k + \Pi'_k + \Gamma_k (\frac{1}{2}(u_{ki}^{Im})^2 + h_k^{Im}) \right] = 0 \tag{2.62}$$

where W_k is neglected. Then, we consider that the interface can not store thermal energy, the net energy transferred to the interface by vapor and droplet corresponds to the phase change by vaporization (or condensation). Thus the mass transfer rate Γ_k is given by

$$\Gamma_2 = -\Gamma_1 = \frac{\Pi'_2 + \Pi'_1}{H_2^\sigma - H_1^\sigma} \tag{2.63}$$

The droplet interface is supposed to be at thermodynamic equilibrium. It is thus supposed to be at saturation conditions (T_{sat}, P_{sat}). Then Π'_k is the rate of heat transfer to the interface, due to the difference between the

temperature of the phase k and the temperature of the interface T_{sat}. $H_2^\sigma - H_1^\sigma$ is the enthalpy difference that corresponds to the latent heat of vaporization at T_{sat}.
Expressions for the interfacial heat transfers are obtained by assuming that each phase has an average temperature denoted by T_k.

$$\Pi'_k = Coef(T_k - T_{sat}) \tag{2.64}$$

where the constant $Coef$ is the heat transfer coefficient between the phase and the interface. This coefficient is given by appropriate closure laws, for example Ranz Marchall's model for the heat transfer in the vapor side and Hendou (1992) model for the heat transfer in the liquid side.
Since our interest is limited to the dynamic section of the flow, no further study about the modeling of these terms will be presented.

2.4 Derivation of dispersed phase Eulerian modeling from particles point of view

The closure of the interfacial momentum transfer is not possible from a pure Eulerian point of view of the particle dynamics. The dispersed phase consists basicly from isolated particles whose size is small in compare of the characteristic scales of mixture properties evolution. The interaction between the particles stays negligible, then the problem can be treated from another point of view, by considering the dispersed phase as isolated particles. The Lagrangian approach permits to study the dynamics of separated particles and their transfer with the surrounding fluid. Then, the summation over a large number of particles permits to obtain a realistic description of the dispersed phase and its influence on the continuous phase. This statistical treatment of the Lagrangian equations permits to derive simple and sufficiently realistic formulations for the interfacial transfers with averaged quantities.

2.4.1 Probability density function

The dispersed phase statistics in turbulent two-phase flows may be described in terms of the probability density function (pdf) $f_2(c_p, \mu_p; x, t)$ defined such that $f_2(c_p, \mu_p; x, t)\delta c_p \delta \mu_p \delta x$ is the probable number of particles who's center of mass at instant t is located in the volume $[x, x + \delta x]$ with a translation velocity u_2 in $[c_p, c_p + \delta c_p]$ and a mass m_2 in $[\mu_p, \mu_p + \delta \mu_p]$.

$$f_2(c_p, \mu_p; x, t) = \langle \delta_2(x, t)\delta(u_2 - c_p)\delta(m_2 - \mu_p) \rangle \tag{2.65}$$

where $\langle . \rangle$ represents an ensemble averaging over a very large number of "identical" realizations of the two-phase flow and $\delta_2(x, t)$ is a dispersed phase

function which is defined to be

$$\delta_2(x,t) = \begin{cases} 1 & \text{if any particle center is located at } x \text{ at time } t \\ 0 & \text{otherwise} \end{cases} \tag{2.66}$$

The evolution equation of the (pdf) can be defined in a general manner as

$$\frac{\partial f_2}{\partial t} + \frac{\partial}{\partial x_j}[c_{p,j} f_2] = -\frac{\partial}{\partial c_{p,j}}\left[\langle \frac{du_{2,j}}{dt} | c_p, \mu_p \rangle f_2\right] - \frac{\partial}{\partial \mu_p}\left[\langle \frac{dm_2}{dt} | c_p, \mu_p \rangle f_2\right] \tag{2.67}$$

d/dt is the material derivative operator following the velocity of a particle defined as

$$\frac{d\cdot}{dt} = \frac{\partial \cdot}{\partial t} + u_{2,j}\frac{\partial \cdot}{\partial x_j} \tag{2.68}$$

Then $\frac{du_{2,j}}{dt}$ is the acceleration of a particle measured along the particle's path due to the exchange with the fluid and to the influence of the external fields. The above approach presents the evolution with respect to the change of velocity. Otherwise, it can account for additional effects such as change in temperature of the particle as well as the particles' collisions. This can be done by a simple extension in the probability density function definition and the corresponding evolution equation.

2.4.2 Discrete particle momentum conservation equation

The classical approach of the study of the interaction between a particle and the surrounding fluid, supposes that we can define at each point of the fluid flow, two fields of characteristic variables, one field of characteristic variables undisturbed and another one disturbed by the presence of the particle. The variables of the undisturbed fields will be noted with an over tilde (ex: θ will be noted $\widetilde{\theta}$). The earlier work to estimate the forces acting on a particle in a fluid, was in the end of the 19 th by Stokes (1850). They studied the case of a spherical non deformable particle placed in a liquid at rest. Lately the Maxey and Riley (1983) and Gatignol (1983) extended the validity of this theory for non-homogeneous flows with low Reynolds numbers and then for high Reynolds numbers. Then the equation of motion of a particle of mass m_2, accounting for the interaction with the fluid and the effect of the external forces is written in a general form

$$m_2 \frac{du_{2,i}}{dt} = m_2 g_i - \frac{\pi d_p^3}{6}\frac{\partial \tilde{p}_1}{\partial x_i} + F_{r,i} + [u_{\sigma,i} - u_{2,i}]\frac{dm_2}{dt} \tag{2.69}$$

This is also the equation of the trajectory of a particle, which is used in the Lagrangian treatment of the dispersed phase. The first term on the right hand side of the above equation represents the force due to the external

fields (gravity). The second and third terms represent the forces applied by the surrounding fluid flow on the particle. The second results from the locally undisturbed fluid flow field which should be considered as if the particle don't exist. It is written in terms of the instantaneous undisturbed pressure $\tilde{p}_1$ gradient measured at the particle center. The third comes from the perturbation induced by the presence of the particle and can be well approximated as the sum of the inter-facial forces (drag, virtual mass, lift force...). The last term accounts for the momentum transported by the mass flux exchange with the continuous phase where u_σ is the averaged velocity of the mass flux crossing the particle surface and it is approximated as $u_\sigma \approx u_2$. Then the corresponding term in the pdf transport equation can be thus written as

$$\begin{aligned}
\frac{\partial}{\partial c_{p,i}}\left[\langle\frac{du_{2,i}}{dt}|c_p\rangle f_2\right] &= \frac{\partial}{\partial c_{p,i}}\left[\left(g_i - \frac{1}{\rho_2}\frac{\partial P_1}{\partial x_i}\right) f_2\right] \\
&- \frac{\partial}{\partial c_{p,i}}\left[\langle\frac{1}{\rho_2}\frac{\partial \tilde{p''}_1}{\partial x_i}|c_p\rangle f_2\right] \\
&+ \frac{\partial}{\partial c_{p,i}}\left[\langle\frac{F_{r,i}}{m_2}|c_p\rangle f_2\right] \\
&+ \frac{\partial}{\partial c_{p,i}}\left[\langle\frac{[u_{\sigma,i} - u_{2,i}]}{m_2}\frac{dm_2}{dt}|c_p\rangle f_2\right] \qquad (2.70)
\end{aligned}$$

The second term on the right hand side represents the effect of the pressure gradient fluctuations on the particle acceleration; where the undisturbed pressure $\tilde{p}_1$ is decomposed into a mean and a fluctuating par

$$\tilde{p}_1 = P_1 + \tilde{p''}$$

2.4.3 Dispersed phase averaging

Defining a probability density function (pdf) of the dispersed phase allows to describe the statistics of this phase and then the possibility to apply an averaging process over the dispersed phase. This averaging process is the passing step from the Lagrangian description into a Eulerian description of the motion. Thus after presenting an expression of the instantaneous forces acting on a particle in equation (2.69), we apply the dispersed phase averaging using the (pdf) in order to have a macroscopic description of the forces.
The dispersed phase average of any function $\psi(u_2)$ may be obtained by the integration over the particle property space as

$$\{\psi\}_2 = \frac{1}{n_2}\int \psi(c_p; x, t) f_2(c_p; x, t) dc_p \qquad (2.71)$$

where n_2 is the mean number of particles per unit volume in the two-phase mixture (or particle number density)

$$n_2(x,t) = \int f_2(c_p;x,t)dc_p \tag{2.72}$$

It is generally more convenient to introduce the dispersed phase mass weighted average

$$\langle\psi\rangle_2 = \frac{1}{\alpha_2\rho_2}\int \mu_p\psi(c_p;x,t)f_2(c_p;x,t)dc_p \tag{2.73}$$

where ρ_2 is the mean particles density and α_2 is the dispersed phase volumetric fraction given by (Simonin (2000))

$$\alpha_2\rho_2 = n_2\{m_2\}_2 = \int \mu_p f_2(c_p;x,t)dc_p \tag{2.74}$$

Then any variable ψ can be averaged by the dispersed phase average, so it can be decomposed into a mean part Ψ and a fluctuating part ψ'' as follows

$$\psi = \Psi + \psi''$$

The mean velocity of the droplets U_2 reads

$$\alpha_2\rho_2 U_{2,i} = \alpha_2\rho_2\langle u_{2,i}\rangle_2 = \int \mu_p c_{p,i} f_2(c_p;x,t)dc_p \qquad u''_{2,i} = u_{2,i} - U_{2,i} \tag{2.75}$$

where $u''_{2,i}$ is fluctuation particle velocity. Therefore the particle's kinetic stress components (or the particle's Reynolds stress tensor components) $\left\langle u''_{2,i}u''_{2,j}\right\rangle_2$ can be expressed as follows

$$\alpha_2\rho_2\langle u''_{2,i}u''_{2,j}\rangle_2 = \int \mu_p[c_{p,i}-U_{2,i}][c_{p,j}-U_{2,j}]f_2(c_p;x,t)dc_p \tag{2.76}$$

General equation for the transport of $\langle\psi\rangle_2$ can be derived from the pdf transport equation (2.67). By integrating over the particle properties (see Simonin (1996)), one can find:

$$\frac{\partial}{\partial t}\alpha_2\rho_2\langle\psi\rangle_2 + \frac{\partial}{\partial x_j}\alpha_2\rho_2\langle u_{2,j}\psi\rangle_2 = \alpha_2\rho_2\left\langle\frac{du_{2,i}}{dt}\frac{\partial\psi}{\partial u_{2,i}}\right\rangle_2 + \alpha_2\rho_2\left\langle\frac{dm_2}{dt}\left[\frac{\partial\psi}{\partial m_2}+\frac{\psi}{m_2}\right]\right\rangle_2 \tag{2.77}$$

2.4.4 Mass balance ($\psi = 1$)

On replacing ψ by the value 1 in equation (2.77) we can write

$$\boxed{\frac{\partial(\alpha_2\rho_2)}{\partial t} + \frac{\partial(\alpha_2\rho_2 U_{2,i})}{\partial x_i} = \Gamma_2} \tag{2.78}$$

The left hand side of the equation is deduced easily since $\langle 1 \rangle_2 = 1$ and $\langle u_{2,i} \rangle_2 = U_{2,i}$. The first term of the right hand side is equal to zero since $\frac{\partial 1}{\partial u_{2,i}} = 0$, and the second term is defined as Γ_2

$$\Gamma_2 = \alpha_2 \rho_2 \left\langle \frac{1}{m_2} \frac{dm_2}{dt} \right\rangle_2 \tag{2.79}$$

Where Γ_2 is the mean interface mass transfer rate.

2.4.5 Momentum balance ($\psi = u_{2,i}$)

By substituting $u_{2,i}$ in place of ψ in equation (2.77) we can write

$$\begin{aligned} \frac{\partial}{\partial t} \alpha_2 \rho_2 \langle u_{2,i} \rangle_2 + \frac{\partial}{\partial x_j} \alpha_2 \rho_2 \langle u_{2,j} u_{2,i} \rangle_2 &= \alpha_2 \rho_2 \left\langle \frac{du_{2,i}}{dt} \frac{\partial u_{2,i}}{\partial u_{2,i}} \right\rangle_2 \\ &+ \alpha_2 \rho_2 \left\langle \frac{dm_2}{dt} \left[\frac{\partial u_{2,i}}{\partial m_2} + \frac{u_{2,i}}{m_2} \right] \right\rangle_2 \end{aligned} \tag{2.80}$$

Then we decompose the velocity of the droplets into as averaged part and fluctuating part

$$u_{2,i} = u''_{2,i} + U_{2,i}$$

so the left hand side (LHS) of the equation can be written

$$\begin{aligned} LHS &= \frac{\partial}{\partial t} \alpha_2 \rho_2 \langle u_{2,i} \rangle_2 + \frac{\partial}{\partial x_j} \alpha_2 \rho_2 \langle u_{2,j} u_{2,i} \rangle_2 \\ &= \frac{\partial}{\partial t} \alpha_2 \rho_2 U_{2,i} + \frac{\partial}{\partial x_j} \alpha_2 \rho_2 U_{2,i} U_{2,j} \\ &+ \frac{\partial}{\partial x_j} \alpha_2 \rho_2 \left\langle u''_{2,i} u''_{2,j} \right\rangle_2 \quad \text{since} \quad (\left\langle u''_{2,j} U_{2,i} \right\rangle_2 = 0) \\ &= \alpha_2 \rho_2 \frac{\partial}{\partial t} U_{2,i} + \alpha_2 \rho_2 U_{2,j} \frac{\partial}{\partial x_j} U_{2,i} + \frac{\partial}{\partial x_j} \alpha_2 \rho_2 \left\langle u''_{2,i} u''_{2,j} \right\rangle_2 \\ &+ U_{2,i} \left[\frac{\partial}{\partial t} \alpha_2 \rho_2 + \frac{\partial}{\partial x_j} \alpha_2 \rho_2 U_{2,j} \right] \end{aligned} \tag{2.81}$$

Using the mass averaged equation (2.78) we can write

$$LHS = \alpha_2 \rho_2 \frac{\partial}{\partial t} U_{2,i} + \alpha_2 \rho_2 U_{2,j} \frac{\partial}{\partial x_j} U_{2,i} + \frac{\partial}{\partial x_j} \alpha_2 \rho_2 \left\langle u''_{2,i} u''_{2,j} \right\rangle_2 + U_{2,i} \Gamma_2 \tag{2.82}$$

The right hand side (RHS) of the equation (2.80) can be written as

$$RHS = \alpha_2 \rho_2 \left\langle \frac{du_{2,i}}{dt} \right\rangle_2 + \alpha_2 \rho_2 \left\langle \frac{dm_2}{dt} \frac{u_{2,i}}{m_2} \right\rangle_2 \tag{2.83}$$

$\frac{du_{2,i}}{dt}$ can be deduced from the equation (2.69) as

$$\frac{du_{2,i}}{dt} = g_i - \frac{1}{\rho_2}\frac{\partial \tilde{p}_1}{\partial x_i} + \frac{F_{r,i}}{m_2} + \frac{1}{m_2}[u_{\sigma,i} - u_{2,i}]\frac{dm_2}{dt} \tag{2.84}$$

then we substitute the equation (2.84) in equation (2.83) to write

$$\begin{aligned} RHS &= \alpha_2\rho_2 g_i - \alpha_2[\frac{\partial P_1}{\partial x_i} + \frac{\partial \langle p_1'' \rangle_2}{\partial x_i}] + \alpha_2\rho_2 \left\langle \frac{F_{r,i}}{m_2} \right\rangle_2 \\ &+ U_{\sigma,i}\Gamma_2 - \alpha_2\rho_2 \left\langle \frac{dm_2}{dt}\frac{u_{2,i}}{m_2} \right\rangle_2 + \alpha_2\rho_2 \left\langle \frac{dm_2}{dt}\frac{u_{2,i}}{m_2} \right\rangle_2 \end{aligned} \tag{2.85}$$

Finally we use the equality between equation (2.82) and equation (2.85) to write the final form of the momentum balance equation as follows

$$\begin{aligned} \alpha_2\rho_2\frac{\partial}{\partial t}U_{2,i} + \alpha_2\rho_2 U_{2,j}\frac{\partial}{\partial x_j}U_{2,i} &= \frac{\partial}{\partial x_j}[-\alpha_2\rho_2 \left\langle u_{2,i}''u_{2,j}'' \right\rangle_2] + \alpha_2\rho_2 g_i \\ &- \alpha_2[\frac{\partial P_1}{\partial x_i} + \frac{\partial \langle p_1'' \rangle_2}{\partial x_i}] + [U_{\sigma,i} - U_{2,i}]\,\Gamma_2 \\ &+ \alpha_2\rho_2 \left\langle \frac{F_{r,i}}{m_2} \right\rangle_2 \end{aligned} \tag{2.86}$$

- The first term on the right hand side of the equation represents the transport momentum by the velocity fluctuations, where the particle kinetic stress tensor needs to be modeled or computed in an additional submodel (model of turbulence of the dispersed phase).
- The second term represents the influence of the external body force fields (gravity) acting on the particle.
- The third term presents the influence of the mean and pressure gradients of the continuous phase. $\alpha_2\frac{\partial\langle p_1''\rangle_2}{\partial x_i}$ represents the effect of the inhomogeneous distribution of the pressure of the "undisturbed" flow on the dispersed phase. This term is generally negligible in gas-solid flows but should be taken into account in liquid-solid or bubbly flows. The closure of this term is not discussed here since in our case, we are interested in vapor-droplet flow which is similar to gas-solid flow, where the density of the dispersed phase is very big with respect to the density of the continuous phase.
- The fourth term represents the influence of the interphase mass transfer,

  $$U_{\sigma,i}\Gamma_2 = \alpha_2\rho_2 \left\langle \frac{u_{\sigma,i}}{m_2}\frac{dm_2}{dt} \right\rangle_2$$

  where $U_{\sigma,i}$ is the mean velocity of the mass flux crossing the particle surfaces ($U_{\sigma,i} \approx U_{2,i}$)

- The last term represents the mean interphase momentum transfer rate coming from the local perturbation induced by the presence of the particle. This term is generally considered as the sum of the drag force, virtual mass force, lift force and history force. The history force should take into account the instationary viscous effects. In the rest of our study we will consider that the effect of this force is negligible with respect to the other forces. Therefore we can write that

$$\alpha_2\rho_2\left\langle\frac{F_{r,i}}{m_2}\right\rangle_2=\alpha_2\rho_2\left\langle\frac{f_i^D}{m_2}\right\rangle_2+\alpha_2\rho_2\left\langle\frac{f_i^{AM}}{m_2}\right\rangle_2+\alpha_2\rho_2\left\langle\frac{f_i^L}{m_2}\right\rangle_2 \quad (2.87)$$

  Where each one of these terms accounts for the rate of interfacial exchange of momentum due to the force. So we will present the models of forces acting on a single isolated droplets then by averaging over the dispersed phase $\langle\rangle_2$ we got the mean rate of momentum transfer corresponding to this force.

Drag force

The drag force is a surface force due to the movement of a droplet in the vapor. It takes into account the drag due to the surface friction and to the droplet shape. This force acts in a direction opposite to the oncoming flow velocity. It exists whenever there is a relative motion between the two phases even if this motion is non-accelerated. The ascending velocity of a droplet is determined thanks to the balance between this force and the gravitational forces. The general form of the drag force, acting on a spherical droplet, reads

$$f_i^D=-\frac{3}{4}\rho_1\frac{C_D}{d_p}V_p|v_r|v_{r,i} \quad (2.88)$$

$v_{r,i}$ is the relative velocity between the two phases. This velocity is expressed in terms of the velocity of the droplet and the velocity of the vapor undisturbed by the presence of this droplet

$$v_{r,i}=u_{2,i}-\tilde{u}_{1,i} \quad (2.89)$$

V_p is the particle volume, d_p is the droplet diameter, and C_D is the drag coefficient. The mean rate of momentum transfer that corresponds to this force, F_i^D, is obtained by averaging equation (2.88) by the dispersed phase average

$$\begin{aligned}F_i^D=\alpha_2\rho_2\left\langle\frac{f_i^D}{m_2}\right\rangle_2 &= -\alpha_2\rho_2\left\langle\frac{3}{4}\rho_1\frac{C_D}{d_p}\frac{V_p}{m_2}|v_r|v_{r,i}\right\rangle_2\\ &= -\alpha_2\rho_2\left\langle\frac{3}{4}\frac{\rho_1}{\rho_2}\frac{C_D}{d_p}|v_r|v_{r,i}\right\rangle_2\end{aligned} \quad (2.90)$$

The closure of this term by Simonin (2000) reads

$$F_i^D = \alpha_2 \rho_2 \left\langle \frac{f_i^D}{m_2} \right\rangle_2 = -\alpha_2 \rho_2 \frac{1}{\tau_{12}^F} \langle v_{r,i} \rangle_2 \tag{2.91}$$

where the τ_{12}^F is the mean particle relaxation time

$$\tau_{12}^F \approx \frac{\rho_2}{\rho_1} \frac{4}{3} \frac{d_p}{C_D} \frac{1}{\langle |v_{r,i}| \rangle_2} \tag{2.92}$$

$\langle v_{r,i} \rangle_2$ is the averaged value of the local relative velocity between each droplet and the surrounding vapor flow

$$\langle v_{r,i} \rangle_2 = \langle u_{2,i} - \tilde{u}_{1,i} \rangle_2$$

A major closure problem that appears here, is the averaging of the undisturbed fluid velocity $\tilde{u}_{1,i}$ via the dispersed phase average. $\tilde{u}_{1,i}$ can be decomposed into a mean and a fluctuating part

$$\tilde{u}_{1,i} = U_{1,i} + \tilde{u}'_{1,i} \tag{2.93}$$

If we suppose that the averaged vapor velocity of the undisturbed flow seen by the droplet is equal to the averaged vapor velocity, then the closure problem becomes related directly to the averaging of the undisturbed vapor velocity fluctuation seen by the droplet $\left\langle \tilde{u}'_{1,i} \right\rangle_2$. In this paragraph we define this term as the drift velocity $V_{d,i}$

$$V_{d,i} = \left\langle \tilde{u}'_{1,i} \right\rangle_2 \tag{2.94}$$

Then the drift velocity $V_{d,i}$ is the conditional average of the locally undisturbed vapor velocity fluctuation with respect to the particle distribution. The closure of this velocity is discussed later in a separate paragraph.
Now we can write

$$V_{r,i} = \langle v_{r,i} \rangle_2 = U_{2,i} - (U_{1,i} + V_{d,i}) \tag{2.95}$$

This permits us to close the relative velocity modulus $\langle |v_r| \rangle_2$. First, we decompose the relative velocity into a mean and a fluctuating parts,

$$v_{r,i} = V_{r,i} + v''_{r,i} \tag{2.96}$$

then we can write

$$\langle |v_r| \rangle_2 = (V_{r,i} V_{r,i} + \left\langle v''_{r,i} v''_{r,i} \right\rangle_2)^{\frac{1}{2}} \tag{2.97}$$

We suppose that the fluctuation of the relative velocity can be written in a simple way as the difference between the droplet's velocity fluctuation and the undisturbed vapor velocity fluctuation

$$v''_{r,i} = u''_{2,i} - \tilde{u}'_{1,i} \tag{2.98}$$

then

$$\langle |v_r| \rangle_2 = ((U_{2,i} - U_{1,i} - V_{d,i})^2 + (\langle u''_{2,i} u''_{2,i} \rangle_2 - 2 \langle \tilde{u}'_{1,i} u''_{2,i} \rangle_2 + \langle u'_{1,i} u'_{1,i} \rangle_2))^{\frac{1}{2}} \quad (2.99)$$

We define k_2 as the turbulent kinetic energy of the dispersed phase, and k_{12} as the particle-fluid velocity fluctuation covariance,

$$k_2 = \frac{1}{2} \langle u''_{2,i} u''_{2,i} \rangle_2 \quad (2.100)$$

$$k_{12} = \langle u''_{2,i} \tilde{u}'_{1,i} \rangle_2 \quad (2.101)$$

and we suppose that the turbulent kinetic energy of the undisturbed fluid seen by the droplet is equal to the turbulent kinetic energy of the vapor averaged over the vapor phase

$$k_1 = \frac{1}{2} \langle u'_{1,i} u'_{1,i} \rangle_2 = \frac{1}{2} \overline{u'_{1,i} u'_{1,i}} \quad (2.102)$$

where $\overline{u'_{1,i} u'_{1,i}}$ is equal to $R_{ij,1}$, which is defined in equation (2.33).
Finally, we can write

$$\langle |v_r| \rangle_2 = ((U_{2,i} - U_{1,i} - V_{d,i})^2 + (2k_2 - 2k_{12} + 2k_1))^{\frac{1}{2}} \quad (2.103)$$

The drag force is written as the sum of a laminar contribution and a turbulent contribution

$$\boxed{F_i^D = \overbrace{-\alpha_2 \rho_1 \frac{3}{4} \frac{C_D}{d} \langle |v_r| \rangle_2 (U_{2,i} - U_{1,i})}^{\text{Laminar part}} + \overbrace{\alpha_2 \rho_1 \frac{3}{4} \frac{C_D}{d} | \langle |v_r| \rangle_2 V_{d,i}}^{\text{Turbulent part}}} \quad (2.104)$$

In the present study, we use a drag coefficient C_D developed by Wallis (1969) for the isolated and diluted particles flow:

$$C_D = \begin{cases} \frac{24}{Re_p} [1 + 0.15 Re_p^{0.687}] \alpha_1^{-1.7} & \text{for} \quad Re_p < 1000 \\ 0.44 \alpha_1^{-1.7} & \text{for} \quad Re_p \geq 1000 \end{cases} \quad (2.105)$$

The particle Reynolds number Re_p is given in terms of the diameter of the droplet d_p, the averaged magnitude of the relative velocity $\langle |v_r| \rangle_2$, the dynamic viscosity of the vapor μ_1, and the density of the vapor ρ_1:

$$Re_p = \rho_1 \frac{\langle |v_r| \rangle_2 d}{\mu_1} \quad (2.106)$$

The limit of validity between the two forms of C_D is associated with very high Reynolds numbers. It expresses that when the drag is dominated by the interaction between the droplets, the calculation of individual drag coefficient is meaningless. But, when the droplets behave as isolated particles, C_D depends only on the droplets particle Reynolds number. In our study case, the particular Reynolds number does not reach the value of 1000 and the droplets behave as isolated particles.

Virtual mass force

When a particle is accelerated through a fluid, the surrounding fluid in the immediate vicinity of the particle will also be accelerated. The particle apparently behaves as if it has a larger mass than the actual mass, thus the net force acting on the particle due to this effect has been called virtual mass or added mass force. In the case of vapor-droplet flow the virtual mass force is considered of second order since the density of the droplets is very high with respect to that of the vapor. We use here the analytical solution derived by Auton et al. (1988) for the virtual mass force in a non-uniform and non-stationary flow. Then the virtual mass force acting on a single spherical particle reads

$$f_i^{Ma} = -\rho_1 V_p C_{Ma} \left(\frac{D\tilde{u}_{1,i}}{Dt} - \frac{du_{2,i}}{dt} \right) \tag{2.107}$$

where d/dt is the material derivative following the particle path, defined in equation (2.68), and D/Dt is the material derivative following the velocity of the undisturbed fluid defined as

$$\frac{D\cdot}{Dt} = \frac{\partial\cdot}{\partial t} + \widetilde{u}_{1,j} \frac{\partial\cdot}{\partial x_j} \tag{2.108}$$

In order to simplify this equation, we suppose that the acceleration of the vapor in this equation can be written following the velocity of a droplet:

$$\frac{Du_{1,i}}{Dt} \simeq \frac{du_{1,i}}{dt} \tag{2.109}$$

This hypothesis may have an impact in the cases where the density of the particles is much smaller than the density of the fluid (e.g. bubbly flows). But in our case droplets flow, the virtual mass force plays a minor role, therefore this hypothesis is considered. Then we obtain the averaged expression of the virtual mass force

$$F_i^{Ma} = \alpha_2 \rho_2 \left\langle \frac{f_i^{Ma}}{m_2} \right\rangle_2 = -\rho_1 C_{Ma} \left[\frac{\partial}{\partial t} (\alpha_2 \langle v_{r,i} \rangle_2) + \frac{\partial}{\partial x_j} (\alpha_2 \langle u_{2,j} v_{r,i} \rangle_2) \right] \tag{2.110}$$

if we split the relative velocity v_r and the velocity of the dispersed phase u_2 into averaged and fluctuating velocity we get:

$$\begin{aligned} F_i^{Ma} &= -\rho_1 C_{Ma} [\alpha_2 \left(\frac{\partial V_{r,i}}{\partial t} + U_{2,j} \frac{\partial V_{r,i}}{\partial x_j}) \right) + V_{r,i} \left(\frac{\partial \alpha_2}{\partial t} + \frac{\partial (\alpha_2 U_{2,j})}{\partial x_j} \right) \\ &+ \frac{\partial}{\partial x_j} (\alpha_2 \left\langle u'_{2,j} v'_{r,i} \right\rangle_2)] \end{aligned} \tag{2.111}$$

using the mass balance equation of the dispersed phase we can write

$$F_i^{Ma} = -\rho_1 C_{Ma}\left[\alpha_2 \frac{\overline{d}V_{r,i}}{\overline{d}t} + \frac{\partial}{\partial x_j}(\alpha_2 \left\langle u'_{2,j} v'_{r,i}\right\rangle_2)\right] \tag{2.112}$$

where $\overline{d}/\overline{d}t$ is the material derivative following the averaged velocity of the dispersed phase. Considering that the relative fluctuating velocity can be written as the difference between the fluctuating velocity of the particles and the fluctuating velocity of the undisturbed fluid

$$v'_{r,i} = u'_{2,i} - \tilde{u}'_{1,i} \tag{2.113}$$

gives

$$F_i^{Ma} = -\rho_1 C_{Ma}\left[\alpha_2 \frac{\overline{d}V_{r,i}}{\overline{d}t} + \frac{\partial}{\partial x_j}(\alpha_2 \left\langle u'_{2,j} u'_{2,i}\right\rangle_2 - \left\langle u'_{2,j} \tilde{u}'_{1,i}\right\rangle_2)\right] \tag{2.114}$$

We consider that $\left\langle u'_{2,j} u'_{2,i}\right\rangle_2$ and $\left\langle u'_{2,j} \tilde{u}'_{1,i}\right\rangle_2$ are isotropic, then we can write

$$k_2 \delta_{ij} = \frac{3}{2}\left\langle u'_{2,i} u'_{2,i}\right\rangle_2 \tag{2.115}$$

$$k_{12} \delta_{ij} = 3\left\langle u'_{2,j} \tilde{u}'_{1,i}\right\rangle_2 \tag{2.116}$$

the averaged form of the virtual mass force is written as

$$F_i^{Ma} = -\rho_1 C_{Ma}\left[\alpha_2 \frac{\overline{d}V_{r,i}}{\overline{d}t} + \frac{\partial}{\partial x_j}(\alpha_2 \left\langle u'_{2,j} u'_{2,i}\right\rangle_2 - \left\langle u'_{2,j} \tilde{u}'_{1,i}\right\rangle_2)\right] \tag{2.117}$$

then the final form virtual mass force is written as follows

$$\boxed{F_i^{Ma} = \overbrace{-\rho_1 \alpha_2 C_{Ma}\left[\frac{\overline{d}\overrightarrow{V_r}}{\overline{d}t}\right]}^{\text{Laminar part}} \overbrace{-\rho_1 C_{Ma}\frac{\partial}{\partial x_i}\left((\frac{2}{3}k_2 - \frac{1}{3}k_{12})\alpha_2\right)}^{\text{Turbulent part}}} \tag{2.118}$$

C_{Ma}, is the virtual mass coefficient which is not general in all the flow configurations and should be adapted to the simulated flow. For the case of diluted flow of isolated spherical inclusions we use

$$C_{Ma} = \frac{1}{2} \tag{2.119}$$

In our special case, the virtual mass force is negligible beside the drag force.

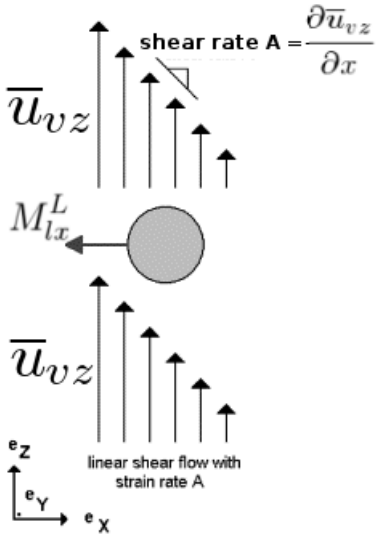

Figure 2.4: Lift force on a particle in a shear flow

Lift force

When a droplet moves in a shear flow and more generally in a rotational flow, it experiences a transverse force. This force is called the lift force, and it is essential for predicting the lateral dispersion of the droplets in vertical pipe flows. The lift force acting on a single particle can be written as

$$f_i^L = \rho_1 V_p C_L (v_r \wedge rot(u_1))_i \tag{2.120}$$

We apply the same steps used for the virtual mass and the drag force in order to average the lift force. The fluctuating part of the lift force is neglected since we suppose that the velocity fluctuations are uncorrelated with the fluctuations of vorticity. So the averaged form of the lift force can be written in the form

$$\boxed{F_i^L = -\alpha_2 \rho_1 C_L \left(V_r \wedge rot(U_1)\right)_i} \tag{2.121}$$

This force is important in our study since it affects the radial distribution of the droplets. According to Auton (1987) the lift coefficient is equal to 0.5. The analytical model of Auton is valid for the case of a spherical particle placed in a weak shear flow of an inviscid fluid. This is somehow far from our study case. Therefore the impact of this force on the simulation results will be quantified in the next chapter.

Drift velocity

In order to model the averaged momentum transfer rate according to the drag and the added mass forces, it is necessary to know the averaged relative velocity between the two phases. This velocity is defined as the difference between the velocity of the droplet and the velocity of the surrounding vapor undisturbed by the presence of the droplet. The major closure problem that appears here is the modeling of the undisturbed vapor velocity, $\tilde{u_1}$, measured along the particle paths. Particularly, to the term of the conditional expectation of the undisturbed fluid velocity fluctuation, $\tilde{u_1'}$, measured along the particle paths,$\langle \tilde{u}'_{1,j} | cp \rangle$. This term is defined as the drift velocity, and it is due to the correlation between the instantaneous distribution of the particles and the fluid large turbulent eddies (large with respect to the size of the particle). The drift velocity takes into account the dispersion effect due to the particle transport by the fluid turbulence.
According to the theoretical case of particles suspended in homogeneous turbulent flow (Simonin et al. (1993a)), the velocity of drift can be written as

$$V_{d,i} = -D^t_{12,ij} \left[\frac{1}{\alpha_2} \frac{\partial \alpha_2}{\partial x_j}_{\frac{1}{\alpha_1}} \frac{\partial \alpha_1}{\partial x_j} \right] \tag{2.122}$$

where the fluid-particle turbulent dispersion tensor $-D^t_{12,ij}$ is expressed in terms of the covariance tensor between the turbulent velocity fluctuations of the two phases and the fluid-particle turbulent characteristic time:

$$D^t_{12,ij} = -\tau^t_{12} \left\langle u'_{2,j} \tilde{u}'_{1,i} \right\rangle_2 \tag{2.123}$$

τ^t_{12} is the turbulence time scale of the vapor viewed by the droplets, the formulation of this term will be given later in the turbulence chapter. This modeling of the drift velocity will be used in the present work. However, in chapter 4 we will present another modeling for the drift velocity based on a stochastic Langvin type Lagrangian description which permits to derive a transport equation for the drift velocity, proposed by Simonin (2000).

2.5 Interfacial momentum transfer

The method presented in the last section permits to close the interfacial momentum transfer term $M'_{2,i}$ of the momentum balance equation of the dispersed phase equation (2.54), developed by a pure Eulerian point of view. Moreover, the interfacial momentum transfer term $M'_{1,i}$ of the continuous phase will be closed by using the interfacial jump condition of the momentum equation (2.16).
First, we compare the dispersed phase momentum balance equations obtained by the Eulerian approach, equation (2.54), and from the particles

point of view, equation (2.86). After neglecting the effect of the viscous tensor on the droplets, we get the following relation

$$-\frac{\partial \alpha_2 \overline{p_2}}{\partial x_j} + M'_{2,i} = -\alpha_2 \frac{\partial P_1}{\partial x_j} + \alpha_2 \rho_2 \left\langle \frac{F_{r,i}}{m_2} \right\rangle_2 \tag{2.124}$$

Let us define $\overline{\overline{M'_{2,i}}}$ as

$$\overline{\overline{M'_{2,i}}} = \alpha_2 \rho_2 \left\langle \frac{F_{r,i}}{m_2} \right\rangle_2 \tag{2.125}$$

Then we can write

$$-\frac{\partial \alpha_2 \overline{p_2}}{\partial x_j} + M'_{2,i} = -\alpha_2 \frac{\partial P_1}{\partial x_j} + \overline{\overline{M'_{2,i}}} \tag{2.126}$$

if we replace the left hand side of the last equation in the equation (2.54), then we can write the final form of the momentum balance equation of the dispersed phase as

$$\begin{aligned} \frac{\partial(\alpha_2 \rho_2 \overline{u_{2i}})}{\partial t} + \frac{\partial(\alpha_2 \rho_2 \overline{u_{2i}}\ \overline{u_{2j}})}{\partial x_j} &= \alpha_2 \rho_2 g_i - \alpha_2 \frac{\partial P_1}{\partial x_j} \\ + \frac{\partial}{\partial x_j}[\alpha_2(\overline{\tau_{ij,2}} - \rho_2 \overline{R_{ij,2}})] + \overline{\overline{M'_{2,i}}} &+ \Gamma_2 u_{2i}^{Im} \end{aligned} \tag{2.127}$$

For the momentum balance equation of the vapor, the closure of the term $M'_{1,i}$ is required. Starting by averaging the momentum interfacial jump condition in equation (2.16)we can write

$$M'_{2,i} + M'_{1,i} = \overline{F_{si}\delta} \tag{2.128}$$

Lhuillier (2003) cited that the force of surface tension per unit volume can be expressed as the divergence of a tensor as follows

$$\overline{F_{si}\delta} = div < \delta_i \sigma (I - n_i n_j) > \tag{2.129}$$

where I is the identity tensor. If σ, the surface tension, is constant (we neglect the Marangoni[1] type effects) , this equation can be written as

$$\begin{aligned} \overline{F_{si}\delta} &= \sigma div(< \delta_i > I - < \delta_i (n_i n_j) >) \\ &= \sigma(div < \delta_i > I - divQ) \end{aligned} \tag{2.130}$$

[1] Marangoni forces are tangential forces that appear at the surface of a fluid because of the change in surface tension along the interface, due to a temperature gradient or the surfactant concentration gradient along the interface. The Marangoni effect is responsible of the jump of tangential stresses across the interface. These forces can cause convection in fluids, even in zero gravity, when the natural convection disappears

according to Lhuillier (2003) Q is the area tensor and its decomposed into a spherical part and its stress deviator tensor as follows

$$Q = (a^I/3)I + q \text{with} q =< \delta_i((n_i n_j) - I/3) > \tag{2.131}$$

The tensor q is the tensor of the anisotropy of the surface, therefore in the case of closed surfaces as spherical particles this tensor is equal to zero. Lhuillier et al. (2000) showed that

$$< \delta_i > \approx a^I \tag{2.132}$$

where a^I is the density of the interfacial area in a unit volume, which permits to write

$$\begin{aligned} \overline{F_{si}\delta} &= \sigma div(< \delta_i > I - < \delta_i(n_i n_j) >) \\ &= \sigma(\frac{\partial}{\partial x_j}(a^I) - \frac{\partial}{\partial x_j}(a^I/3) - divq \\ &= 2/3\sigma\frac{\partial}{\partial x_j}\sigma(a^I) \end{aligned} \tag{2.133}$$

For the case of dispersed spherical droplets with constant diameter, a^I is expressed in terms of the droplets volume fraction $alpha_2$

$$a^I = \frac{6\alpha_2}{d} \tag{2.134}$$

So finally we can write

$$\overline{F_{si}\delta} = \frac{4}{d}\sigma\frac{\partial}{\partial x_j}\alpha_2 \tag{2.135}$$

We use the equations (2.126) and (2.128) to write

$$\begin{aligned} M'_{1,i} &= \overline{F_{si}\delta} + \alpha_2\frac{\partial P_1}{\partial x_j} - \frac{\partial \alpha_2\overline{p_2}}{\partial x_j} - \overline{\overline{M'_{2,i}}} \\ &= -\overline{\overline{M'_{2,i}}} + \overline{F_{si}\delta} + \frac{\partial}{\partial x_j}(\alpha_2(P_1 - \overline{p}_2)) - P_1\frac{\partial \alpha_2}{\partial x_j} \end{aligned} \tag{2.136}$$

and

$$\frac{\partial \alpha_2}{\partial x_j} = -\frac{\partial \alpha_1}{\partial x_j} \quad (\alpha_1 = 1 - \alpha_2) \tag{2.137}$$

so

$$M'_{1,i} = -\overline{\overline{M'_{2,i}}} + \overline{F_{si}\delta} + \frac{\partial}{\partial x_j}(\alpha_2(P_1 - \overline{p}_2)) + P_1\frac{\partial \alpha_1}{\partial x_j} \tag{2.138}$$

Then we define

$$\overline{\overline{M'_{1,i}}} = M'_{1,i} - P_1\frac{\partial \alpha_1}{\partial x_j} \tag{2.139}$$

to write

$$\overline{\overline{M'_{1,i}}} = -\overline{\overline{M'_{2,i}}} + \frac{\partial}{\partial x_j}(\alpha_2(P_1 - \overline{p}_2)) + \overline{F_{si}\delta} \tag{2.140}$$

From Delhaye (1974) we can conclude that the jump condition of the pressure near the interface apply the low of Laplace

$$(\overline{p}_2 - P_1)\delta = \frac{4\sigma}{d}\delta \tag{2.141}$$

we substitute equation (2.141) in equation (2.140) to get

$$\begin{aligned}\overline{\overline{M'_{1,i}}} &= -\overline{\overline{M'_{2,i}}} - \frac{\partial}{\partial x_j}\left(\alpha_2\left[\frac{4\sigma}{d}\right]\right) + \overline{F_{si}\delta} \\ &= -\overline{\overline{M'_{2,i}}} - \alpha_2\frac{\partial}{\partial x_j}\left[\frac{4\sigma}{d}\right] - \left[\frac{4\sigma}{d}\right]\frac{\partial}{\partial x_j}\alpha_2 + \overline{F_{si}\delta}\end{aligned} \tag{2.142}$$

using the equation (2.135), to write

$$\overline{\overline{M'_{1,i}}} = -\overline{\overline{M'_{2,i}}} + \alpha_2\frac{\partial}{\partial x_j}\left[\frac{4\sigma}{d}\right] \tag{2.143}$$

Since we consider that we are in a case where the diameter of the droplets is constant, the second term of the right hand side of the equation is neglected and we can deduce that

$$\overline{\overline{M'_{1,i}}} = -\overline{\overline{M'_{2,i}}} = -\alpha_2\rho_2\left\langle\frac{F_{r,i}}{m_2}\right\rangle_2 \tag{2.144}$$

According to this, we can use the equation (2.139) to write the final form of the momentum balance equation of the continuous phase as follows

$$\begin{aligned}&\frac{\partial(\alpha_1\rho_1\overline{u_{1i}})}{\partial t} + \frac{\partial(\alpha_1\rho_1\overline{u_{1i}}\,\overline{u_{1j}})}{\partial x_j} = \alpha_1\rho_1 g_i - \alpha_1\frac{\partial P_1}{\partial x_j} \\ &+\frac{\partial}{\partial x_j}[\alpha_1(\overline{\tau_{ij,1}} - \rho_1\overline{R_{ij,1}})] + \overline{\overline{M'_{1,i}}} + \Gamma_1 u_{1i}^{Im}\end{aligned} \tag{2.145}$$

By this method we close the momentum balance equations of the two phases using one pressure P_1, which is called one pressure model.
This coupling step shows the importance of starting from a Lagrangian description of the particles motion inorder to reach the final closure of the Eulerian formulations. The interfacial forces will play the major role on the motion of the droplets inside the vapor. So as the drag force and the virtual mass force control the droplet motion in the sense of the flow the lift force will affect the traversal motion of the droplets. The earlier closure of the forces regarded the general form of each force without discussing the model of closure of the forces' coefficients (C_{MA}, C_D, C_L). The impact of these forces and the models of closure of the coefficients are discussed in the following chapters.

2.6 Turbulence modeling

In our study case, vapor-droplet vertical upward flow, the flow is initiated at the level of the quench front by a violent evaporation in a depressurized nuclear reactor. The velocity of the vapor between fuel bars is large enough to create a turbulent flow. The turbulence phenomenon may have a major effect on the flow characteristics, and the turbulent structures may interact with the droplets and modify their distribution. The averaging process on the balance equations yields the appearance of turbulent quantities corresponding to the mean of the fluctuating velocities $\overline{u'_{ki}u'_{kj}}$. These terms are also called Reynolds stress tensor of the phase k and are noted $\overline{R_{ij,k}}$.
In the momentum balance equations the turbulence terms act as a momentum source. So the gradients of the tensor $\overline{R_{ij,2}}$ acts as a momentum source term for the droplets and may modify the distribution of the droplets. The turbulence of the dispersed phase interacts on the turbulence of the continuous phase. This interaction is modeled via algebraic relations or via interfacial transfer terms of the turbulent quantities. Therefore $\overline{R_{ij,1}}$ has an indirect impact on the droplets distribution. A successful modeling of turbulence of both phases greatly increases the quality of our simulations. In the next chapter we quantify the impact of turbulence modeling on the droplets distribution. The turbulence modeling is discussed in details in a separate chapter.

2.7 Conclusion

This chapter presents a detailed derivation of the RANS equations used in Euler/Euler model for two phase flow. The averaging process yields the appearance of unknown terms which requires extra sub models to simulate the physical phenomena. We limit our interest to the terms that impact the spatial distribution of the droplets. These terms are the Reynolds stress tensors of the two phases and the momentum interfacial transfer term. Averaging the Lagrangian particle's trajectory equation using the particle distribution function (pdf) permits to close the interfacial momentum transfer term. The gradient of the Reynolds tensor is understood as a source term in the momentum equation and it impacts the mean motion of the particles. After a brief presentation of the forces we could understand the role of each interfacial force on the motion of the droplet. The virtual mass force and the drag force play the major role on the propagation of the droplet in the main direction of the flow, while the lift force plays the major role in the radial direction. The gradients of the Reynolds tensor act as forces in both directions. Therefore this chapter ameliorates our comprehension of the problem by limiting it to the sub models that simulate these forces. The general form of each interfacial force had been presented

in this chapter without discussing the models of closure for the coefficients of these forces. In the next chapter, we will quantify the effect of these forces on the results by analyzing experimental and numerical data. This analysis will help to test the compatibility of the used models in our case and to specify where more concentration is required.

Chapter 3

Main forces involved in droplets dispersion

3.1 Introduction

In the previous chapter, we identified that the motion of the droplets is affected by the modeling of two main terms, the turbulence term, and the interfacial momentum transfer term. The interfacial momentum transfer term is decomposed into three main forces: drag force, virtual mass force and lift force. The gradient of the turbulent term presents a source term in the momentum balance equation and can be understood as a force acting on the mean droplets motion. Besides, we saw that the turbulent term is used in the closure of the fluctuating parts of the forces. The modeling of each term is a research aspect that has been studied before by other authors. In previous studies of two-phase dispersed flow, we can find different models proposed for the closure of these terms. The choice of the appropriate model usually depends on the flow conditions as the geometry and the nature of the dispersed phase. So the choice of some models can be evident for our study case since they have been tested before in similar cases. While the research projects about other models are still under discussion. In this chapter we restrict our research to the models that have a main impact on the results and in the same time that are not well defined yet for our study case.
For this aim, a parametric study is proposed to show the effect of the modeling of the various terms specified in the theoretical chapter. First we present the calculation tool and a study case geometry with the choice of the mesh. A simulation test case with basic models is executed and the results are presented. This test case helps us draw a general description of the droplets distribution. During the description, we specify the role of each term in the mechanism of droplets distribution. Some parametric tests are presented to show the important impact of some terms. After that we discuss briefly the modeling of each term regarding the basic models used in the test case. At

the end of this chapter, we specify the models that will be the subject of the rest of our study.

3.2 Calculation tool

NEPTUNE_CFD is a three dimensional two-fluid code developed more especially for nuclear reactor applications. This local three-dimensional model is based on the classical two-fluid one pressure approach, including mass, momentum and energy balances for each phase. The NEPTUNE_CFD solver, based on a pressure correction approach, is able to simulate multi-component multiphase flows by solving a set of three balance equations for each field (fluid component and/or phase) (Guelfi, 2007), (Mimouni, 2008, 2009). These fields can represent many kinds of multiphase flows: distinct physical components (e.g. gas, liquid and solid particles); thermodynamic phases of the same component (e.g.: liquid water and its vapor); distinct physical components, some of which split into different groups (e.g.: water and several groups of different diameter bubbles); different forms of the same physical components (e.g.: a continuous liquid field, a dispersed liquid field, a continuous vapor field, a dispersed vapor field). The solver is based on a finite volume discretization, together with a collocated arrangement for all variables. The data structure is totally face-based, which allows the use of arbitrary shaped cells (tetrahedral, hexahedral, prism, pyramid ...) including non conforming meshes.

3.3 Geometry and mesh

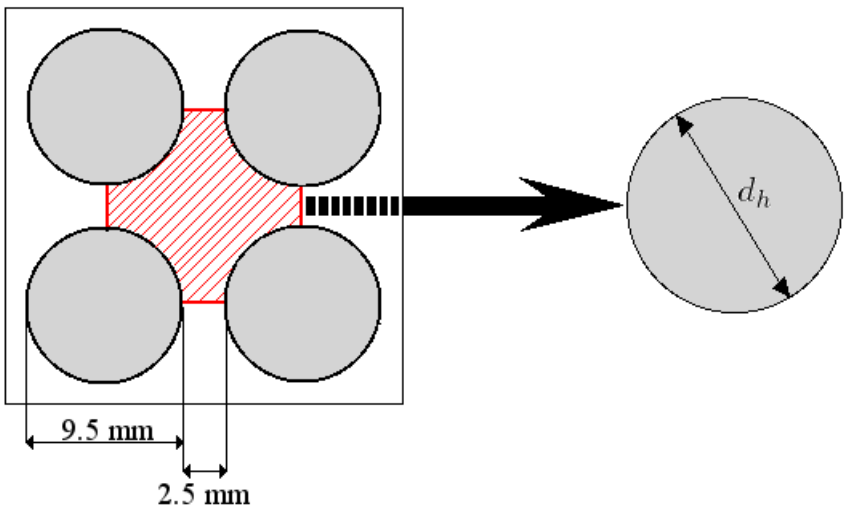

Figure 3.1: Minimal surface called "sub-channel"

As it is mentioned, the context of our study is the treatment of a LOCA accident that may occur in a PWR nuclear reactor. The main problem in simulating the flow in the PWR is the complex geometries where the flow between the fuel rods is bounded by the rods but it is an open medium, where the flow traverses between the rods. Our particular application is the cooling process of the rods that contain the nuclear fuel. In the core of a PWR, the fuel assemblies consists of cylindrical rods of circular section (mostly 9.5 mm in diameter). For numerical simulations it is necessary to define an elementary geometry that represents the physical feature but also small enough to be compatible with the computing power and memory of computers. Such a geometry (shown in figure 3.1) is called "sub-channel" and represents the area between 4 rods. We then define an equivalent hydraulic diameter d_h, and our simulations are effected in a circular pipe:

$$d_h = \frac{4A}{P} \tag{3.1}$$

where A is the flow section and P is the perimeter. In this case $d_h \simeq 11.7$ mm so in our study case we consider a cylindrical pipe with a diameter of the same order of magnitude $d = 20$ mm. In PWR the fuel rods are about 4 meters long but the vapor-droplet flow occurs in the lower part of the core after the quench front. Therefore, we consider a 3 meters long tube, after verifying that this distance is sufficiently long.

The inlet conditions of the general study case are chosen in the same data

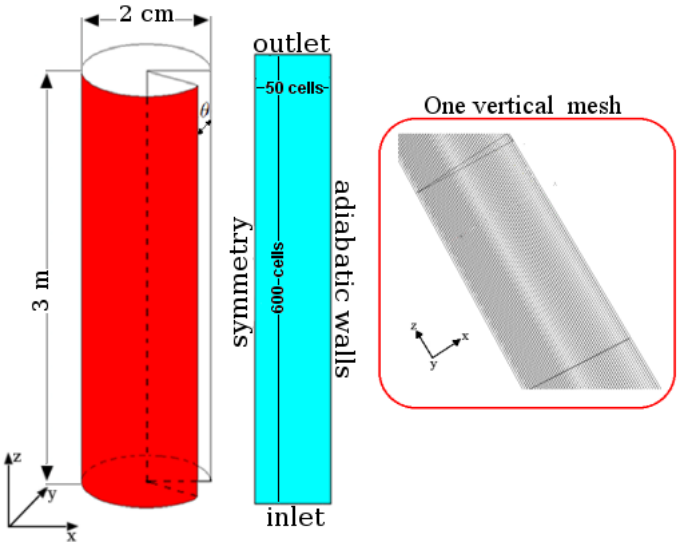

Figure 3.2: The geometry

range that may occur in LOCA accident. The inlet volumetric fractions are 99.5 % of vapor and 0.5 % of water droplets. The droplets and the vapor

enter with a uniform radial distribution from the bottom of the tube. This is thus a dilute flow. The diameter of the droplets is considered to be constant and equal to 0.5 mm. The temperature of the vapor at the inlet is equal to 573 K while the droplets temperature is 372 K. The condition of adiabatic walls is considered in this study case in order to concentrate on the dynamic characteristics of the flow. The vapor enters with a velocity equal to 10 m/s at the bottom of the pipe while the droplets velocity is 2 m/s.
Neptune_CFD can simulate only 3D cases, so we will take a small section of the pipe considering two symmetry planes. The angle formed by the two symmetric planes is $\theta \simeq 10$ degrees. The used mesh is composed of 61800 cells and the majority of the cells are of hexagonal shapes. While constructing the mesh we took into account two main factors. The width of the first cell near the wall (dr^+), and the ratio of the cell height over the cell width (dZ/dR) or cell elongation. This simulation is very sensitive to the ratio of the cell height over the cell width. A very long cell may have a negative impact, and (dZ/dR) should normally not be bigger than 10. Therefore a very fine mesh near the wall require a large number of longitudinal cells. Thus, the discretization of mesh is regular in the longitudinal direction with 600 cells and also regular in the radial direction with 50 cells (figure 3.2). This gives us a wall coordinate $dr^+ \simeq 5$ near the wall, and cell elongation of order 25 (dZ/dR). This mesh has been chosen after several mesh sensitivity tests. In figure 3.3, we present the volume fraction distribution of the vapor over the pipe section produced by using four different meshes. We can notice the importance of the cell elongation by comparing the case of the mesh (50x150) with the case (50x600). Then, the simulation becomes not sensitive to the vertical refinement as we see in the case (50x1500) neither to horizontal refinement as in the case (100x3000). Moreover a simulation over full 3D tube has been done and similar results have been obtained.

3.4 General study case flow description

First of all a general description of the flow is drawn regarding the dynamic mechanism of the dispersion of the droplets over the tube. A general case of simulation was done using the model $k - \varepsilon$ for the vapor phase turbulence, the model Tchen-Hinze for the droplets turbulence, the model of Auton for the lift force, and the model developed by Wallis (1969) for the drag coefficient. In figure 3.4, we present the volume fraction distribution over the tube section. Directly after the inlet, the droplets get away from the wall. After a small distance the concentration of the droplets in the center decreases so the droplets go toward the wall. It means that there is a force that pushes the droplets away from the wall and a force that pushes the droplets away from the center.

In figure 3.5, we present the vapor volume fraction distribution for several

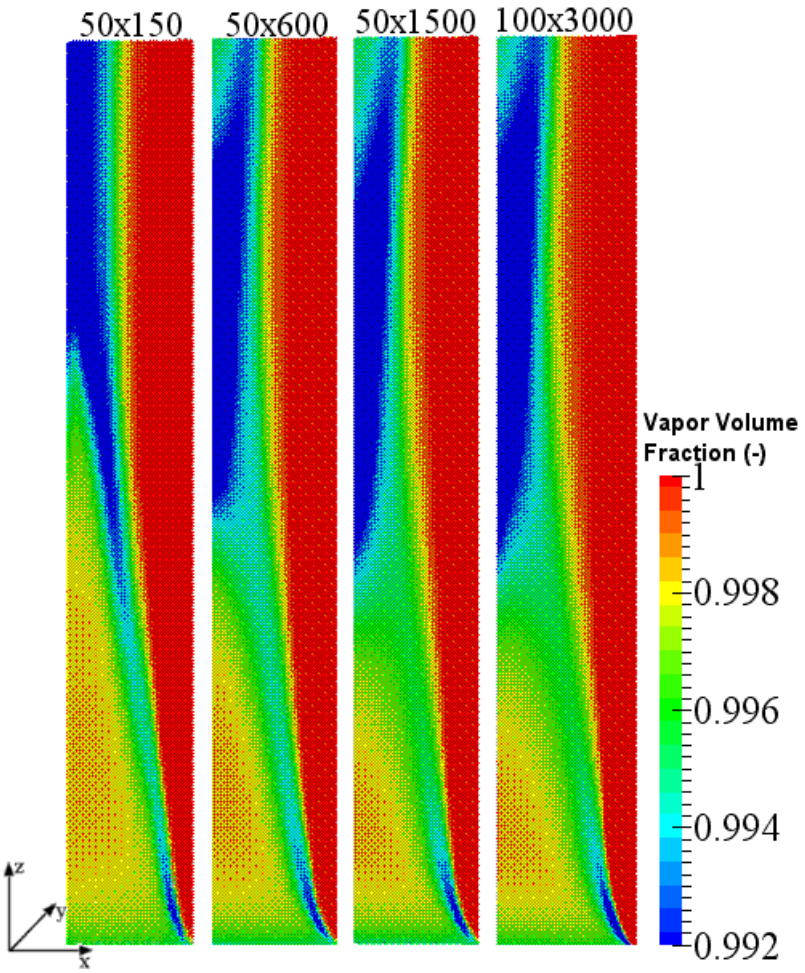

Figure 3.3: Mesh sensitivity

cases obtained by varying the kinetic turbulent energy of the vapor at the inlet of the tube. It shows that as we increase the turbulent kinetic energy of the vapor at the inlet, the concentration of the droplets at the center decreases more quickly. This suggests that the force that pushes the droplets away from the center is directly related to the turbulence intensity in the flow. This force is the source term caused by the gradient of the Reynolds stress tensor of the droplets $\overline{R_{ij,2}}$ in the momentum balance equation. The relation between the turbulent kinetic energy of the vapor and that of the droplets will be discussed later in the next chapters. For now our aim is only to show the direct impact of the turbulence on the radial distribution of the droplets.

As seen in the tests of figure 3.5 for example, the droplets are always far from the wall. After analyzing the forces in these tests, we figured out that the force that pushes the droplets away from the wall toward the center,

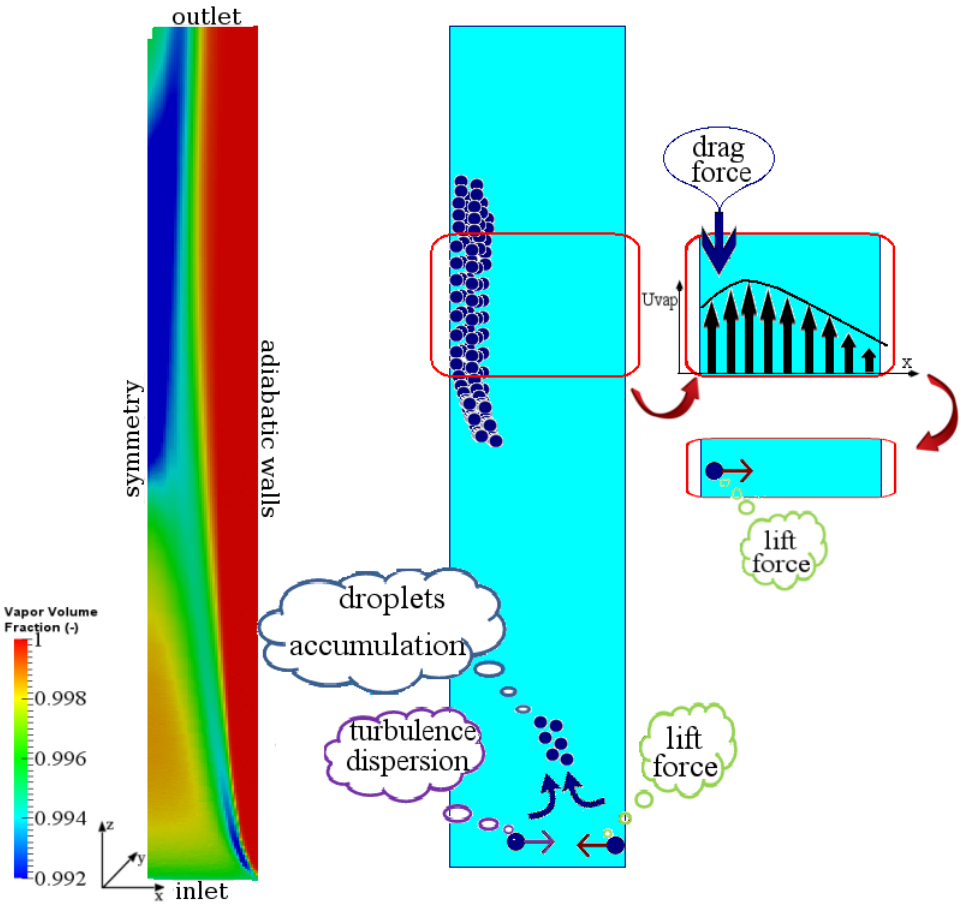

Figure 3.4: The volume fraction distribution over the tube section for a general case

just after the inlet, is the lift force. The importance of this force is shown in figure 3.6, where we present two tests, the first one with the lift force and the second one in neglecting the lift force. When the lift force is neglected, the concentration of the droplets increases in the near wall area. Therefore, we can conclude that the lift force plays a major role in the radial distribution of the droplets over the tube section.
Droplets pushed from the wall meet droplets pushed from the center to form a concentration zone of the droplets, (here we notice that the volume fraction of the droplets is locally more than 0.8 % while the uniform volume fraction at the inlet was 0.5 %). This concentration zone goes up through the tube until it reaches the center. The competition of the two forces after the inlet controls the main direction of the droplets velocity. The large inertia of droplets permits them to retain this velocity direction far from the inlet. Thus, the phenomena at the pipe inlet affect the flow evolution

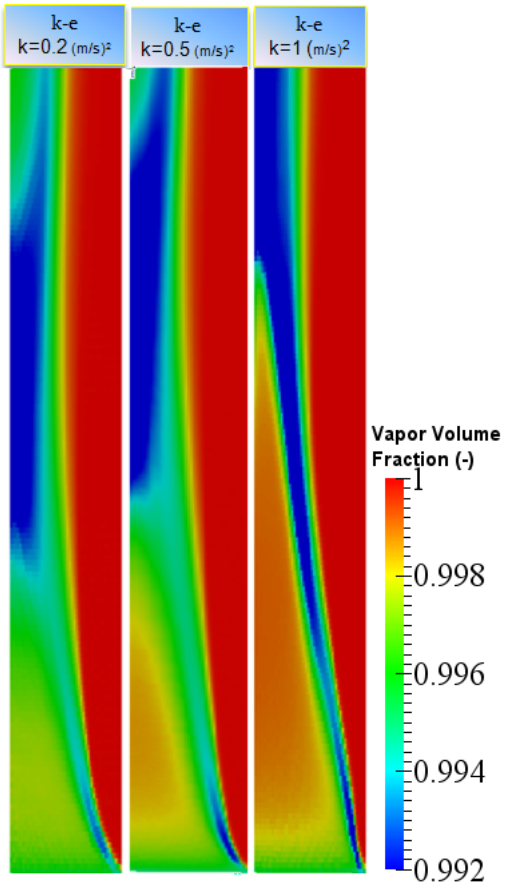

Figure 3.5: The effect of increasing the turbulent kinetic energy of the vapor on the droplets distribution over the tube

all over the pipe. For example, the competition between the two forces after the inlet determines the resulting acceleration direction of the concentrated droplets and affects the height at which they meet the center. This effect can be seen in figure 3.5, which shows that the effect of the turbulence increase as we increases the turbulent kinetic energy of the droplets at the inlet. In these tests the lift force is the same for the three tests. In other words, we increased the force that pushes the droplets toward the wall which changes direction of the acceleration of the concentrated droplets. Consequently, the zone with higher droplets concentration meets the center at a higher point.
If the upper part of the pipe, also in figure 3.4, we can see that after certain height the concentrated droplets move away from the center toward the wall. This orientation of the droplets toward the wall, in this zone, is explained as follow. The important concentration of the droplets at the center causes important vertical deceleration of the vapor in this zone. This deceleration

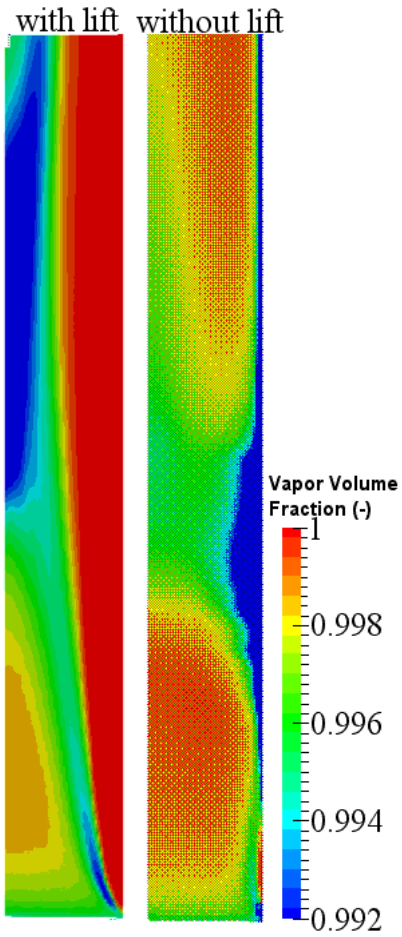

Figure 3.6: The effect of the lift force on the droplets distribution over the tube

of the vapor inverses the gradient of the vapor's mean velocity, so it inverses the sign of the shear. Since the lift force direction depends on the sign of the shear rate, it inverses its sense and it pushes the droplets from the center to the wall. The vertical deceleration and acceleration of the droplets is controlled by the vertical component of the forces mainly the drag force. Then beside its effect in the vertical distribution of the droplets the drag force has an indirect impact on the radial distribution of the droplets.

3.5 Discussion about the model of each force

After explaining the role of each term on the distribution of the droplets, now we discuss briefly the importance and the modeling of these terms. This

discussion aims at restricting our study toward the models that play a critical role and seems not to be compatible with the dispersed droplets case. For the closure of interfacial forces, the bibliographical review shows that the models of the closure of the drag force and the lift force usually depend on two main characteristics of the flow: the particle Reynolds number Re_p defined in equation (2.106) and the non dimensional shear rate of the flow α defined as

$$\alpha = \left(\frac{d_p/2}{\overline{u_{1z}}}\right)\left(\frac{\partial \overline{u_{1z}}}{\partial x}\right) \tag{3.2}$$

Where d_p is the particle diameter, and $\overline{u_{1z}}$ is the mean vapor velocity in the vertical direction.
So first of all we will place our study with respect to these two variables. According to the presented geometry and the considered inlet conditions, Re_p is greater than one and reaches an order of 10^2. The non dimensional shear rate α reaches high values near the wall but it stays lower than 0.5 in the major part of the flow. Theoretically, the drag force, the virtual mass force, and the gravity forces play the major role in the vertical propagation of the droplets. In the case of droplets flow, the virtual mass force shows to be so small, and the vertical propagation of the droplets is mainly controlled by the competition between the drag and the gravity force. In the previous chapter, we presented the model of the drag force with a drag coefficient developed by Wallis (1969) in equation (2.105). This model was initially developed for the flows with solid particles. In recent studies, the validity of this model has been confirmed by the DNS calculations predicted by Kurose and Komori (1999) as shown in the figure 3.7. This figure shows the evolution of the drag coefficient with respect to the particle Reynolds number Re_p, in a shearless flow. Sugioka and Komori (2006) studied the sensitivity of the drag coefficient to the shear rate of the flow. As shown in figure 3.8, the drag coefficient on a spherical droplet increases with the shear rate for a fixed value of the particle Reynolds number, and the dependence of the drag coefficient on the shear rate is more obvious for higher particle Reynolds numbers. The difference in the drag between a spherical droplet and a rigid sphere in a linear shear flow never exceeds 4%, but the drag on a spherical droplet is a little smaller than that on a rigid sphere. For our study case, the flow of spherical droplets, the used model is able to predict the drag coefficient with a degree of uncertainty that varies according to the particular Reynolds number and shear rate. This uncertainty stays in the range of 10% which is acceptable for our study case. Therefore the actual model will be considered for the rest of our study.

The analysis of the results shows the important role of the lift force on the radial distribution of the droplets in the pipe. In the previous chapter, we presented a general model of the lift force proposed by Auton (1987). This model concerns the flow about a sphere placed in a weak shear flow of

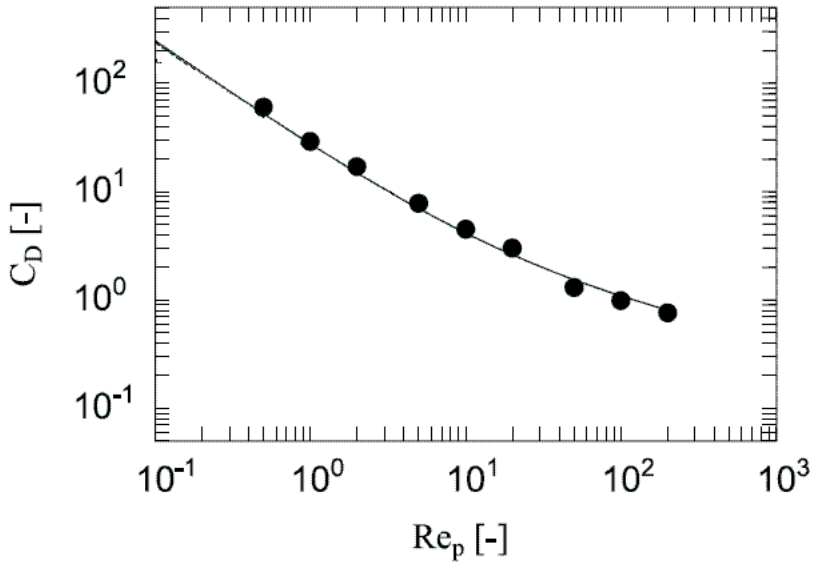

Figure 3.7: Comparison of the drag coefficient in a uniform shearless flow for a solid particle: (•) DNS results predicted by Kurose and Komori (1999); solid line: the drag coefficient prediction by the empirical expression of Wallis (1969)

.

an inviscid fluid. A wall-bounded flow with high particle Reynolds number does not satisfy the hypothesis of Auton. The lift force appears to be over-predicted where we see that all the droplets are pushed away from the wall and concentrated in the center of the pipe. Therefore, the closure of this force will be discussed in a separate chapter.
The other important term is the turbulence term. In the test case we showed briefly the effect of the value of this term on the droplet distribution by changing the inlet condition. The change of the value of the turbulent kinetic energy at the inlet had an effect on the forces acting on the droplets distribution. That means that the value and the gradients of the turbulent Reynolds tensor has an impact on the droplets distribution. As it is shown in momentum balance equations we have two main turbulent terms which are the two Reynolds stress tensors of the continuous phase and dispersed phase. These two turbulent quantities are not independent because of the turbulent interaction expected between the two phases. The turbulence of the continuous phase is already a complex phenomenon. Turbulent dispersed two-phase flow with the co-existing droplets and vapor is more complex. For a good simulation of the turbulence phenomena, we should simulate the turbulence of the dispersed phase, the turbulence of the continuous phase and the turbulent interaction between the two phases.
Simulation of turbulent flows at CFD scale poses the challenge of choosing a

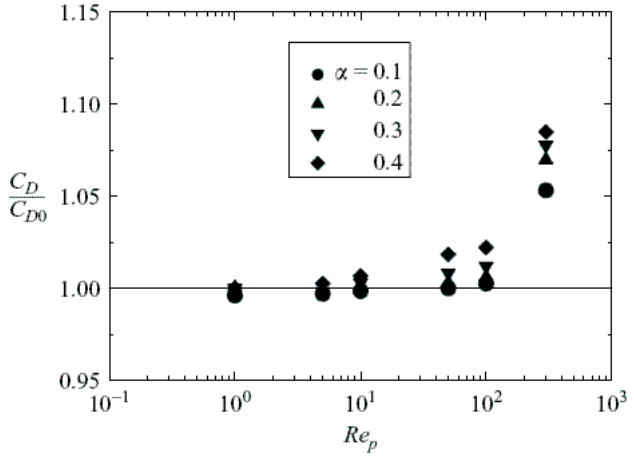

Figure 3.8: The ratio of the drag coefficient C_D, on a spherical droplet in a linear shear flow to that in a uniform shearless flow,c_{D0}, versus the particle Reynolds number, Re_p, Sugioka and Komori (2006).

model that introduces the minimum amount of complexity while capturing main physical phenomena. In the presented case, $k-\varepsilon$ model was used to simulate the turbulence of the continuous phase and Tchen-Hinze model was chosen for the turbulence of the dispersed phase. These models are considered as low-cost models from the numerical point of view. In a separate chapter, we will discuss the compatibility of these models in our case. Moreover more complex models will be tested to show the impact of the strong hypothesis of $k-\varepsilon$ and Tchen-Hinze on the results.

3.6 Conclusion

An overall description of the flow permitted to identify the role of the different terms on the droplets distribution. A test case with common generic models was done. A brief bibliographical study was presented to confirm the use of the model of Wallis (1969) for the prediction of the drag force coefficient. The radial distribution of the droplets over the pipe section is mainly affected by the lift force, the model of turbulence of the continuous phase, and the model of turbulence of the dispersed phase. Auton model used for the prediction of the lift force apparently predicts an important effect of this force. To our knowledge, a lift model suitable for the case of the droplets does not exist. Moreover, the choice of the turbulence models is not evident. Therefore, the modeling of the lift force and the turbulence modeling will be presented in separated chapters. While studying the turbulence modeling we will test the low cost models and the impact of the considered hypothesis

on the results. Moreover more complex models will be tested to check their ability on ameliorating the results. Finally, the problem is now restricted into three main models, the lift force model, the turbulence model of the continuous phase and the turbulence model of the dispersed phase.

Chapter 4

Turbulence modeling

4.1 Introduction

In the context of the reflooding phase of a LOCA (Loss Of Coolant Accident), the vapor-droplet upward flow is initiated at the level of the quench front by a violent evaporation in a depressurized core of the nuclear reactor. The velocity of the vapor between fuel rods is large enough to create a turbulent flow. Moreover the real geometry of the core contains the spacer grids between the fuel rods. The high temperature of the fuel rods during the accident may cause the ballooning of some rods and flow section restrictions. All these complex geometries are extra effects that favor the turbulence of the flow. Therefore turbulence is an essential phenomenon for the targeted application of our study. In the simulation, these extra geometry effects are not taken into account. A simple geometry is considered in order to concentrate on the phenomena that occur in two-phase turbulent flow. The co-existence of dispersed phase and continuous phase, implies extra complex phenomena as the turbulence of the two phases and the turbulent interaction between the two phases, beside the effect of the turbulence on the droplets' spatial distribution.
As shown in the previous chapters, the turbulence quantities have a remarkable effect on the droplets' distribution. The corresponding terms are related to the mean of the fluctuating velocities $\overline{u'_{ki}u'_{kj}}$. These terms are also called Reynolds stress tensor of the phase k and are denoted by $\overline{R_{ij,k}}$.
In the Euler/Euler approach, these turbulent quantities are estimated via turbulence models. There is a large variety of turbulence models proposed, and the choice of the suitable model presents a crucial question. The model should introduce the minimum amount of numerical complexity (CPU time), while capturing the essence of the relevant physics. In two-phase flows, we should choose the appropriate model to calculate turbulence of the continuous phase, and another model to calculate the agitation of the dispersed phase. Besides, special attention should be paid to the modeling of the tur-

bulent interaction between the two phases.
This chapter is organized as follows: first the isotropic turbulence model $k-\varepsilon$ and the nonisotropic model $R_{ij}-\varepsilon$, are presented for the modeling of the turbulence of the continuous phase in section 4.2. Second, two turbulence models for the dispersed phase are presented in section 4.3, one based on simple algebraic relations that calculates the dispersed phase turbulence from the continuous phase turbulence, Tchen-Hinze, and the other based on adding two transport equations for the turbulence characteristics of the dispersed phase, Q2Q12. The adequacy of these turbulence models is discussed theoretically with respect to the case of vapor-droplet pipe flow. Third, numerical simulations using these different models are compared with a gas-particle experimental case in section 4.4. In section 4.5, a detailed study is presented for the modeling of the two-way coupling terms, that we showed to be a key issue of the modeling. Then, we propose a new formulation for the turbulence coupling term and show how it allows to recover the experimental results. In section 4.6, we analyze the impact of the modeling of the two phase turbulence on the spatial distribution of the droplets in a configuration close to our case of interest. And finally, a conclusion on the turbulence modeling is drawn.

4.2 Turbulence modeling of the continuous phase

The turbulence of the continuous phase, vapor, is modeled in the framework of RANS turbulence models. The models of turbulence of the continuous phase in a two-phase flow differ from models of single-phase flow through several additional production and destruction (sink) terms arising from the interaction with the dispersed phase. The majority of industrial CFD applications today are conducted with two-equation eddy viscosity model (EVM), especially the $k-\varepsilon$ model, while the Reynolds stresses transport model (RSTM) or $R_{ij}-\varepsilon$, remains exceptional. Several studies were done to evaluate RSTM model in other flow configurations. In the case of single-phase flows in presence of mixing vanes, Lee and Choi (2007) have concluded that RSTM is helpful to see the effect of secondary flow. Ikeda et al. (2006) used $k-\varepsilon$ model, they confirmed its ability to predict the averaged velocity, but they mentioned that it may be insufficient for narrow channel flow conditions that include non isotropic effects. In our case, both mixing vanes and narrow channels have to be considered. Moreover two-phase flow cases induce new effects, like the accumulation of dispersed phase particles, and interaction between these particles and the continuous phase turbulence. Several authors studied the turbulence modeling in the case of water flow with gas bubbles. As an example, a RSTM model adapted to bubbly flows is studied in Chahed (1999) and used to perform simulations of basic bubbly flows. This model is interesting

but it requires a doubled computational effort; because it accounts for two scales of turbulence, the first one is the turbulence of the fluid seen in a single phase flow and the second is the pseudo turbulence which considers the fluctuation caused by the motion of the bubble. In Mimouni et al. (2009), the authors proposed a turbulence modeling that takes into account the Reynolds tensor for the continuous phase only, while a more basic modeling is used for the dispersed phase. Also in Mimouni et al. (2009) it is concluded that the use of eddy viscosity models may be sufficient for water bubbly flows in vertical pipes but not for complex geometries especially when swirling flows are involved. In our case, unlike the gas bubbles, water droplets have important inertia and the anisotropy of the vapor turbulence may influence the concentration of the droplets. Therefore this anisotropy may play an important role even in a simple pipe. To analyze these effects, the two models $k-\varepsilon$ and $R_{ij}-\varepsilon$ will be studied in details in this section.

4.2.1 $k-\varepsilon$ turbulence model

This model is based on Bousinesq's analogy employing the eddy viscosity as the model parameter. The eddy viscosity assumption transforms the Reynolds stress gradient into a diffusion-like transport term. $k-\varepsilon$ model describes energy process in terms of production and dissipation, as well as transport through the mean flow or by turbulent diffusion. The formulation of the standard $k-\varepsilon$ modeling concept for the single-phase flow is provided in Jones and Launder (1972). In this approach two quantities are defined: the turbulent kinetic energy of the vapor k_1

$$k_1 = \frac{1}{2}\overline{u'_{1i}u'_{1i}} \tag{4.1}$$

and the turbulent dissipation rate of the vapor ε_1

$$\varepsilon_1 = \nu_1 \overline{\frac{\partial u'_{1i}}{\partial x_k}\frac{\partial u'_{1i}}{\partial x_k}} \tag{4.2}$$

where ν_1 is the molecular kinetic viscosity of the vapor. The Bousinesq-eddy viscosity approximation assumes that the principal axes of the Reynolds stress tensor $R_{ij,1}$ are aligned with those of the mean strain-rate tensor at all points of the turbulent flow and that the ratio of proportionality between the two stresses is the turbulent eddy viscosity of the vapor ν_1^T.

$$-\overline{R_{ij,1}} + \frac{2}{3}k_1\delta_{ij} = \nu_1^T\left(\frac{\partial \overline{u_{1i}}}{\partial x_j} + \frac{\partial \overline{u_{1j}}}{\partial x_i} - \frac{2}{3}\frac{\partial \overline{u_{1m}}}{\partial x_m}\delta_{ij}\right) \tag{4.3}$$

and

$$\nu_1^T = C_\mu \frac{k_1^2}{\varepsilon_1} \tag{4.4}$$

where $C_\mu = 0.09$.
In the case of two-phase flow, the turbulent predictions of the continuous phase are carried out with the standard $k-\varepsilon$ model supplemented with additional terms accounting for the interfacial turbulent momentum transfer Π_{q1}. Then the transport equations allowing to compute k_1 and ε_1 are written in the approximate forms:

- The transport equation of the turbulent kinetic energy, k_1

$$\alpha_1\rho_1\left[\frac{\partial k_1}{\partial t}+\overline{u_{1,j}}\frac{\partial k_1}{\partial x_j}\right]=\frac{\partial}{\partial x_j}[\alpha_1\rho_1\frac{\nu_1^T}{\sigma_k}\frac{\partial k_1}{\partial x_j}]+\alpha_1\rho_1(Prod_1+G_1-\varepsilon_1)+\Pi_{q1} \tag{4.5}$$

  with the constant $\sigma_k = 1$.

- The transport equation of the turbulent dissipation rate, ε_1, reads

$$\begin{aligned}\alpha_1\rho_1\left[\frac{\partial \varepsilon_1}{\partial t}+\overline{u_{1,j}}\frac{\partial \varepsilon_1}{\partial x_j}\right] &= \frac{\partial}{\partial x_j}[\alpha_1\rho_1\frac{\nu_1^T}{\sigma_\varepsilon}\frac{\partial \varepsilon_1}{\partial x_j}] \\ &+ \alpha_1\rho_1\frac{\varepsilon_1}{k_1}\left[C_{\varepsilon1}Prod_1+C_{\varepsilon1}max(G_1,0)-C_{\varepsilon2}\varepsilon_1\right] \\ &+ C_{\varepsilon4}\frac{\varepsilon_1}{k_1}\Pi_{q1}\end{aligned} \tag{4.6}$$

  with $C_{\varepsilon1} = 1.44$, $C_{\varepsilon2} = 1.92$, $C_{\varepsilon4} = 1.2$ and $\sigma_\varepsilon = 1.3$.

where $Prod_1$ is the production contribution

$$Prod_1 = -\overline{R_{ij,1}}\frac{\partial \overline{u_{1i}}}{\partial x_j} \tag{4.7}$$

G_1 is the stratification attenuation term modeling the correlation between fluctuating density and velocity.

$$G_1 = -\frac{\nu_1^T}{Pr^T}\frac{1}{\rho_1}\frac{\partial \rho_1}{\partial x_i}g_i \tag{4.8}$$

where Pr^T is Prandtl turbulent number which is equal to 0.9.
Π_{q1} models the influence (destruction or production) of the dispersed phase on the continuous phase (in our case the influence of the droplets on the vapor)

$$\Pi_{q1} = \alpha_2 F_D^{12}\frac{\rho_2}{\rho_2+\rho_1 C_{ma}}(k_{12}-2k_1)+\alpha_2 F_D^{12}V_{di}(\overline{u_{2i}}-\overline{u_{1i}}-V_{di}) \tag{4.9}$$

where C_{ma} is the virtual mass coefficient, and $k_{12} = \overline{u'_{1i}u'_{2i}}$ is the covariance of the fluctuating velocities of the two phases which is calculated in the

model of turbulence of the dispersed phase. The averaged drag force F_D^{12}, is expressed in terms of the drag coefficient C_D and the relative velocity $|V_r|$ and the droplet diameter d as follows

$$F_D^{12} = \frac{3}{4}\frac{\rho_1}{\alpha_1}\frac{C_D}{d}|V_r| \tag{4.10}$$

where

$$|V_r| = ((\overrightarrow{U_2} - \overrightarrow{U_1} - \overrightarrow{V_d}) + 2k_1 - k_{12} + 2k_2)^{1/2} \tag{4.11}$$

For the case of the droplets where ($\rho_2 >> \rho_1$), the virtual mass coefficient can be neglected from the equation of Π_{q1}. More details about the modeling and the role of this term is discussed in section 4.5.

4.2.2 $R_{ij} - \varepsilon$ turbulence model

The Reynolds stresses transport model (RSTM) $R_{ij} - \varepsilon$ is a higher level, elaborated turbulence model. In RSTM, the eddy viscosity approach has been discarded and the Reynolds stresses are directly computed. The exact transport equation of the vapor Reynolds stress tensor $\overline{R_{1,ij}}$, accounts for the directional effects of the Reynolds stress fields and it is written in the following way:

$$\begin{aligned}
\frac{\partial R_{1,ij}}{\partial t} + \overline{u_{1,j}}\frac{\partial R_{1,ij}}{\partial x_j} &= \overbrace{-\left(\overline{u'_{1,i}u'_{1,m}}\frac{\partial \overline{u_{1,j}}}{\partial x_m} + \overline{u'_{1,j}u'_{1,m}}\frac{\partial \overline{u_{1,i}}}{\partial x_m}\right)}^{P_{ij}} + \overbrace{\left(\overline{f_i u'_{1,j}} + \overline{f_j u'_{1,i}}\right)}^{G_{ij}} \\
&+ \overbrace{\overline{\frac{p'}{\rho}\left(\frac{\partial u'_{1,i}}{\partial x_j} + \frac{\partial u'_{1,j}}{\partial x_i}\right)}}^{\Phi_{ij}} - \overbrace{2\nu\left(\overline{\frac{\partial u'_{1,i}}{\partial x_m}\frac{\partial u'_{1,i}}{\partial x_m}}\right)}^{\epsilon_{ij}} + \Pi_{q1} \\
&+ \overbrace{\frac{\partial}{\partial x_m}\left[\underbrace{\nu\frac{\partial \overline{u'_{1,i}u'_{1,j}}}{\partial x_m}}_{D_{ij}^{\nu}} - \underbrace{\overline{u'_{1,i}u'_{1,j}u'_{1,m}}}_{D_{ij}^{t}} - \underbrace{\overline{\frac{p'}{\rho}\left(u'_{1,j}\delta_{jm} + u'_{1,i}\delta_{im}\right)}}_{D_{ij}^{p}}\right]}^{D_{ij}}
\end{aligned} \tag{4.12}$$

The right hand side of the transport equation is decomposed into the following terms: P_{ij} is the production contribution due to the velocity gradients, G_{ij} is the production due to body forces, Φ_{ij} is the redistribution due to pressure fluctuations, ϵ_{ij} is the viscous destruction, $D_{ij} = D_{ij}^{\nu} + D_{ij}^{t} + D_{ij}^{p}$ are the diffusion terms due to viscosity, turbulence and pressure respectively,

and Π_{q1} is the influence (destruction or production) of the dispersed phase on the continuous phase.
The modeling of $R_{ij} - \varepsilon$ depends on the same principles applied in the modeling of $k - \varepsilon$, by referring to the turbulent characteristic scales of time and length:

$$\tau = \frac{k}{\varepsilon}, L = \frac{k^{\frac{2}{3}}}{\varepsilon}$$

The turbulent production term, P_{ij}, comes from the shear of the mean velocity. The expression of P_{ij} does not require any particular modelling. Also the turbulent production term by the body forces, G_{ij}, which concerns the gravity force, does not require any special modeling.
Some terms in the Reynolds stress tensor transport equation can not be computed directly and must be modeled. A modeling from Hanjalic and Laurence (2002) is presented below.

- The turbulent energy interfacial transfer term, Π_{q1}:
  This term comes from the interfacial forces between the continuous and the dispersed phase, and it is modeled in the same way as for the model $k - \varepsilon$.

- The viscous dissipation,ϵ_{ij}:
  The large turbulent structures are not affected by the viscosity, while small eddies may be considered locally isotropic. Therefore, the viscous dissipation, which is associated to small structures, is considered locally isotropic:

$$\epsilon_{ij} = \frac{2}{3}\varepsilon\delta_{ij} \tag{4.13}$$

- The diffusion term, D_{ij}:
  The term of turbulent diffusion is modeled due to a generalized gradient diffusion expression as follows:

$$D_{ij}^{t} = \frac{\partial}{\partial x_n}\left[C_s\overline{u_n' u_{1,m}'}\frac{k}{\varepsilon}\frac{\partial\overline{u_{1,i}' u_{1,j}'}}{\partial x_m}\right] \tag{4.14}$$

  The terms of diffusion due to pressure and viscosity, D_{ij}^{p} and D_{ij}^{ν}, are generally neglected. It is sufficient to adjust the constant C_s to take them into account.

- The term of pressure redistribution, Φ_{ij}:
  Experience shows that the pressure fluctuations tend to redistribute the turbulent stresses in a way that makes them tend toward an isotropic state. This term is decomposed into several expressions that can affect the sources of turbulence. After some calculations and physical

considerations, Hanjalic and Laurence (2002) obtain the following decomposition:

$$\Phi_{ij} = \Phi_{ij,1} + \Phi_{ij,2} + \Phi_{ij,3}$$

- $\Phi_{ij,1}$ is the term of slow return toward the isotropy. In the absence of turbulent shear production or volume forces, far from the wall, the force fluctuations become isotropic turbulence. Based on this observation, Hanjalic and Laurence (2002) proposed the following model:

$$\Phi_{ij,1} = -C_1\varepsilon_1 \left(\frac{\overline{u'_{1,i}u'_{1,j}}}{k} - \frac{2}{3}\delta_{ij} \right)$$

  In two-phase flows, the dispersed particles also affect the mechanisms of redistribution of turbulent energy. The tendency of sheared dispersed flows towards the isotropy may be faster than the corresponding single-phase flows. To account for that diphasic property, the term of the slow return to isotropy $\Phi_{ij,1}$, according to Chahed (1999) reads:

$$\Phi_{ij,1} = -C_1 \left(\frac{1}{\tau_1^T} + \frac{\alpha}{\tau_p} \right) \left(\overline{u'_{1,i}u'_{1,j}} - \frac{2}{3}k\delta_{ij} \right)$$

  where $\tau_1^T = \frac{k_1}{\varepsilon_1}$ is the characteristic time scale of the vapor turbulence and τ_p is the characteristic time scale of a particle with $\tau_p = C_D d/V_r$

- $\Phi_{ij,2}$ and $\Phi_{ij,3}$ are the terms of the fast return toward the isotropy. These terms act directly on the terms of production P_{ij} and G_{ij} as follows:
  $\Phi_{ij,2} = -C_2 \left(P_{ij} - \frac{2}{3}P\delta_{ij}\right)$ with $P = \frac{1}{2}P_{mm}$
  $\Phi_{ij,3} = -C_3 \left(G_{ij} - \frac{2}{3}G\delta_{ij}\right)$ with $G = \frac{1}{2}G_{mm}$

Hence, the model equation for ε has the form:

$$\frac{\partial \varepsilon}{\partial t} + \overline{u_{1,j}}\frac{\partial \varepsilon}{\partial x_j} = \frac{\partial}{\partial x_i}\left(C_\varepsilon \frac{k}{\varepsilon}\overline{u'_{1,i}u'_{1,j}}\frac{\partial \varepsilon}{\partial x_j} \right) + (C_{\varepsilon_1}P + C_{\varepsilon_3}G + C_{\varepsilon_4}k\frac{\partial \overline{u_{1,j}}}{\partial x_j} - C_{\varepsilon_2}\varepsilon)\frac{\varepsilon}{k}$$

The coefficients of the $R_{ij} - \varepsilon$ model are given in (Table 4.1).

C_s	C_1	C_2	C_1^ω	C_2^ω	C_ε	C_{ε_1}	C_{ε_2}	C_{ε_3}	C_{ε_4}
0.2	1.8	0.6	0.5	0.3	0.18	1.44	1.92	1.44	0.33

Table 4.1: Constants of the model $R_{ij} - \varepsilon$

4.2.3 Adequacy of the models $k-\varepsilon$ and $R_{ij}-\varepsilon$ in the studied case

RSTM model may be more time and storage-consuming, however, EVM models may have major weaknesses. Mimouni et al. (2009) resumed the short coming and deficiencies of EVM models and among them $k-\varepsilon$ model, as follows

1. limitation to linear algebraic stress-strain relationship (poor performances whenever the stress transport is important, e.g., non equilibrium, fast evolving, and separating flows),

2. insensitivity to the orientation of turbulence structure and stress anisotropy (poor performance where normal stresses play an important role),

3. inability to account for extra strain (streamline curvature, skewing, rotation).

In our case of a vapor-droplet upward flow inside a vertical thin tube, the normal turbulent stresses are expected to be more important than the radial turbulent stresses, this induces shear stresses and turbulence anisotropy. Besides, the existence of inertial droplets in some areas decelerates the vapor flow, and this induces local shear stress far from the wall. This also implies streamlines curvatures. These predictions drive us to test the two models in order to check if, in this case, $R_{ij}-\varepsilon$ is able to capture extra physical phenomena that are ignored by the $k-\varepsilon$. In section 4.6, we will quantify the effect of these phenomena on other flow properties, particularly on the droplets dispersion.

4.3 Turbulence of the dispersed phase

The turbulence of the continuous phase (vapor) is already a complex phenomenon, turbulence of dispersed multi-phase flows makes the problem more complex. As soon as the droplets have sufficient inertia and finite size their agitation are less correlated with the agitation of the vapor and meanwhile the presence of the droplets influences the continuous phase turbulence intensity. The importance of the turbulence of the dispersed phase comes from its direct effect on the spatial distribution of the droplets. Hence it may have an important effect on the heat and the mass transfer between the two phases. There was less understanding of the dispersed phase turbulence until the late 80's of the last century. Over a long period, of time the most popular theory

was Tchen-Hinze's "particle-tracking-fluid" theory (see Hinze (1975)). This theory considers a strong hypothesis which imposes a large dependency of the particle turbulence on the fluid turbulence. According to this theory the particle turbulent fluctuation is always weaker than the fluid turbulent fluctuation. It is valid when the Stokes number is very small. In the frame work of two fluid-models, Elghobashi et al. (1984) combined the continuous phase $k-\varepsilon$ turbulence model with an algebraic particle turbulence model. Similar approaches have been taken by Melville and Bray (1979), Chen and Wood (1985), Mostafa and Mongia (1988), etc. All of these approaches are based on the idea of Tchen-Hinze's theory. Others model the particle's agitation and take into account its own convection diffusion and production due to its mean motion and not only the effect of the fluid turbulence as predicted by the Tchen-Hinze's theory. Some models calculate the turbulence quantities characterizing the dispersed phase from one-equation model (a transport equation for the turbulent kinetic energy of the dispersed phase and an algebraic relation for the dissipation rate) as the model $k-\varepsilon-k_p$ proposed by Zhou and Huang (1990). In dilute dispersed two-phase flows, turbulent transport has a different nature due to the non viscous character of the particles' flow, thus the dissipation rate, whose existence as a viscous-dependent variable is not possible. Therefore in the present work, a different modeling method proposed by Simonin (2000) namely the Q2Q12, is used. Besides transport equation for the turbulent kinetic energy of the dispersed phase, the model employs a transport equation for the vapor-droplet velocity covariance. This variable allows to model a sink of turbulence instead of the dissipation rate, and it takes into account the turbulence destruction effect caused by the drag force. The impact of the choice between the model Q2Q12 and Tchen-Hinze on the droplets distribution is studied here.
In the momentum balance equations of the vapor and the droplets, the fluctuation of the droplets is presented by mean of two terms that need proper closures

- The particle kinetic stress tensor $\overline{u'_{2i}u'_{2j}}$ represents the mean transport of particle momentum by the velocity fluctuations. By considering that the droplets' fluctuations are isotropic, this stress tensor is considered equal to the turbulent kinetic energy of the droplets k_2:

$$k_2 = \frac{1}{2}\overline{u'_{2i}u'_{2i}} \tag{4.15}$$

  The energy k_2 characterizes the droplets' agitation, and not a liquid phase turbulence inside the droplet.

- The tensor of covariance between the velocity fluctuations of the two phases $\overline{u'_{1,i}u'_{2j}}$, is also considered isotropic

$$k_{12} = \overline{u'_{1,i}u'_{2i}} \tag{4.16}$$

These two turbulent terms appear in the momentum balance equation of the dispersed phase. Also, these terms are used in the closure of the interfacial forces. In the previous chapters, it appears that the value and the evolution of these terms particularly the kinetic turbulent energy k_2 is of high importance. The gradient of k_2 acts as a radial force and impacts directly the spatial distribution of the droplets. Two turbulence models are considered: Tchen-Hinze model and Q2Q12 model.

Tchen-Hinze model

Tchen-Hinze model is an algebraic model that evaluates the turbulent kinetic energy k_2 of the dispersed phase and the covariance k_{12} mainly from the turbulent kinetic energy k_1. Tchen (1947) was the first who developed this method under restrictive hypotheses.
Other work were done on the same subject, as the work of Hinze (1975) and Deutch (1992) which aimed to limit some of these very restrictive hypotheses. Here we present a brief study of this work starting with the hypotheses of Tchen (1947) then the consequent modifications proposed to reach the final modeling of k_2 and k_{12} used in our study.
The aim of Tchen (1947) was to estimate the coefficient of dispersion of particles in function of the flow characteristics for small non-deformable spheres in a turbulent field. This theory is based on five hypotheses.

1. The turbulence of the liquid is stationary and homogeneous in a finite dimensional domain. Therefore, the fluctuating movement of the inclusions may reach an asymptotic value.

2. The particle Reynolds number Re_p is smaller than unity. Then the drag force can be calculated via linear model. The Stokes law can be used.

3. The characteristic diameter of the particle is less than the scale of Kolmogorov. Then the size of inclusions does not provoke spatial filtering of the turbulence of liquid. With the assumption (2), the derivative along the particle path is equivalent to the derivative following a fluid particle.

4. During its motion the particle follows always the same fluid element. Therefore the Lagrangian statistics following a fluid particle is equivalent to the Lagrangian statistics following a particle.

5. No external forces are acting on the particles. This can be deduced from hypothesis 4.

Using these five hypothesis, Tchen (1947) could write a linear equation of trajectory of a particle.

$$\frac{du_{2,i}(t)}{dt} = -\frac{u_{2,i}(t) - u_{1,i}(t)}{\tau_{12}^F} + b\frac{u_{1,i}(t)}{dt} - c\int_{t_0}^{t} \frac{d}{d\tau}(u_{2,i}(\tau) - u_{1,i}(\tau))\frac{d\tau}{\sqrt{t-\tau}} \tag{4.17}$$

with τ_{12}^F is the characteristic time scale of the particle in the motion of the fluid

$$\tau_{12}^F = \frac{1}{F_D}(\frac{\rho_2}{\rho_1} + C_{Ma}) \tag{4.18}$$

and the coefficients b and c are respectively equal to:

$$\begin{aligned} b &= \frac{1 + C_{Ma}}{\frac{\rho_2}{\rho_1} + C_{Ma}} \\ c &= \frac{9}{d_p}\frac{\sqrt{\frac{\nu_1}{\pi}}}{\frac{\rho_2}{\rho_1} + C_{Ma}} \end{aligned} \tag{4.19}$$

Tchen (1947) showed that the dispersion of the particles tends toward the diffusion of the fluid particles. Hinze (1975) added other hypothesis to the work of Tchen (1947) considering that the fluid turbulence is isotropic. Due to linearity of the transport equation of the particle's velocity, the isotropy of the liquid is transmitted to the particle's fluctuation. Consequently, the terms of velocity variance, Lagrangian correlations of the velocity, and the Lagrange spectrum of the inclusions can be written more simply as follows:

- The variance of the particle velocity:

$$\left\langle u_2'^2 \right\rangle_2 = \frac{1}{2}\left\langle u_{2,i}' u_{2,i}' \right\rangle_2$$

- The Lagrangian autocorrelation of the fluctuating velocity of the particles:

$$\Re_{2,ii}(\tau) = \frac{\left\langle u_{2,i}'(t_0) u_{2,i}'(t_0+\tau) \right\rangle_2}{\left\langle u_{2,i}'(t_0) u_{2,i}'(t_0) \right\rangle_2} \tag{4.20}$$

  and the Lagrangian correlation

$$\Re_2 = \frac{1}{3}\Re_{2,ii}(t)$$

- The Lagrangian spectrum of the particles' fluctuating velocities

$$\xi_2(t) = \frac{1}{3}\xi_{2,ii}(t)$$

where

$$\xi_{2,ij}(w) = \frac{\sqrt{\left\langle u'_{2,i}u'_{2,i}\right\rangle_2 \left\langle u'_{2,j}u'_{2,j}\right\rangle_2}}{2\pi} \int_{-\infty}^{\infty} \Re_{2,ij}(\tau) exp(-Iw\tau) d\tau$$

- Lagrangian integral time scale

$$\tau_2^t = \frac{1}{3}\tau_{2,ii}^t$$

where

$$\tau_{2,ii}^t = \int_0^{\infty} \Re_{2,ij}(\tau) d\tau$$

Tchen (1947) applied Fourier transformation to this linearized trajectory equation. After neglecting the Basset force, he could write the Lagrangian Spectrum of the particles ξ_2 in terms of that of the fluid ξ_1.

$$\frac{\xi_2}{\xi_1} = \frac{(\tau_{12}^F)^{-2} + bw^2}{(\tau_{12}^F)^{-2} + w^2} \tag{4.21}$$

Consequently, the variance of the fluctuating velocity of the particles could be written in terms of the Lagrangian spectrum of the liquid

$$\left\langle u_2'^2 \right\rangle_2 = \int_0^{\infty} \xi_2(w) dw = \int_0^{\infty} \frac{(\tau_{12}^F)^{-2} + bw^2}{(\tau_{12}^F)^{-2} + w^2} \xi_1(w) dw \tag{4.22}$$

Then Hinze (1975) considered that the Lagrangian correlation of the fluid velocity can be written in the following exponential form

$$\xi_1 = exp(\frac{\tau}{\tau_1^t}) \tag{4.23}$$

with τ_1^t the characteristic time scale of the liquid turbulence. Integrating the equation (4.22) leads to

$$\left\langle u_2'^2 \right\rangle_2 = \frac{b^2 + \dfrac{\tau_1^t}{\tau_{12}^F}}{1 + \dfrac{\tau_1^t}{\tau_{12}^F}} \left\langle \tilde{u}_1'^2 \right\rangle_2 \tag{4.24}$$

With the same method, Desjonqueres et al. (1986) derives the equation of the fluid-particle velocity covariance in terms of the turbulent kinetic energy of the fluid:

$$\left\langle \tilde{u}_1' u_2' \right\rangle_2 = \frac{b + \dfrac{\tau_1^t}{\tau_{12}^F}}{1 + \dfrac{\tau_1^t}{\tau_{12}^F}} \left\langle \tilde{u}_1'^2 \right\rangle_2 \tag{4.25}$$

with

$$\left\langle \tilde{u}'_1 u'_2 \right\rangle_2 = \frac{1}{3} \left\langle \tilde{u}'_{1,i} u'_{2,i} \right\rangle_2 \tag{4.26}$$

The theory of Tchen-Hinze presents the major inconvenience that the particles follow, the same fluid elements during their motion. This hypothesis does not allow to take into account the slip velocity between the two phases. Consequently, this hypothesis neglects the effect of concentration of the droplets in some zones. In the present case, the droplets may have tendency to migrate away or toward the tube walls to form concentration zones. In this case the turbulent kinetic energy of the fluid "seen" by the particles is different from the turbulent kinetic energy of the fluid.
The second inconvenient of this hypothesis is neglecting the slip velocity between the particle, then it does not take into account the external forces acting on the particle.
Deutch (1992) proposed an extension of the theory of Tchen-Hinze to take into account these phenomena. This extension is based on the work of Csanady (1963) who studied the effect of the slip velocity on the dispersion of particles in a cloud in the atmosphere. This phenomenon is called the "crossing -trajectories effect". Csanady (1963) showed that the function of auto-correlation of the liquid turbulence "seen" by the liquid could be written in the following form:

$$\Re_{12}(\tau) = exp(-\frac{\tau}{\tau_{12}^t}) \tag{4.27}$$

with τ_{12}^t which represents the characteristic time scale of the liquid turbulence "seen" by the particles:

$$\tau_{12}^t = \tau_1^t (1 + \beta^2 \frac{|V_r|^2}{\left\langle u'^2_{1,i} \right\rangle_2})^{-\frac{1}{2}} \tag{4.28}$$

with β the ratio of the Lagrangian integral time scale over the Eulerian integral time scale and it is taken $(0.7 < \beta < 1)$.
Deutch (1992) took the principal results of Csanady (1963) and wrote an equation of movement equation (4.17) for a bubble, considering that the particle Reynolds number Re_p is greater than unity. He considered that the interaction time between the inclusion and the large turbulent eddies in the slip direction is identical to that of Csanady (1963). But in the perpendicular direction to the slip, Deutch (1992) modeled the time scale in the following way:

$$\tau_{12,\perp}^t = \tau_1^t (1 + 4\beta^2 \frac{|V_r|^2}{\left\langle u'^2_{1,i} \right\rangle_2})^{-\frac{1}{2}} \tag{4.29}$$

After all this process, the final equations of the Tchen-Hinze model, that we will consider here, are

$$\boxed{k_2 = k_1 \left[\frac{b^2+\eta_r}{1+\eta_r}\right] \qquad k_{12} = 2k_1 \left[\frac{b+\eta_r}{1+\eta_r}\right]} \tag{4.30}$$

b and η_r are functions of the drag coefficient F_D^{12} and the virtual mass coefficient C_{ma}, and two specific time scales:

$$b = \frac{\rho_1 + \alpha_1 C_{ma}}{\rho_2 + \alpha_1 C_{ma}} \qquad \eta_r = \frac{\tau_{12}^T}{\tau_{12}^F} \tag{4.31}$$

τ_{12}^F is the characteristic time scale of the momentum transfer between the two phases, and τ_{12}^T represent the time scale of the continuous phase turbulence, viewed by the dispersed phase that takes into account the crossing trajectory effect.

$$\tau_{12}^F = \frac{\alpha_1 C_{ma} + \rho_2}{\alpha_1 F_D^{12}} \qquad \tau_{12}^T = \frac{\tau_1^T}{\sigma_\alpha}\left(1 + C_\beta \xi_r^2\right)^{-0.5} \tag{4.32}$$

with σ_α equal to Prandtl turbulent number, C_β is the crossing trajectory coefficient equal to 1.8, and $\xi_r = \frac{\langle|\overrightarrow{V_r}|\rangle_2}{\sqrt{\frac{2}{3}k_1}}$.
In the case of the droplets ρ_2 is larger than ρ_1 then the factor b is very small with respect to one,

$$\rho_1 << \rho_2 \quad \Rightarrow \quad b = \frac{\rho_1 + \alpha_1 C_{ma}}{\rho_2 + \alpha_1 C_{ma}} << 1 \quad \text{when} \quad (\alpha_1 C_{ma}) \simeq 1$$

Also in the case of heavy particles as droplets the Stokes number is considered to be larger than one. Then, η_r, which is the inverse of the turbulent Stokes number, is smaller with respect to one, and k_2 is so small with respect to k_1.

$$b << 1 \quad \text{and} \quad \eta_r << 1 \Rightarrow \left[\frac{b^2+\eta_r}{1+\eta_r}\right] << 1 \Rightarrow k_2 << k_1$$

In a case where η_r much larger than one, k_2 will stay smaller than k_1 but it can reach a value comparable to k_1.
It is necessary to note here that there are two ways to use the model Tchen-Hinze with the model $R_{ij} - \varepsilon$. The first method is to calculate each component of the Reynolds turbulent stress tensor of the droplets $R_{ij,2}$ from its corresponding term in $R_{ij,1}$ via the algebraic formulas of Tchen model equation (4.30),

$$R_{ij,2} = R_{ij,1}\left[\frac{b^2+\eta_r}{1+\eta_r}\right] \qquad R_{ij,12} = 2R_{ij,1}\left[\frac{b+\eta_r}{1+\eta_r}\right] \tag{4.33}$$

Due to this method the turbulence anisotropy of the continuous phase is transmitted to the turbulence of the dispersed phase via the linearity of Tchen formulas. The second method is to calculate the turbulent kinetic energy of the continuous phase k_1 as half of the sum of the diagonal components of the Reynolds stress tensor of the continuous phase $R_{ij,1}$. Then, the calculated k_1 is used in the calculation of k_2 considering that the dispersed phase turbulence is isotropic.

Q2-Q12 model

This model assumes that kinetic stress tensor of the droplets $R_{ij,2}$ is isotropic, therefore this stress tensor is calculated by using Boussinesq analogy employing eddy viscosity as a model quantity. The transport equations of the turbulence kinetic energy of the droplets k_2, and the vapor-droplet velocity covariance k_{12}, are derived in the framework of the Lagrangian method using the probability distribution function (pdf) defined in section 2.4.3. The turbulent momentum transfer between fluctuating motions is obtained in terms of fluid particle velocity covariance given by an additional transport equation derived from a stochastic Lagrangian description of the fluid velocity fluctuation along the particle paths based on Langevin-type model.
This model can take into account the effects of collision between the particles, but we will not consider it in the present study where droplet flow is diluted.

Modeling of the droplets' kinetic energy transport equation: k_2 equation In section 2.4, we showed that the transport equation of any mean quantity $\langle\psi\rangle_2$ can be derived in equation via the equation (2.77). Then, here we will start by deriving the transport equation of the particles fluctuating stress tensor $R_{ij,2}$ by substituting ($\psi = u_{2,i}u_{2,j}$) in the equation (2.77), so that

$$\begin{aligned}
\alpha_2\rho_2\left[\frac{\partial}{\partial t}+U_{2,m}\frac{\partial}{\partial x_m}\right]\left\langle u''_{2,i}u''_{2,j}\right\rangle_2 &= \frac{\partial}{\partial x_m}\left[-\alpha_2\rho_2\left\langle u''_{2,m}u''_{2,i}u''_{2,j}\right\rangle_2\right] \\
&- \alpha_2\rho_2\left[\left\langle u''_{2,m}u''_{2,i}\right\rangle_2\frac{\partial U_{2,j}}{\partial x_m}\right. \\
&+ \left.\left\langle u''_{2,m}u''_{2,j}\right\rangle_2\frac{\partial U_{2,i}}{\partial x_m}\right] \\
&+ \left[R_{\sigma,ij}-\left\langle u''_{2,i}u''_{2,j}\right\rangle_2\right]\Gamma_2 \\
&- \alpha_2\rho_2\left[\left\langle\frac{F_{r,i}}{m_2}u''_{2,j}\right\rangle_2+\left\langle\frac{F_{r,j}}{m_2}u''_{2,i}\right\rangle_2\right]
\end{aligned} \tag{4.34}$$

- The first term on the right hand side of the equation represents the transport of the kinetic stress by the velocity fluctuations and is approximated using an eddy-diffusivity closure assumption derived from the third-momentum mean transport and velocity shear influence

$$\frac{\partial}{\partial x_m}\alpha_2\rho_2\left\langle u''_{2,m}u''_{2,i}u''_{2,j}\right\rangle_2 = -\frac{\partial}{\partial x_m}\left[\alpha_2\rho_2 K^{kin}_{2,mn}\frac{\partial}{\partial x_n}\left\langle u''_{2,i}u''_{2,j}\right\rangle_2\right] \quad (4.35)$$

where, $K^{kin}_{2,mn}$, the kinetic stress diffusivity tensor is written

$$K^{kin}_{2,mn} = \left[\frac{\tau^t_{12}}{\xi^t_{12}}R_{mn,12} + \frac{\tau^F_{12}}{\xi^F_{12}}\left\langle u''_{2,m}u''_{2,n}\right\rangle_2\right] \qquad \sigma_q = 1 \quad (4.36)$$

where

$$\xi^F_{12} = \frac{5}{9} \quad \xi^c = \frac{8}{25} \quad \xi^t_{12} = \frac{3}{2}\frac{C_\mu}{C_s} \quad C_s = 0.25$$

- The second term is the production by the mean particle velocity gradient, and does not need to be modeled.

- The third term is the influence of the interfacial mass transfer, and it is neglected in our present case.

- The last term is the interaction with the fluid turbulent motion, and leads to production or destruction of the particle velocity variance with respect to the fluid particle velocity covariance. This term represents the influence of the interfacial momentum transfer which is noted by M'_k or $F_{r,m}$ in the previous chapters. The derivation of this term is an important point and it reads

$$\begin{aligned}
\left\langle \frac{F_{r,m}}{m_2}\frac{\partial u_{2,i}u_{2,j}}{\partial u_{2,m}}\right\rangle_2 &= \left\langle \frac{F_{r,m}}{m_2}\left[u_{2,j}\frac{\partial u_{2,i}}{\partial u_{2,m}} + u_{2,i}\frac{\partial u_{2,j}}{\partial u_{2,m}}\right]\right\rangle_2 \\
&= \left\langle \frac{F_{r,m}}{m_2}\left[u_{2,j}\delta_{im} + u_{2,i}\delta_{jm}\right]\right\rangle_2 \\
&= \left\langle \frac{F_{r,m}}{m_2}u_{2,j}\delta_{im} + \frac{F_{r,m}}{m_2}u_{2,i}\delta_{jm}\right\rangle_2 (\delta_{im} = 1 \text{ if } i = m) \\
&= \left\langle \frac{F_{r,i}}{m_2}(U_{2,j} + u''_{2,j})\right\rangle_2 + \left\langle \frac{F_{r,j}}{m_2}(U_{2,i} + u''_{2,i})\right\rangle_2 \\
&= \overbrace{\left\langle \frac{F_{r,j}}{m_2}U_{2,i} + \frac{F_{r,i}}{m_2}U_{2,j})\right\rangle_2}^{\text{mean part}} + \overbrace{\left\langle \frac{F_{r,i}}{m_2}u''_{2,j} + \frac{F_{r,j}}{m_2}u''_{2,i}\right\rangle_2}^{\text{turbulent part}}
\end{aligned} \quad (4.37)$$

In the derivation process of the transport equation of the particles kinetic stress tensor, we substract the momentum balance equation. It leads to the disappearance of the mean part of the equation (4.37).

The transport equation of the particle kinetic stress tensor (equation (4.34)), takes into account the anisotropy of the particle's turbulence. But this requires the computation of a large number of equations, an equation for each component of the tensor, this imply high CPU time. Therefore, a simpler equation for the particle turbulent kinetic energy, based on the eddy-viscosity assumption, may be derived from the particle kinetic stress equation (equation (4.34)). Assuming that the tensor anisotropy remains small and locally in equilibrium. Thus the kinetic stress tensor components are computed with the help of eddy viscosity as follows:

$$\left\langle u''_{2,i}u''_{2,j}\right\rangle_2 = -\nu_2^{kin}\left[\frac{\partial U_{2i}}{\partial x_j}+\frac{\partial U_{2j}}{\partial x_i}\right]+\frac{2}{3}\delta_{ij}\left[k_2+\nu_2^{kin}\frac{\partial U_{2m}}{\partial x_m}\right] \tag{4.38}$$

Where ν_2^{kin} is the particle eddy-viscosity, which accounts directly for the combined effects of different mechanisms such as: the transport of particle momentum by the fluid turbulence and by their own random motion. The algebraic expression for the eddy-viscosity is obtained from the off-diagonal correlations of equation (4.34) written in quasi- equilibrium homogeneous shear flow, providing that the difference between the fluid and the particle mean velocity gradients remains negligible:

$$\nu_2^{kin} = \left[\nu_{12}^T + \frac{\tau_{12}^F}{2}\frac{2}{3}k_2\right] \tag{4.39}$$

ν_{12}^T is the vapor-droplet turbulent viscosity which is directly referred to the vapor-droplet velocity covariance.

$$\nu_{12}^T = \frac{1}{3}k_{12}\tau_{12}^T \tag{4.40}$$

Then the transport equation governing the particle kinetic energy equation is obtained by summation from the separate diagonal kinetic stress tensor components:

$$\boxed{\frac{\partial}{\partial t}k_2+\overline{u_{2,j}}\frac{\partial}{\partial x_j}k_2=\frac{\partial}{\partial x_j}K_2^{kin}\frac{\partial}{\partial x_j}k_2-\overline{u'_{2,i}u'_{2,j}}\frac{\partial}{\partial x_j}\overline{u_{2,j}}+\Pi_{q2}} \tag{4.41}$$

The first term is the transport term by the velocity fluctuations, where the eddy-diffusivity coefficient K_2^{kin} is

$$K_2^{kin} = \left[\frac{\nu_{12}^T}{\sigma_q}+\frac{5}{9}\tau_{12}^F\frac{2}{3}k_2\right] \qquad \text{with } \sigma_q = 1 \tag{4.42}$$

The second term accounts for the production by the mean particle velocity. The third term represents the inter-phase turbulent kinetic energy transfer rate. For isotropic flows, the expression in equation (4.37) becomes

$$\Pi_{q2} = -2\alpha_2\rho_2\left[\left\langle\frac{F_{r,i}}{m_2}u''_{2,i}\right\rangle_2\right] \tag{4.43}$$

A detailed closure of this term is presented in the following sections.

Modeling of the vapor-droplet velocity correlations: transport equation of k_{12} The term of velocity correlation between the vapor and the droplet, $k_{12} = \left\langle \tilde{u}'_{1,i} u''_{2,j} \right\rangle_2$, appears during the closure of the turbulent parts of the interfacial forces and in the closure model of the particle's kinetic energy. This term plays a role in the turbulent momentum transfer rate between the two phase. The closure problem of this term relates to the condition expectation of the undisturbed fluid velocity fluctuation measured along the particle paths, $\left\langle \tilde{u}'_{1,i} | c_p \right\rangle_2$. The closure of this term, that we defined before as the drift velocity in section 2.4.5, is needed for the closure of the vapor-droplet velocity correlation $\left\langle \tilde{u}'_{1,i} u''_{2,j} \right\rangle_2$. In section 2.4.5, we proposed a simple relation for the modeling of the drift velocity. Here in this section we present a complete closure of this term proposed by Simonin (2000) derived from the stochastic Lagrangian description of the fluid turbulent velocity measured along the particle path using a Langevin-type model.
First, to express this conditional expectation of the undisturbed fluid velocity fluctuation $\left\langle \tilde{u}'_{1,i} | c_p \right\rangle_2$, we define the conditional fluid velocity distribution $f_1(c_f | c_p; x, t)$. Where $f_1(c_f | c_p; x, t)$ is the probability that any given particle with translation velocity u_2 equal to c_p views a locally undisturbed fluid velocity $\tilde{u}_1$ in $[c_f, c_f + \delta c_f]$ who is located in the volume $[x, x + \delta x]$ at instant t.

$$\left\langle \tilde{u}'_{1,j} | cp \right\rangle = \int [c_{f,j} - U_{1,j}] f_1(c_f | c_p; x, t) dc_f \tag{4.44}$$

We should note that this conditional fluid distribution is different than the standard fluid velocity pdf $f_1(c_f; x, t)$. Where $f_1(c_f; x, t)$ is the probable number of fluid particles (discrete vapor elements) with translation velocity u_1 equal to c_f who are located in the volume $[x, x + \delta x]$ at instant t.

$$f_1(c_f | c_p; x, t) \neq f_1(c_f; x, t) \tag{4.45}$$

Then the fluid-particle velocity moments appearing in the momentum balance equation can be written as

$$V_{d,i} = \frac{1}{n_2} \int \left\langle \tilde{u}'_{1,i} | cp \right\rangle f_2 dc_p \tag{4.46}$$

and

$$\left\langle \tilde{u}'_{1,i} u''_{2,j} \right\rangle_2 = \frac{1}{n_2} \int \left\langle \tilde{u}'_{1,j} | cp \right\rangle [c_{p,j} - U_{2,j}] f_2 dc_p \tag{4.47}$$

To simplify these equations, we define the fluid-particle velocity joint probability density function $f_{12}(c_f, c_p; x, t)$ which presents the local instantaneous probable number of particle centers with a given translation velocity $u_p = c_p$ and viewing a fluid velocity $\tilde{u}_f = c_f$. By definition the standard particle

velocity pdf f_2 can be derived from f_{12} by simple integration over the fluid velocity space,

$$f_2(c_p;x,t) = \int f_{12}(c_f,c_p;x,t)dc_f \tag{4.48}$$

and the conditional probability distribution $f_1(c_f|c_p)$ can be written as

$$f_1(c_f|c_p;x,t) = f_{12}(c_f,c_p;x,t)/f_2(c_p;x,t) \tag{4.49}$$

the fluid velocity measured at the particle position and the corresponding particle velocity are random but correlated variables

$$f_{12}(c_f,c_p;x,t) \neq f_1(c_f;x,t)f_2(c_p;x,t) \tag{4.50}$$

Then we can write

$$V_{d,i} = \frac{1}{n_2}\int \left[c_{f,i} - U_{1,i}\right] f_{12}(c_f,c_p;x,t)dc_f c_p \tag{4.51}$$

and

$$\left\langle \tilde{u}'_{1,i}u''_{2,j}\right\rangle_2 = \frac{1}{n_2}\int \left[c_{f,i} - U_{1,i}\right]\left[c_{p,j} - U_{2,j}\right] f_{12}(c_f,c_p;x,t)dc_f c_p \tag{4.52}$$

The evolution equation of f_{12} can be derived in a general manner as follows

$$\frac{\partial f_{12}}{\partial t} + \frac{\partial}{\partial x_j}[c_{p,j}f_{12}] = -\frac{\partial}{\partial c_{p,j}}\left[\langle \frac{du_{2,j}}{dt}|c_p,c_f\rangle f_{12}\right] - \frac{\partial}{\partial c_{f,j}}\left[\langle \frac{d\tilde{u}_{1,j}}{dt}|c_p,c_f\rangle f_{12}\right] \tag{4.53}$$

The closure of the transport equation governing the fluid particle velocity joint probability density function $f_{12}(c_f,c_p;x,t)dc_f c_p$ requires to know the two increment terms $\frac{du_{2,j}}{dt}$ and $\frac{d\tilde{u}_{1,j}}{dt}$. The velocity increment $\frac{du_{2,j}}{dt}$ is already defined in equation (2.69). While the fluid velocity increment measured along the particle paths, $\frac{d\tilde{u}_{1,j}}{dt}$, can be written according to a Langevin type equation. Simonin (2000) writes the Langevin equation of the locally undisturbed fluid velocity increment measured along the particle paths as

$$\begin{aligned}\tilde{u}_{1,i}(x+u_2\delta t, t+\delta t) &= \tilde{u}_{1,i}(x,t) + g_i\delta t - \frac{1}{\rho_1}\frac{\partial P_1}{\partial x_i}\delta t + \frac{\partial}{\partial x_j}\left[\nu_1\frac{\partial U_{1,i}}{\partial x_j}\right]\delta t \\ &+ \left[u_{2,j} - \tilde{u}_{1,j}\right]\frac{\partial U_{1,i}}{\partial x_j}\delta t \\ &+ G_{12,ij}[\tilde{u}_{1,j} - U_{1,j}]\delta t \end{aligned} \tag{4.54}$$

$G_{12,ij}$ is a tensor of order two which is function of averaged values. It refers to the anisotropy of the Lagrangian correlation of the fluid along the trajectory of a particle. So it symbolizes the effects of the crossing trajectories on the

fluid turbulent velocity fluctuations viewed by the particles. Simonin (2000) closed $G_{12,ij}$ by the following approximation.

$$G_{12,ij} = \frac{1}{\tau^t_{12,\perp}}\delta_{ij} - \left(\frac{1}{\tau^t_{12,\parallel}} - \frac{1}{\tau^t_{12,\perp}}\right) p_i p_j \qquad \left(p_i = \frac{V_{r,i}}{|V_r|}\right) \tag{4.55}$$

where $\tau^t_{12,\parallel}$ and $\tau^t_{12,\perp}$ are respectively the Lagrangian time scale of the fluid turbulent measured along the particle path in the direction parallel and orthogonal to the mean relative velocity.
The term accounting for the interaction with the fluid and the effect of external force fields can be written under the explicit form

$$\frac{\partial}{\partial c_{p,j}}\left[\langle\frac{du_{2,j}}{dt}|c_p, c_f\rangle f_{12}\right] = \frac{\partial}{\partial c_{p,j}}\left[\left(g_i - \frac{\rho_1}{\rho_2}\frac{3}{4}\frac{C_D}{d_p}|C_r|[c_{p,j} - c_{f,j}] - \frac{1}{\rho_2}\frac{\partial P_1}{\partial x_j}\right) f_{12}\right] \tag{4.56}$$

According to Langevin type equation, the term in the joint fluid particle pdf equation accounting for the fluid velocity rate of change is

$$\begin{aligned}\frac{\partial}{\partial c_{f,j}}\left[\langle\frac{d\tilde{u}_{1,j}}{dt}|c_p, c_f\rangle f_{12}\right] &= \frac{\partial}{\partial c_{f,j}}\left[\left(g_i - \frac{1}{\rho_1}\frac{\partial P_1}{\partial x_j} + \frac{\partial}{\partial x_m}\left[\nu_1\frac{\partial U_{1,j}}{\partial x_m}\right]\right) f_{12}\right] \\ &+ \frac{\partial}{\partial c_{f,j}}\left[([c_{p,m} - c_{f,m}]\frac{\partial U_{1,i}}{\partial x_m}\right. \\ &+ \left. G_{12,jm}[c_{f,m} - U_{1,m}])f_{12}\right] \\ &- \frac{\partial}{\partial c_{f,j}}\left[\frac{\partial}{\partial c_{f,j}}\left(\frac{1}{2}C_{12}f_{12}\right)\right]\end{aligned} \tag{4.57}$$

From the closed form of the fluid-particle joint pdf equation, we can derive directly transport equation for the drift velocity $V_{d,i}$ using equation (4.53) and equation (4.51)

$$\begin{aligned}\alpha_2\rho_2\left[\frac{\partial}{\partial t} + U_{2,j}\frac{\partial}{\partial x_j}\right] V_{d,i} &= \alpha_2\rho_2\frac{\partial}{\partial x_j}\left[\langle\tilde{u}'_{1,i}u''_{2,j}\rangle_2 - \langle u'_{1,i}u'_{1,j}\rangle_1\right] \\ &- \langle\tilde{u}'_{1,i}u''_{2,j}\rangle_2\frac{\partial}{\partial x_j}\alpha_2\rho_2 \\ &- \alpha_2\rho_2\frac{\partial U_{1,i}}{\partial x_j}V_{d,j} + \alpha_2\rho_2 G_{12,ij}V_{d,j}\end{aligned} \tag{4.58}$$

The substitution of the fluid-particle velocity covariance in the equation (4.53) allows to write the following transport equation:

$$\begin{aligned}\alpha_2\rho_2\left[\frac{\partial}{\partial t}+U_{2,m}\frac{\partial}{\partial x_m}\right]\left\langle\tilde{u}'_{1,i}u''_{2,j}\right\rangle_2 &= \frac{\partial}{\partial x_m}\left[-\alpha_2\rho_2\left\langle\tilde{u}'_{1,i}u''_{2,j}u''_{2,m}\right\rangle_2\right]\\ &- \alpha_2\rho_2\left[\left\langle\tilde{u}'_{1,i}u''_{2,m}\right\rangle_2\frac{\partial U_{2,j}}{\partial x_m}\right.\\ &+ \left.\left\langle u''_{2,m}\tilde{u}'_{1,m}\right\rangle_2\frac{\partial\left\langle\tilde{u}_{1,i}\right\rangle_2}{\partial x_m}\right]\\ &- \alpha_2\rho_2\frac{1}{\tau_{12}^F}\left[\left\langle\tilde{u}'_{1,i}u''_{2,j}\right\rangle_2-\left\langle\tilde{u}'_{1,i}\tilde{u}'_{1,j}\right\rangle_2\right]\\ &+ \alpha_2\rho_2G_{12,im}\left\langle\tilde{u}'_{1,m}u''_{2,j}\right\rangle_2 \qquad (4.59)\end{aligned}$$

- The first term on the right hand side of the equation represents the transport of the velocity covariance by the particle velocity fluctuations, and it is modeled using Boussinesq approximation.
- The second term represents the separate production by the mean particle and fluid velocity gradients respectively.
- The third term is the production rate due to the particle interaction with the fluid turbulent motion.
- The fourth term accounts for viscous dissipation and crossing trajectory effect.

Assuming that the tensor anisotropy remains small and locally in equilibrium, the modeling of the vapor-droplet velocity correlation tensor is also based on an eddy-viscosity assumption, or Boussinesq approximation:

$$\begin{aligned}\left\langle\tilde{u}'_{1,i}u''_{2,j}\right\rangle_2 &= -\frac{\nu_{12}^T}{1+\eta_r}\left[\frac{\partial\overline{u_{1,i}}}{\partial x_j}+\frac{\partial\overline{u_{2,i}}}{\partial x_j}\right]+\frac{1}{3}\delta_{ij}\left[k_{12}+\frac{\nu_{12}^T}{1+\eta_r}\left(\frac{\partial\overline{u}_{1,m}}{\partial x_m}+\frac{\partial\overline{u_{2,m}}}{\partial x_m}\right)\right]\\ &+ \frac{\eta_r}{1+\eta_r}\left[R_{1,ij}-\frac{2}{3}k_1\delta_{ij}\right] \qquad (4.60)\end{aligned}$$

where $k_{12}=\left\langle\tilde{u}'_{1,i}u''_{2,i}\right\rangle_2$, and ν_{12}^T is the vapor-droplet turbulent viscosity accounting for the droplet momentum transport by the vapor turbulence. The transport equation of k_{12} is derived from the separate transport equation governing the vapor-droplet correlation tensor components:

$$\begin{aligned}\frac{\partial k_{12}}{\partial t}+\overline{u_{2,j}}\frac{\partial k_{12}}{\partial x_j} &= \frac{1}{\alpha_2\rho_2}\frac{\partial}{\partial x_j}\left(\alpha_2\rho_2\frac{\nu_{12}^T}{\sigma_q}\frac{\partial k_{12}}{\partial x_j}\right)\\ &- \overline{R_{ij,12}}\frac{\partial\overline{u_{2,i}}}{\partial x_j}-\overline{R_{ij,12}}\frac{\partial\overline{u_{1,i}}}{\partial x_j}-\varepsilon_{12}+\Pi_{q12} \qquad (4.61)\end{aligned}$$

The first term on the right hand side represents the closure of the transport of the covariance k_{12} by the velocity fluctuations, the constant $\sigma_q = 1$. The vapor-droplet covariance dissipation rate due to viscous dissipation and crossing-trajectory effect is

$$\varepsilon_{12} = \frac{k_{12}}{\tau_{12}^T} \tag{4.62}$$

and the inter-phase interaction term Π_{q12} reads

$$\Pi_{q12} = -\alpha_2\rho_2\frac{1}{\tau_{12}^F}\left[\left(1+\frac{\alpha_2\rho_2}{\alpha_1\rho_1}\right)k_{12} - 2k_1 - 2\frac{\alpha_2\rho_2}{\alpha_1\rho_1}k_2\right] \tag{4.63}$$

Interests and applications of the models Tchen-Hinze and Q2Q12

The algebraic model of particle dispersion Tchen-Hinze has been restricted to idealized cases of homogeneous and isotropic turbulence, with small particles and very diluted flows. This model was validated by several authors; it can predict the particle dispersion in simple flows where the density of the particles is smaller than the density of the liquid. Simonin (1991b) has also applied this model to the problem of particle dispersion in turbulent jets, and has shown that this simplified approach predicts the turbulent dispersion of the particles accurately far downstream of the nozzle. But the model cannot accurately predict particle dispersion close to the nozzle exit where the particle radial fluctuation velocity is significantly affected by the injection method. Moreover this model provides an important starting (just after the nozzle) for simulation of droplet evaporation in simple burners typically used in combustion studies, e.g. Masri et al. (1996), which are often carefully designed to produce very little turbulence at the nozzle exit.
As shown in section 4.3, for the case of heavy particles, k_2 is always small with respect to k_1. This conclusion already contradicts with some experimental results in the literature that noticed that the particles may have a turbulent energy that can be even bigger than the turbulent kinetic energy of the fluid.
Owing to their greater inertia, heavy particles retain longer memories of their velocities. Therefore the local particle velocity fluctuation intensity is a function of both inertial influence response to local turbulent fluctuations and a particle's velocity history, so that the particle velocity fluctuation intensity can be larger than the turbulence intensity of the carrier fluid. Higher order closure models, as Q2Q12, is more flexible than Tchen-Hinze model in this regard because the particle and the fluid-particle fluctuating velocity correlations are modeled more rigorously using transport equations rather than algebraic formulations. Q2Q12 should give better results since it separates the production effect due to the shear of the mean particles' velocity and to the interaction with the fluid turbulence.

In our case, droplets are considered as inertial particles, then they may have fluctuations, uncorrelated to those of the carrier fluid, leading to their own dispersion. The droplets in our case are originated from a violent evaporation at the level of the quench front. Therefore, particles may have important turbulent kinetic energy at the inlet of the flow and here the model of Tchen may fail at this level as it was shown for the case of a nozzle. The size of the droplets and the inlet conditions may play a role in reducing the deficiencies of Tchen-Hinze model. Then this simplified modeling stays as a considerable choice, especially when the additional computational expense of the more complex models is considered. A numerical test for these two models, is done in the next chapter to evaluate the advantages and the deficiencies of both models in our case.

4.4 Interpretation of the effect of the prediction of the particles' agitation in channel flow

The turbulence characteristics calculated by the models should be verified experimentally, but unfortunately, no experimental data is available for vapor-droplet flow. Some experimental data exist for the gas-liquid flow but usually they treat cases of spray flow in which special inlet conditions are imposed and they do not account for wall bounded flows e.g Sommerfeld et al. (1993). Experimental data are available for gas-solid flows, for different flow configurations (e.g. geometries, particle sizes, and types). Although gas-particles experiments do not take into account phenomena as droplets evaporation and mass transfer between the two phases, these experiments can give the dynamic characteristics of the flow. Groll et al. (2009) used the experiment of Kulick et al. (1994) to validate his computational code in which he used the model $k - \varepsilon$ for the turbulence modeling of the continuous phase and the model Q2Q12 for the model of the turbulence of the dispersed phase. The experiment of Kulick et al. (1994) is representative of wall bounded flows, and the particles flow is in the same order of scale of the Stokes number of the droplets in our study case. Therefore this experimental database is used to validate our computational code and the turbulence models. But this step is not sufficient, since the experimental data does not provide the spatial distribution of the particles over the tube which is a main characteristic in our work. Therefore this experimental interpretation gives us only a general idea about the numerical code and the models of turbulence. The effects of the turbulence modeling on the droplets distribution is studied, in details, by analyzing numerical simulations results.

A gas-solid flow in a fully developed channel is tested by Kulick et al. (1994). It is a representative configuration dealing with wall-bounded and dispersed flow. The interaction between air, representing the continuous phase, and copper, taken as the dispersed phase is investigated. This flow

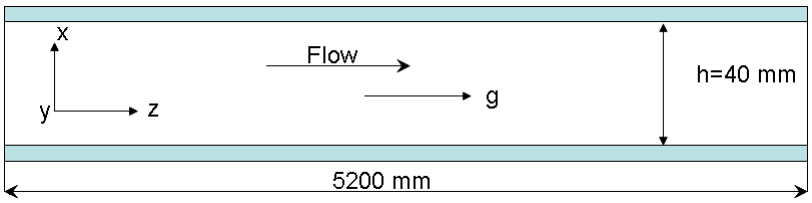

Figure 4.1: Schematic of the channel flow considered

is downward channel flow as shown in figure 4.1, Reynolds number based on the channel height($h = 40mm$) and a single phase centerline velocity ($U_0 = 10.5m/s$), is $Re = 27600$. The flow is considered as fully developed after 150 channel width and at this position it is assumed that the particle velocity and particle turbulence reached an asymptotic state. The copper particles have a density of $\rho^C = 8800kg/m^3$ and the diameter of the particle is $D_p = 70\mu m$. The inlet mass loading of the particles is $Z_0 = 10\%$ (the corresponding volume fraction of the copper α^C can be obtained directly from the formulation: $\alpha^C = \rho^{air} Z/(\rho^C + \rho^{air} Z)$). Groll et al. (2009) used this experiment for the validation of his turbulence modeling with $k - \varepsilon$ for the continuous phase and the model Q2Q12 for the turbulence of the dispersed phase. We simulated the same experimental configuration using different combinations of turbulence models. These simulations are realized by the code Neptune_CFD, with a mesh representing a thin ranch of the channel. The discretization of the mesh is regular in the longitudinal direction with 2450 cells, while in the radial direction the mesh is composed of 100 cells and the size of the cells increase from $y^+ = 1$ near the wall to $y^+ = 25$ at the center of the tube. The first case is done with the model $k - \varepsilon$ for the continuous phase and the model Tchen-Hinze for the dispersed phase, while the second case is done with the model $R_{ij} - \varepsilon$ for the continuous phase and the model Q2Q12 for the dispersed phase. In the following, the different results are compared and evaluated with respect to the experimental results.

Figure 4.2 and figure 4.3 show the comparison between the experimental data and numerical simulations for the streamwise mean velocity and the streamwise and normal-to-wall turbulence intensities for the continuous phase. For the gaseous phase both models give a very good agreement with the experimental results for the streamwise mean velocity component. The experiment shows an anisotropy in the turbulence components of the gaseous phase. The isotropic values simulated by $k - \varepsilon$ are near to the streamwise turbulent intensity and overestimate the normal-to-wall turbulent intensity; this result is similar to the result obtained by Groll et al. (2009). $R_{ij} - \varepsilon$ is more able to produce this anisotropy but the values are overpredicted especially the normal-to-wall turbulence intensity. The peak near to the wall is not reached by any model. The modeling of the

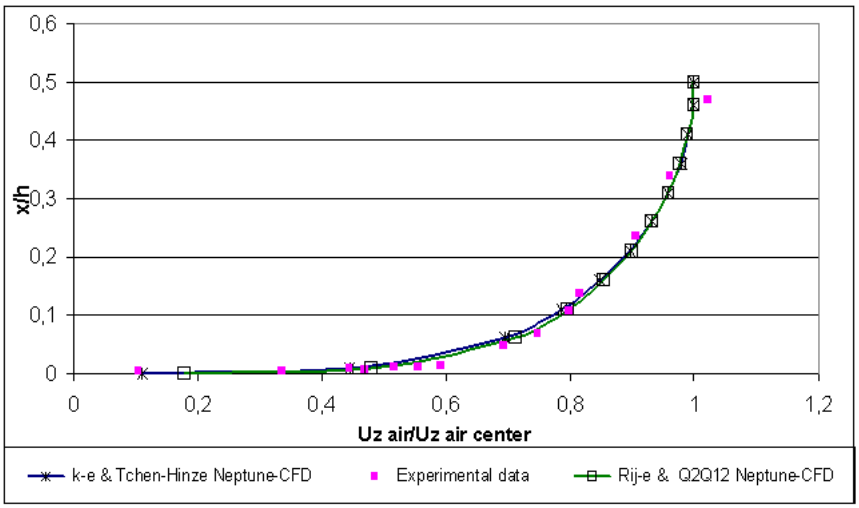

Figure 4.2: Comparison of mean value velocity of air(x/h: normalized distance from the wall; $U_{z,air}/U_{z,air,center}$: normalized mean air velocity with respect to the air velocity at the channel center

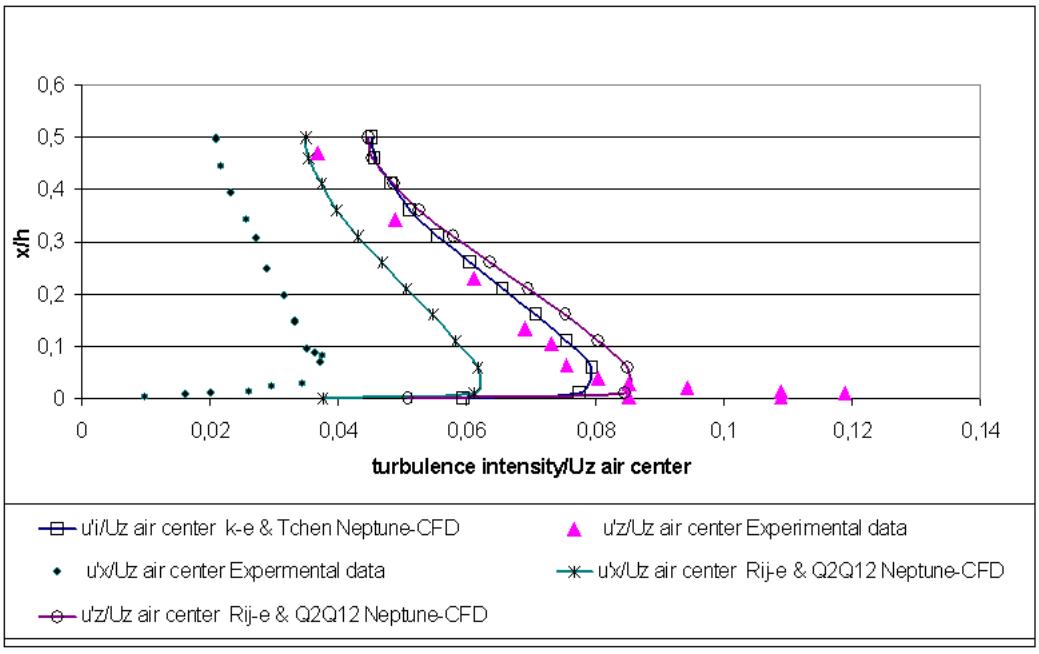

Figure 4.3: Stream wise and normal to wall turbulence intensities of the continuous phase

turbulence anisotropy may have an impact on the droplets distribution, but the experimental database does not provide any data to analyze this impact.

Figures 4.4 and 4.5 show the comparison between the experimental

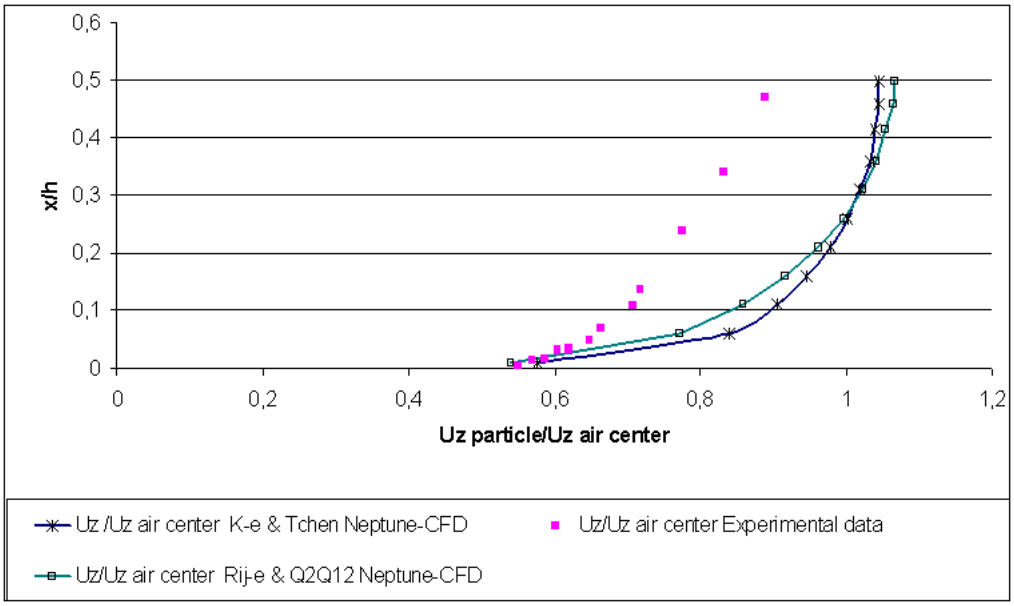

Figure 4.4: Comparison of mean value velocity of the dispersed phase

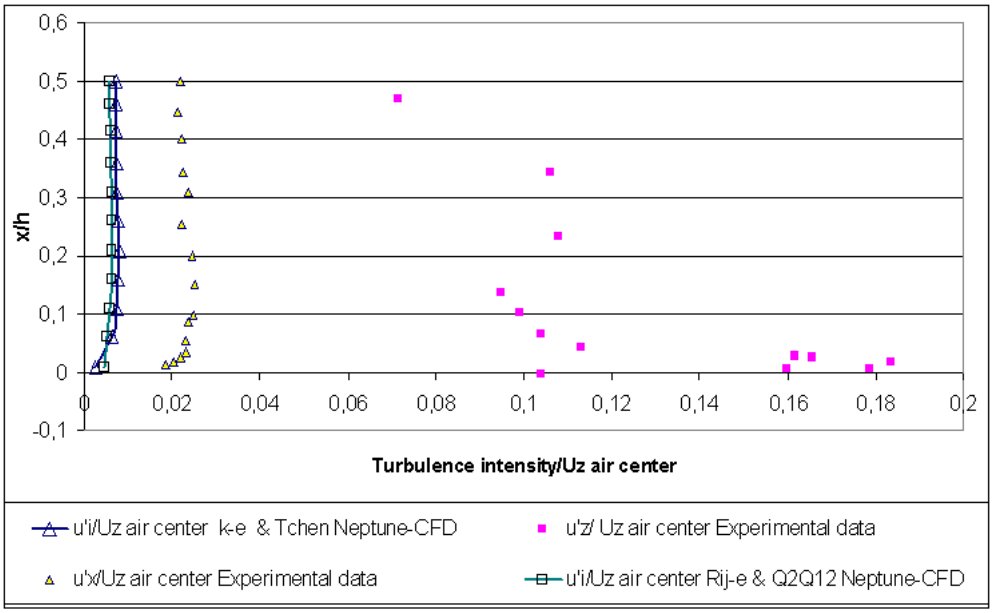

Figure 4.5: Stream wise and normal-to-wall turbulence intensities of the dispersed phase

and numerical results for the streamwise mean velocity, the stream-wise

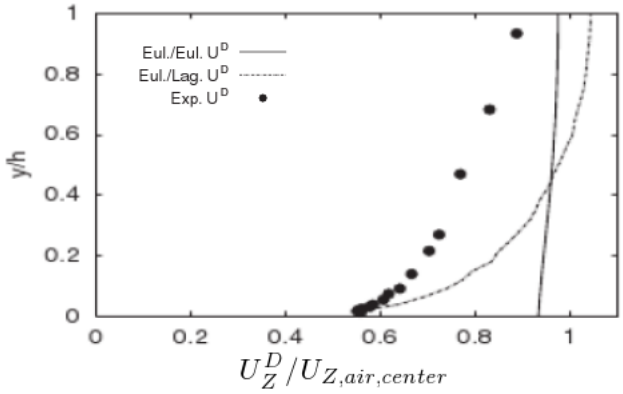

Figure 4.6: Comparison of mean value velocity of the dispersed phase, figure taken from Groll et al. (2009) to show the results obtained by the method Euler/Lagrange

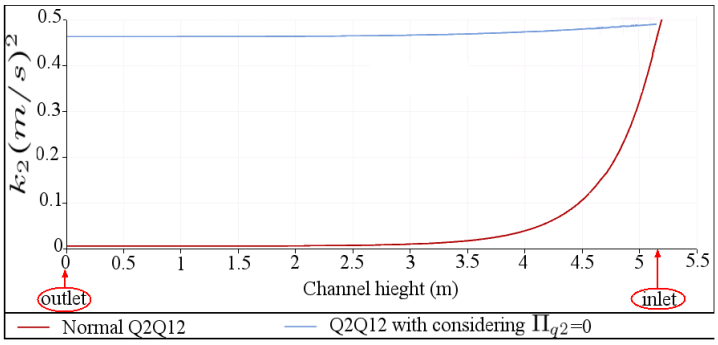

Figure 4.7: Two cases with considering a high value of particles turbulent kinetic energy at the inlet $k_2 = 0.5(m/s)^2$: first case using Q2Q12 with no modification; second case considering that the effect of the vapor on the droplets turbulence is equal to zero $\Pi_{q2} = 0$

and normal-to-wall turbulent intensities for the dispersed phase. In the two simulated cases, the calculated values of the particle velocity is over predicted with respect to the experimental values. Experiments show that the particles are decelerated by the vapor all over the channel radial section. All the computational approaches show no capability in reproducing this feature. This effect of deceleration of the particles in the experimental case can not be explained since in used modeling there is no force that acts against the gravitational force on the heavy particles. Groll et al. (2009) have simulated this case by using two approaches, Euler/Euler and Euler/Lagrange as shown in figure 4.6. In the Euler/Euler approach the calculated particle's velocity is uniform over the entire channel cross section, while Euler/Lagrange approach gives the similar profile shape of

the experimental results but also with the overpredicted values. Our results are more comparable to Euler/Lagrange results, this may be explained due to model used for calculating the drag coefficient. In our model the drag coefficient is calculated in terms of the particulate Reynolds number which is, in term, based on the particle diameter and the relative velocity modulus that takes into account turbulence and fluctuating velocity covariance as seen in equation (4.11). While for the drag force model in Euler/Euler approach of Groll's simulation the relative velocity was calculated simply as the difference between the averaged velocities of the two phases.
The analysis of the experimental data for the vapor and the particle agitations show that the particle turbulence is important and comparable to the air turbulence. Moreover the experimental results show strong anisotropy of the particles turbulence, figure 4.5. The simulated cases show incapability of both models Tchen-Hinze and Q2Q12 to calculate these characteristics of the particles fluctuations. For the anisotropy, it is expected that both models fail since both of them are based on a theory of isotropy. Moreover while analyzing the model Tchen-Hinze, it is expected that this model underestimate the turbulent kinetic energy of the droplets. But Q2Q12 is expected to have a better simulation for the magnitude of the turbulent kinetic energy of the dispersed phase k_2 since it takes into account the particle's own fluctuations. Therefore the detailed analysis about this result had been done to verify the reasons behind this failure of the model Q2Q12. Unlike Tchen-Hinze model, Q2Q12 model permits us to impose a value for the turbulent kinetic energy and the gas-particle velocity correlation at the inlet of the channel. Since these values are not specified from the experimental data, several values of the turbulent kinetic energy of the particle are imposed as entry boundary conditions. These cases showed us that, the for established flows the model estimates a value of k_2 which is independent of the values at the inlet. In figure 4.7, we show a test case where we imposed a high turbulent kinetic energy of the vapor at the inlet $k_2 = 0.5$. We noticed that in the case where we used the model Q2Q12 without any modification, this value of k_2 decays to the environ of zero and its value becomes similar to the value calculated by the model of Tchen-Hinze. Therefore more detailed analysis of the modeling method has been done. The analysis over the several terms of the transport equation of k_2 shows that the term of the inter phase-turbulent energy transfer is the main term that cause the attenuation of k_2. Also in figure 4.7 we show another test case where we neglected the interfacial transfer term of the turbulent kinetic energy. This test case shows that k_2 maintains its high value when $\Pi_{q2} = 0$. Therefore a detailed study about the closure of this term is presented in the next section of this chapter.

4.5 Turbulent coupling

The dispersion of the droplets and the turbulence of the ambient vapor by the dispersed droplets are two coupled phenomena. The effect of the vapor turbulence on the droplets dispersion and agitation as well as the effect of the presence of the droplets on the vapor turbulence are major phenomena in vapor-droplet flow. This is known as turbulence modification or two-way coupling. The effect of the droplets on the fluid turbulence is presented in the model of the term Π_{q1} while the effect of the vapor turbulence on the droplets dispersion is presented by the term Π_{q2}.

4.5.1 Bibliographical review

In the past, numerous studies have been performed on the effect of the dispersed particles on the fluid turbulence. These studies show that many parameters have been involved in the determination of the turbulent modification. First Gore and Crowe (1989) summarized the previous works and concluded that the ratio between the particle diameter and the fluid length scale could be used to distinguish the regimes of turbulence increase or attenuation. They noted that small particles tends to attenuate the turbulence while large particles increase the turbulence. But Yarin and Hestroni (1993) found that small particles could also enhance the turbulence in some cases. Hestroni (1989) proposed that particles with low particles Reynolds number Re_p tend to suppress the turbulence whereas particles with high Re_p would enhance the turbulence. However, the experimental work of Hardalupas et al. (1989) showed that particles without wake shedding (small Re_p) could also increase the turbulence. Eaton and Fessler (1994) reviewed previous experimental and numerical studies and pointed out that dramatic turbulence attenuation took place when the mass loading ratio was greater than 0.1. Sato et al. (2000) claimed that the inter-particle spacing was a more critical parameter for turbulence modification than the particle diameter. The experimental results of Kulick et al. (1994) show that particles attenuate the turbulence, as the Stokes number, mass loading and the distance from the wall increases . This agrees with the DNS results of Sundaram and Collins (1999) which show that when the Stokes number increases, the fluid turbulence decreases. Lately in a detailed DNS, Lucci et al. (2010) cited the following: particles with diameter of the order of Taylor's length-scale always reduce the turbulent kinetic energy of the fluid. If the volume fraction and diameter of particles are fixed, the turbulence decreases as we increase the ratio of the particle density over the fluid density. If the inertia and volume are fixed, smaller particles diameters attenuate the turbulence more than the larger particles. Among these studies, although some consensus has been reached, many of the explanations remain not clear and even contra-

dict with each other. This bibliographical review shows that the effect of the presence of the droplets on the fluid turbulence depends on a large number of important parameters as particle diameter, particles Stokes number, particle Reynolds number, particle/fluid density ratio, flow structure and presence of the walls.
On the other hand, we have the effect of the fluid turbulence on the droplets dispersion. In turbulent flows droplets motion is directly connected to the ability of the droplets to respond to the large turbulent structure. The response of the particles to the fluctuations in the fluid velocity is also a challenging phenomena which is difficult to predict. For several authors, Stokes number is the main parameter that characterizes how quickly a particle responds to the turbulent fluctuation of carrier phase. Luo et al. (2006) have realized a DNS of gas-particle flow considering particles with different Stokes numbers (calculated as the ratio of the particle aerodynamic response time to the time scale associated with the large-scale organized vortex structures in the free shear flows) in a turbulent jet flow. They noted that for large scale turbulent structures, particles with low Stokes number (st=0.01) follow the vortex motion, also for (st=0.1) the particles tends to distribute uniformly, while for (st=1) particles concentrate in the outer layers of the large turbulent structures and finally for (st=10) particles move down stream through the vortex structure with small lateral dispersion. Besides, for small turbulence structures particles with (st=0.01, 0.1 and 1) tends to distribute uniformly in the flow while for (st=10) most particles directly move down stream with rectilinear paths with very small lateral dispersion.
In our case the volume fraction of the dispersed phase is small enough to assure that the dispersion is governed by the turbulent flow (i.e. particle collisions can be neglected). However, the droplet mass-loading ratio $\phi = \dot{m}_d/\dot{m}_1$ (where $\dot{m}_d$ and $\dot{m}_1$ represents the droplets and the vapor mass flow rates respectively) is large enough to introduce significant mean and turbulent energy exchanges between the two phases. Moreover in the study of water-vapor flow, we are interested to a wide spectrum of droplets sizes. Therefore, some droplets may be small enough to respond to some of the vapor velocity fluctuations but they remain too massive to act as a vapor element. More massive particles can be partially responsive or not responsive to the vapor velocity fluctuation.
In Euler/Euler simulations these two-way coupling phenomena are modeled via the inter-phase turbulent kinetic energy transfer terms. Turbulent quantities of the continuous phase such as the kinetic energy and dissipation, are modified directly by the dispersed phase through the interfacial momentum transfer. To take this into account extra source/sink terms are added to the transport equations of the continuous phase turbulence. Although large number of experimental and DNS studies had been done to characterize these phenomena, few references study the modeling of these terms in Euler/Euler modeling. In the previous chapters, two terms of turbulent

kinetic energy inter-phase transfer appear: First term is Π_{q1} which appears in the transport equation of the continuous phase (in both cases $k-\varepsilon$ and $R_{ij}-\varepsilon$). The second term is Π_{q2} which appears in the transport equation of the turbulent kinetic energy of the dispersed phase when Q2Q12 model is used. Our analysis shows that the term Π_{q1} plays a secondary role in the turbulent kinetic energy modeling of the continuous phase beside the other terms. While the term Π_{q2} plays a major role in the turbulent kinetic energy of the dispersed phase as shown in figure 4.6. The analysis of the experimental case of Kulick et al. (1994) shows that the turbulent kinetic energy of the droplets is under-estimated, because of an overestimation of Π_{q2}. In the following, the closure of the two terms is studied and finally a new closure is proposed for the modeling of Π_{q2}

4.5.2 Closure Models of Π_{q1} and Π_{q2} in Q2Q12

The term Π_{q2} is defined in equation (4.43). By applying the same steps of derivation presented in equation (4.37) we can write

$$\Pi_{q1} = -2\frac{\alpha_2\rho_2}{\alpha_1\rho_1}\left[\left\langle \frac{F_{r,i}}{m_2}\tilde{u}'_{1,i}\right\rangle_2\right] \tag{4.64}$$

For modeling this term, Simonin (2000) used the work of Gatignol (1983) that proposes an approximate form for the fluid forces acting on a particle in terms of the undisturbed surrounding fluid flow velocity. According to Gatignol's analysis, the given approximation is valid for low particle Reynolds number, if the size of the sphere is of the order of (or smaller than) the characteristic length scale of the undisturbed fluid flow. For heavy particles (with respect to gas density: $\rho_2 >> \rho_1$) the volume force induced by the surrounding flow reduces to the drag force contribution.

$$f_{r,i} = -\rho_1\frac{3}{4}\frac{C_D}{d_p}|v_r|v_{r,i} \tag{4.65}$$

where $v_r = u_2 - \tilde{u}_1$ is the local instantaneous relative velocity. It is the difference between the particles with velocity u_2 and the surrounding fluid velocity $\tilde{u}_1$, locally undisturbed by the presence of the particle measured at the particle position. C_D, and d_p are the respectively the drag coefficient and the particle diameter defined in previous chapters. By averaging

$$\left\langle \frac{f_{r,i}}{m_2}\right\rangle_2 = -\frac{1}{\tau_{12}^F}\left\langle v_{r,i}\right\rangle_2 \tag{4.66}$$

where the τ_{12}^F is the mean particle relaxation time defined before as

$$\tau_{12}^F = \frac{\rho_2}{\rho_1}\frac{4}{3}\frac{d_p}{C_D}\frac{1}{\left\langle|v_{r,i}|\right\rangle_2} \tag{4.67}$$

An important note here, that this complex form of the particle response time scale can be simplified to the well known form of Stokes number.

$$st = \frac{\rho_2 d_p^2}{18\mu_1}$$

If we consider that $Re_p = 1$ for all particles then the product of C_D and Re_p is approximately equal to 24 (according to the definition of C_D in equation (2.105)). If we replace $\langle |v_{r,i}| \rangle_2$ by $\frac{\nu_1 Re_p}{d_p}$ in equation (4.67) we can write

$$\tau_{12}^F = \frac{\rho_2}{\rho_1} \frac{4}{3} \frac{d_p^2}{C_D} \frac{1}{\nu_1 Re_p} \simeq \frac{\rho_2 d_p^2}{18\mu_1} \tag{4.68}$$

τ_{12}^F is another form of the Stokes number that can be broadened to larger values of Re_p, because it accounts roughly for the non-linear dependence of the drag coefficient on the instantaneous relative velocity.
The closure of the term Π_{q2} can be derived as follows, starting from

$$\Pi_{q2} = 2\alpha_2 \rho_2 \left\langle \frac{F_{r,i}}{m_2} u''_{2,i} \right\rangle_2$$

we use the equation (4.66) to write

$$\Pi_{q2} = -2\alpha_2 \rho_2 \frac{1}{\tau_{12}^F} \left\langle u''_{2,i} v_{r,i} \right\rangle_2$$

by decomposing v_r into a mean and a fluctuating part

$$\begin{aligned} \Pi_{q2} &= -2\alpha_2 \rho_2 \frac{1}{\tau_{12}^F} \left\langle u''_{2,i} [V_{r,i} + v'_{r,i}] \right\rangle_2 \\ &= -2\alpha_2 \rho_2 \frac{1}{\tau_{12}^F} \left\langle u''_{2,i} v'_{r,i} \right\rangle_2 \end{aligned}$$

then we replace $v'_{r,i}$ by $u''_{2,i} \tilde{-} u'_{1,i}$

$$\Pi_{q2} = -2\alpha_2 \rho_2 \frac{1}{\tau_{12}^F} [\left\langle u''_{2,i} u''_{2,i} \right\rangle_2 - \left\langle \tilde{u}''_{2,i} \tilde{u}'_{1,i} \right\rangle_2]$$

finally we use $k_2 = 1/2 \left\langle u''_{2,i} u''_{2,i} \right\rangle_2$ and $k_{12} = \left\langle \tilde{u}''_{2,i} \tilde{u}'_{1,i} \right\rangle_2$ to write

$$\Pi_{q2} = -2\alpha_2 \rho_2 \frac{1}{\tau_{12}^F} [2k_2 - k_{12}] \tag{4.69}$$

For Π_{q1}, we repeat the same steps. The only difference that appears here is that $\left\langle \tilde{u}'_{1,i} \right\rangle_2 = V_{d,i}$ and not equal to zero. Therefore we have an extra term

in the final closure of Π_{q1}

$$\begin{aligned}
\Pi_{q1} &= 2\frac{\alpha_2\rho_2}{\alpha_1\rho_1}\left\langle \tilde{u}'_{1,i}\frac{F_{r,i}}{m_2}\right\rangle_2 \\
&= -2\frac{\alpha_2\rho_2}{\alpha_1\rho_1}\frac{1}{\tau_{12}^F}\left\langle \tilde{u}'_{1,i}v_{r,i}\right\rangle_2 \\
&= -2\frac{\alpha_2\rho_2}{\alpha_1\rho_1}\frac{1}{\tau_{12}^F}\left\langle \tilde{u}'_{1,i}[V_{r,i}+v'_{r,i}]\right\rangle_2 \\
&= -2\frac{\alpha_2\rho_2}{\alpha_1\rho_1}\frac{1}{\tau_{12}^F}[\left\langle \tilde{u}'_{1,i}u''_{2,i}\right\rangle_2 - \left\langle \tilde{u}'_{1,i}\tilde{u}'_{1,i}\right\rangle_2 + \left\langle \tilde{u}'_{1,i}V_{r,i}\right\rangle_2] \\
&= -2\frac{\alpha_2\rho_2}{\alpha_1\rho_1}\frac{1}{\tau_{12}^F}[V_{r,i}V_{d,i}+k_{12}-2k_1] \qquad (4.70)
\end{aligned}$$

4.5.3 Models' limitations from bibliography

This closure method has been analyzed and compared to other methods by several authors. That allows us to make a critical review of this modeling.
First, Ferrand et al. (2003) have realized an experimental study on the gas-droplets interaction, in an axisymmetric jet laden with partly responsive droplets. They tested the modeling of the term Π_{q1} presented above to droplets flow with several Stokes number. Their tests start from totally responsive droplets with very low Stokes number (st«1), which are able to follow the smallest turbulent scales. Then they noted that all droplets becomes at least partially responsive to the gaseous fluctuations. Ferrand et al. (2003) lighted on the interest of gas-droplet turbulent velocity correlation k_{12} while working with wide range of partially responsive droplets. These correlations are expected to be negligible for the big droplets (st»1). On the contrary they are equivalent to the fluid Reynolds stress for the smallest droplets (st«1). An intermediate behavior depending on the droplet size is expected for partially responsive droplets. Therefore they evaluated experimentally the weight of the gas-droplets correlations on the direct turbulent interaction between phases. And finally concluded that neglecting these terms leads to overestimate the magnitude of the attenuation term. Besides, for the droplets turbulence Ferrand et al. (2003) detected a different behavior between the radial and the longitudinal kinetic stresses of the droplets. The radial stress decreases when the droplet diameter increases, while the longitudinal stress remains corresponding for the fluid longitudinal Reynolds stress for droplet diameters smaller than 50 μm and grows up for larger sizes. This is due to the production of the longitudinal kinetic stress by the mean particle velocity gradient. This production term is the source of the strong anisotropy observed for the droplet fluctuating motion.
Other studies were done by Xu and Subramaniam (2006) and Xu and Subramaniam (2007) who present one of the rare detailed studies on this subject. Xu and Subramaniam (2006) tested the model of Simonin against the

DNS results obtained by Sundaram and Collins (1999). These DNS results simulate the case of spherical solid particles evolving in freely decaying homogeneous turbulent flow. The flow is diluted, with particle density much larger than fluid density ($\rho_2/\rho_1 \simeq 1000$); and particle size is in the sub-Kolmogorov range. In this study, the Stokes number $St = \tau_p/\tau_f$, is defined as the ratio of the characteristic particle momentum response time τ_p to a characteristic flow time scale τ_f which is chosen to be the Kolmogorov time scale. These DNS results show that the turbulent energy of both phases decreases monotonically and that the net effect of particles is to reduce fluid energy. Moreover, the attenuation effect of the particles on the fluid turbulence grows with increasing particle Stokes number. The particle turbulent energy also decays monotonously in time, and the decay rate increases with increasing particle Stokes number (for fixed mass loading). Xu and Subramaniam (2006) found that the prediction from model of Simonin agrees with the DNS that turbulent kinetic energy of the fluid phase decreases monotonically, but the net effect of particles to reduce fluid energy is found to decrease with increasing Stokes numbers, which is opposite to the DNS result. The model predictions for fluid energy evolution also show a much steeper decay at the beginning than the DNS result. The same steep decay is also observed in the particle energy evolution. The decay of particle energy is observed to increase with increasing particle Stokes numbers, which is consistent with DNS data but there is some crossover at the beginning of evolution. The physical reason behind the incorrect behavior of k_1 evolution with increasing particle Stokes number in Simonin model, and the anomalous steep decay of k_2 at early time lies in the fact that the particle response time is the appropriate time scale for only a limited range of particle-eddy interactions. In reality, particle-turbulence interaction is a complex multi-scale process. Even for a mono-disperse gas-solid two-phase flow, particles interact with a range of eddies with different lengths and time scales. Furthermore, the particle response time and the Stokes number for each particle are different, since each particle has a different instantaneous velocity. The particle response time, defined here, can only represent the characteristic time scale of particles interacting with the eddies in the dissipation range. To solve this problem Xu and Subramaniam (2006) proposed a multi scale interaction model. This model impose a new time scale that is able to estimate small Stokes number for energetic eddies and large Stokes number for small fluctuations. When this modeling of the time scale was implemented in the model of Simonin the steep decay of k_1 and k_2 was corrected. Moreover it corrects the prediction of the fluid turbulent kinetic energy evolution with variation of particles Stokes number.

Xu and Subramaniam (2007) proved a constraint associated with mean momentum equation for particle-laden flows. In a limiting study case of turbulent multiphase flows, the flow is statistically homogeneous, isothermal and in zero-gravity environment. If the gravity is considered equal to zero and

the mean velocity fields are homogeneous, the mean pressure gradient is zero and the mean momentum equation system results in the trivial solution of zero mean velocity in each phase, which implies a zero mean slip velocity. Also collisions are assumed to be elastic and therefore there is no energy loss through collisions. If the flow field is initialized with zero mean velocity in both phases, the mean velocities will remain zero. In this case, the evolution of second-moments of fluctuating velocity is solely influenced by inter-phase turbulent kinetic energy TKE transfer and viscous dissipation in the fluid phase(without effects of the mean velocity gradients). For this limiting case, the turbulent flow equations are written in the following form:

$$\begin{aligned} \alpha_1\rho_1\frac{\partial k_1}{\partial t} &= \Pi_{q1} - \alpha_1\rho_1\varepsilon_1 \\ \alpha_2\rho_2\frac{\partial k_2}{\partial t} &= \Pi_{q2} \end{aligned} \tag{4.71}$$

The constraint of Xu and Subramaniam (2007) is that the mean inter-phase turbulent momentum transfer is conservative, i.e., equal and with opposite signs for both phases.

$$\Pi_{q1} = -\Pi_{q2} \tag{4.72}$$

If we define the turbulent kinetic energy of the mixture as

$$e_m = \alpha_1\rho_1 k_1 + \alpha_2\rho_2 k_2$$

then according to the conservation of the mean inter-phase momentum transfer in the special case we can write

$$\frac{\partial e_m}{\partial t} = -\alpha_1\rho_1\varepsilon_1 \tag{4.73}$$

This relation should be applied by any model to consider it as a conservative model. The implication of this constraint on the model of Simonin yields

$$\begin{aligned} \alpha_1\rho_1\frac{\partial k_1}{\partial t} &= \alpha_2\rho_2\frac{1}{\tau_{12}^F}(k_{12} - 2k_1) - \alpha_1\rho_1\varepsilon_1 \\ \alpha_2\rho_2\frac{\partial k_2}{\partial t} &= \alpha_2\rho_2\frac{1}{\tau_{12}^F}(2k_2 - k_{12}) \end{aligned} \tag{4.74}$$

$$\tag{4.75}$$

The resulting evolution equation of the specific mixture energy is

$$\frac{\partial e_m}{\partial t} = 2\alpha_2\rho_2\frac{1}{\tau_{12}^F}(k_{12} - k_1 - k_2) - \alpha_1\rho_1\varepsilon_1 \tag{4.76}$$

Then the model of Simonin is not conservative.
In this bibliographical review above, we showed the advantages of the used

turbulence coupling closure model as found by Ferrand et al. (2003). In their study, Ferrand et al. (2003) focused on the modeling of the term Π_{q1} and the importance of the term k_{12} while they did not discuss the closure of the term Π_{q2}. In the previous section, we showed the critical role played by the term Π_{q2} and the need to close this term in a different way. The work of Xu and Subramaniam (2007), Xu and Subramaniam (2006), and Sundaram and Collins (1999) present a good analysis of the closure of the turbulence coupling and provided some arguments about the modeling. These references propose two ways to ameliorate this modeling. The first one is by considering a multi time scale interaction model whereas the second way is to find a model that applies the conservative constraint ($\Pi_{q1} = -\Pi_{q2}$). According to our knowledge these studies are from the rare studies that treat this particularity of the flow and can provide a good reference for proposing any amelioration to the model. In the next section, we will propose another modeling for the term Π_{q2} based on the hypothesis of separating the turbulence scales.

4.5.4 Turbulence coupling model based on multi turbulent scales

In this model we propose a correction solution for the term Π_{q2} by analogy with the work of the separation of the scale which has been proposed by several authors for the closure of the term Π_{q1} (Chahed (1999), "Standard" model[1], etc.). We show that it is possible to define a turbulent scale separation on the different terms that compose the turbulent kinetic energy interfacial transfer. This separation is important for our modeling which aims to ameliorate the prediction of the turbulent energy of the droplets inside the flow.

This is based on separating the turbulence interaction between the particle and its surrounding fluid into two scales. From the fluid point of view, a particle can enhance the turbulence of the fluid by the fluctuations in the wake. This is considered as fluid turbulence production, and it is produced at a scale smaller than the size of the particle (which means small turbulent scales). On the other hand the particle acts on the destruction of the fluid turbulence when it traverse the large eddies. Looking from a particle point of view permits us to assume that the production term for the fluid in the wake is viewed as destruction term for the particles fluctuation; and on the other side the destruction of the fluid turbulence, when particle crosses a large eddy, represents a production term for the particle fluctuation.

This understanding of the turbulence exchange is modeled by decomposing the term of the turbulent interaction between the two phases into two terms. One represents the destruction at the level of the wake for small eddies. The second one represents the production particle velocity fluctuation at the scale

[1] Turbulent model used in the calculation code ASTRID

of large eddies.
Starting from the definition of the term Π_{q2}

$$\Pi_{q2} = -\left\langle u''_{2,i}\frac{F_{r,i}}{m_2}\right\rangle_2 \tag{4.77}$$

Then the fluctuating relative velocity is decomposed as the difference between the fluctuating velocity of the particle and the fluctuating velocity of the fluid

$$v'_{r,i} = u''_{2,i} - \tilde{u}'_{1,i} \rightarrow u''_{2,i} = v'_{r,i} + \tilde{u}'_{1,i} \tag{4.78}$$

then $\left\langle \frac{F_{r,i}}{m_2}u''_{2,i}\right\rangle_2$ is decomposed as

$$\left\langle \frac{F_{r,i}}{m_2}u''_{2,i}\right\rangle_2 = \overbrace{\left\langle \tilde{u}'_{1,i}\frac{F_{r,i}}{m_2}\right\rangle_2}^{\tilde{\Pi}_{q2}} + \overbrace{\left\langle v'_{r,i}\frac{F_{r,i}}{m_2}\right\rangle_2}^{\Pi_w} \tag{4.79}$$

Π_w is considered to be the term of destruction of the particle agitation and it equals the energy of the eddies produced in the wake of the droplet. $\tilde{\Pi}_{q2}$ is the term of the production of the turbulence agitation when it crosses the large eddies. This term can be written as

$$\begin{aligned}
\tilde{\Pi}_{q2} &= \left\langle \tilde{u}'_{1,i}\frac{F_{r,i}}{m_2}\right\rangle_2 \qquad (4.80)\\
&= -\frac{1}{\tau_{12}^F}\left\langle \tilde{u}'_{1,i}[u_{2,i} - \tilde{u}_{1,i}]\right\rangle_2\\
&= -\frac{1}{\tau_{12}^F}\left\langle \tilde{u}'_{1,i}[U_{2,i} + u''_{2,i} - U_{1,i} - \tilde{u}'_{1,i}]\right\rangle_2\\
&= -\frac{1}{\tau_{12}^F}[\left\langle \tilde{u}'_{1,i}U_{2,i}\right\rangle_2 + \left\langle \tilde{u}'_{1,i}u''_{2,i}\right\rangle_2 - \left\langle \tilde{u}'_{1,i}U_{1,i}\right\rangle_2 - \left\langle \tilde{u}'_{1,i}\tilde{u}'_{1,i}\right\rangle_2]\\
&= -\frac{1}{\tau_{12}^F}[U_{2,i}V_{d,i} + k_{12} - U_{1,i}V_{d,i} - 2k_1^L]
\end{aligned}$$

In the same steps we can get

$$\begin{aligned}
\Pi_w &= \left\langle v'_{r,i}\frac{F_{r,i}}{m_2}\right\rangle_2\\
&= -\frac{1}{\tau_{12}^F}[2k_2 - U_{2,i}V_{d,i} - 2k_{12} + U_{1,i}V_{d,i} + 2k_1^S] \qquad (4.81)
\end{aligned}$$

Where k_1^L represents the turbulent kinetic energy in the large eddies and k_1^S represents the turbulent kinetic energy in the small eddies. We suppose that the movement of the particle in the fluid is affected by the turbulent kinetic energy of the fluid at two different scales. Therefore the turbulent kinetic

energy of the fluid used in the closure of the two terms does not refer to the same turbulent scale. We suppose that turbulent kinetic energy of the fluid is contained in big turbulent scales and the energy of the small structures is negligible (the notion of large and small scales are considered with respect to the size of the droplet). This hypothesis is true when droplets are small and near the dissipation scale of Kolmogorov. According to this hypothesis we can consider that the term k_1^S in the equation (4.81) is negligible since the turbulent kinetic energy of the fluid seen in the wake of the droplet is of small scale. Then we can write

$$\Pi_w = -\frac{1}{\tau_{12}^F}[2k_2 - U_{2,i}V_{d,i} - 2k_{12} + U_{1,i}V_{d,i}] \tag{4.82}$$

then the final form of Π_{q2} reads

$$\Pi_{q2} = -\frac{1}{\tau_{12}^F}[2k_2 - k_{12} - 2k_1] \tag{4.83}$$

For cases with larger sizes of droplets the turbulent kinetic energy in the small eddies can not be simply neglected. But the estimation of the energy of these small eddies can not be solved easily. One of the most used methods is the multi scale turbulent model for the continuous phase in which a system of four transport equations should be solved. Two transport equations to calculate the turbulent energy and the turbulent dissipation for large scales and two other transport equations for turbulent energy and dissipation at small scales. This model permits to estimate the neglected term in our approach. In the present work this multi scale model is not considered, keeping on the hypothesis that the droplet's size is near the length scale of Kolmogorov.

The correction in the closure of the inter-phase turbulent energy transfer term had been applied for the gas particle flow of Kulick et al. (1994) in order to compare it with the experimental data. In this reference experimental case, the diameter of the particles is around 70 μm, thus the hypothesis of neglecting the fluctuation energy of the eddies formed in wake remains valid in this case. Figure 4.8 presents the experimental values of the vertical and the radial components of the velocity fluctuation of the droplets with the estimated isotropic agitation calculated by the models Tchen, Q2Q12 (with equation (4.69)), and Q2Q12 with modifying the inter-phase transfer term (equation (4.83)). The correction closure has an important impact over the results, since it estimates an isotropic agitation of the droplets which lay in the correct area between the vertical and the radial agitation. While with the model Q2Q12 without any correction, this value is sharply underestimated. Moreover several tests done on this closure have shown a total independence from the initial conditions; but the correction model appears to have some limitations since it presents a flat profile of the turbulent kinetic energy of the particles overall the radial section of the tube. This may be referred to

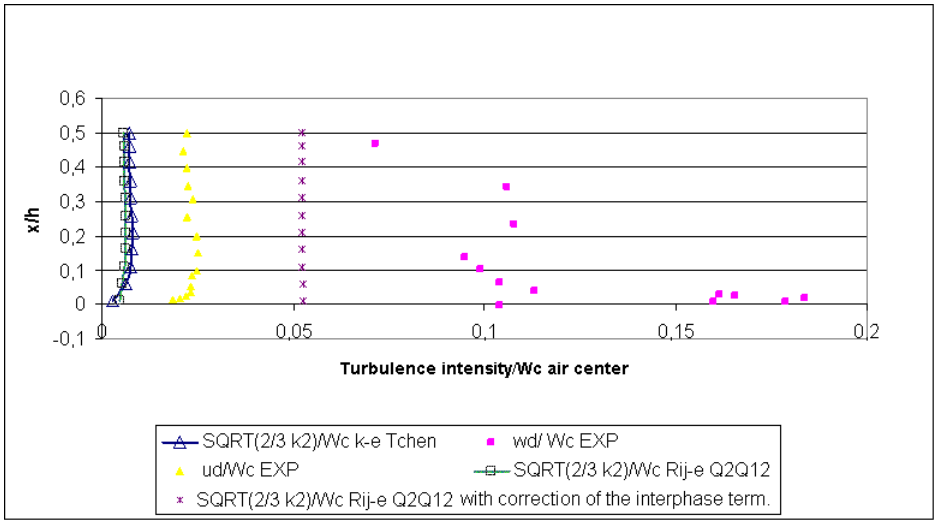

Figure 4.8: Stream wise and normal to wall turbulence intensities of the dispersed phase

the strong hypothesis of neglecting the vapor turbulent energy in the small eddies seen by the particle. But this result is satisfactory in our case, since it corrects the order of magnitude of the agitation of the droplets.

4.6 Numerical simulation in a long vertical tube

The analysis of the experimental case shows the adequacy and the deficiencies of the turbulence models regarding the mean velocity and the turbulence characteristics of the two phases. It shows that the difference between the turbulence models of the continuous phase is limited in detecting the anisotropy as it is expected. In the other hand, for the particles turbulence both models underestimate the particle turbulence. The new modeling of the turbulent interfacial transfer makes the turbulent kinetic energy of the droplets lie in the same order of magnitude as that of the experimental results. Unfortunately the experimental results do not give any information about the impact of the turbulence modeling on the particles distribution.
In order to study the effect of these differences on the droplets distribution, simulation cases are realized using the study case defined in section 3.4 by varying the turbulence models of the two phases. First the effect of the turbulence model of the continuous phase is studied by analyzing the impact of the vapor turbulence anisotropy on the results. Then, the impact of the two models Tchen and Q2Q12 (without any modification) are studied. Finally, we apply the modification proposed in Q2Q12 and analyze its impact.

4.6.1 Effect of the turbulence modeling of the continuous phase

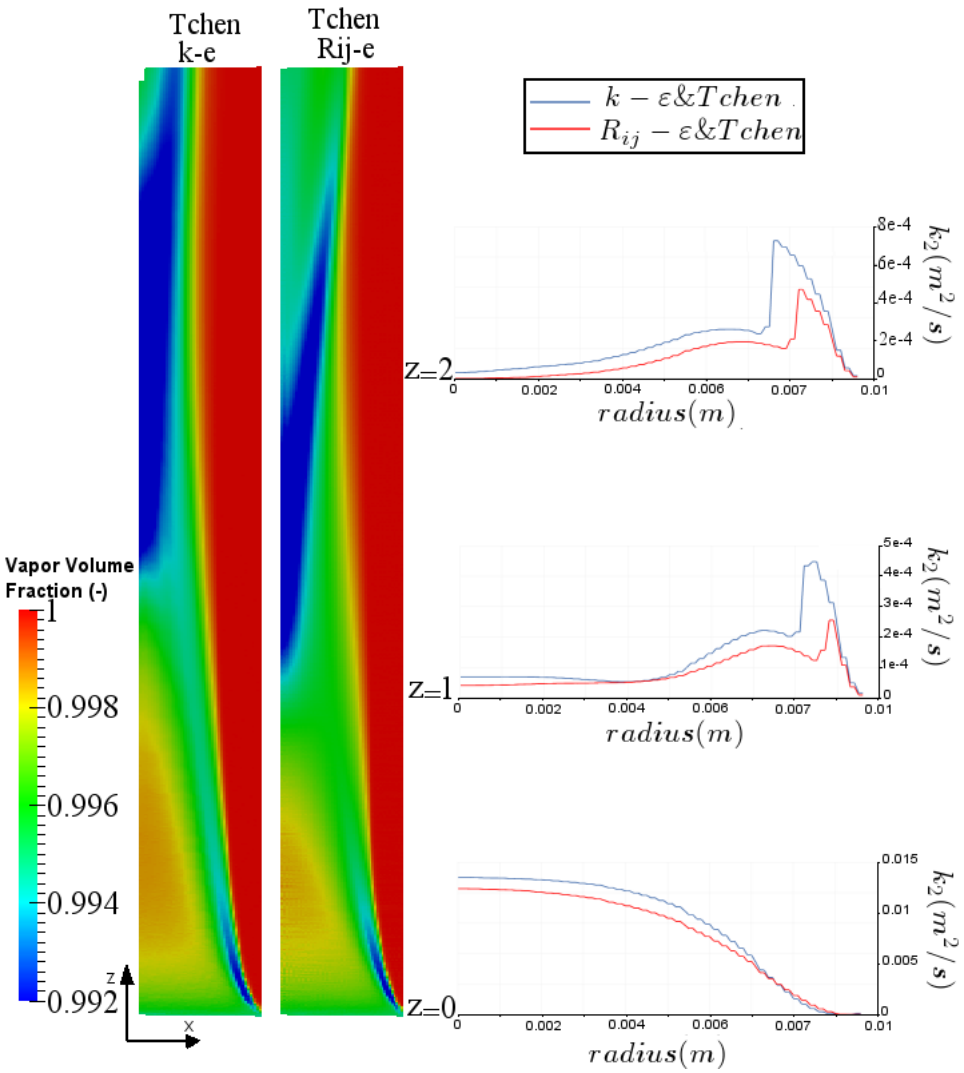

Figure 4.9: The vapor volume fraction distribution field for two simulation cases one with $k-\varepsilon\&Tchen$ and the other with $R_{ij}-\varepsilon\&Tchen$. Beside, the radial profiles of the turbulent kinetic energy of the droplets at three different heights.

The comparison with the experimental data showed that both $k-\varepsilon$ and $R_{ij}-\varepsilon$ are able to predict the mean vapor velocity profile. The experimental results show a remarkable anisotropy for the vapor turbulence in such a geometry. Evidently $R_{ij}-\varepsilon$ is more able to reproduce this anisotropy. In this section, tests have been done with $k-\varepsilon$ and others with $R_{ij}-\varepsilon$. The

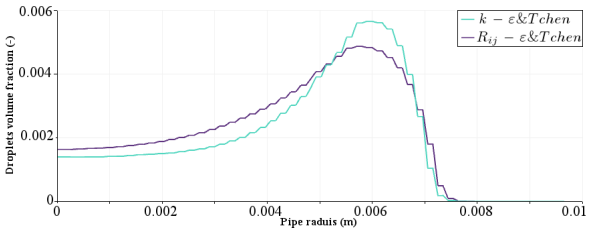

Figure 4.10: The radial profiles of the droplets' volume fraction for two simulation cases one with $k-\varepsilon\&Tchen$ and the other with $R_{ij}-\varepsilon\&Tchen$ at the height Z=0.5 m

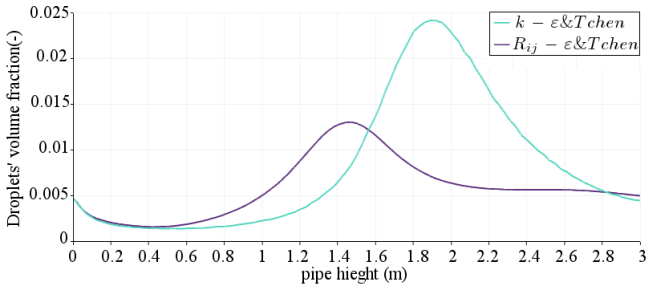

Figure 4.11: The vertical profiles of the droplets' volume fraction for two simulation cases one with $k-\varepsilon\&Tchen$ and the other with $R_{ij}-\varepsilon\&Tchen$ at center of the pipe X=0 m

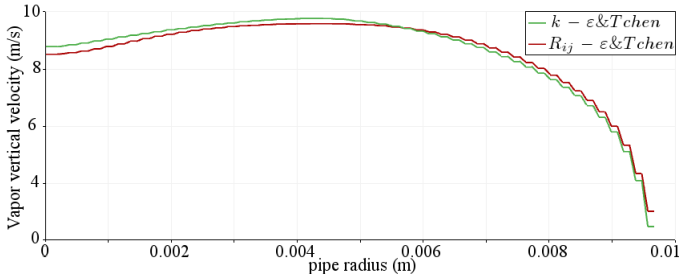

Figure 4.12: The radial profiles of the vapor velocity at the peak concentration point, Z=1.9 m for the case $k-\varepsilon\&Tchen$ and Z=1.5 m for the case $R_{ij}-\varepsilon\&Tchen$ at the height Z=0.5 m

effect of the vapor turbulence on the droplets distribution has been done via several terms. First, modeling the vapor turbulence affects the vapor flow characteristics, mainly the vapor mean and fluctuating velocities. These vapor characteristics may impact the droplet distribution as follow:

- The mean vapor velocity has a direct effect on the modeling of the interfacial forces acting on the droplets.

- The vapor kinetic energy is used in the modeling of the fluctuating parts of the interfacial forces.
- The vapor kinetic energy impacts mainly the modeling the turbulent characteristics of the droplets, k_2 and k_{12}. Since, as it has been shown before, there is always a kind of dependency between the turbulence of the vapor and turbulence of the droplets.

These three impacts are considered as indirect influence of the vapor turbulence modeling on the droplets spatial distribution. The impact of the vapor turbulence on the modeling of k_2 and k_{12} is the main effect due to the important role of the gradient of k_2 on the droplet distribution. The dependency of the droplets turbulence on the vapor turbulence is usually controlled by the model of turbulence of the dispersed phase. Therefore, the comparison of the modeling between $k-\varepsilon$ and $R_{ij}-\varepsilon$ is done first by using Tchen-Hinze model as a model of turbulence for the dispersed phase, then by using the model Q2Q12. These two cases are analyzed in order to verify if the impact of the modeling between $k-\varepsilon$ and $R_{ij}-\varepsilon$ on the droplets distribution changes if we change the turbulence model of the dispersed phase. Since the effect of the turbulence of the vapor on the droplets is complicated and indirect, a detailed analysis of the differences is done in order to draw the main lines at the end.
Figure 4.9 shows the vapor volume fraction distribution fields for two study cases, done with the model Tchen-Hinze model. The radial profiles of the droplets' turbulent kinetic energy at different heights are presented. For the case of $R_{ij}-\varepsilon$ & $Tchen$ shown in figure 4.9 the turbulence of the droplets is considered isotropic (review the two different ways of using the model Tchen in section 4.3). Figure 4.9 shows that, from a general point of view, the structure of the spatial distribution of the droplets is similar in both cases (i.e. concentration zones are formed in both cases and they have similar trajectories). A more detailed analysis of the droplets distribution shows the following differences.

1. The concentration of the droplets in the blue zone is higher in the case of $k-\varepsilon$. (a unified scale has been chosen for the two cases)
2. In the first part of the tube after the inlet, the concentration of the droplets in the zone around the tube center is higher in the case of $R_{ij}-\varepsilon$.
3. The inclination of the concentration zone of the droplets (blue zone) is different in the two cases. The concentration zone at the tube center is higher in the case of $k-\varepsilon$. Figure 4.11 shows the profiles of the droplets concentration at the tube center of the tube. The peak point in the case $k-\varepsilon$ is at 1.9 m while it is at 1.5 m in the case $R_{ij}-\varepsilon$. Moreover, the peak concentration point in the case of $k-\varepsilon$ is more

important (0.023) than the case of $R_{ij}-\varepsilon$ where it stays in the environ of (0.012).

4. The droplets in the concentrated zones in the center change their orientation and flow toward the wall after a certain distance in both cases. It it noticed that the distance necessary for the droplets to change their orientation is shorter in the case of $R_{ij}-\varepsilon$.

After specifying the general differences between the two cases, we propose an interpretation that explains the indirect impact of the vapor turbulence modeling on the droplets distribution.

- The model $k-\varepsilon$ overestimates the value of the turbulent kinetic energy of the vapor k_1. Therefore the value of the turbulent kinetic energy of the droplets estimated in the case of $k-\varepsilon$ is always higher than that estimated in the case of $R_{ij}-\varepsilon$ as shown in the curves of figure 4.9. This difference in the value of k_2, especially at the tube inlet ($z=0$), causes a larger centrifugal force (or turbulent dispersion force) that push more droplets from the center toward the wall. This interprets the first two differences noted above: More droplet in the concentrated (blue) zone in the case of $k-\varepsilon$ and more droplets stays in the center in the case of $R_{ij}-\varepsilon$. This is shown clearly in the concentration profiles in figure 4.10.

- The third difference is about the inclination of the concentration zone and the height at which it is located in the center. The inclination of the concentrated zones is determined via the competition between a turbulent dispersion force which pushes the droplets toward the wall and the lift force which pushes the droplets near the wall toward the center. As the turbulent dispersion force is more important in the case of $k-\varepsilon$, the concentrated zone is more inclined upward; and this interprets that the position of the concentrated zone is higher in the case of $k-\varepsilon$.

- The fourth difference can be interpreted as follows: in the case of $R_{ij}-\varepsilon$ more droplets stay in the center and in the lower part of the tube. Therefore the vapor velocity is more decelerated in the case of $R_{ij}-\varepsilon$. This is shown in figure 4.12 which shows the radial profiles of the vapor velocity at the height of the peak of each case (1.9 m for $k-\varepsilon$ and 1.5 m for $R_{ij}-\varepsilon$). Then the shear rate of the mean velocity of the vapor becomes more important in the case of $R_{ij}-\varepsilon$. Consequently the lift force, acting on the droplets after the concentration zone, reaches a sufficient value to push the droplets toward the wall after a shorter distance in the case of $R_{ij}-\varepsilon$ (figure 4.9).

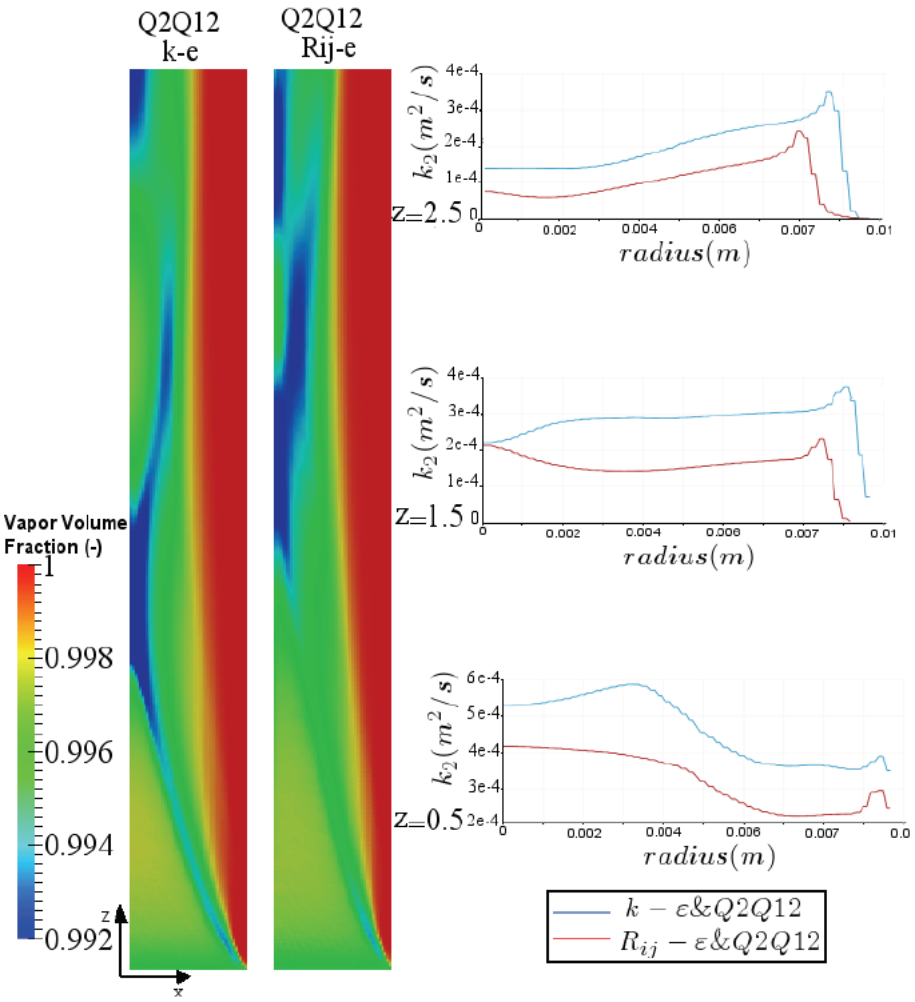

Figure 4.13: The vapor volume fraction distribution field for the two simulation cases one with $k-\varepsilon\&Q2Q12$ and the other with $R_{ij}-\varepsilon\&Q2Q12$. Besides, the radial profiles of the turbulent kinetic energy of the droplets at three different heights.

Another study for the impact of the model of turbulence of the continuous phase has been done, with Q2Q12 as a model of turbulence of the dispersed phase. The profiles of k_2 in figure 4.13 show that the value of the turbulent kinetic energy of the droplets estimated in the case of $k-\varepsilon$ is always higher than that estimated in the case of $R_{ij}-\varepsilon$. In the case of Q2Q12, this difference can not be explained easily referring to a linear algebraic relation as done for the case of Tchen. Here we show why k_2 increases if we increase k_1 via the model Q2Q12. First we remind the system of equations of the

model Q2Q12 that can be written as follows

$$\frac{\partial k_{12}}{\partial t} + \overline{u_{2,j}}\frac{\partial k_{12}}{\partial x_j} = \cdots \overbrace{-\frac{1}{\tau_{12}^F}\left[(k_{12}-2k_1)+\frac{\alpha_2\rho_2}{\alpha_1\rho_1}(k_{12}-2k_2)\right]}^{\Pi_{qvl}}$$

$$\frac{\partial}{\partial t}k_2 + \overline{u_{2,j}}\frac{\partial}{\partial x_j}k_2 = \cdots \overbrace{-\frac{2}{\tau_{12}^F}[2k_2-k_{12}]}^{\Pi_{q2}}$$

Since k_1 is very big with respect to k_{12} then

$$k_1 \nearrow \Rightarrow [-(k_{12}-2k_1)] \nearrow \Rightarrow \Pi_{qvl} \nearrow \Rightarrow k_{12} \nearrow$$

and k_{12} is the same order of k_2 then

$$k_{12} \nearrow \Rightarrow [-(2k_2-k_{12})] \searrow \Rightarrow \Pi_{q2} \searrow \Rightarrow k_2 \nearrow$$

Figure 4.13 presents the vapor volume fraction distribution field for two

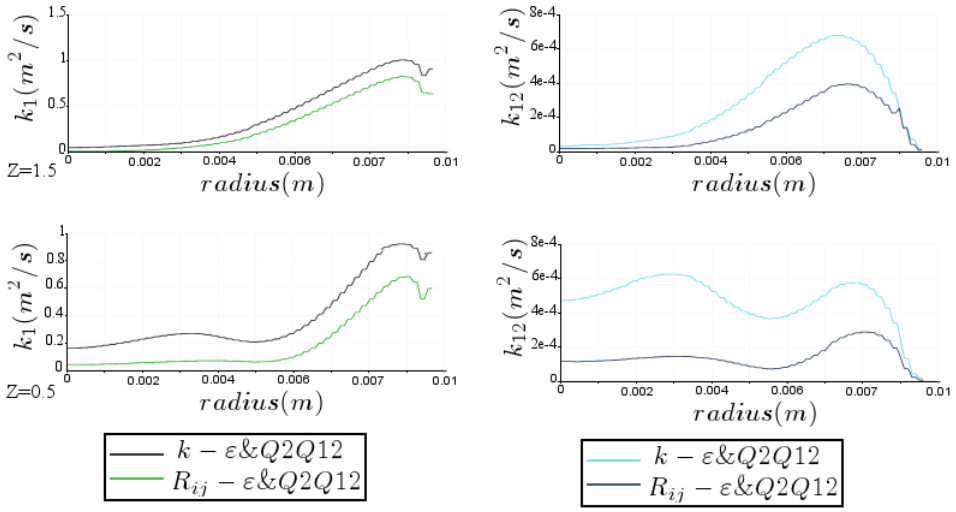

Figure 4.14: The radial profiles of k_2 and k_{12} at two different heights

simulation cases: one with $k-\varepsilon$ and the other with $R_{ij}-\varepsilon$. Here we also notice the importance of the phenomena of the lower part of the pipe just after the inlet. The higher value of k_2 in the case of $k-\varepsilon$ generates a turbulent dispersion force that pushes more droplets from the center toward the wall. This leads to form more concentrated accumulation zones and the consequences will be of the same type seen in the case of Tchen.
The choice of the continuous phase turbulence model has not an important influence on the characteristics of the vapor phase, i.e. both models show good prediction for the vapor averaged velocity. This is why $k-\varepsilon$ is widely

used in simulation of single-phase flows or two-phase flows with particles of low density as bubbly flows. The impact of the vapor turbulence modeling on droplets dispersion is indirect, since this impact is produced by other models that use k_1. Therefore the final impact changes by changing other models, as the model of turbulence of the dispersed phase as shown above. In this section, the impact of the vapor turbulence modeling is analyzed in a case study according to a special flow mechanism occurring here. The detailed differences at each section of the tube can not be generalized; but major lines can be drawn. The inertia of the droplets is an important parameter that magnifies the impact of the vapor turbulence. It is clearly shown that a little difference in the direction or the concentration of the droplets in the entrance zone of the pipe changes the overall distribution even far away from the entrance. This is related to the inertia of the droplets and their ability to retain the memory of their velocities for long distances. This drives us to conclude that the small differences in modeling k_1 could not be neglected in case of the droplets, since their impact can be magnified. Therefore, a first conclusion can be drawn here, that $R_{ij} - \varepsilon$ model is required for this type of flow in order to avoid the impact of the extra hypothesis considered by the model $k - \varepsilon$. Nevertheless, the choice between the two models does not modify the structure of the phase spatial distribution.

4.6.2 Effect of the turbulence modeling for the dispersed phase

The comparison with the experimental data shows us that both Tchen-Hinze and Q2Q12 models give similar results when the flow becomes fully developed. Even if the two models fail to reproduce the value of the droplets' turbulent kinetic energy found in the experiment, it is still important to analyze the impact of the two modeling methods on the droplets distribution. Four study cases have been formulated to analyze this impact, two cases with $k - \varepsilon$ shown in figure 4.15 and two others with $R_{ij} - \varepsilon$ shown in figure 4.16.

Changing the model of turbulence of the vapor does not impact the differences between Q2Q12 and Tchen. These numerical tests show two main differences between Tchen-Hinze and Q2Q12 model in our case. The first one is that Tchen-Hinze imposes inlet boundary condition for the droplet's turbulent energy, since it calculates the inlet value k_2 automatically based on the inlet boundary conditions of the continuous phase. This model calculates a value of k_2 very small with respect to the value k_1. On the other hand, Q2Q12 model allows to take into account an independent inlet value of k_2, which allows to study some cases where k_2 is considered to be important or comparable to k_1. This may be required for the targeted

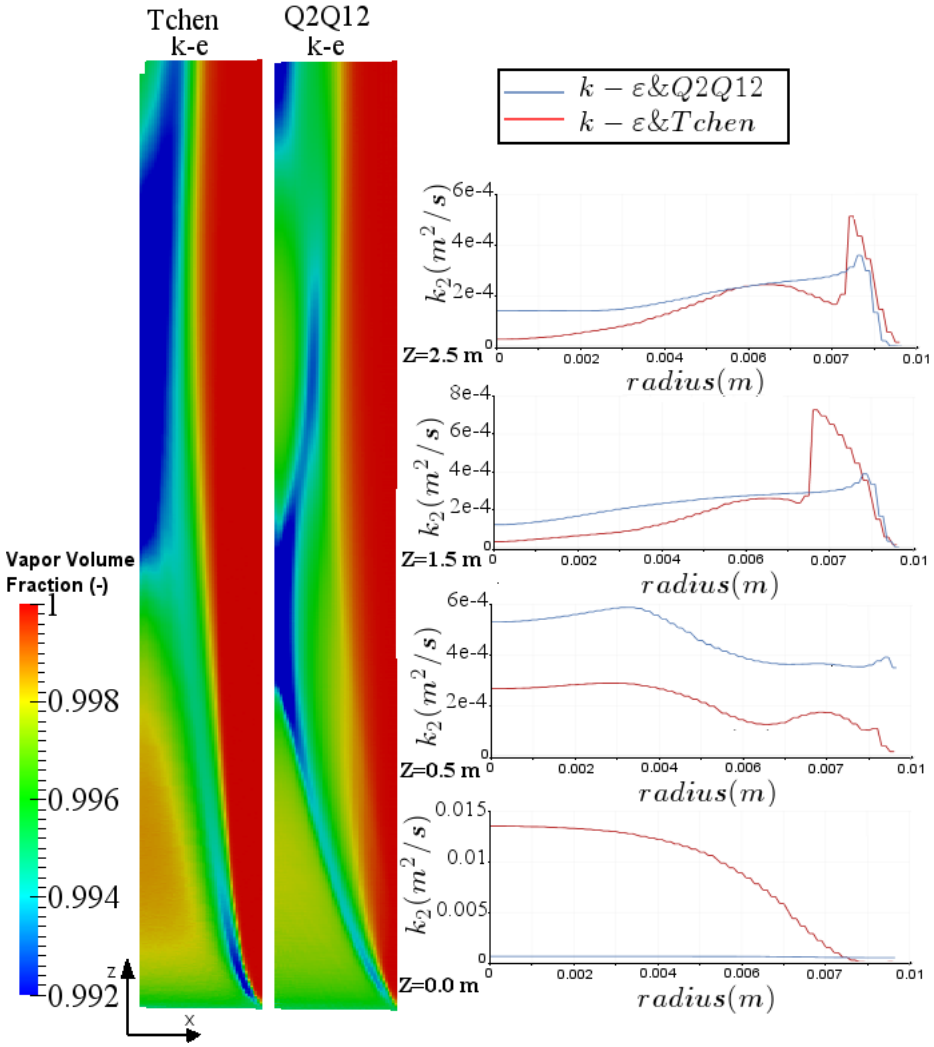

Figure 4.15: The vapor volume fraction distribution field for two simulation cases one with $k-\varepsilon\&Tchen$ and the other with $k-\varepsilon\&Q2Q12$

study, especially if a violent departure of the droplets at the level of the quench front should be taken into account. But several tests show that even if an important value of k_2 is imposed at the inlet this energy vanishes and finally it reaches a value of the same order of that calculated by Tchen. Beside the magnitude of the k_2, k_2 calculated by Tchen-Hinze model takes a sharp profile just after the inlet (center of the first cell). The radial profiles of k_2 at the first cell after the inlet, presented in figures 4.15 and 4.16, show the difference in the evolution of the profile of k_2. The inlet boundary condition value of k_2 used in the case of Q2Q12 is chosen to be of the same order of that calculated by Tchen-Hinze model. The inlet

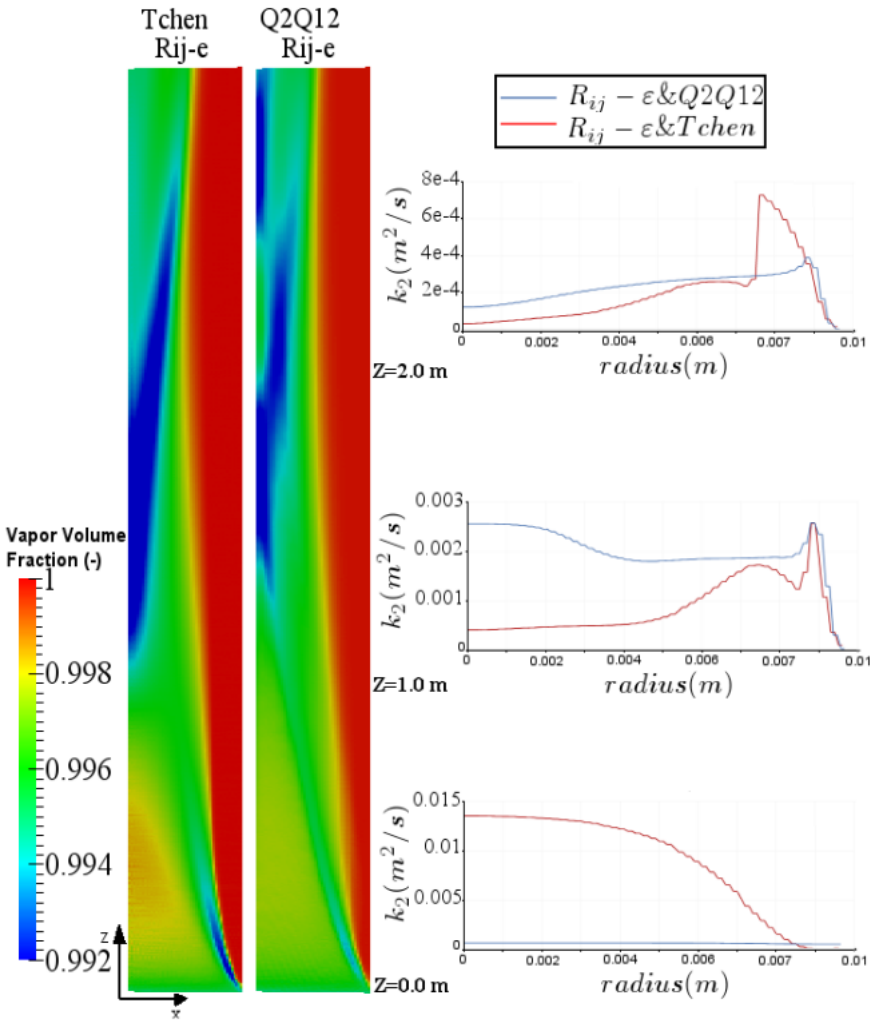

Figure 4.16: The vapor volume fraction distribution field for two simulation cases one with $R_{ij} - \varepsilon\&Tchen$ and the other with $R_{ij} - \varepsilon\&Q2Q12$

profile of k_2 induces the gradient of the droplets Reynolds tensor which acts as a momentum source term (the turbulent dispersion force acting on the droplets). The sharp profile of k_2 in the case of Tchen-Hinze model generates an important force in comparison with the case of Q2Q12 where the profile of k_2 is almost uniform. The impact on the droplets distribution is seen in the vapor volume fraction fields in both figures 4.15 and 4.16. In the cases where Tchen is used, the droplets are more accumulated in the concentration zones just after the inlet. The departure of the droplets at the inlet, affects their distribution all over the tube, because of their high inertia.

The second difference between the two models is noticed in the radial

profiles of k_2 at high levels in the pipe as shown in figures 4.15 and 4.16. The profiles of the turbulent kinetic energy of the dispersed phase calculated by Tchen-Hinze follows the shape of the profile of the turbulent kinetic energy of the continuous phase. Besides, the profile of k_2 calculated by the model Q2Q12 shows appears to be independent from the shape of the profile of k_1. Q2Q12 is able to take into account the turbulent agitation of the droplets produced by the droplets motion beside the influence of the continuous phase. On the other hand, Tchen-Hinze model calculates only the agitation of the droplets due to the influence of the continuous phase turbulence.
The two models give similar results when the flow is fully developed (i.e. at the outlet of the tube) and independent from inlet conditions. Q2Q12 permits to control the inlet boundary condition of k_2 and it shows more ability to account for the own agitations of the droplets independent of the vapor. But finally this model is also incapable to maintain the high agitation of the droplets when the flow becomes fully developed, as shown in the comparison with the experimental results.
Therefore, a new test case is done with modifying the model of Q2Q12 by implanting the proposed modeling of the turbulent interfacial transfer term presented in the previous section.

Figure 4.17 presents the vapor volume fraction distribution field for a simulation case using $R_{ij} - \varepsilon$ as turbulence model of the continuous phase and the modified model Q2Q12 for the dispersed phase. This case is done keeping on all the initial conditions of the previous cases. An important impact of this modeling is noticed that no concentration zones are viewed all over the tube section. All the phenomena seen in the previous cases disappear and the important effect of the inlet phenomena disappears. The flow is homogeneous and the droplet volume fraction decreases consequently up in the tube due to the evaporation of the droplets.
This test case shows the important impact of the dispersed phase turbulence on the simulation of our targeted case. The underestimation of the value of the droplets turbulence causes droplets accumulation in specific trajectories inside the flow which has no physical interpretation. Moreover the experimental results show that the turbulence of the particles may be as important as the vapor turbulence. The modification of the interfacial turbulent energy transfer in the model Q2Q12 permits us to estimate a value of k_2 which is of the same order of magnitude found in the experimental results. The good estimation of the droplets turbulence changes the overall structure of the spatial dispersion of the droplets.

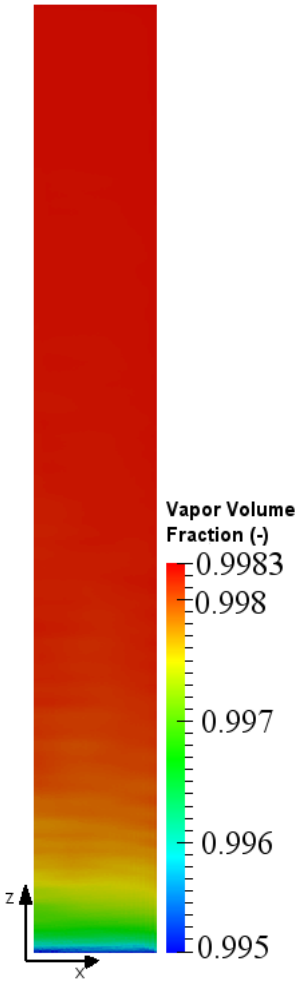

Figure 4.17: The vapor volume fraction distribution field for simulation case one with $R_{ij} - \varepsilon$ model and the modified model of Q2Q12

4.7 Conclusion

This chapter discusses the turbulence modeling in a droplets-vapor dispersed flow and its effect on the droplets volume fraction distribution in a vertical tube. Turbulence models of the continuous phase and the dispersed phase are discussed theoretically. Due to the lack of experimental data for this kind of flows, an experimental data of air-particles vertical channel flow is used to test the turbulence models. The experimental data does not provide enough information about the droplets' spatial distribution. Therefore the effect of the turbulence modeling on the droplets distribution is studied numerically by analyzing different simulation cases of vapor-droplet flow in a vertical tube employing different turbulence models. The main results are

as follow:
The turbulence modeling shows a significant impact on the droplets distribution. The value and the profile of the turbulent kinetic energy of the droplets k_2 is the main term that impacts directly the distribution of the droplets through what we defined as a turbulent dispersion force. There are three models that participate in the prediction of k_2: the turbulence model of the continuous phase, the turbulence model of the dispersed phase and the model of the turbulent coupling between the two phases.
The turbulence model of the continuous phase predicts the value of $R_{ij,1}$. This may impact directly the vapor characteristics as the vapor velocity. Besides, it has an indirect impact on the droplet distribution. Comparison with the experimental data shows that both models, $k-\varepsilon$ and $R_{ij}-\varepsilon$ succeed in estimating the velocity of the vapor, while the model $R_{ij}-\varepsilon$ is evidently more able to take into account the anisotropy of the vapor turbulence. The used models for the dispersed phase turbulence are not able to transform the effect of the vapor turbulence anisotropy into the droplets turbulence. Then the difference between the two models is limited. $k-\varepsilon$ overestimates the value of k_1 with respect to $R_{ij}-\varepsilon$. Although the difference of the values of k_1 calculated by the two models is small; but it is transmitted, through the turbulence model of the dispersed phase, to make a difference in the value of k_2. This difference in the estimated value of k_2 leads to change the turbulent dispersion force, which influences in turn the radial distribution of the droplets. Inertial particles as droplets are able to retain memories of their velocity for long distances. Therefore a small difference in the sense of the velocity or droplets' concentration in the entrance zone of the tube, is able to change the distribution of the droplets all over the tube. This inertial criteria of the droplets tends to magnify the effect of the turbulence modeling of the vapor phase. We conclude that the results of $k-\varepsilon$ can be satisfying while the model $R_{ij}-\varepsilon$ is requested for more accuracy.

The turbulence model of the dispersed phase is important in determining the value of k_2 and evidently has more impact on the droplet distribution. This model determines the degree of dependency of the droplets agitation on the vapor's turbulence. Two models have been studied, an algebraic model Tchen-Hinze and a higher level model Q2Q12 which calculates a transport equation for k_2. From a theoretical point of view, the droplets agitation estimated by Q2Q12 should be more independent from the vapor turbulence, than that estimated by the model Tchen-Hinze. This refers to the ability of Q2Q12 to take into account the production terms due to the droplets motion beside the effect of the vapor. This effect can be clearly noticed in the numerical study case, when the profiles of k_2 are more independent from the profiles of k_1 in the case of Q2Q12. But the experimental case, shows that heavy particles may have a turbulent agitation comparable to that of the continuous phase with strong turbulence anisotropy. The comparison of the

values predicted by the two models with the experimental values shows that both, Tchen-Hinze and Q2Q12, underestimate the turbulent kinetic energy of the droplets. The analysis of the different terms of the transport equation of k_2 in the model Q2Q12 indicates that the term of the inter-phase turbulent energy transfer is behind this underestimation of k_2. A detailed bibliographical study about the modeling of this term is presented . Some studies clarify the disadvantages of the actual modeling of the inter-phase transfer and proposed some solutions. In analogy with the work of separating the turbulence scale, which has been proposed for the closure the reverse coupling term Π_{q1}, we proposed a new closure method for Π_{q2}. This method is based on separation of the turbulence interaction between the two phases into destruction of droplets agitation at small turbulence scales in the wake of the droplet; and production of droplets agitation at big turbulent scales when it cross large eddies. A strong hypothesis had been considered to neglect the turbulent energy of the, k_1^S, vapor at scales smaller than droplets diameter. This can be justified for the cases with small droplets near the scale length of Kolmogorov, but it is not so evident for big droplets. The proposed closure helps us to estimate a particle's turbulent energy k_2 that lays in the same order of scale measured in the experiment. For this present study this solution is enough but our analysis enlights the importance of the closure of this term for future research projects. The application of this closure on the numerical study case shows a very important impact. This closure enhanced the effect of the turbulence on the droplets distribution. No more concentration zones were seen and the droplets became uniformly distributed all over the tube section. The model of Tchen-Hinze is not suitable for the case of droplets and higher level model as Q2Q12 is required to this case study. More attention should be paid on the modeling of the inter-phase turbulent transfer. Moreover, all the present study is based on the hypothesis that the droplets turbulence is isotropic while several experimental references cited a strong anisotropy of the droplets' turbulence. Therefore a high level model that is able to take into account the anisotropy of the droplets turbulence should be analyzed in future studies.

Chapter 5

Lift force

As we showed in the previous chapters, the spatial distribution of the droplets in vapor-droplet turbulent flow in a long vertical tube is controlled mainly by the interfacial forces and the turbulent dispersion. The main interfacial forces are the drag force which plays the major role in the vertical propagation of the droplets and the lift force which impacts the radial distribution of the droplets. The lift force, although often much smaller in magnitude than the drag force, can play a central role in the preferential accumulation of the droplets either close or away from the wall. Due to the important impact of the radial distribution on the dynamic as well as on the thermal transfer in the flow, the lift force modeling becomes of fundamental importance in this study.
In Stokes flows[1], a moving particle in one-dimensional shear flow does not experience a transverse lift force. With the introduction of the inertial effects there are three primary contributions to lift force: shear-induced lift, rotation-induced lift, and wall-induced lift. In the present study, the droplet surface is assumed to be clean so that the outer flow does not induce any rotation of the droplet. Note that the deformation of the droplet can induce a lateral force even in zero Reynolds number flow (Stokes limit). Here we restrict our attention to inertial effect on non-deformable spherical particles. Therefore, the problem of the lift force for a particle translating in a shear flow near to the wall is characterized by three parameters:

1. The non-dimensional distance from the wall, calculated as the ratio of the distance between the wall and the droplet center over the droplet's diameter.

2. The particle Reynolds number, being based on the droplet diameter.

[1] Stokes flow is a type of fluid flow where inertial forces are small compared with viscous forces. The Reynolds number is low, i.e. $Re << 1$. This is a typical situation in flows where the fluid velocities are very slow, the viscosities are very large.

3. The non-dimensional shear rate, being the ratio between the velocity difference across the droplet due to the shear and the relative velocity at the droplet center.

When a particle moves in a shear flow it experiences a transverse force. The existence of the lift force for small rigid spheres was demonstrated experimentally by Segré and Silberberg (1962) who studied the migration of buoyant spheres in a Poiseuille flow. Because of its practical applications, the analytical calculations of the lift force on spherical particles has been the subject of constant interest since a long time. There are two series of analytical work that has been carried out on this problem. The first one considers the effect of inviscid[2] rotational flow on a sphere. After several studies by several authors, Auton (1987) succeeded in performing the complete calculation of the secondary velocity field induced by the vorticity and evaluated the resulting lift force. The range of validity of the analytical solutions derived by Auton (1987) is unknown. In other words, according to our knowledge, no reference specifies the upper limit of the particle Reynolds number Re_p and the shear rate for a valid application of Auton's solution. The second series of work concerns low Reynolds-numbers flow. Combining several techniques, Saffman (1965) derived the force on a particle due to the velocity shear by considering the motion far away from any boundaries and in the limit of small Reynolds number and large shear. Saffman (1965) assumed that the particle Reynolds number Re_p and the velocity gradient Reynolds number Re_s (being based on the shear rate) are small with respect to unity, and that $Re_p << Re_s^{\frac{1}{2}}$. McLaughlin (1991) extended Saffman's analysis by considering the case of an unbounded shear flow, where the inertial effects induced by the mean flow are of the same order of those induced by the shear. In other words, McLaughlin (1991) removes the restriction of Saffman $Re_p << Re_s^{\frac{1}{2}}$. McLaughlin (1993) derived an expression of the lift force due to the presence of the wall. McLaughlin and Cherukat (1994) obtained an expression for the lift force on a particle which is valid when particle is very close to the wall. The Lift force modeling changes according to the conditions on Re_p, Sr, and the distance from the wall. Therefore, McLaughlin et al. (1997) proposed what he called optimum modeling of the lift force. This optimum modeling is a conditional modeling that uses different models for each special case. All these models are restricted under the condition that $Re_p << 1$. This brief summary shows that the analytical modeling of the lift force on a solid particle is not clear at the present time, except for low Reynolds number limit for which asymptotic results are available. Compared to the amount of the analytical work, the number of the computational studies that have

[2] The flow of a fluid is called inviscid flow when it is assumed to have no viscosity. The flow of fluids with low values of viscosity agree closely with inviscid flow everywhere except close to the fluid boundary where the boundary layer plays a significant role.

considered the case of spherical particle embedded in shear flow was very small. First, Dandy and Dwyer (1990) obtained the numerical estimation of the lift force on a rigid sphere for particle Reynolds number ranging between 0.01 and 100. Nevertheless, other authors cited that their results display some troubling features. Recently, a series of computational studies clarified the effect of the lift on a rigid sphere for high Reynolds numbers. Komori and Kurose (1996) considered the same problem up to particles Reynolds number of several hundreds. The later found that beyond a certain Reynolds number the coefficient becomes negative and depends strongly of shear rate. Later on, Kurose and Komori (1999) performed a three dimensional direct numerical simulation for the flow field outside a rigid sphere in the range of particle Reynolds numbers of $Re_p = 1 - 500$. They confirmed the phenomenon of reversal of the sign of the lift. The lift force on a stationary sphere in a linear shear flow acts from low-fluid-velocity side to high-fluid-velocity side for low particle Reynolds numbers of $Re_p < 60$, whereas it acts from high-velocity side to low-velocity side for high particle Reynolds numbers of $Re_p > 60$. Sugioka and Komori (2006) investigated the effects of fluid shear on the lift force acting on a spherical water droplet in a viscous linear shear air flow for moderate and high Reynolds number. Their study aims to clarify the difference in the mechanism of the lift force between a water droplet and a rigid sphere. They found that the behavior of the lift coefficient on a spherical droplet is similar to that on a stationary rigid sphere. Moreover the lift force acting on a spherical droplet changes its sign from a positive to a negative value at a particle Reynolds number of $Re_p \simeq 50$ in a linear shear flow and it acts from the high-speed side to the low-speed side for $Re_p \geq 50$.

Beside the shear-induced lift, the presence of the wall tends to increase the lift force. The effect of the wall is strongest when the particle is in close contact with the wall. This effect decays rapidly as the distance between the particle and the wall increases until it becomes negligible for distance in the environ of 10 particle diameters.

Lately, Zeng et al. (2009) performed a computational study for a rigid sphere in a linear wall bounded shear flow, to understand the effect of the wall on the lift force. In Zeng et al. (2009) computations, the particle Reynolds number ranges from 2 to 250 at separation distances to the wall from nearly sitting on the wall to far away from the wall. They showed that the value of the critical Reynolds number, at which the lift force inverses its sign, is also dependent on the distance from the wall. For a droplet nearly sitting on the wall the lift force changes its sign at very high Reynolds number while for a droplet far from the wall the critical Reynolds number will be similar to the value calculated by the Sugioka and Komori (2006), i.e. $Re_{p,cr} \simeq 50$.

The main goal of this chapter is to provide a complete description of the lift force experienced by a droplet over a wide range of the particle Reynolds

number and shear flow taking into account the effect of the wall.

5.1 Problem Description

In our study case, we are interested in a flow of water droplets in vapor wall-bounded shear flow. As explained in the introduction, the lift force in this case should be characterized by the non-dimensional distance from the wall, the particle Reynolds number Re_p, and the non-dimensional shear rate S_r. Therefore, it is important to place our study according to these parameters. For this sake, a simulation of vapor droplets flow in a long vertical pipe is considered. This study case is defined in section 3.4. It is done with basic turbulent models for both phases ($k-\varepsilon$ and Tchen-Hinze), which has not an important impact on the order of magnitude of the calculated parameters. So only the effect of the lift force modeling on the droplets dispersion, is analyzed.

Figure 5.1 shows the radial profile of particle Reynolds number Re_p over

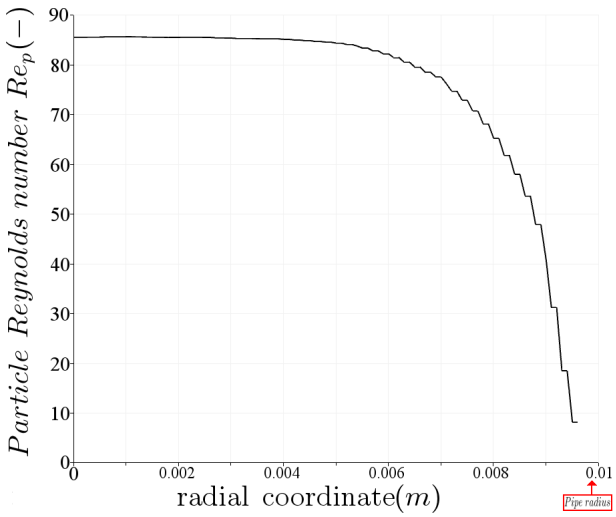

Figure 5.1: The radial profile of particle Reynolds number Re_p over the tube section in vapor droplets pipe flow

the tube section in vapor droplets pipe flow in the inlet zone (bottom of the simulated domain). The particle Reynolds number ranges between 5 and 100 at this elevation. Although this range can changes a little as we change the elevation in the pipe, we can generalize by considering that Re_p is greater than 1 and may reach a value more than 100. Figure 5.2 shows the radial profile of non-dimensional shear rate S_r over the tube section. S_r ranges between 1 in the near wall zone and zero at the tube center.

Equation (2.120) presents the general model of the lift force acting on a single

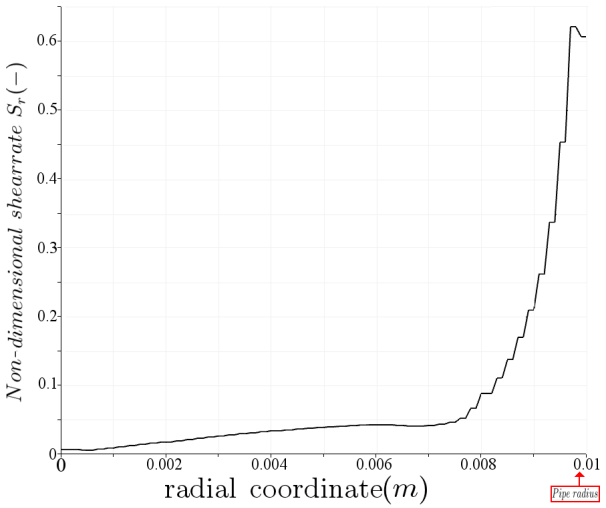

Figure 5.2: The radial profile of non-dimensional shear rate S_r over the tube section in vapor droplets pipe flow

droplet, it has been averaged to get equation (2.121) which presents volumic interfacial momentum transfer due to the lift force. In this chapter, the equation (2.120) will be considered for simplicity reasons while comparing with other models. Moreover, the radial component (x-axis) of the lift force is the most important, and the other components can be neglected. Therefore, we are interested only by the vertical component (z-axis) of the vapor velocity and its shear rate.

We will state a simple problem of a fixed spherical droplet of radius R

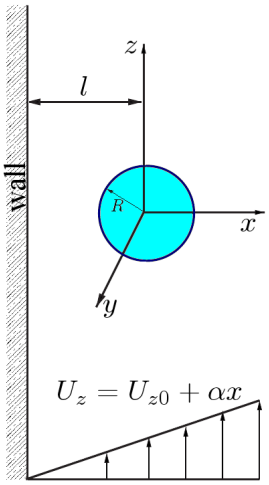

Figure 5.3: A representative scheme of a droplet in a wall-bounded shear flow

located at the origin of a Cartesian frame. The droplet is embedded in a wall-bounded shear flow corresponding to the undisturbed vapor velocity field U_z, where l is the distance between the wall and the particle center. Then under these conditions the main characteristic parameters of the flow are defined as follows

$$Re_p = \frac{2RU_z}{\nu}, \quad \alpha = \frac{dU_z}{dx}, \quad S_r = \frac{R\alpha}{U_z} \quad L = \frac{l}{2R}$$

The non-dimensional shear rate compares the streamwise vapor velocity U_z to the velocity difference induced by the shear over a distance corresponding to the one droplet diameter. First, the general equation of the lift (equation (2.120)) is recalled

$$f^L = \rho_1 V_p C_L (v_r \wedge rot(u_1)) \tag{5.1}$$

Here V_p is the volume of the spherical droplet, v_r is the relative velocity which corresponds to U_z in the simple case of a reference frame moving with the droplet and u_1 is the velocity of the vapor which also correspond to U_z here. Then $rot(u_1)$ corresponds to

$$\frac{dU_z}{dx}\overrightarrow{e_y} = \alpha\overrightarrow{e_y}$$

and

$$v_r \wedge rot(u_1) = U_z \frac{dU_z}{dx}\overrightarrow{e_x}$$

Finally, the lift force is in the x-axis direction reads

$$f^L = C_L \rho_1 V_p \alpha U_z \tag{5.2}$$

As noted out in the introduction, two analytical solutions giving the lift coefficient on a spherical particle in the simple shear flow have been derived. For an inviscid fluid satisfying the condition $S_r << 1$, Auton (1987) obtained the result

$$f^L = C_L \frac{2}{3}\pi \rho_1 R^3 \alpha U_z \tag{5.3}$$

which yields to a lift coefficient $C_{L,Auton} = 0.5$. All the simulation cases in the previous chapters have been done using this lift model. But the vapor is a viscous fluid, and the flow is far to be considered inviscid especially close to the wall where the boundary layer plays a significant role. For viscous flows, Saffman (1965) proposed the following model

$$f^L = 6.46\mu R^2 U_z \sqrt{\frac{\alpha}{\nu}} \tag{5.4}$$

which yields a lift coefficient

$$C_{L,Saff} = \frac{1.54}{R}\sqrt{\frac{\nu}{\alpha}}$$

Saffman (1965) derived this analytical expression of the lift force under the following assumptions,

$$Re_p << 1$$
$$Re_s \left[= \frac{\alpha(2R)^2}{\nu}\right] << 1$$

where Re_s is the shear Reynolds number defined in terms of the velocity shear.
Re_p is assumed to be much smaller than Re_s by defining the variable ξ

$$\xi \left[= \frac{Re_s^{\frac{1}{2}}}{Re_p} = \left(\frac{S_r}{Re_p}\right)^{\frac{1}{2}}\right] >> 1$$

Figure 5.1 shows that in the present study Re_p is not smaller than unity

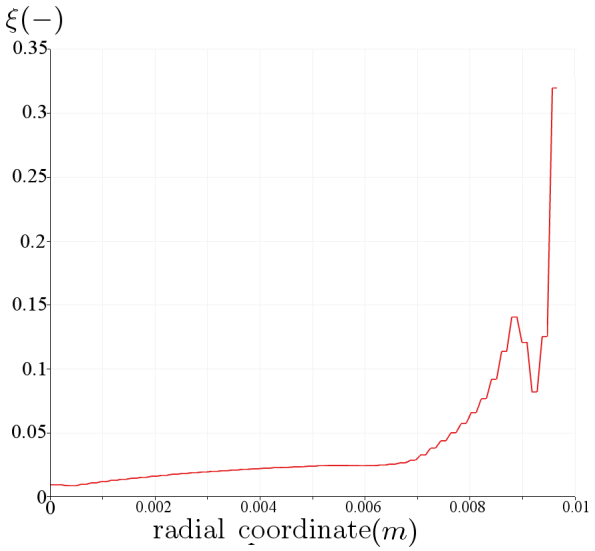

Figure 5.4: The radial profile of the ratio ξ between the shear Reynolds number and the particle Reynolds number

and can reach high values more than 100. Besides in figure 5.4, that shows the radial profile of the variable ξ, ξ is always smaller than one. That makes the use of Saffman's expression of the lift coefficient irrelevant in our case.

McLaughlin (1991) relaxed the restriction for cases with small ξ, and derived the following expression for the lift force.

$$f^L = \frac{9}{\pi}\mu R^2 U_z \sqrt{\frac{\alpha}{\nu}} J^u \tag{5.5}$$

where the function J^u is dependent upon the dimensionless parameter ξ. Since the general form of J^u is complicated, McLaughlin (1991) defined the values of J^u as follows

$$\begin{aligned} J^u &= -32\pi^2\xi^5 \ln(1/\xi^2), \quad \text{for} \quad \xi << 1 \\ J^u &= \text{the values are provided in a special table for} \quad 0.025 \leq \xi \leq 5 \\ J^u &= 2.255 - 0.6463/\xi^2, \quad \text{for} \quad \xi >> 1 \end{aligned} \tag{5.6}$$

Due to these formulation, the solution of Saffman (1965) in equation (5.4)

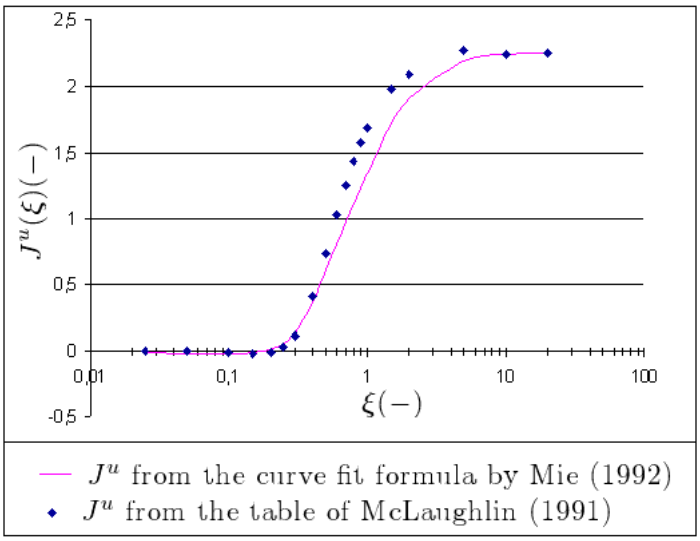

Figure 5.5: Comparison between the values from the table and the proposed expression of Mie (1992) of J^u

is recovered for the case $\xi \longrightarrow \infty$ as $J^u \longrightarrow 2.255$. McLaughlin found that J^u decreases rapidly as ξ tends to zero which means that Saffman's model may overestimate the lift force in our case. From the table of the values of J^u in McLaughlin (1991), Mie (1992) constructed a curve fit formula. Figure 5.5 confirms that formula given by Mie (1992) fits with the values from the table of McLaughlin (1991). This formula reads

$$J^u(\xi) = 0.6765\{1+\tanh[2.5\log_{10}(\xi+0.191)]\}\{0.667+\tanh[6(\xi-0.32)]\} \tag{5.7}$$

Mie (1994) obtained an expression on a spherical bubble in a linear shear flow. Although McLaughlin (1991) relaxes the condition over ξ, it stays in

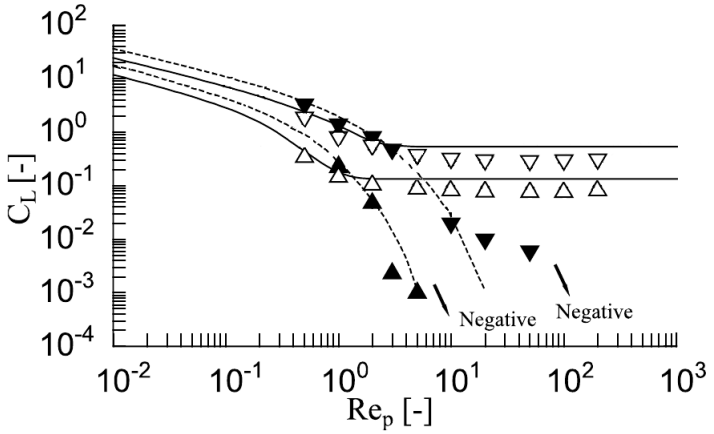

Figure 5.6: Figure from Kurose et al. (2001), comparison of the lift coefficient C_L in a linear shear flow for a bubble (open symbols) with that for a solid particle (closed symbols): ($\triangle$,$\blacktriangle$) $S_r = 0.1$;($\bigtriangledown$,$\blacktriangledown$)$S_r = 0.4$, the solid and the dashed lines show the predictions for $S_r = 0.1, 0.4$ by Mie (1994) and McLaughlin (1991), respectively

the limit $Re_p << 1$. According to our knowledge, there is no analytical model for the lift force on heavy particles (solid particles, or droplets) for the case of high Reynolds numbers. But recently, several authors approached this problem by effecting DNS for moderate and high Reynolds number. Therefore new models have been proposed for the closure of the lift force in this case based on the correlation of the DNS results.
Komori and Kurose (1996) and Kurose and Komori (1999) performed a three dimensional direct numerical simulation for the flow field outside a rigid sphere in the range of particle Reynolds numbers of $Re_p = 1 - 500$. They found that the direction of the lift force action on a stationary rigid sphere at higher Re_p is opposite to that predicted by the inviscid and low-Reynolds-numbers theories. Kurose and Komori (1999) specified that the lift force on a stationary rigid sphere in a linear shear flow acts from the low-fluid-velocity side to the high-fluid velocity side for low particle Reynolds number of $Re_p < 60$, where as it acts from the high velocity side to the low-velocity side for high particle Reynolds numbers $Re_p > 60$. Later Sugioka and Komori (2006) found that the behavior of the lift coefficient on a spherical droplet is similar to that on a stationary rigid sphere; and that the lift force acting on a spherical droplet changes its sign from a positive to a negative value at a particle Reynolds number of $Re_p \simeq 50$ in a linear shear flow. It acts from the high-speed side to the low-speed side for $Re_p \geq 50$.
Kurose et al. (2001) studied the lift force acting on a spherical bubble for high Reynolds number. They noted that the lift force acting on a spherical solid particle is quite different from that acting on a bubble. The lift force

on a solid particle changes its sign, while it keeps the same for a bubble. They compared the results of this model with the DNS results obtained by Kurose and Komori (1999). Figure 5.6 shows the difference between the lift force on a bubble and a solid particle. The model of Mie (1994) is good for the case of bubbles. Kurose et al. (2001) applied the model of Saffman with the empirical function from McLaughlin (1991), equation (5.7), for the case of solid particles at high Reynolds numbers. Figure 5.6 shows good agreement of the model of McLaughlin with the DNS results up to a certain limit. Figure 5.6, does not show clearly the limit of validity of this combination, particularly it does not show at which Reynolds number the lift force changes its sign according to this formula. In the present study, we extended the analysis about this point. According to the combination between the model of Saffman (1965) with the correlation of McLaughlin (1991) the critical value of the particle Reynolds number $Re_{p,cr}$ (the value at which the lift inverses its sense) is not fixed in the environ of 50 as predicted in Sugioka and Komori (2006) but rather depends on S_r. Table 5.1 shows how the values of $Re_{p,cr}$ for different values of S_r. Therefore, we propose to

S_r	$Re_{p,cr}$
0.1	5.8
0.2	11.6
0.3	17.4
0.4	23.2
0.5	29
0.6	34.8
0.8	46.4

Table 5.1: The value of $Re_{p,cr}$ at which C_L inverses its sign for different values of shear rate if we apply Saffman model with the empirical function of McLaughlin

adjust the empirical function of McLaughlin in equation (5.7) by replacing the constant 32 by a variable b. b is a function of S_r, which permits the lift force to inverse its sign around $Re_{p,cr} = 50$ independently from the value of S_r. Then the new proposed correlation reads.

$$J^u(\varepsilon) = 0.6765\{1+tanh[2.5log_{10}(\varepsilon+0.191)]\}\{0.667+tanh[6(\varepsilon-b)]\} \quad (5.8)$$

where

$$b(S_r) = -0.6916S_r^4 + 1.4522S_r^3 + 1.1313S_r^2 + 0.532S_r + 0.1533 \quad (5.9)$$

This new empirical function allows to calculate a lift coefficient in the same order of magnitude of the results calculated by the empirical function of McLaughlin. Besides the lift coefficient changes its sign for $Re_p \simeq 50$ which

is consistent with the DNS results. Although this solution allows the lift force to change its sign, it still presents some deficiencies when it is compared with DNS results and it does not take into account the effect of the wall.
A particle moving in a shear stress near the wall experiences a transverse force that is directed away from the wall. The wall-induced lift force arises as a result of two fundamental mechanisms. Using inviscid arguments, the flow relative to the particle can be expected to accelerate more within the gap between the particle and the wall than above the particle away from the wall. The resulting difference in pressure around the sphere will contribute to a wall-ward force on the particle. On the other hand, vorticity generated on the particle surface is not symmetrically distributed in the wake due to the presence of the nearby wall. The asymmetry in the vorticity distribution contributes to an asymmetric induced flow, whose effect is to generate a lift force on the particle directed away from the wall. Zeng et al. (2009) performed a computational study for a rigid sphere in a linear wall bounded shear flow to understand the effect of the wall on the lift force. In Zeng et al. (2009) computations, the particle Reynolds number ranges from 2 to 250 at separation distances to the wall from nearly sitting on the wall, $L = 0.505$, to far away from the wall, $L = 4$. They noted that for separation distances larger than $L = 0.75$, C_L changes sign at some Re_p and becomes negative. However, for $L < 0.75$, the lift coefficient remains positive over the entire range of Re_p considered. Therefore near the wall, the critical Reynolds $Re_{p,cr}$ number at which $C_L = 0$, is not constant and it depends on the distance from the wall. The values of $Re_{p,cr}$ for different L as found by Zeng et al. (2009) lie in table 5.1. It is seen that at $L = 0.75$, the critical Reynolds number is close to 200 and decreases substantially to $Re_{p,cr} = 60$ at $L = 4$. For distances smaller than $L = 0.75$ Zeng et al. (2009) did not determine whether the lift coefficient will become negative at even higher Re_p since their calculations were limited to $Re_p < 250$. Due to these results, Zeng et al. (2009) noted that for distances far from $L = 4$ the value of the critical particle Reynolds number $Re_{p,cr} \simeq 60$ can be compared to the value found by Kurose and Komori (1999). In the present case of the droplets, Sugioka and Komori (2006) has specified for the case of the droplets in unbounded shear flow that the value reads $Re_{p,cr} \simeq 50$.

In the pipe flow concerned and for the typical droplet diameter considered in the present study case, the non-dimensional distance from the wall ranges between 0.5 and 20. Therefore, near the wall the wall-induced lift should be considered, while far away from the wall the conditions of the unbounded shear flow can be applied.
Zeng et al. (2009) presented a numerical correlation for the lift coefficient based on his DNS results. This correlation is valid over a range $1 < Re_p < 200$ and $L > 0.5$. This correlation has a complicated form and it reads:

$$C_L = C_{L,w} exp(-0.5\delta(Re_p/250)^{4/3})[exp(\alpha_L^{\beta_L}) - \lambda_L] \tag{5.10}$$

L	$Re_{p,cr}$
0.75	198.19
1	125.5
2	74.70
4	59.11

Table 5.2: The value of $Re_{p,cr}$ at which C_L inverses its sign at different distances from the wall, table provided by Zeng et al. (2009)

where

$$\begin{aligned} \delta &= L - 1/2 \\ C_{L,w} &= \frac{3.663}{(Re_p^2 + 0.1173)^{0.22}} \\ \alpha_L(Re_p) &= -exp(-0.3 + 0.025Re_p) \\ \beta_L(Re_p) &= 0.8 + 0.01Re_p \\ \lambda_L(\delta, Re_p) &= (1 - exp(-\delta))(Re_p/250)^{5/2} \end{aligned} \tag{5.11}$$

The validity of this correlation is presented in figure 5.7, where the value of the lift coefficient from the DNS results and the correlation of Zeng et al. (2009) are plotted in terms of the Re_p at several distances from the wall. The correlation of Zeng fits the DNS results for the zone near the wall ($L \in [0,505; 2]$). For distances far from the wall ($L = 4$) the correlation gives values in the same order of magnitude that's calculated by DNS, but this result presents a deficiency: the lift coefficient changes its sign before $Re_p = 50$. Therefore, an extra curve is presented considering that $L = 10$. In this case, figure (5.7,d) shows that if we apply Zeng formula far away from the wall $Re_{p,cr}$ becomes very small with respect to 50, the value estimated by Sugioka and Komori (2006) to be the critical Reynolds number in unbounded shear flow. Then we can conclude that the correlation of Zeng fails as the distance between the wall and the particle increases.

It has been shown earlier that in the zone of the tube center, the flow is considered to be unbounded shear flow. Therefore, the correlation of Zeng et al. (2009) is not valid for all the domain of the flow of interest in the present study. According to our knowledge, there is no model for the lift coefficient for the case of unbounded shear flow. In this chapter we propose a correlation that fits with the DNS results of Sugioka and Komori (2006) that are valid for the particle in an unbounded shear flow for particle Reynolds number that ranges between 1 and 500. This correlation reads

$$\begin{aligned} C_L &= \left(15.5\frac{S_r}{Re_p^2}\exp^{-2Re_p^{-1.4}} + 0.12\right) \\ &+ \left(\frac{5}{Re_p} - 0.05S_r - 0.08\right)\left(\frac{\tanh(Re_p - 55) + 1}{2}\right) \end{aligned} \tag{5.12}$$

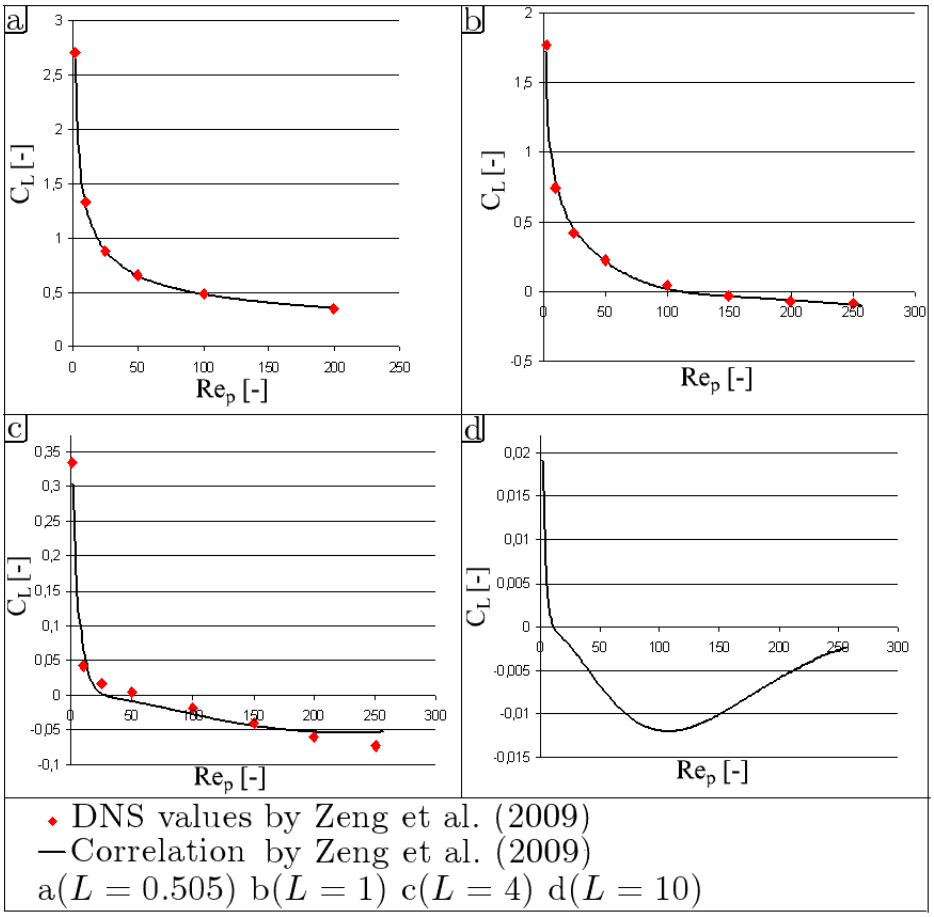

Figure 5.7: Comparing the DNS values and the correlation of Zeng et al. (2009) at several distances from the wall

Figure 5.8 presents the comparison of the new correlation with the DNS results of Sugioka and Komori (2006). Although it is not perfect, the above correlation shows a favorable agreement with the DNS results and respect the characteristic of inverting the sign in the limit between 50 and 60. Moreover this correlations stays valid in the zone far from the wall, which is better than the values predicted by the correlation of Zeng.

5.2 Impact of the lift force modeling on the study case

After this detailed study about the different modelings of the lift force, the impact of these modelings on our study case is analyzed in this section. In

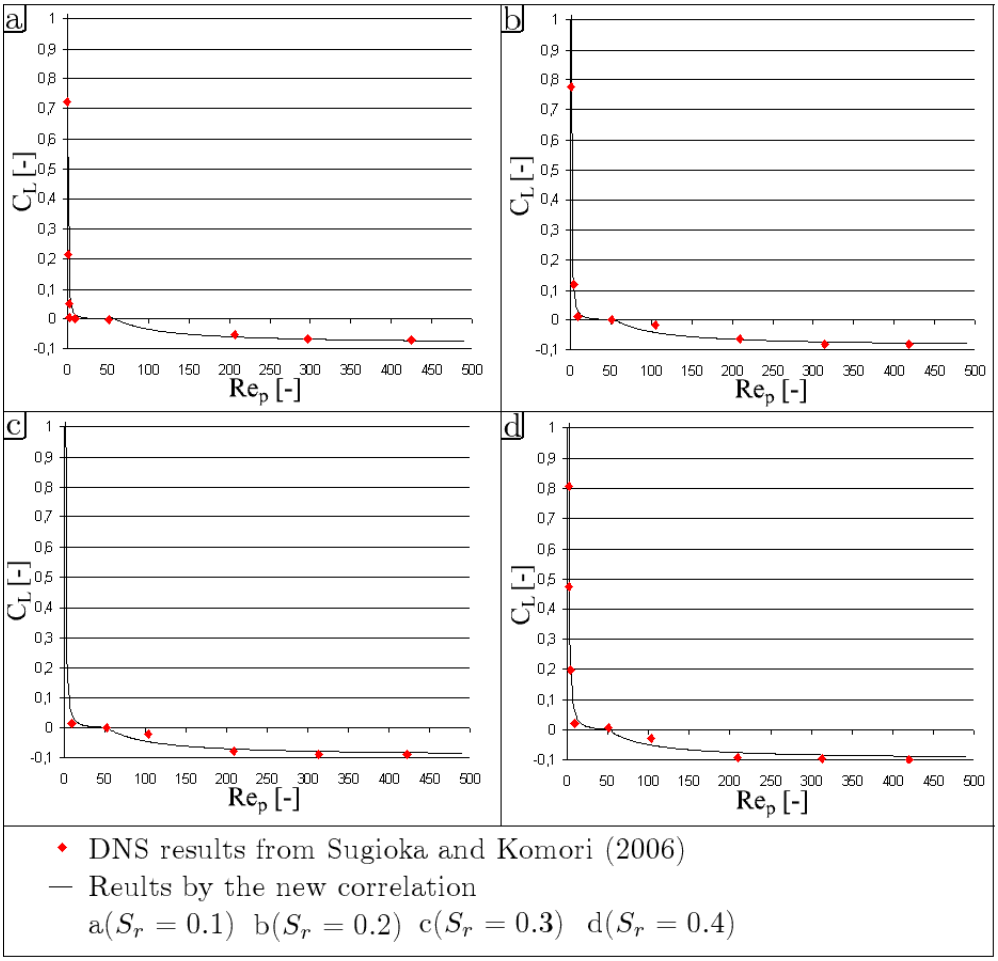

Figure 5.8: Comparing the DNS values of Sugioka and Komori (2006) and the new correlation at several distances shear rates for unbounded shear flow

figure 5.9, the vapor volume fraction fields are presented for five simulation cases with different models of the lift. First in case (a) the model of Auton (1987) is used, this model has been used in all the previous chapters. The lift force here is overestimated and it pushes the droplets from the wall to the center. In case (b) the model of Saffman (1965) is used, here also all the droplets are pushed away from the wall and concentrated zones are found in the center. In case (c) the model of Saffman (1965) is applied with the empirical function from McLaughlin (1991) and correction of equation (5.9). Here the effect of the wall is taken into account roughly by considering $C_L = 0.29$ near the wall. Therefore in this case it is shown that the droplets do not approach the wall because of the strong lift near the wall. But from the other side a lift force with opposite sign will push the droplets from the center to the wall, this force is due to the change of the sign of the lift force

estimated by empirical function from McLaughlin (1991). The same case is done again in case (d) but this time the correlation of Zeng et al. (2009) is used near the wall instead of considering roughly that $C_L = 0.29$. The results are similar to the case (c). Finally, in case (e) the correlation of Zeng et al. (2009) is used all over the domain and similar results are found.

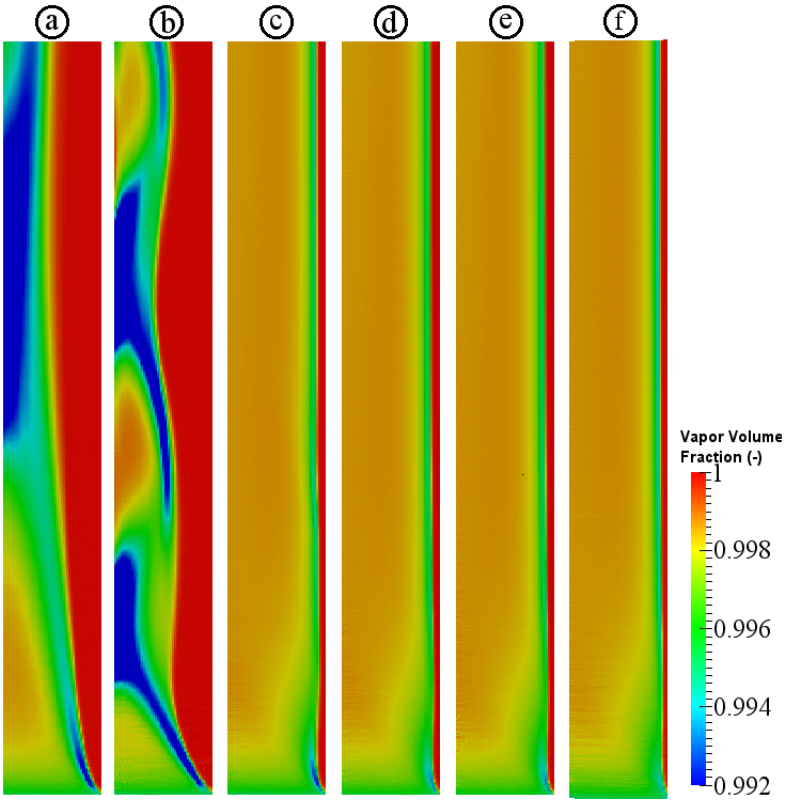

Figure 5.9: The impact of different lift modeling on the spatial distribution of the droplets over the pipe section: a) Model of Auton (1987)- b) Model of Saffman (1965)- c) Model of Saffman (1965) + empirical function from McLaughlin (1991) + Correction of equation (5.9) + $C_L = 0.29$ near the wall- d) Model of Saffman (1965) + empirical function from McLaughlin (1991) + Correction of equation (5.9) + model Zeng et al. (2009) near the wall- e) Model of Zeng et al. (2009)- f) New correlation proposed in equation (5.12) + model Zeng et al. (2009) near the wall

5.3 Conclusion

The impact of the different modelings of the lift force on the distribution of the droplets over the pipe radial section, shows that the modeling of

this force is of substantial importance in our study. Our case of interest requires a good modeling for the lift force in a domain where the particle Reynolds number reaches high values and the shear rate range lies between 0 and 1. Also, the present study can be divided into two main domains, near-wall shear flow and unbounded shear flow. Therefore the wall-induced shear can not be ignored. The detailed revision of the modeling of this force shows the following. The lift force action on a droplet is different from that acting on a bubble and it is very similar to the lift force action on a solid sphere. The basic analytical models of Auton (1987) and Saffman (1965) overestimate the lift force and they do not allow to fit the values found in DNS calculations. The review of the different DNS results shows us that two main characteristics should be taken into account. First, the lift force is always positive and proportionally high near the wall. Second, that far from the wall the lift force inverses its sign for a critical value of the particle Reynolds number. Several solutions have been proposed in this chapter in order to take into account these phenomena. All the proposed solutions gave similar impact on the droplets distribution. For more accuracy for the value of the lift force a new correlation is proposed based on the DNS results of Sugioka and Komori (2006) for the unbounded shear flow. For an accurate modeling of the lift, we propose to use the correlation of Zeng et al. (2009) in the near-wall region and the new correlation proposed in this chapter for the zone away from the wall.

Chapter 6

Application on the cooling of a damaged PWR reactor core

The targeted study that motivates this work is the estimation of the cooling capacity of the vapor-droplet flow in a damaged PWR reactor core. It has been postulated that the spatial distribution of the droplets is a main characteristic of the flow and that has a direct impact on the cooling capacity of the flow. It is the time to state about this hypothesis and to examine whether the proposed modification on the modeling of the droplet dynamics actually impacts the rate of heat transfer with the wall.
As it is shown in the previous chapters, the modeling of the turbulence and the lift force have an important impact on the spatial distribution of the droplets. Moreover we noted that the existing turbulence models underestimate the turbulence impact on the droplets distribution, while the existing lift force model overestimates the impact of this force on the droplets. These wrong estimations impact the simulation of the droplets' distribution. The numerical results in this case show that droplets tend to concentrate in the center of the tube where the near-wall zone stays empty from any droplet. In a try to ameliorate these results, modifications were proposed on the modeling of these forces, which changed the over all distribution of the droplets. In this chapter, we analyze the consequences of these modelings on the quantity of heat that the flow can absorb from the wall. A new series of test cases has been done replacing the adiabatic wall considered in all the previous cases by a hot wall of temperature $573K$.
In figure 1.2, we enumerated the different heat transfer mechanisms those occur in this type of the flow, which can be summarized as follows: the convection of the vapor with the wall, the convection between the vapor and the droplets, the conduction between the droplet and the wall in a case of direct contact of the droplet on the wall, and the radiation of the wall toward the vapor and the droplets. The latter two effects are not considered in the present work, but they are treated in parallel projects due to their impor-

tance and complexity. It is worth noting that the estimation of these effects also depends on the distribution of the droplets. Actually the radiation depends on the distance between the droplet and the wall. Besides the direct conduction between the droplets and the wall depends on estimating the quantity of droplets that can be in contact with the wall. Therefore adding these models in the future will be an additional proof on the importance of the present study.
Four study cases have been realized to show the role of each modeling change of the droplet distribution on the heat transfer rate. These five cases are done with the same geometry mesh and initial conditions defined in section 3.4 by adding the hot wall condition. Only the models of turbulence and the model of lift force will be changed from a case to another. Let us define the five cases and the corresponding problematic:

1. The first case is a basic case done with the model $k-\varepsilon$ for the turbulence of the vapor, the model Tchen-Hinze for the turbulence of the droplets, and the model of Auton et al. (1988) for the lift force.

2. The second case is done with the model $R_{ij}-\varepsilon$ for the turbulence of the vapor, the model Q2Q12 for the turbulence of the droplets, and the model of Auton et al. (1988) for the lift force. This case is already done for the adiabatic case and it aims here to show importance of the choice of the turbulence models even without any modification.

3. The third case is done with the $R_{ij}-\varepsilon$ for the turbulence of the vapor, and the model Q2Q12 for the turbulence of the droplets. But in this case we replaced the model of Auton et al. (1988) of the lift force by the model proposed in chapter 5. This test aim at showing separately the impact of the overestimation of the lift force on the heat transfer.

4. The fourth case is done with the model $R_{ij}-\varepsilon$ for the turbulence of the vapor, the modified model of Q2Q12 for the turbulence of the droplets, and the new proposed model for the lift force. This case aims at the impact of all the proposed models on the heat transfer.

In the following, for simplicity purpose, these cases will be noted as case 1, case 2, ... consequently.

First of all, figure 6.1 shows how the distribution of the droplets changes with each change in the modeling for the four presented cases. These cases are already described in the previous chapters in the case of adiabatic walls. We do not remark any special effect of the hot wall on the dynamic structure of the flow. The differences between the cases stay of the same type described before in chapters 4 and 5. We will remind rapidly the difference between the cases. In case 1, the droplets are concentrated in the center of the tube and no droplet approaches the near wall zone. In case 2, when we replace the turbulent models $k-\varepsilon$ by $R_j-\varepsilon$ and $Tchen-Hinze$ by Q2Q12, the droplets

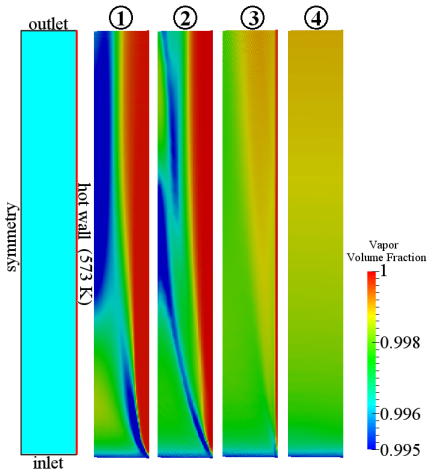

Figure 6.1: The volume fraction distribution of the vapor for the four modeling cases

are more dispersed but they stay in the center of the tube. The flow has the same structure as in the case 1, because of the over estimation of the lift force that pushes all the droplets away from the wall in the two cases. Therefore in case 3, when the model of the lift force Auton et al. (1988) is replaced by the new lift force model, the droplets become distributed almost overall the tube section but they do not reach the wall (see the thin red line near the wall in case 3 of figure 6.1). In this case, an important wall-induced lift force prevents the droplets to approach the wall, besides the underestimated effect of the turbulence dispersion is not enough to make the droplets reach the wall. In case 4, the lift force and the turbulence models are modified and the droplets are distributed all over the tube section.

The difference in the droplets distribution impacts the evaporation process. Figure 6.2 shows the interfacial mass transfer rate Γ_1 in the four cases. Evaporation increases in the zones where the droplets concentrate. The evaporation of the droplets decreases the temperature of the vapor. Then when the evaporation is concentrated in a specific zone the vapor will become locally cooler in this zone. This decreases its ability to evaporate more droplets in this zone. Figure 6.3 shows the mean mass transfer rate over the whole simulated domain in the four cases in the form of a histogram. The mass transfer rate is minimum in the case 1 where the droplets are accumulated in the center and the maximum is case 4 where the droplets are totally dispersed. This histogram shows that the more the droplets are dispersed all over the tube section the more the mass transfer rate increases.

In figure 6.4, the vapor temperature field of the four cases is presented. The droplets evaporation directly impacts the vapor temperature fields. In case 1 and 2 the vapor is locally cooled in the accumulation zones in the tube center

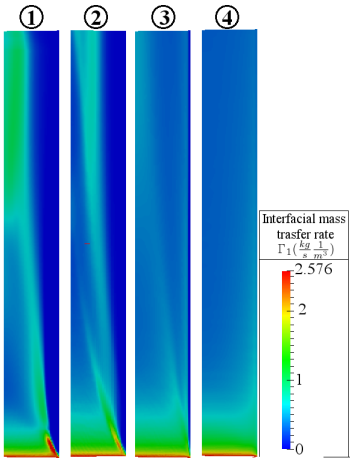

Figure 6.2: The quantity of vapor that results from the droplet evaporation for the four modeling cases

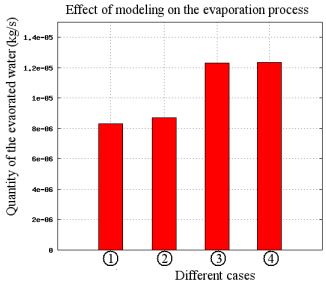

Figure 6.3: The quantity rate of vapor that results from the droplet evaporation for the four modeling cases

while the vapor near the wall stays proportionally hot with respect to other cases. In case 3, the temperature of the vapor is more homogeneous all over the tube section as in case 4. The heat transfer with the wall depends mainly on the temperature of the vapor and its gradient in the near-wall zone. The temperature profile of the vapor is an interesting factor in determining the quantity of heat that is absorbed by the flow.

Figure 6.5 shows the enthalpy transfer rate with the wall in all the four cases as a histogram. The flow extracts the maximum of enthalpy when the droplets are totally dispersed (case 4). On the other side, the minimum enthalpy transfer rate is extracted when the droplets are concentrated in the center of the tube (case 1).

In this analysis, we show consequently the impact of the estimation of the droplets distribution on the wall cooling process. Each amelioration in the modeling of the droplets distribution impacts the quantity of heat extracted from the wall. The heat transfer in case 2 is more important than the heat

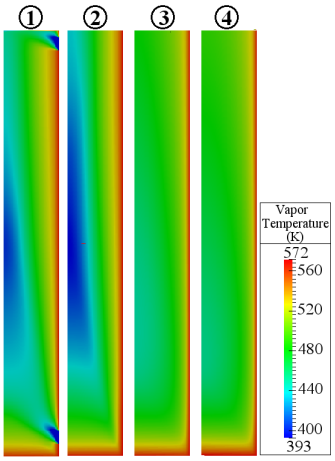

Figure 6.4: The vapor temperature distribution field for the four modeling cases

transfer in case 1 since the droplets are more dispersed even if they stay in the center of the tube. In case 3, the quantity of heat absorbed from the wall increases since we removed the effect of the lift force which concentrates the droplets. Finally in case 4, the results are comparable to that in case 3. But we should note an important remark here, that in case 3 the droplets are simulated to never touch the wall but in case 4 droplets can be in direct contact with the wall. Therefore in a case where we model the direct heat transfer between the wall and the droplets in contact, the heat transfer in case 4 will be more important than in case 3. Finally, this study shows the importance of improving the estimation of the droplets distribution on the estimation of the wall cooling. The heat transfer rate estimated after choosing the good turbulence models and integrating the modifications on the models in case 4 is 118% more than the value estimated in the case 1 done with basic models.

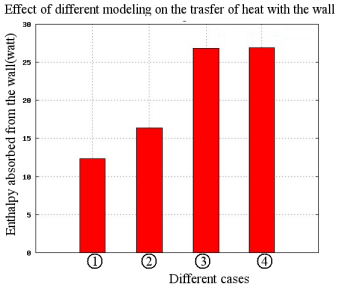

Figure 6.5: The quantity of enthalpy transfer rate with the wall for the four modeling cases

Chapter 7

General conclusion

Our work aims to improve the understanding of the fluid-gas non isothermal turbulent wall bounded flow. In particular, for the vapor droplets flow there is still open questions about the heat transfer with the wall. Only CFD codes can help a better understanding for the wall to fluid heat transfer in a DFFB[1]. Specifically, in the context of ameliorating the estimation of the heat transfer during a LOCA accident in the core of a PWR, this study deals with the adaptation of the code Neptune_CFD to the cases of dispersed droplets flow. The flow is considered diluted and the droplets are considered to be spherical and not deformable.
First, we introduced the various hypothesis in the methodology Euler-Euler used by CFD approach and particularly in this computer code. A description of two-phase flow model is presented, using separate mass, momentum, and energy equations for the two phases. These separate balance equations are obtained in an averaging process starting from the local instantaneous conservation equations of the individual phases. During the averaging process, important information on local flow processes is lost and, consequently, additional correlations were needed in order to close the system of equations. The terms that need closure models are identified, such as the terms of turbulence of the two phases and the terms of the interfacial transfer of mass, momentum, and energy. The treatment of these models lays on several physical aspects starting from the models of the heat transfer to the dynamics of the two phases, beside the existence of several sizes of droplets and the evolution of their sizes. The treatment of all these problems is a very wide physical issue therefore we restricted our study to a main characteristic of the flow which is the spatial distribution of the droplets, due to its direct impact on the wall to flow heat transfer. The modeling of the droplets distribution is also a composed problem since it depends on several phenomena. Thanks to a physical and a theoretical analysis in chapter 2, we identified that the main phenomena that affect the droplets distribution

[1] Dispersed Flow Film Boiling

are the forces between the vapor and the droplets and the turbulence of the vapor and the droplets. After a brief presentation of the different forces that impact the droplets distribution, a simulation test case was done in chapter 3 using basic models to specify the importance of the modeling of each term. This study case allows us to draw general conclusions concerning the main mechanism that control the simulated flow:

- Because of their important inertia, droplets are able to retain memories of their velocity for long distances. Therefore the phenomena that occurs at the inlet of the channel influences the structure of the flow for long distances in the tube.

- The main force that drives the propagation of the droplet in the stream flow direction is the drag force. Depending on the DNS results of Kurose and Komori (1999) and Sugioka and Komori (2006) we deduced that in our case the model of Wallis (1969) is able to predict the drag coefficient with a degree of uncertainty that do not exceed 10% which is acceptable for our study case.

- The radial motion of the droplets depends mainly on two main forces: lift force and the force of turbulent dispersion.

- The lift force model Auton et al. (1988), used in the test case, estimates a very important effect of the lift force which leads to push all the droplets away from the wall and makes the near-wall zone empty from any droplets. In the other hand, the turbulent dispersion force pushes the droplets in the inverse sense in the entry zone which leads to form concentration zones.

- These concentration zones appear to be not realistic, this drives us to conclude that the lift force and the turbulent dispersion force are not well estimated. Therefore in the rest of the present document, we extend the research about the closure of these terms.

The turbulence modeling shows a significant impact on the droplets distribution. The value and the profile of the turbulent kinetic energy of the droplets k_2 is the main term that impacts directly the distribution of the droplets since the gradient of the kinetic stress tensor of the dispersed phase is understood as a source term in the droplets momentum averaged equation. Three models participate in the prediction of k_2 with different degrees of importance: the turbulence modeling of the continuous phase, the turbulence model of the dispersed phase and the turbulent coupling between the two phases. These two models of different levels of numerical complexity and physical accuracy are considered for each phase. For the continuous phase the choice between an isotropic model $k-\varepsilon$ and a non-isotropic model $R_{ij}-\varepsilon$ is studied, to check if the modeling of the anisotropy of the vapor

turbulence has an important impact on the droplets distribution. For the droplets turbulence two models are also studied, the simple algebraic model called Tchen-Hinze (Tchen (1947)) is compared with the model Q2Q12 (Simonin (2000)) based on two transport equations for the turbulent kinetic energy of the dispersed phase k_2 and the fluctuation energy covariance k_{12}. Then we discussed the modeling of the turbulent energy transfer between the two phase and new modeling proposed for this issue.
First we discussed these models theoretically. Then two simulation cases with different combination of the turbulence models ($k-\varepsilon$ & Tchen-Hinze or $R_j-\varepsilon$ & Q2Q12) were compared to the experimental data of Kulick et al. (1994) of air-particles vertical channel flow. These comparisons aim to test the ability of these different turbulence models to reproduce the characteristics of the continuous and the dispersed phase. The comparison with the experimental data shows that both models $k-\varepsilon$ and $R_{ij}-\varepsilon$ are able to predict the streamwise mean velocity of the gaseous phase. Besides, $R_{ij}-\varepsilon$ is evidently more able to produce the anisotropy of the air turbulence. The experimental data shows that for the case of heavy particles of Kulick et al. (1994), the velocity fluctuations of the particles are anisotropic and they are important and comparable to the fluctuations of the gaseous phase. From theoretical analysis of the two models, it was expected that the model Tchen-Hinze may underestimate the value of the turbulent kinetic energy of the dispersed phase. But Q2Q12 is expected to have a better estimation for the value of k_2 since it takes into account the particle's own agitation beside the effect of the gas on the particles. Results show that both turbulence models sharply underestimate the value of the turbulent kinetic energy of the dispersed phase. Therefore we decided to extend our research about the modeling different terms of the model Q2Q12 in order to verify which term causes this attenuation of the value of k_2. We noticed that the term of the interfacial turbulent energy transfer in the model Q2Q12 causes the destruction of the turbulent kinetic energy of the particles. A detailed bibliographical study about the modeling of the turbulent coupling term helps to precise the disadvantages of the actual modeling and proposed some solutions in the work of Xu and Subramaniam (2007), Xu and Subramaniam (2006), and Sundaram and Collins (1999). In the present study, we proposed a new closure method in analogy with the work of turbulence scale separation that has been proposed for the closure of the turbulent coupling term in the two-phase model of $k-\varepsilon$ (Chahed (1999), "Standard" model etc.). This method is based on separation of the turbulence interaction between the two phases into destruction of droplets agitation at small turbulence scales in the wake of the droplet; and production of droplets agitation at big turbulent scales when it cross large eddies. A strong hypothesis had been considered to neglect the turbulent energy of the vapor at scales smaller than droplets diameter. This can be justified for cases with small droplets near the scale length scale of

Kolmogorov like those in the experiment of Kulick et al. (1994), but it is not so evident for big droplets. The proposed closure helps us to estimate a particle's turbulent energy k_2 that lays in the same order of scale measured in the experiment. For the present study this solution is enough but our analysis lights on the importance of the closure of this term for future research projects, where turbulent energy of the vapor in the wake of the droplet should be calculated differently regarding the scale of the droplet size.
The experimental data do not provide enough information about the particles' spatial distribution, therefore the impact of the turbulence modeling on the droplets distribution is studied numerically by analyzing different simulation cases of vapor-droplet flow in a vertical tube using different turbulence models. The main results can be summarized as follows:

- The two models $k-\varepsilon$ and $R_{ij}-\varepsilon$ produce the same type of flow structures with minor differences. The impact of these models on the droplets distribution is indirect. The differences between the two models had been explained in details to show that the impact of the vapor turbulence on the droplets distribution depends also on the consequences through other models as the model of the drag force and the model of the turbulence of the dispersed phase. As a conclusion, the results of the model $k-\varepsilon$ are acceptable although we know that $R_{ij}-\varepsilon$ is better.

- Although we showed that both models Tchen-Hinze and Q2Q12 underestimate the value of the droplets turbulent kinetic energy, we analyzed the different impact of these models on the droplets distribution. First, we note that Q2Q12 permits to control the inlet condition of the channel while Tchen-Hinze impose an estimated value for the entry conditions calculated from the agitation of the continuous phase. Tests show that the entry value of k_2 calculated by the model of Tchen impacts the structure of the flow. Moreover, the profiles of k_2 shows that Q2Q12 estimates k_2 more independently from k_1 in comparison with Tchen.

- The proposed closure of the interfacial turbulent energy transfer in the Q2Q12 model permits to have a good estimation of the droplets agitation. The correction of the value of k_2 changes the overall structure of the spatial dispersion of the droplets, where no concentrated zones were formed and the droplets were dispersed all over the tube section.

The impact of the different modeling of the lift force on the distribution of the droplets over the pipe radial section, shows that the modeling of this force is of substantial importance in our study. The lift force plays a central

role in the preferential accumulation of the droplets either close or away from the wall. There are three primary contributions to the lift force: the shear induced lift force, the rotation induced lift force, and the wall induced lift force. The lift force is characterized by the non-dimensional distance from the wall, the particle Reynolds number, and the non-dimensional shear rate. Our case of interest requires a good modeling for the lift force in a domain where the particle Reynolds number reaches high values and the shear rate range lies between 0 and 1. Also, the present study can be divided into two main domains, near-wall shear flow and unbounded shear flow. Therefore the wall-induced shear can not be ignored. The basic analytical models of Auton (1987) and Saffman (1965) overestimate the lift force and they do not allow to fit the values found in DNS calculations. As a conclusion from several DNS numerical results (e.g. Sugioka and Komori (2006), Zeng et al. (2009),..) we note that: the lift force acting on a droplet is different from that acting on a bubble and it is very similar to the lift force action on a solid sphere. The lift force is always positive and proportionally high near the wall (droplet almost in touch with the wall). For a small distance far from the wall the lift force inverses its sign for a critical value of the particle Reynolds number. This critical value decreases as the distance from the wall increases until it reaches the value $Re_p \simeq 50$ for unbounded flows. In order to fit with these numerical facts we proposed two solutions

- Kurose et al. (2001) noticed that the combination of the model of Saffman (1965) and the correlation of McLaughlin (1991) shows a good agreement with the experimental results proportionally to other analytical models. This combination presents a disadvantage that the critical Re_p is smaller than 50. Therefore we proposed an extension of the correlation of McLaughlin (1991) to correct this. This solution allows to calculate a lift coefficient in the same order of magnitude of the results of McLaughlin and to change the sign at $Re_p \simeq 50$. This result can be accepted but it does not fits exactly the DNS results therefore we continued our research.

- Based on his DNS values Zeng et al. (2009) proposed a correlation to calculate the lift coefficient that takes into account the effect of the wall-induced lift. This correlation failed in the zone far from the wall and do not fits the DNS results of Sugioka and Komori (2006). Therefore, we proposed a numerical correlation based on the DNS results of Sugioka and Komori (2006) for the case of unbounded shear flow. Then for an accurate modeling of the lift, we proposed to use the correlation of Zeng et al. (2009) in the near-wall region and the new correlation proposed in this document for the zone away from the wall.

Finally we studied the impact of all these modeling methods on the heat transfer with the wall in a simulation test case with hot walls. This test

takes into account only the effect of the convection of the vapor with the wall and the droplets. Our results show that the more the droplets are dispersed, more the extracted heat by the vapor from the wall increases. The heat transfer rate estimated after choosing the good turbulence models and integrating the modifications on the models Q2Q12 and the lift is 118% more than the value estimated in the basic study case done with models $k-\varepsilon$, Tchen-Hinze for the turbulence and the model of Auton et al. (1988) for the lift force. This shows the importance of our study for the context case.
Starting from a very general problem which is the modeling of a turbulent vapor droplets dispersed flow, we could precise that the droplets distribution is the main characteristic that should be studied. Then by analyzing all the models those impacts the droplets distribution, we concluded that the lift force model is overestimated while the turbulent dispersion effect is underestimated. Extended research was done to ameliorate the estimation of these phenomena and satisfying solutions had been proposed.
This study can be extended and several perspectives can be proposed as follows:

1. A major problem in the treatment of this subject is the lack in the experimental data. An experimental research counting for the conditions at the entry or at the level of the quench front and providing a clear view about the preferential zone of concentration of the droplets can provide a big help in conforming most of the modeling doubts.

2. The size of the droplet is a main factor that can impact most of the dynamic and the thermal models of the flow. Therefore modeling the change of size of the droplets is an essential issue in these type of flows.

3. The modeling of the turbulence of the droplets in the present study is done by isotropic models. Tests show that the dispersed phase turbulence may present an important anisotropy that should be taken into account.

4. The modeling of the term of the turbulent energy transfer between the two phases is treated in this study based on hypothesis that can not be applied for all types of flow. This study precises that the modeling of this term is of high importance. Therefore we propose that future studies should be done on the modeling of this term.

Chapter 8

Résumé en français

Chapter I

Introduction générale

Les écoulements diphasiques, gaz-gouttes, sont des phénomènes qui se produisent dans des situations naturelles et industrielles. Ces écoulements sont l'objet de recherche dans de nombreux secteurs industriels comme la production d'énergie électrique (générateurs de vapeur des centrales électriques, les condensateurs, échangeurs thermiques), l'industrie pétrolière (extraction et transport de produits pétroliers), la combustion de l'essence et de l'air dans un moteur d'automobile etc. Le développement d'outils de calcul numérique pour simuler ce type d'écoulement est utile. Puisque les méthodes de simulation numérique directe sont trop coûteuses pour les applications industrielles, la simulation de valeurs moyennes apparaît comme la solution optimale. D'autre part, la simulation de valeurs moyennes nécessite un effort de modélisation élevé pour reproduire la physique locale, avec une précision satisfaisante. Dans la présente étude, nous traitons ce problème dans le contexte de la sûreté nucléaire.

I.1. Contexte de l'étude

Un des accidents de référence pouvant se produire dans un REP (Réacteur à Eau Pressurisée) est l'APRP (Accident de Perte de Réfrigérant Primaire). Cet accident est associé à une perte de pression qui conduit à la vaporisation de l'eau dans le cIJur du réacteur, et à l'augmentation de la température des assemblages. Dans la suite, de l'eau est injectée et une évaporation violente de l'eau se produit au niveau de l'interface entre l'eau et de vapeur, qui est appelée le front de trempe. L'évaporation violente au front de trempe provoque l'arrachement de gouttes d'eau et l'écoulement de vapeur-gouttes domine dans la partie supérieure du cIJur de réacteur. L'efficacité du refroidissement de ce mélange est importante pour évaluer la suite de l'accident. Les gouttelettes agissent comme des puits de chaleur pour la vapeur. Elles contrôlent ainsi le profil de température de vapeur qui, à son tour, détermine

le transfert de chaleur avec la paroi.

Figure I.1 montre un schema représentatif de l'écoulement de vapeur-

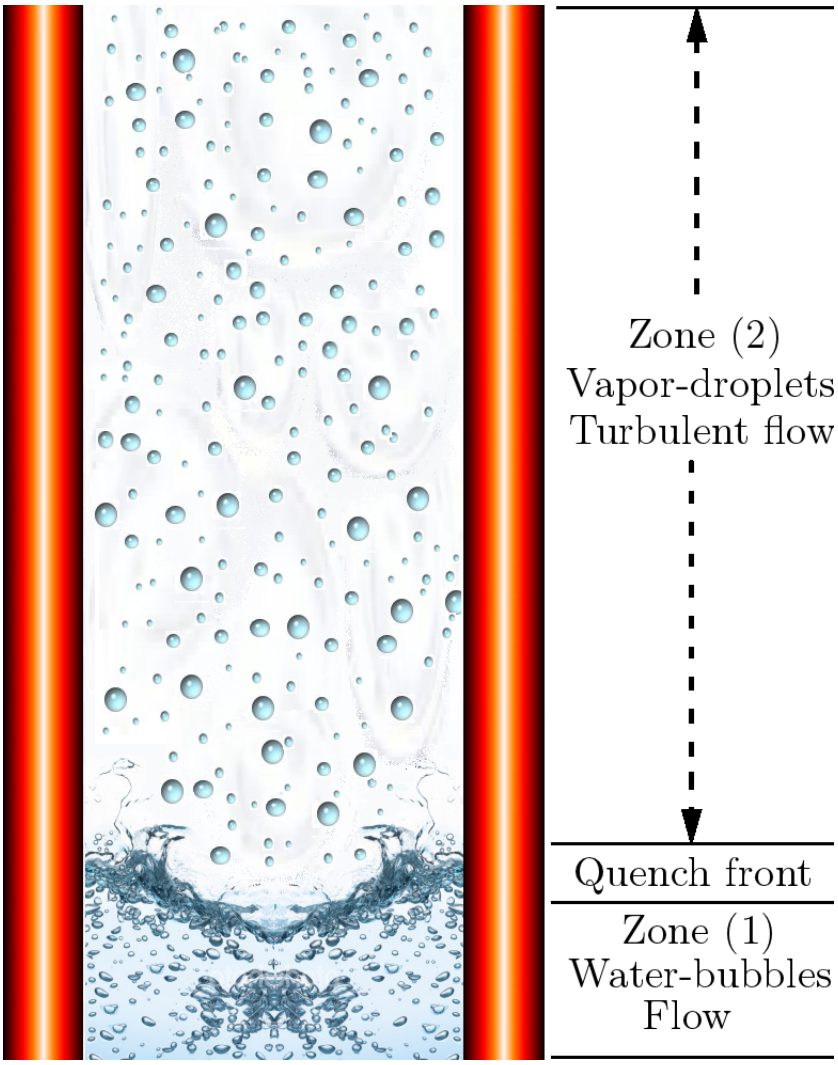

Figure I.1: Figure qui représente l'écoulement de vapeur-gouttelettes turbulente entre deux crayons de combustible chaud dans un coeur de réacteur PWR

gouttelettes turbulente, au dessus du front de trempe, entre deux barres de combustible chaud dans un coeur de réacteur REP accidenté. Les mécanismes de transfert de chaleur dans cet écoulement dispersé sont illustrés dans la figure I.2. Ces effets sont distingués par Andreani and Yadigaroglu (1997) comme suit:

- Le transfert de chaleur par convection entre la paroi, la vapeur, et les gouttelettes.

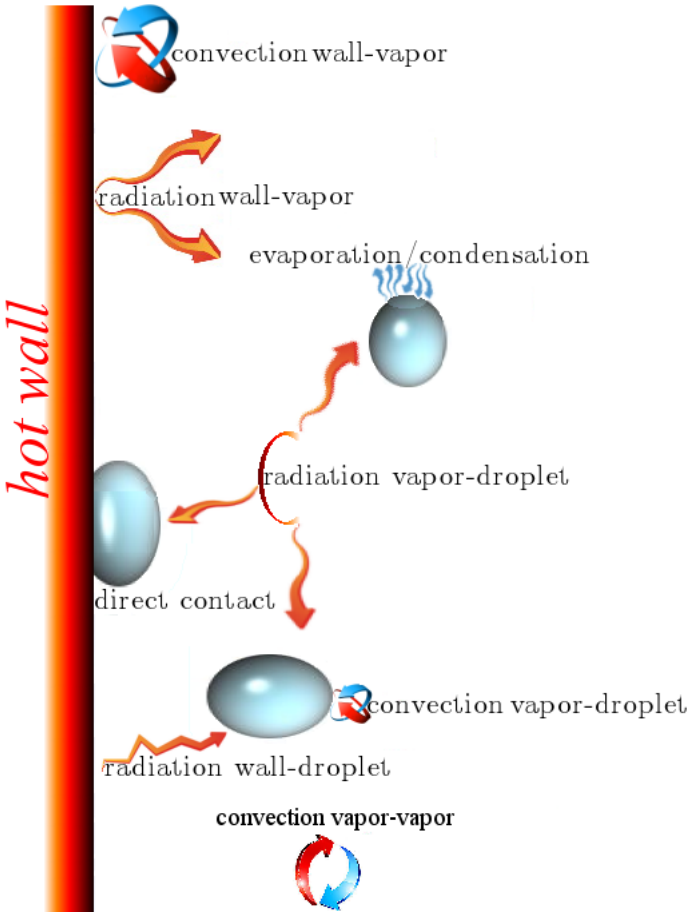

Figure I.2: Figure qui représente les mécanismes de transfert de chaleur entre une paroi chaude et un écoulement vapeur-gouttelettes

- Le transfert de chaleur radiatif entre la paroi, la vapeur, et les gouttelettes.
- Le transfert de chaleur par contact direct entre les gouttes et la paroi.
- Transfert par l'évaporation des gouttelettes ou condensation de vapeur

La répartition spatiale des gouttelettes est un facteur important qui influe la modélisation de la plupart de ces mécanismes. Par conséquence, l'estimation de la concentration des gouttelettes est nécessaire pour estimer le taux de transfert de chaleur dans le coeur du réacteur. La modélisation de la distribution des gouttelettes est un problème composé car il dépend de plusieurs phénomènes comme les forces entre la vapeur et les gouttelettes et la turbulence. Notre objectif général est d'améliorer la modélisation de la distribution spatiale des gouttelettes au sein d'un outil de simulation à

l'échelle de la CFD.

Chapter II

Modélisation des écoulements diphasiques

Le code NEPTUNE-CFD est basé sur une approche de type Euler/Euler pour laquelle chaque phase de l'écoulement est décrite à l'aide des variables continues. L'évolution des grandeurs locales de l'écoulement est régie par les équations de conservation locales moyennées :

- l'équation de bilan moyennée de masse,
- l'équation de bilan moyennée de Quantité De Mouvement (QDM),
- l'équation de bilan moyennée d'enthalpie totale.

Ces équations sont obtenues à partir des équations locales instantanées. Chaque phase de l'écoulement étant considérée comme continue, le milieu dans son ensemble possède des discontinuités, rendant les grandeurs locales de l'écoulement non dérivables au sens des fonctions. Le passage des équations locales instantanées aux équations locales moyennées nécessite alors :

- de se placer dans l'espace des distributions afin de rendre l'ensemble du milieu dérivable, les équations de conservation locales instantanées sont alors multipliées par la fonction caractéristique de phase $\chi_k(M,t)$:

  $\chi_k(M,t) = 1$ Si le point M est situé dans la phase k à l'instant t (II.1)

  sinon:

  $$\chi_k(M,t) = 0 \tag{II.2}$$

  Par convention on note que $k = 1$ pour la phase vapeur et $k = 2$ pour la phase de gouttes.

- puis, de moyenner ces équations à l'aide d'un opérateur de moyenne statistique pondérée par la masse volumique. La moyenne statistique phasique d'une fonction ϕ_k de la phase k est définie par :

$$\underline{\phi} = \frac{\overline{\phi\chi_k}}{\alpha_k} \tag{II.3}$$

ou $\alpha_k = \overline{\chi_k}$ est la fraction volumique de la phase k. Ensuite la densité moyenne de la phase k est définie par:

$$\underline{\rho_k} = \frac{\overline{\rho_k\chi_k}}{\alpha_k} \tag{II.4}$$

Pour les équations d'équilibre local, il est plus pratique, pour les cas avec une densité variable de définir une moyenne pondérée par la densité de type Favre, qui s'écrit

$$\overline{\theta} \equiv \frac{\overline{\rho_k\theta\chi_k}}{\overline{\rho_k\chi_k}} = \frac{\overline{\rho_k\theta\chi_k}}{\alpha_k\widetilde{\rho_k}} \tag{II.5}$$

Ensuite une variable locale instantanée se décompose en une partie moyenne et une partie fluctuante comme suit:

$$\phi = \overline{\phi} + \phi' \qquad \overline{\phi'} = 0 \tag{II.6}$$

On applique par la suite ce moyen pour écrire le système d'équations moyennées à résoudre.

II.1. Les équations de conservation locales moyennées

II.1.1. Equation de bilan locale moyennée de masse

$$\boxed{\frac{\partial(\alpha_k\rho_k)}{\partial t} + \frac{\partial(\alpha_k\rho_k\overline{u_{ki}})}{\partial x_i} = \Gamma_k \qquad k = 1,2} \tag{II.7}$$

avec :

- α_k le taux de présence de la phase k,
- ρ_k la masse volumique de la phase k,
- $\overline{u_{ki}}$ les composantes de la vitesse locale moyenne de la phase k,
- Γ_k le transfert interfacial de masse à la phase k

$$\Gamma_k = \overline{\rho_k(\omega_i - u_{ki})n_{ki}\delta} \tag{II.8}$$

et :

- ω_i les composantes de la vitesse locale de l'interface,
- u_{ki} les composantes de la vitesse locale instantanée de la phase k,
- n_{ki} les composantes du vecteur unitaire normal à l'interface,
- δ la distribution de Dirac associée à l'interface

La relation locale moyennée de saut à l'interface s'écrit :

$$\boxed{\sum_{k=1,2} \Gamma_k = 0} \tag{II.9}$$

II.1.2. Equation de conservation locale moyennée de Quantité De Mouvement

$$\frac{\partial(\alpha_k \rho_k \overline{u_{ki}})}{\partial t} + \frac{\partial(\alpha_k \rho_k \overline{u_{ki}}\ \overline{u_{kj}})}{\partial x_j} = \alpha_k \rho_k g_i - \frac{\partial \alpha_k \overline{p_k}}{\partial x_j} + \frac{\partial}{\partial x_j}[\alpha_k(\overline{\tau_{ij,k}} - \rho_k \overline{R_{ij,k}})] + \overline{[(-p_k \delta_{ij} + \tau_{ij,k}) - \rho_k u_{ki}(u_{kj} - \omega_j)] n_{kj} \delta} \tag{II.10}$$

- g_i la résultante des forces volumiques,
- $\overline{\tau_{ij,k}}$ le tenseur des contraintes visqueuses de la phase k,
- $\overline{R_{ij,k}}$ le tenseur des contraintes turbulentes de la phase k,

$$\alpha_k \rho_k \overline{R_{ij,k}} = \overline{\rho_k u'_{ki} u'_{kj} \chi_k}$$

- u'_{ki} les composantes de la fluctuation de la vitesse de la phase k,
- le transfert interfacial de QDM à la phase k.

$$\overline{[(-p_k \delta_{ij} + \tau_{ij,k}) - \rho_k u_{ki}(u_{kj} - \omega_j)] n_{kj} \delta}$$

La relation locale moyennées de saut à l'interface s'ecrit:

$$\boxed{\sum_{k=1,2} \overline{[(-p_k \delta_{ij} + \tau_{ij,k}) - \rho_k u_{ki}(u_{kj} - \omega_j)] n_{kj} \delta} = \overline{f_{s,i} \delta}} \tag{II.11}$$

avec, $f_{s,i}$ la composante de la force de tension de surface par unité d'aire interfaciale.
La fermeture du transfert interfaciale de QDM n'est pas possible à partir d'un point de vue purement Eulérien du fait de la perte d'information de la localisation de l'interface. Dans notre cas, la phase dispersée est constituée

de particules isolées et l'interaction entre les particules reste négligeable. Le problème peut alors être traité par un autre point de vue. L'approche lagrangienne permet d'étudier la dynamique des particules séparées et de leur transfert avec le fluide environnant.
Cette méthode peut être résumée par les étapes suivantes : On introduit une fonction de densité de probabilité des gouttelettes. L'équation d'évolution de la pdf, puis appliquer une moyenne statistique. Le couplage entre les approches lagrangienne et eulérienne permet d'écrire

$$\frac{\partial(\alpha_k\rho_k\overline{u_{ji}})}{\partial t}+\frac{\partial(\alpha_k\rho_k\overline{u_{ki}}\ \overline{u_{kj}})}{\partial x_j}=\alpha_k\rho_k g_i-\alpha_k\frac{\partial P_k}{\partial x_j}$$
$$+\frac{\partial}{\partial x_j}[\alpha_k(\overline{\tau_{ij,k}}-\rho_k\overline{R_{ij,k}})]+\overline{\overline{M'_{k,i}}}+\Gamma_k u_{ki}^{Im} \quad \text{(II.12)}$$

Le transfert interfacial de QDM, comporte deux composantes :

- $\Gamma_k u_{ki}^{Im}$ liée à l'échange de QDM provoqué par le transfert de masse
- $\overline{\overline{M'_{k,i}}}$ liée à l'action des contraintes sur l'interface (pression + contrainte visqueuse sur l'interface),

A partir de la fermeture lagrangienne du mouvement de la goutte, $\overline{\overline{M'_{k,i}}}$ est fermé comme la somme de la force de traînée, la force de masse virtuelle, et la force de portance. Chacune de ces forces est décrit par un modèle distinct.

Force de traînée

La force de traînée est une force de surface due au mouvement relatif entre la goutte et la vapeur. Il prend en compte la traînée due au frottement de surface. La forme générale de la force de traînée agissant sur une goutte sphérique est

$$f_i^D=-\frac{3}{4}\rho_1\frac{C_D}{d_p}V_p|v_r|v_{r,i} \quad \text{(II.13)}$$

$v_{r,i}$ est la vitesse relative entre les deux phases. Cette vitesse est exprimée en termes de vitesse de la gouttelette $u_{2,i}$ et la vitesse de la vapeur non perturbée par la présence de cette goutte $\tilde{u}_{1,i}$

$$v_{r,i}=u_{2,i}-\tilde{u}_{1,i} \quad \text{(II.14)}$$

V_p est le volume de la goutte, d_p est le diamètre de la goutte, et C_D est le coefficient de traînée.

La moyenne de la force de traînée sur la population de gouttes, s'écrit comme la somme d'une contribution laminaire et d'une contribution turbulente

$$\boxed{F_i^D = \overbrace{-\alpha_2\rho_1\frac{3}{4}\frac{C_D}{d}\left\langle|v_r|\right\rangle_2\left(U_{2,i}-U_{1,i}\right)}^{\text{laminaire}} + \overbrace{\alpha_2\rho_1\frac{3}{4}\frac{C_D}{d}|\left\langle|v_r|\right\rangle_2 V_{d,i}}^{\text{turbulent}}} \quad \text{(II.15)}$$

avec :

- $U_{k,i}$ les composantes de la vitesse locale moyenne de la phase k,
- $\langle|v_r|\rangle_2$ est la moyenne de la vitesse relative,

$$\langle|v_r|\rangle_2 = ((U_{2,i}-U_{1,i}-V_{d,i})^2 + (2k_2 - 2k_{12} + 2k_1))^{\frac{1}{2}} \quad \text{(II.16)}$$

Ou :
k_1 est l'énergie cinétique turbulente de la vapeur

$$k_1 = \frac{1}{2}\overline{u'_{1,i}u'_{1,i}}$$

k_2 est l'énergie cinétique turbulente de la phase dispersée,

$$k_2 = \frac{1}{2}\overline{u'_{2,i}u'_{2,i}}$$

k_{12} est la covariance des fluctuations des vitesse vapeur-gouttes,

$$k_{12} = \overline{u'_{1,i}u'_{2,i}}$$

- ρ_k la masse volumique de la phase k,
- $V_{d,i}$ est défini comme la vitesse de drift, et elle traduit la corrélation entre la distribution instantanée des particules et les grands tourbillons turbulents de fluide. La vitesse de drift peut être modélisée par

$$V_{d,i} = -D^t_{12,ij}\left[\frac{1}{\alpha_2}\frac{\partial\alpha_2}{\partial x_j} - \frac{1}{\alpha_1}\frac{\partial\alpha_1}{\partial x_j}\right] \quad \text{(II.17)}$$

où $D^t_{12,ij}$, le tenseur de dispersion turbulente vapeur-gouttes, est exprimé en termes du tenseur de covariance entre les fluctuations de vitesse turbulente des deux phases et le temps caractéristique de la turbulence de la vapeur vu par les gouttelettes τ^t_{12} (chapitre IV)

$$D^t_{12,ij} = -\tau^t_{12}\left\langle u'_{2,j}\tilde{u}'_{1,i}\right\rangle_2 \quad \text{(II.18)}$$

Dans la présente étude, nous utilisons le coefficient de traînée C_D développé par Wallis (1969) pour l'écoulement dilué de particules isolées :

$$C_D = \begin{cases} \frac{24}{Re_p}[1 + 0.15Re_p^{0.687}]\alpha_1^{-1.7} & \text{for} \quad Re_p < 1000 \\ 0.44\alpha_1^{-1.7} & \text{for} \quad Re_p \geq 1000 \end{cases} \tag{II.19}$$

Le nombre de Reynolds particuliare Re_p est calculé en fonction du diamètre de la gouttelette d_p, de le moyenne de la vitesse relative $\langle |v_r| \rangle_2$, de la viscosité dynamique de la vapeur μ_1, et de la densité de la vapeur ρ_1:

$$Re_p = \rho_1 \frac{\langle |v_r| \rangle_2 \, d}{\mu_1} \tag{II.20}$$

Force de mass ajoutée

Quand une particule est accélérée par un fluide, le fluide environnant dans le voisinage immédiat de la particule sera également accéléré. La particule se comporte apparemment comme si elle a une masse plus importante que la masse réelle, donc la force nette agissant sur la particule due à cet effet a été appelée force de masse ajoutée. Cette force agissant sur une seule particule sphérique est s'écrit comme

$$f_i^{Ma} = -\rho_1 V_p C_{Ma} \left(\frac{D\tilde{u}_{1,i}}{Dt} - \frac{du_{2,i}}{dt} \right) \tag{II.21}$$

La moyenne de la force de mass ajoutée s'écrit comme la somme d'une contribution laminaire et d'une contribution turbulente.

$$F_i^{Ma} = \overbrace{-\rho_1 \alpha_2 C_{Ma} \left[\frac{\overline{d\vec{V}_r}}{\overline{dt}} \right]}^{\text{Laminar part}} \overbrace{- \rho_1 C_{Ma} \frac{\partial}{\partial x_i} \left((\frac{2}{3}k_2 - \frac{1}{3}k_{12})\alpha_2 \right)}^{\text{Turbulent part}} \tag{II.22}$$

Pour le cas d'un écoulement dilué de inclusions sphériques isolée, le coefficient de masse ajoutée C_{Ma} s'écrit

$$C_{Ma} = \frac{1}{2} \tag{II.23}$$

Dans notre cas particulier, la force de masse ajoutée est négligeable par rapport à la force de traînée.

Force de la portance

Quand une goutte se déplace dans un écoulement cisaillée, elle est soumise à une force transversale. Cette force est appelée force de portance. La forme

moyenne de la force de portance s'écrit sous la forme

$$\boxed{F_i^L = -\alpha_2 \rho_1 C_L \left(V_r \wedge rot(U_1)\right)_i} \tag{II.24}$$

Cette force est importante dans notre étude car elle affecte la distribution radiale des gouttelettes. Selon Auton et al. (1988) le coefficient de portance est égal à 0,5. Le modèle analytique d'Auton est valable pour le cas d'une particule sphérique placée dans un écoulement à faible cisaillement. Ceci ne corresponde pas à notre cas d'étude.

II.1.3. Equation de bilan locale moyennée de l'énergie

L'équation de l'énergie totale moyenne est écrite en termes de l'enthalpie totale:

$$h_k = e_k + \frac{\overline{p_k}}{\rho_k} \quad ; \quad H_k = h_k + \frac{\overline{u_{ki}}^2}{2} \tag{II.25}$$

où H_k est l'enthalpie totale, h_k est l'enthalpie massique, et E_K est l'énergie totale de la phase k.
L'équation moyennée de l'enthalpie totale s'écrite comme suit:

$$\begin{aligned} \frac{\partial}{\partial t}(\alpha_k \rho_k \overline{H_k}) + \frac{\partial}{\partial x_i}(\alpha_k \rho_k \overline{H_k}\,\overline{u}_{ki}) &= \alpha_k \frac{\partial \overline{p_k}}{\partial t} - \frac{\partial}{\partial x_i}[\alpha_k(\overline{q_{ki}} + \overline{q_{ki}}^T)] \\ &+ \frac{\partial(\alpha_k \overline{\tau_{ij,k} u_{kj}})}{\partial x_i} + \alpha_k \rho_k g_i \overline{u_{ki}} + \alpha_k \overline{Q_k}^k \\ &+ W_k + \Pi'_k + \Gamma_k(\frac{1}{2}(u_{ki}^{Im})^2 + h_k^{Im}) \end{aligned} \tag{II.26}$$

Le flux de chaleur turbulente $\overline{q_q}^T$ est défini par:

$$-\alpha_k \overline{q_k}^T = -\alpha_k \rho_k \overline{H'_k u'_{ki}} + \overline{\chi_k \tau_{ij,k} u'_{kj}} \tag{II.27}$$

Pour le transfert d'énergie interfaciale on présente les termes suivants:

- Puissance des contraintes interfaciales:

$$W_k = \overline{\sigma_{kij} u_{kj} n_{ki} \delta} \tag{II.28}$$

- Transfert de chaleur interfaciale par conductivité thermique :

$$\Pi'_k = \overline{-q_{ki} n_{ki} \delta} \tag{II.29}$$

- Transfert d'énergie cinétique due au transfert de masse:

$$\frac{1}{2}(u_{ki}^{Im})^2\Gamma_k = -\frac{1}{2}\overline{\rho_k u_k^2(u_{ki}-\omega_i)n_{ki}\delta} \tag{II.30}$$

- Transfert d'enthalpie due au transfert de masse:

$$h_k^{Im}\Gamma_k = -\overline{\rho_k h_k(u_{ki}-\omega_i)n_{ki}\delta} \tag{II.31}$$

L'écoulement de gouttelettes d'eau dans la vapeur chaude, implique un transfert de chaleur et de masse entre les deux phases. Les échanges thermiques entre les deux phases, sont considérés comme des termes source dans les équations de bilans d'énergie et de masse des deux phases. Pour modéliser ces termes, nous utilisons la condition de saut de l'énergie à l'interface

$$\sum_{k=1,2}\left[W_k + \Pi_k' + \Gamma_k(\frac{1}{2}(u_{ki}^{Im})^2 + h_k^{Im})\right] = 0 \tag{II.32}$$

où W_k est négligé. Nous considérons ainsi que l'interface ne stocke pas l'énergie thermique, l'énergie nette transférée à l'interface par la vapeur et de gouttelettes correspond au changement de phase par vaporisation (ou condensation). Ainsi, le taux de transfert de masse Γ_k est donnée par

$$\Gamma_2 = -\Gamma_1 = \frac{\Pi_2' + \Pi_1'}{H_2^\sigma - H_1^\sigma} \tag{II.33}$$

L'interface des gouttelettes est supposé aux conditions de saturation (T_{sat}, P_{sat}). Ainsi Π_K' est le taux de transfert de chaleur à l'interface, due à la différence entre la température de la phase de k et la température de l'interface de T_{sat}. T_{sat}. $H_2^\sigma - H_1^\sigma$ est la différence d'enthalpie qui correspond à la chaleur latente de vaporisation à T_{sat}.
Les expressions des transferts de chaleur interfaciaux sont obtenus en supposant que chaque phase a une température moyenne notée par T_k.

$$\Pi_k' = Coef(T_k - T_{sat}) \tag{II.34}$$

où la constante $Coef$ est le coefficient de transfert thermique entre la phase et l'interface. Ce coefficient est calculé par les lois de fermeture appropriées, par exemple le modèle Marchall Ranz pour le transfert de chaleur dans la phase vapeur et le modèle Hendou (1992) pour le transfert de chaleur dans la phase liquide.
Puisque notre intérêt est limité à la dynamique de l'écoulement, aucune autre étude sur la modélisation de ces termes ne sera présentée.

II.2. Modélisation de la turbulence

La prise de moyenne d'équations provoque l'apparition de quantités turbulentes correspondant à la moyenne des vitesses fluctuantes $\overline{u'_{ki}u'_{kj}}$. Ce terme est le tenseur de Reynolds de la phase de k noté $\overline{R_{ij,k}}$.
Dans l'équation de QDM de la phase dispersée, les gradients du tenseur $\overline{R_{ij,2}}$ agit comme un terme source. Ainsi, ces gradients peuvent modifier la répartition des gouttelettes. L'interaction entre les turbulences des deux phases est modélisée via des relations algébriques ou via les termes de transfert interfaciaux de turbulence. La présentation plus détaillée de ces modèles fait l'objet chapitre IV.

II.3. Conclusion

Ce chapitre présente les équations RANS utilisées dans le modèle Euler/Euler pour l'écoulement diphasique. Le procédé de moyenne fait apparaître des termes inconnus, qui nécessitent des modèles supplémentaires pour leur fermeture. Nous limitons notre intérêt aux termes qui ont un impact sur la répartition spatiale des gouttelettes. Ces termes sont les tenseurs de Reynolds des deux phases et le terme de transfert interfacial de QDM. La forme générale de chaque force interfaciale a été présentée dans ce chapitre sans préciser les modèles de fermeture pour les coefficients de ces forces. Dans le prochain chapitre, nous allons quantifier l'effet de ces forces sur la répartition spatiale des gouttes en analysant les données expérimentales et numériques. Cette analyse permettra d'analyser la compatibilité des modèles utilisés avec notre cas d'intérêt.

Chapter III

Simulation

Une étude paramétrique est proposée pour montrer l'effet de la modélisation des différents termes spécifiés dans le chapitre théorique. Un cas test de simulation avec des modèles de base est résolu et les résultats sont présentés. Ce test nous permet d'établir une description générale de la distribution de gouttelettes. Cette description, nous permet de préciser le rôle de chaque terme dans le mécanisme de répartition des gouttelettes. Par la suite, on examine brièvement la modélisation de chacun et la compatibilité des modèles de base utilisés dans le cas de test. A la fin de ce chapitre, nous précisons les modèles qui feront l'objet du reste de notre étude.

Dans le but de présenter l'écoulement entre quatre barres de combustible celui de REP, nous considérons un tube cylindrique d'un diamètre $d = 20$ mm et de 3 m de longueur. Les conditions d'entrée de ce cas d'étude sont choisies dans la même gamme de données d'un accident APRP. Les fractions volumiques d'entrée sont de $99,5$ % de vapeur et de $0,5$ % de gouttelettes d'eau. Les gouttelettes et la vapeur ont une distribution radiale uniforme à l'entrée. Le diamètre des gouttelettes est constant et égal à 0,5 mm. La paroi est considéré adiabatique. La vapeur entre avec une vitesse égale à 10 m/s dans le bas du tube tandis que la vitesse des gouttelettes y est de 2 m/s.

Tout d'abord une description générale de l'écoulement est établie concernant le mécanisme dynamique de la dispersion des gouttelettes. Un cas général de la simulation a été effectuée en utilisant le modèle $k - \varepsilon$ pour la turbulence en phase vapeur, le modèle Tchen-Hinze de la turbulence des gouttelettes, le modèle d'Auton de la force de portance.

Dans la figure III.1, nous représentons la répartition de la fraction de volumique de vapeur sur la section du tube. Après une analyse détaillée, nous pouvons expliquer le mécanisme de l'écoulement comme suit: la force de portance pousse les gouttelettes vers la centre et le turbulence

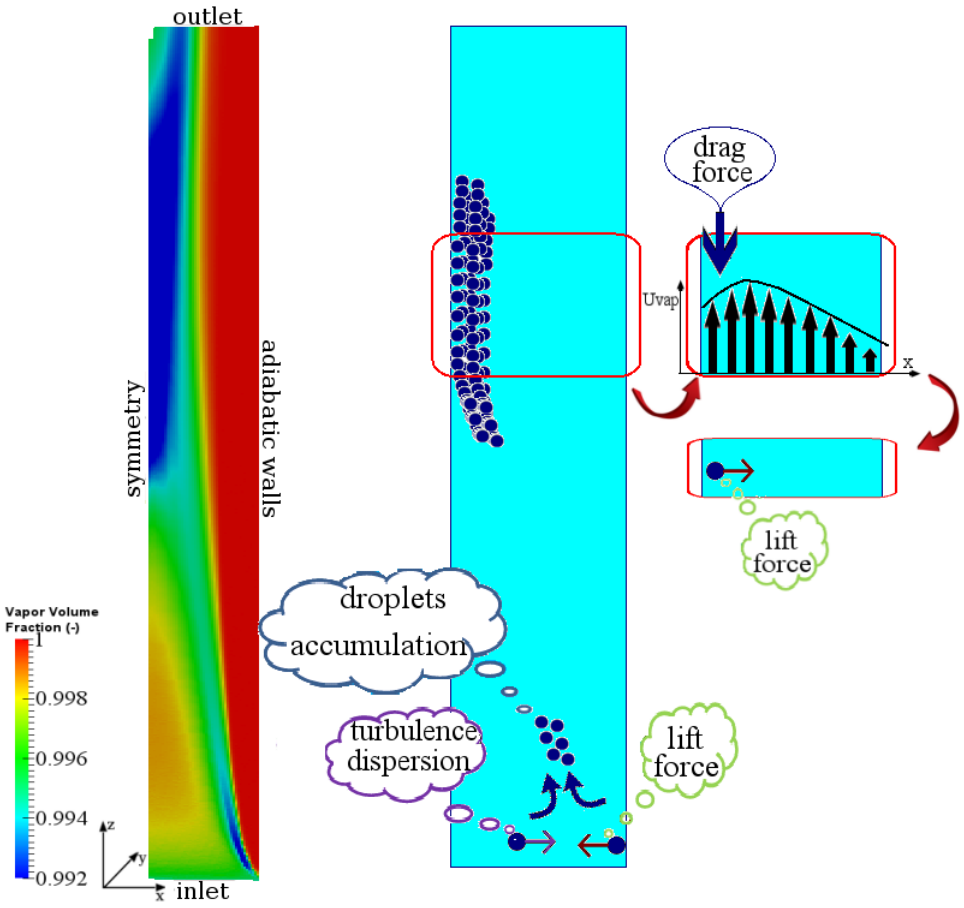

Figure III.1: La répartition de la fraction de volumique de vapeur sur la section de tube pour un cas général

les pousse vers la paroi pour former une zone de concentration. Cette zone de concentration monte dans le tube jusqu'à ce qu'il atteigne le centre. Dans la partie supérieure du tube, après une certaine hauteur, les gouttelettes concentrées s'éloignent du centre vers le paroi. Ceci est du au fait parce que la concentration importante des gouttelettes au centre cause une décélération verticale de la vapeur dans cette zone (effet de la force de trainée). Cette décélération de la vapeur inverse le gradient de vitesse moyenne de la vapeur. Puisque la direction de la force de portance dépend de l'orientation du cisaillement, elle tend alors à pousser les gouttelettes de centre vers la mur dans la partie haute du tube.

De cette analyse, nous concluons que les modèles principaux qui impactent la répartition des gouttelettes sont la force de traînée, la force de portance et les modèles de turbulence. Une brève étude bibliographique

a été menée pour confirmer l'utilisation du modèle de Wallis (1969) pour la prédiction du coefficient de force de traînée. La distribution radiale des gouttelettes sur la section de tube est principalement contrôlée par la force de portance, le modèle de turbulence de la phase continue, et le modèle de turbulence de la phase dispersée. Le modèle d'Auton utilisé pour la prédiction de la force de portance, apparemment surestime l'effet de cette force. Selon nos connaissances, il n'existe pas un modèle adapté au cas des gouttelettes. Par ailleurs, le choix des modèles de turbulence n'est pas évident. Par conséquent, la modélisation de la force de portance et la modélisation de la turbulence seront présentés dans des chapitres séparés.

Chapter IV

Turbulence

IV.1. Introduction

Dans l'approche Euler/Euler, les quantités turbulentes sont estimées en utilisant des modèles de turbulence. Il y a une grande variété de modèles de turbulence proposée, et le choix du modèle approprié présente une question essentielle. Le modèle doit introduire le montant minimum de complexité numérique (temps CPU), et devrait être capable de reproduire les principaux phénomènes physiques. Pour l'écoulement diphasique, il faut choisir le modèle approprié pour calculer la turbulence de la phase continue et un autre modèle pour calculer l'agitation de la phase dispersée.

IV.2. Modèle de turbulence de la phase continue

Les modèles de turbulence de la phase continue dans un écoulement diphasique, sont diffèrent des modèles d'écoulement monophasique par des termes supplémentaires de production et destruction de turbulence résultant de l'interaction avec la phase dispersée. La majorité des applications CFD industriels sont effectuées avec un modèle à deux-équations pour l'estimation de la viscosité turbulente, en particulier le modèle $k-\varepsilon$, tandis que l'utilisation du modèle $R_{ij}-\varepsilon$, reste exceptionnelle. $R_{ij}-\varepsilon$ et plus coûteux (temps de calcul et stockage numérique, cependant, $k-\varepsilon$ a certaines défauts car elle ne prend pas en compte l'anisotropie de la turbulence. Ces deux méthodes seront étudiées en détail par rapport à notre cas d'application.

Modèle $k-\varepsilon$

Ce modèle est basé sur l'analogie de Boussinesq introduisant un terme de viscosité turbulente. Dans cette approche deux quantités sont définies:

l'énergie cinétique turbulente de la vapeur k_1

$$k_1 = \frac{1}{2}\overline{u'_{1i}u'_{1i}} \tag{IV.1}$$

et le taux de dissipation turbulente de la vapeur ε_1

$$\varepsilon_1 = \nu_1 \overline{\frac{\partial u'_{1i}}{\partial x_k}\frac{\partial u'_{1i}}{\partial x_k}} \tag{IV.2}$$

où ν_1 est la viscosité cinétique moléculaire de la vapeur. L'approximation de Boussinesq permet d'écrire le tenseur des contraintes de Reynolds de la vapeur $R_{ij,1}$ comme:

$$-\overline{R_{ij,1}} + \frac{2}{3}k_1\delta_{ij} = \nu_1^T\left(\frac{\partial \overline{u_{1i}}}{\partial x_j} + \frac{\partial \overline{u_{1j}}}{\partial x_i} - \frac{2}{3}\frac{\partial \overline{u_{1m}}}{\partial x_m}\delta_{ij}\right) \tag{IV.3}$$

et

$$\nu_1^T = C_\mu \frac{k_1^2}{\varepsilon_1} \tag{IV.4}$$

ou $C_\mu = 0.09$.

Les équations de transport des k_1 et ε_1 sont écrites sous la forme approchée suivante:

$$\alpha_1\rho_1\left[\frac{\partial k_1}{\partial t} + \overline{u_{1,j}}\frac{\partial k_1}{\partial x_j}\right] = \frac{\partial}{\partial x_j}[\alpha_1\rho_1\frac{\nu_1^T}{\sigma_k}\frac{\partial k_1}{\partial x_j}] + \alpha_1\rho_1(Prod_1 + G_1 - \varepsilon_1) + \Pi_{q1} \tag{IV.5}$$

avec le constant $\sigma_k = 1$.

$$\begin{aligned}\alpha_1\rho_1\left[\frac{\partial \varepsilon_1}{\partial t} + \overline{u_{1,j}}\frac{\partial \varepsilon_1}{\partial x_j}\right] &= \frac{\partial}{\partial x_j}[\alpha_1\rho_1\frac{\nu_1^T}{\sigma_\varepsilon}\frac{\partial \varepsilon_1}{\partial x_j}] \\ &+ \alpha_1\rho_1\frac{\varepsilon_1}{k_1}\left[C_{\varepsilon 1}Prod_1 + C_{\varepsilon 1}max(G_1, 0) - C_{\varepsilon 2}\varepsilon_1\right] \\ &+ C_{\varepsilon 4}\frac{\varepsilon_1}{k_1}\Pi_{q1}\end{aligned} \tag{IV.6}$$

avec $C_{\varepsilon 1} = 1.44$, $C_{\varepsilon 2} = 1.92$, $C_{\varepsilon 4} = 1.2$ et $\sigma_\varepsilon = 1.3$.

ou $Prod_1$ est le terme de production

$$Prod_1 = -\overline{R_{ij,1}}\frac{\partial \overline{u_{1i}}}{\partial x_j} \tag{IV.7}$$

G_1 est le terme de l'atténuation de stratification

$$G_1 = -\frac{\nu_1^T}{Pr^T}\frac{1}{\rho_1}\frac{\partial \rho_1}{\partial x_i}g_i \tag{IV.8}$$

ou Pr^T est le nombre de Prandtl turbulent number et il est égal à 0.9.
Π_{q1} représente l'influence (la destruction ou la production) de la phase dispersée sur la phase continue. Il se modélise

$$\Pi_{q1} = \alpha_2 F_D^{12}\frac{\rho_2}{\rho_2 + \rho_1 C_{ma}}(k_{12} - 2k_1) + \alpha_2 F_D^{12} V_{di}(\overline{u_{2i}} - \overline{u_{1i}} - V_{di}) \tag{IV.9}$$

IV.2.1. $R_{ij} - \varepsilon$ modele

Le modèle $R_{ij} - \varepsilon$ est un modèle ou l'approche de viscosité turbulente n'est pas utilisé et les contraintes de Reynolds sont directement calculées. L'équation de transport exacte du tenseur de Reynolds $\overline{R_{1,ij}}$, prend en compte les effets directionnels et s'écrit de la façon suivante:

$$\begin{aligned}
\frac{\partial R_{1,ij}}{\partial t} + \overline{u_{1,j}}\frac{\partial R_{1,ij}}{\partial x_j} &= \overbrace{-\left(\overline{u'_{1,i}u'_{1,m}}\frac{\partial \overline{u_{1,j}}}{\partial x_m} + \overline{u'_{1,j}u'_{1,m}}\frac{\partial \overline{u_{1,i}}}{\partial x_m}\right)}^{P_{ij}} + \overbrace{\left(\overline{f_i u'_{1,j}} + \overline{f_j u'_{1,i}}\right)}^{G_{ij}} \\
&+ \overbrace{\overline{\frac{p'}{\rho}\left(\frac{\partial u'_{1,i}}{\partial x_j} + \frac{\partial u'_{1,j}}{\partial x_i}\right)}}^{\Phi_{ij}} - \overbrace{2\nu\left(\frac{\partial u'_{1,i}}{\partial x_m}\frac{\partial u'_{1,i}}{\partial x_m}\right)}^{\epsilon_{ij}} + \Pi_{q1} \\
&+ \overbrace{\frac{\partial}{\partial x_m}\left[\underbrace{\nu\frac{\partial \overline{u'_{1,i}u'_{1,j}}}{\partial x_m}}_{D_{ij}^{\nu}} - \underbrace{\overline{u'_{1,i}u'_{1,j}u'_{1,m}}}_{D_{ij}^{t}} - \underbrace{\overline{\frac{p'}{\rho}\left(u'_{1,j}\delta_{jm} + u'_{1,i}\delta_{im}\right)}}_{D_{ij}^{p}}\right]}^{D_{ij}}
\end{aligned} \tag{IV.10}$$

Le partie droite de l'équation de transport est décomposée en les termes suivants: P_{ij} est la contribution de la production due aux gradients de vitesse, G_{ij} est la production due aux forces extérieurs, ϕ_{ij} est le terme de redistribution en raison des fluctuations de pression, ϵ_{ij} est le terme de destruction visqueux, $D_{ij} = D_{ij}^{\nu} + D_{ij}^{t} + D_{ij}^{p}$ sont les termes de diffusion en raison de la viscosité, de la turbulence et de la pression, respectivement, et Π_{q1} est l'influence (la destruction ou la production) de la phase dispersée sur la phase continue.
L'équation de ε s'écrit sous la forme:

$$\frac{\partial \varepsilon}{\partial t} + \overline{u_{1,j}} \frac{\partial \varepsilon}{\partial x_j} = \frac{\partial}{\partial x_i} \left(C_\varepsilon \frac{k}{\varepsilon} \overline{u'_{1,i} u'_{1,j}} \frac{\partial \varepsilon}{\partial x_j} \right) + (C_{\varepsilon_1} P + C_{\varepsilon_3} G + C_{\varepsilon_4} k \frac{\partial \overline{u_{1,j}}}{\partial x_j} - C_{\varepsilon_2} \varepsilon) \frac{\varepsilon}{k}$$

Les coefficients du modèle $R_{ij} - \varepsilon$ sont donnés dans (Table IV.1).

C_s	C_1	C_2	C_1^ω	C_2^ω	C_ε	C_{ε_1}	C_{ε_2}	C_{ε_3}	C_{ε_4}
0.2	1.8	0.6	0.5	0.3	0.18	1.44	1.92	1.44	0.33

Table IV.1: Constantes du modèle $R_{ij} - \varepsilon$

IV.2.2. Compatibilité des modèles $k - \varepsilon$ et $R_{ij} - \varepsilon$ dans le cas étudié

Dans notre cas, d'écoulement de vapeur-gouttes ascendant dans un tube vertical, les contraintes turbulentes verticales sont censées à être plus importantes que les contraintes turbulentes radiales, ce qui induit de l'anisotropie de turbulence. Par ailleurs, l'existence de gouttelettes dans certaines zones décélère le vapeur, ce qui induit des contraintes de cisaillement locales loin de la paroi. Ces prévisions nous conduisent à tester les deux modèles afin de vérifier si $R_{ij} - \varepsilon$ est capable de capturer des phénomènes physiques qui sont ignorés par $k - \varepsilon$.

IV.3. Turbulence des phases dispersées

L'importance de la turbulence de la phase dispersée vient de son effet direct sur la distribution spatiale des gouttelettes. L'agitation des gouttelettes est présentée par deux termes qui ont besoin de fermetures

- Le tenseur de contraintes cinétiques de particules $\overline{u'_{2i} u'_{2j}}$, ce tenseur est considéré égal à l'énergie cinétique turbulente des gouttelettes K_2:

$$k_2 = \frac{1}{2} \overline{u'_{2i} u'_{2i}} \tag{IV.11}$$

- Le tenseur de covariance entre les fluctuations de vitesse des deux phases $\overline{u'_{1,i} u'_{2j}}$, est également considéré comme isotrope

$$k_{12} = \overline{u'_{1,i} u'_{2i}} \tag{IV.12}$$

Ces deux termes turbulents apparaissent dans l'équation de bilan de QDM. L'analyse menée a déterminer que la valeur et l'évolution de ces termes, et plus particulièrement de l'énergie cinétique turbulente k_2 est importante. Le gradient de k_2 agit comme une force radiale et influence directement la distribution spatiale des gouttelettes. Deux modèles de turbulence sont considérés: Tchen-Hinze et Q2Q12.

IV.3.1. Tchen-Hinze

Tchen-Hinze modèle est un modèle algébrique qui évalue l'énergie cinétique turbulente k_2 de la phase dispersée et la covariance k_{12} à partir de l'énergie cinétique turbulente k_1. Tchen (1947) été le premier qui a développé cette méthode sous l'hypothèse restrictive. D'autres travaux ont été effectués sur le même sujet, comme le travail de Hinze (1975) et Deutch (1992) qui visent à limiter ces hypothèses très restrictives originelle. Les équations finales du modèle Tchen-Hinze sont

$$\boxed{k_2 = k_1 \left[\frac{b^2+\eta_r}{1+\eta_r}\right] \qquad k_{12} = 2k_1 \left[\frac{b+\eta_r}{1+\eta_r}\right]} \tag{IV.13}$$

b et η_r sont fonction du coefficient de traînée F_D^{12} et du coefficient de masse ajoutée C_{ma}, et de deux échelles de temps spécifiques:

$$b = \frac{\rho_1 + \alpha_1 C_{ma}}{\rho_2 + \alpha_1 C_{ma}} \qquad \eta_r = \frac{\tau_{12}^T}{\tau_{12}^F} \tag{IV.14}$$

τ_{12}^F est l'échelle de temps caractéristique du transfert du QDM entre les deux phases, et τ_{12}^T représente l'échelle de temps de la turbulence de la phase continue, vue par la phase dispersée.

$$\tau_{12}^F = \frac{\alpha_1 C_{ma} + \rho_2}{\alpha_1 F_D^{12}} \qquad \tau_{12}^T = \frac{\tau_1^T}{\sigma_\alpha}\left(1 + C_\beta \xi_r^2\right)^{-0.5} \tag{IV.15}$$

ou σ_α égal au nombre de Prandtl turbulent, C_β est égal à 1.8 et $\xi_r = \frac{\langle|\overrightarrow{V_r}|\rangle_2}{\sqrt{\frac{2}{3}k_1}}$.

IV.3.2. Q2-Q12

Ce modèle suppose que le tenseur des contraintes cinétiques des gouttelettes $R_{ij,2}$ est isotrope. Ce tenseur des contraintes est calculé en utilisant l'analogie de Boussinesq et le terme de viscosité turbulente. Les équations de transport de l'énergie cinétique turbulente des gouttelettes k_2, et la covariance des vitesses vapeur-gouttelettes k_{12}, sont dérivés dans le cadre de la méthode lagrangienne en utilisant la fonction de distribution de probabilité (pdf). Le transfert d'énergie cinétique turbulente entre les deux phase est obtenu en fonction de k_{12}. Ceci nécessite une équation de transport supplémentaire dérivée de d'une description stochastique lagrangienne de la fluctuation de la vitesse du fluide suivant le chemin de particule basé sur un modèle de type Langevin.
En supposant que l'anisotropie reste faible et localement en équilibre, les composantes du tenseur des contraintes cinétiques sont calculées à l'aide de la viscosité turbulente comme suit:

$$\left\langle u''_{2,i} u''_{2,j} \right\rangle_2 = -\nu_2^{kin}\left[\frac{\partial U_{2i}}{\partial x_j} + \frac{\partial U_{2j}}{\partial x_i}\right] + \frac{2}{3}\delta_{ij}\left[k_2 + \nu_2^{kin}\frac{\partial U_{2m}}{\partial x_m}\right] \tag{IV.16}$$

ou ν_2^{kin} est la viscosité turbulente des particules,

$$\nu_2^{kin} = \left[\nu_{12}^T + \frac{\tau_{12}^F}{2}\frac{2}{3}k_2\right] \tag{IV.17}$$

ν_{12}^T est la viscosité turbulente de qui est liée à la covariance vitesse de la vapeur-gouttelettes.

$$\nu_{12}^T = \frac{1}{3}k_{12}\tau_{12}^T \tag{IV.18}$$

Puis l'équation de transport de l'énergie cinétique turbulente des particules est obtenue par sommation des composantes diagonales du tenseur :

$$\boxed{\frac{\partial}{\partial t}k_2 + \overline{u_{2,j}}\frac{\partial}{\partial x_j}k_2 = \frac{\partial}{\partial x_j}K_2^{kin}\frac{\partial}{\partial x_j}k_2 - \overline{u'_{2,i}u'_{2,j}}\frac{\partial}{\partial x_j}\overline{u_{2,j}} + \Pi_{q2}} \tag{IV.19}$$

Le premier terme du membre de droite de cette équation est le terme de transport par les fluctuations de vitesse, où K_2^{kin} est le coefficient de diffusivité turbulente

$$K_2^{kin} = \left[\frac{\nu_{12}^T}{\sigma_q} + \frac{5}{9}\tau_{12}^F\frac{2}{3}k_2\right] \qquad \text{with } \sigma_q = 1 \tag{IV.20}$$

Le second terme est la production par la vitesse moyenne des particules. Le troisième terme présente le transfert interfacial d'énergie cinétique turbulente.

$$\Pi_{q2} = -2\alpha_2\rho_2\left[\left\langle\frac{F_{r,i}}{m_2}u''_{2,i}\right\rangle_2\right] \tag{IV.21}$$

En supposant que l'anisotropie du tenseur k_{12} reste faible on applique également une hypothèse de viscosité turbulente, ou approximation de Boussinesq:

$$\begin{aligned}\left\langle\tilde{u}'_{1,i}u''_{2,j}\right\rangle_2 &= -\frac{\nu_{12}^T}{1+\eta_r}\left[\frac{\partial\overline{u_{1,i}}}{\partial x_j} + \frac{\partial\overline{u_{2,i}}}{\partial x_j}\right] + \frac{1}{3}\delta_{ij}\left[k_{12} + \frac{\nu_{12}^T}{1+\eta_r}\left(\frac{\partial\overline{u}_{1,m}}{\partial x_m} + \frac{\partial\overline{u_{2,m}}}{\partial x_m}\right)\right] \\ &+ \frac{\eta_r}{1+\eta_r}\left[R_{1,ij} - \frac{2}{3}k_1\delta_{ij}\right]\end{aligned} \tag{IV.22}$$

ou $k_{12} = \left\langle\tilde{u}'_{1,i}u''_{2,i}\right\rangle_2$, et ν_{12}^T est la viscosité turbulente vapeur-gouttes L'equation de transport de k_{12} est:

$$\boxed{\begin{aligned}\frac{\partial k_{12}}{\partial t} + \overline{u_{2,j}}\frac{\partial k_{12}}{\partial x_j} &= \frac{1}{\alpha_2\rho_2}\frac{\partial}{\partial x_j}\left(\alpha_2\rho_2\frac{\nu_{12}^T}{\sigma_q}\frac{\partial k_{12}}{\partial x_j}\right) \\ &- \overline{R_{ij,12}}\frac{\partial\overline{u_{2,i}}}{\partial x_j} - \overline{R_{ij,12}}\frac{\partial\overline{u_{1,i}}}{\partial x_j} - \varepsilon_{12} + \Pi_{q12}\end{aligned}} \tag{IV.23}$$

Le premier terme du côté droit représente la fermeture du transport de la covariance k_{12} par les fluctuations de vitesse, la constante $\sigma_q = 1$. Le taux de dissipation visqueuse s'écrit

$$\varepsilon_{12} = \frac{k_{12}}{\tau_{12}^T} \tag{IV.24}$$

et le terme de interaction entre les phases Π_{q12} est

$$\Pi_{q12} = -\alpha_2\rho_2 \frac{1}{\tau_{12}^F}\left[\left(1 + \frac{\alpha_2\rho_2}{\alpha_1\rho_1}\right)k_{12} - 2k_1 - 2\frac{\alpha_2\rho_2}{\alpha_1\rho_1}k_2\right] \tag{IV.25}$$

IV.4. Comparaison avec les données expérimentales dans un écoulement canal

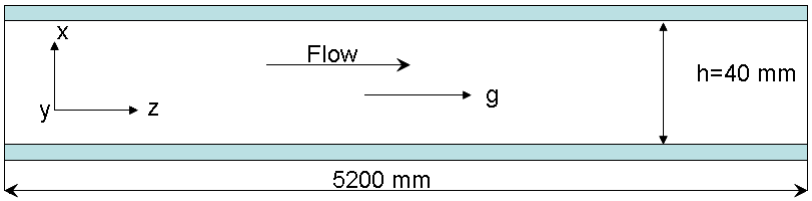

Figure IV.1: Schéma de l'écoulement en conduite considéré

Les caractéristiques de la turbulence calculées par les modèles doivent être vérifiées expérimentalement, mais aucune donnée expérimentale n'est disponible pour des écoulements vapeur-gouttelettes. L'expérience de Kulick et al. (1994) est représentative d'un écoulement gaz-solide en conduite et le nombre de Stokes des particules est du même ordre de grandeur que celui des gouttelettes dans notre cas. L'interaction entre l'air, qui représente la phase continue, et le cuivre la phase dispersée est étudié. Cet écoulement est dans une canal descendent comme le montre la figure IV.1, le nombre de Reynolds est basé sur la hauteur de canal ($h = 40mm$) et une vitesse de l'air à l'entrée ($u_0 = 10,5m/s$) , est $Re = 27600$. Les particules de cuivre ont une densité $\rho^C = 8800kg/m^3$ et le diamètre de la particule est $D_p = 70\mu m$. Nous simulons la même configuration expérimentale en utilisant différentes combinaisons de modèles de turbulence. Le premier cas est réalisé avec le modèle $k - \varepsilon$ pour la phase continue et le modèle de Tchen-Hinze pour la phase dispersée, tandis que le second cas est faite avec le modèle $R_{ij} - \varepsilon$ pour la phase continue et le modèle Q2Q12 pour la phase dispersée. Dans la suite, les différents résultats sont comparés et évalués par rapport aux résultats expérimentaux.

Figuree IV.2 et IV.3 montrent la comparaison entre les données expérimentales et des simulations numériques, pour la vitesse moyenne dans la

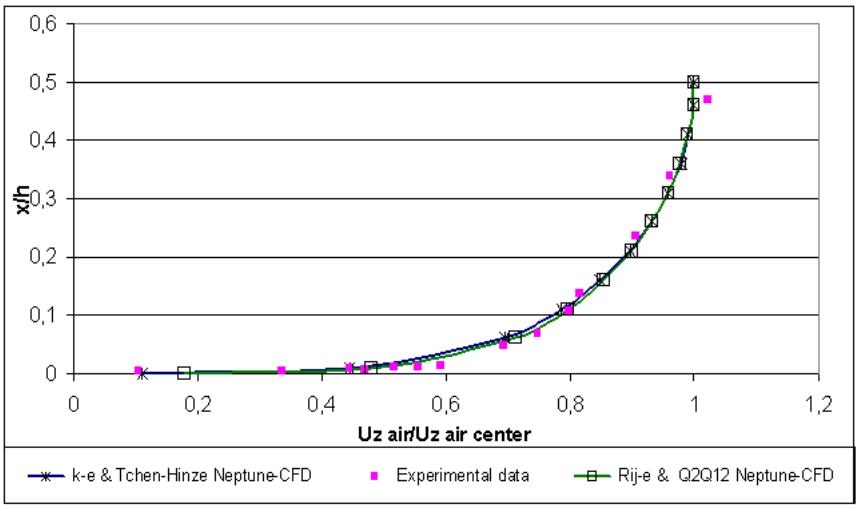

Figure IV.2: Comparaison de la vitesse moyenne de l'air (x/h: La distance adimensionnelle de la paroi; $U_{z,air}/U_{z,air,center}$: la vitesse moyenne normalisé de l'air par rapport à la vitesse de l'air à la center de canal)

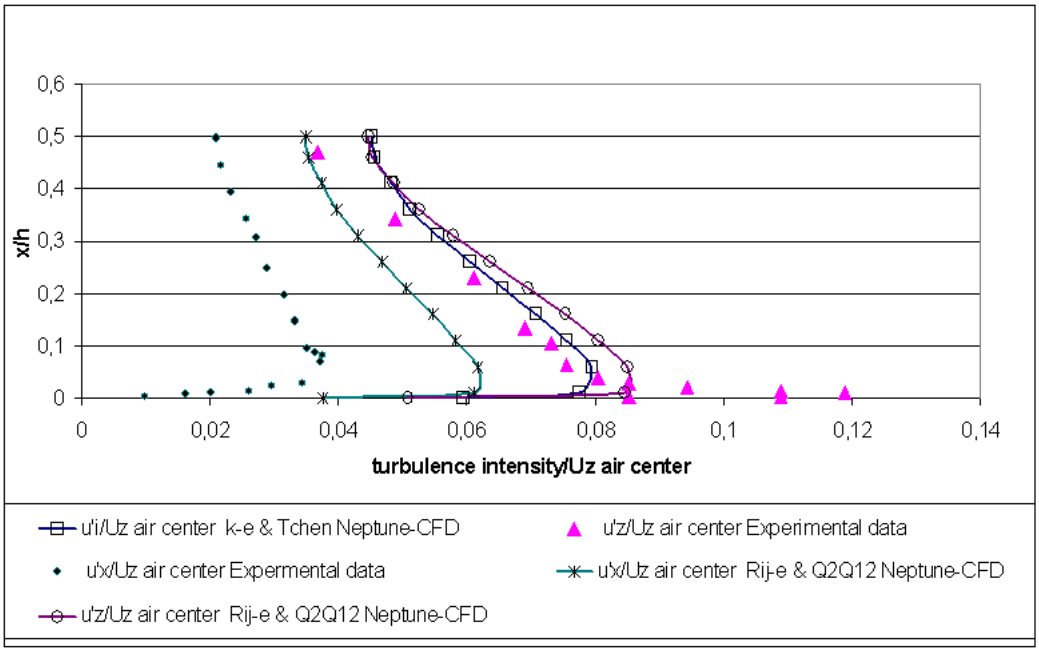

Figure IV.3: Fluctuation longitudinale et transversal de la phase continue

direction d'écoulement et les intensités de turbulence longitudinale et radiale pour la phase continue. Pour la phase gazeuse, les deux modèles donnent un bon accord avec les résultats expérimentaux pour la composante longi-

tudinale de la vitesse moyenne. L'expérience montre une anisotropie de la turbulence de la phase gazeuse, et seul $R_{ij} - \varepsilon$ est plus capable de reproduire cette anisotropie. Les figures IV.4 et IV.5 montrent la comparaison entre

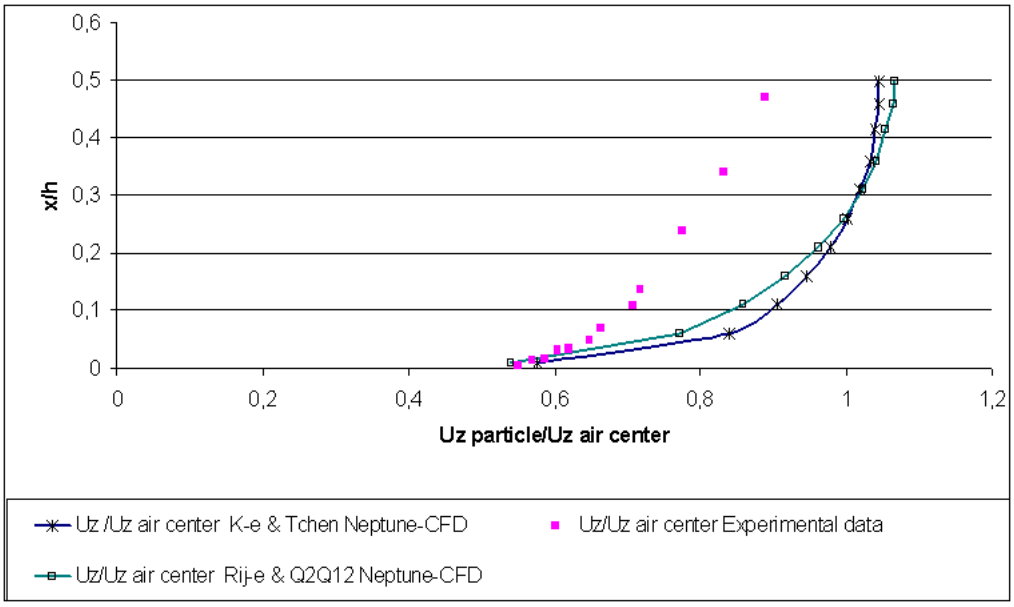

Figure IV.4: Comparaison de la vitesse moyenne de la phase dispersée

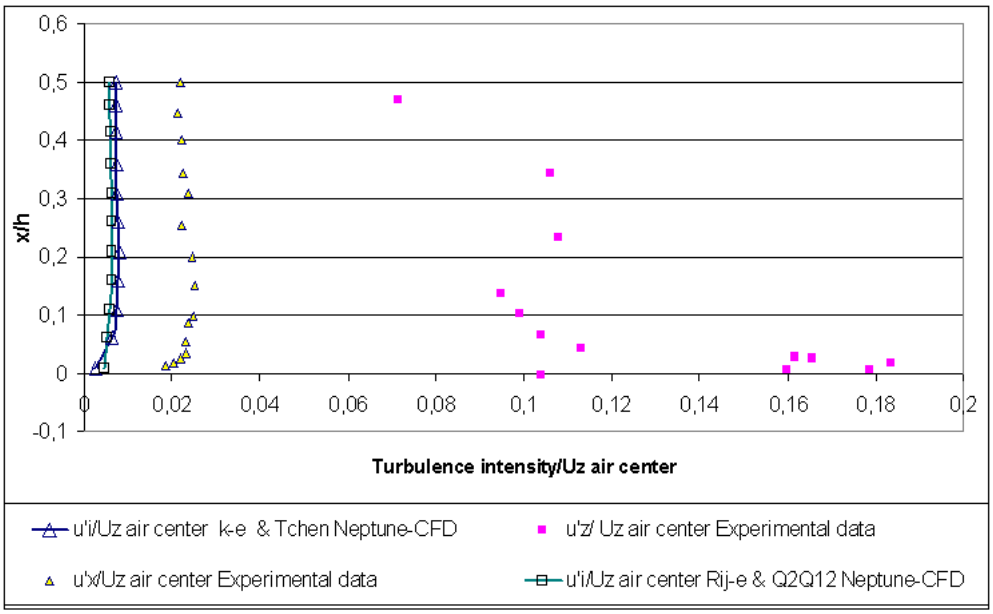

Figure IV.5: Fluctuation longitudinale et transversal de la phase dispersée

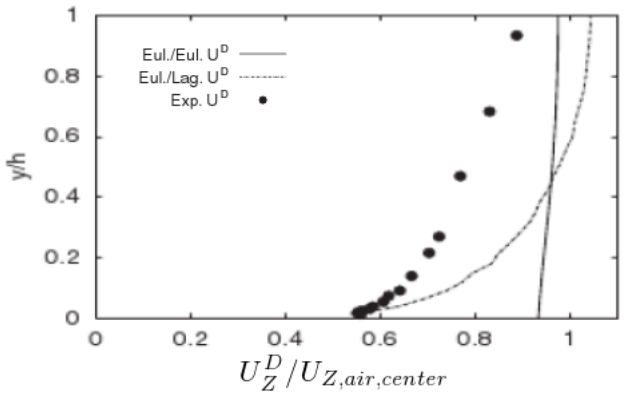

Figure IV.6: Comparaison de la vitesse moyenne de la phase dispersée, figure de Groll et al. (2009) pour montrer les résultats obtenus par la méthode Euler/Lagrange

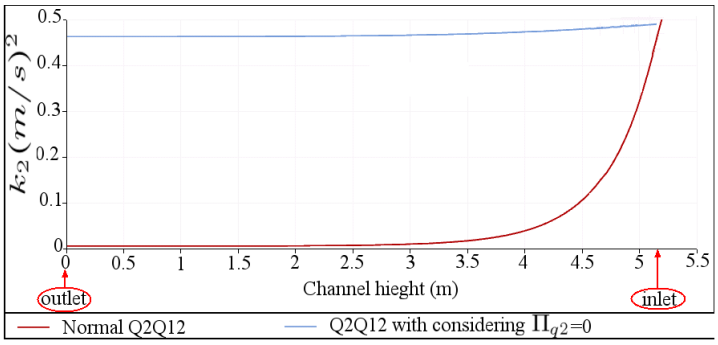

Figure IV.7: Deux cas avec une valeur élevée d'énergie cinétique turbulente de particules à l'entrée du canal $k_2 = 0,5(m/s)^2$: premier cas en utilisant Q2Q12; deuxième cas on considère que l'effet de la vapeur sur la turbulence gouttelettes est nul $\Pi_{q2} = 0$

les résultats expérimentaux et numériques pour la vitesse longitudinale moyenne, et les intensités longitudinale et radiale de turbulence de la phase dispersée. Dans les deux cas simulés, la valeur calculée de la vitesse des particules est surestimé par rapport aux valeurs expérimentales. L'analyse des données expérimentales montre que la turbulence des particules est importante et comparable à la turbulence de l'air. Par ailleurs les résultats expérimentaux montrent une forte anisotropie de la turbulence des particules. Les cas simulés montrent que les deux modèles Tchen-Hinze et Q2Q12 ne sont pas capables de reproduire ces caractéristiques. On s'entendait à ce que le modèle Q2Q12 donne de meilleurs résultats pour la valeur de l'énergie cinétique turbulente de la phase dispersée k_2. Par conséquent, une analyse détaillée de ce résultat a été réalisée. Dans la figure IV.7, nous montrons

un cas de test, où nous avons imposé une forte énergie cinétique turbulente des particules à l'entrée du canal $k_2 = 0,5$. Nous avons remarqué que dans le cas où nous avons utilisé le modèle de Q2Q12 sans aucune modification, cette valeur de k_2 décroît et sa valeur devient semblable à la valeur calculée par le modèle de Tchen-Hinze. L'analyse des différents termes de l'équation de transport de k_2 montre que le terme de transfert d'interfacial d'énergie cinétique turbulente est le terme principal qui causent l'atténuation de k_2. Aussi dans la figure IV.7, nous montrons un autre cas test où nous avons négligé le terme de transfert interfacial de l'énergie cinétique turbulente. Ce test montre que k_2 maintient une valeur très élevée lorsque $\Pi_{q2} = 0$. Par conséquent, une étude détaillée au sujet de la fermeture de ce terme est présentée dans la prochaine section de ce chapitre.

IV.4.1. Modèle d'échange interfacial de turbulence basé sur l'hypothèse de une turbulence multi échelle

Dans ce modèle, nous proposons une solution de correction pour le terme Π_{q2} par analogie avec les travaux de séparation de l'échelle qui ont été proposé par plusieurs auteurs pour la fermeture du terme Π_{q1} (Chahed (1999), modèle "standard" [1], etc.) Nous montrons qu'il est possible de définir une séparation de l'échelle turbulente sur les différents termes qui composent le transfert interfacial d'énergie cinétique turbulente.
On distingue deux échelles de turbulence. Une particule peut augmenter la turbulence du fluide par les fluctuations dans le sillage. Il s'agit d'une production de turbulence, et elle est produite à une échelle plus petite que la taille de la particule (ce qui veut dire de petites échelles turbulentes). D'autre part la particule agit sur la destruction de la turbulence des fluides quand elle traverse des grands tourbillons. Regardant d'un point de vue des particules, nous supposons que le terme de production de fluide dans le sillage est considéré comme un terme de destruction de la fluctuation des particules. Par ailleurs de la destruction de la turbulence du fluide, quand des particules traversent un grand tourbillon, représente un terme de production de la fluctuation du particules.
Cette compréhension est modélisée en décomposant le terme de l'interaction turbulente entre les deux phases en deux termes. Le premier représente la destruction au niveau des petits tourbillons dans le sillage. Le second représente la production de turbulence des particules à l'échelle des grands tourbillons.

$$\Pi_{q2} = \tilde{\Pi}_{q2} + \Pi_w \tag{IV.26}$$

[1] modèle de turbulence utilisé dans le code calcul ASTRID

Π_w est considéré comme le terme de destruction de l'agitation des particules et il est égal à l'énergie des tourbillons produits dans le sillage de la gouttelette. $\tilde{\Pi}_{q2}$ est le terme de la production de l'agitation turbulences quand il traverse des grands tourbillons. Ces termes peuvent s'écrire

$$\begin{aligned} \tilde{\Pi}_{q2} &= -\frac{1}{\tau_{12}^F}[U_{2,i}V_{d,i} + k_{12} - U_{1,i}V_{d,i} - 2k_1^L] \\ \Pi_w &= -\frac{1}{\tau_{12}^F}[2k_2 - U_{2,i}V_{d,i} - 2k_{12} + U_{1,i}V_{d,i} + 2k_1^s] \end{aligned} \tag{IV.27}$$

Où k_1^L représente l'énergie cinétique turbulente dans les grands tourbillons et k_1^S représente l'énergie cinétique turbulente dans les petits tourbillons. Nous supposons que le mouvement de la particule dans le fluide est affecté par l'énergie cinétique turbulente du fluide à deux échelles différentes. Par conséquent, l'énergie cinétique turbulente du fluide utilisée dans la fermeture des deux termes ne se réfère pas à la même échelle turbulente. Nous supposons que l'énergie cinétique turbulente du fluide est contenue dans les grandes échelles turbulentes et que l'énergie des petites structures est négligeable (la notion de grande et petite échelle sont considérés par rapport à la taille de la goutte). Cette hypothèse est vraie lorsque les gouttelettes sont petites et proches de l'échelle de dissipation de Kolmogorov. Selon cette hypothèse, nous pouvons considérer que le terme k_1^S est négligeable, car l'énergie cinétique turbulente du fluide vue dans le sillage de la goutte est de petite échelle. Ensuite, nous pouvons écrire

$$\Pi_w = -\frac{1}{\tau_{12}^F}[2k_2 - U_{2,i}V_{d,i} - 2k_{12} + U_{1,i}V_{d,i}] \tag{IV.28}$$

la forme finale de Π_{q2} s'écrit

$$\Pi_{q2} = -\frac{1}{\tau_{12}^F}[2k_2 - k_{12} - 2k_1] \tag{IV.29}$$

La correction de la fermeture de terme de transfert d'énergie turbulente à l'interface a été utilisésur Kulick et al. (1994), afin de le comparer avec les données expérimentales. Dans ce cas de référence expérimental, le diamètre des particules est d'environ 70 μm, donc l'hypothèse de négliger l'énergie turbulente de la vapeur dans le sillage reste valable dans ce cas. La figure IV.8 représente les valeurs expérimentales des composantes verticale et radiale de la fluctuation de vitesse des gouttelettes et l'agitation isotrope estimée en modifiant le terme de transfert interfacial. La correction proposée a un impact important sur les résultats, et l'estimation donne le bon ordre de grandeur (entre la valeur des fluctuations verticale et radiale). Mais le modèle de correction semble avoir quelques limites car il présente un profil plat de l'énergie cinétique turbulente des particules sur toute la section radiale du tube. Cela peut être lié à l'hypothèse forte de négliger l'énergie vapeur turbulente dans les petites tourbillons. Mais ce résultat est satisfaisant dans notre cas, car il corrige l'ordre de grandeur de l'agitation des gouttelettes.

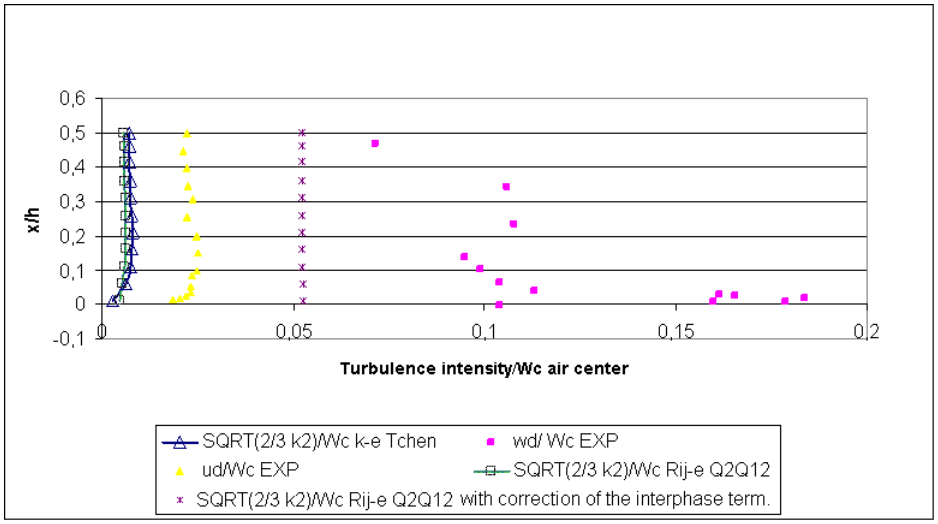

Figure IV.8: Stream wise and normal to wall turbulence intensities of the dispersed phase

IV.4.2. L'impact de la modélisation de la turbulence sur la distribution des gouttelettes

L'analyse de précédente montre les avantages et les lacunes des modèles de turbulence. Malheureusement, les résultats expérimentaux ne donnent aucune information sur l'impact de la modélisation de la turbulence sur la distribution des particules. Afin d'étudier cet effet des simulations sont réalisées en variant les modèles de turbulence des deux phases. La figure IV.9 montre les champs de fraction volumique de vapeur pour deux cas d'étude, l'un fait avec le modèle $k-\varepsilon$ et l'autre fait avec le modèle $R_{ij}-\varepsilon$. D'un point de vue général, la structure de la distribution spatiale des gouttelettes est similaire dans les deux cas. Une analyse plus détaillée de la répartition des gouttelettes montre de petites différences, (ex: les zones de concentration ne sont pas situées au même endroit). On verra que ces différences peuvent être considérées comme un impact mineur en comparaison avec l'impact des autres modèles. Dans ce cas, $k-\varepsilon$ peut être suffisant tandis que Rij-e devient nécessaire quand les différences seront augmentées avec la complexité du cas par exemple la géométrie. La figure IV.10 montre les champs de distribution de fraction volumique de vapeur pour deux cas d'étude, l'un réalisé avec le modèle Tchen-Hinze et l'autre réalisé avec le modèle Q2Q12. D'un point de vue général, Q2Q12 et Tchen-Hinze donnent le même type de distribution spatiale des gouttelettes car comme on l'a vu ils prédisent une faible agitation des gouttelettes. Par conséquent, un nouveau calcul a été fait en intégrant la modélisation proposée de l'interaction turbulente entre les deux phases. La figure IV.11 présente le champ de distribution de fraction volumique

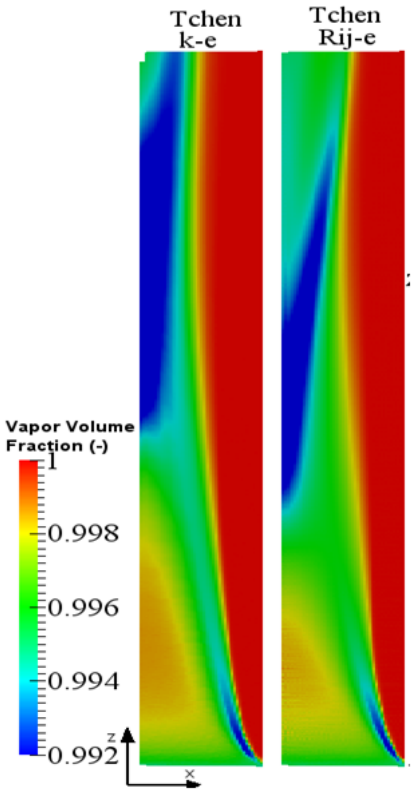

Figure IV.9: Impact du modèle de turbulence de la phase continue sur la distribution des gouttelettes

de vapeur pour un cas de simulation utilisant le modèle modifié Q2Q12 pour la phase dispersée. Un impact important de cette modélisation est la disparition des zones de concentration. Tous les phénomènes observés dans les cas précédents disparaissent. L'écoulement est homogène et la fraction volumique des gouttelettes diminue par conséquent dans le tube du fait de leur évaporation et de leur accélération. Ce test montre l'impact important de la turbulence de la phase dispersée sur la simulation de notre cas. La sous-estimation de la valeur de la turbulence des gouttelettes cause l'accumulation de gouttelettes. La modification du transfert d'énergie turbulente interfaciale dans le modèle Q2Q12 nous permet d'estimer une valeur de k_2 qui est du même ordre de grandeur que dans les résultats expérimentaux. La bonne estimation de la turbulence des gouttelettes change la structure globale de la dispersion spatiale des gouttelettes.

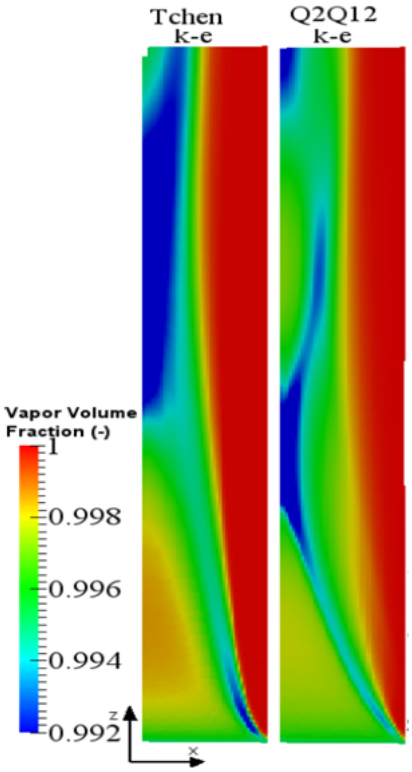

Figure IV.10: Impact du modèle de turbulence de la phase dispersée sur la distribution des gouttelettes

IV.5. Conclusion

Nous avons montré que la modélisation de la turbulence d'une phase dispersée à grand nombre de Stokes nécessite l'utilisation d'une équation de transport pour l'énergie cinétique turbulente et pour la covariance en vitesse. Néanmoins le modèle Q2Q12 classique ne permet pas de retrouver de manière satisfaisante des niveaux élèves d'agitation comme attesté par les résultats expérimentaux de Kulick et al. (1994). Nous avons montré que l'origine de cette mauvaise prédiction était la surestimation du terme de destruction de l'agitation des particules par création d'un sillage turbulent. Nous avons proposé une modélisation différente de ce terme en nous basant sur une séparation de la turbulence de la phase porteuse en deux échelles. Cette modification permet de retrouver les niveaux d'agitation expérimentaux. En appliquant le nouveau model à notre cas d'intérêt nous avons observe une modification radical de la structure de l'écoulement les gouttelettes se répartissant de manière homogène dans le tube.

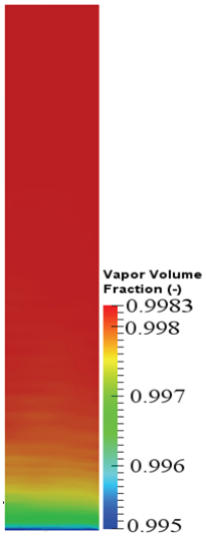

Figure IV.11: Le champ de distribution de fraction volumique de vapeur dans un cas avec Q2Q12 modifé

Chapter V

Force de Portance

La force de portance est une force transversale exercée sur une particule dans un écoulement cisaillée. Du fait de à son impact important sur la distribution radiale des gouttelettes, la modélisation de la force de portance devient fondamentale dans cette étude. Il existe trois principales contributions de la force de portance: la portance induite par le cisaillement, la portance induite par la rotation induite, et la portance induite par la paroi. Dans la présente étude, la surface des gouttelettes est supposée être lisse ce qui entraine que l'écoulement externe n'induit pas de rotation de la gouttelette.

On va considerer un simple problème d'une gouttelette sphérique de rayon

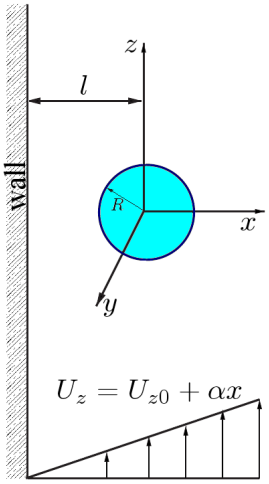

Figure V.1: Un schéma représentant d'une goutte dans un écoulement cisaillée en proche paroi

R situé à l'origine d'un repère cartésien. La goutte est dans un écoulement de cisaillée en proche paroi caractérisé par le vitesse de vapeur U_z, où l est la distance entre le mur et le centre de la particule. Dans ces conditions, les principaux paramètres caractéristiques principaux de l'écoulement sont

la distance adimensionnelle de la paroi L, le nombre de Reynolds particulaire Re_p, et le taux de cisaillement non-dimensionnel S_r définis comme suit

$$Re_p = \frac{2RU_z}{\nu}, \quad \alpha = \frac{dU_z}{dx}, \quad S_r = \frac{R\alpha}{U_z} \quad L = \frac{l}{2R}$$

Une analyse rapide de notre cas d'étude montre que Re_p est toujours supérieur à 1 et atteint des valeurs supérieures à 100. S_r varie entre zéro et un, tandis que L varie entre $0,5$ et 20.

Tout d'abord, l'équation générale de la portance est rappelée

$$f^L = \rho_1 V_p C_L (v_r \wedge rot(u_1)) \tag{V.1}$$

Ici V_p est le volume de la goutte sphérique, v_r est la vitesse relative qui correspond à U_z et u_1 est la vitesse de la vapeur qui corresponde aussi à U_z. Ainsi la $rot(u_1)$ s'écrit

$$\frac{dU_z}{dx}\overrightarrow{e_y} = \alpha\overrightarrow{e_y}$$

et

$$v_r \wedge rot(u_1) = U_z \frac{dU_z}{dx}\overrightarrow{e_x}$$

Ainsi, la force de portance est dans la direction de l'axe x s'écrit

$$f^L = C_L \rho_1 V_p \alpha U_z \tag{V.2}$$

Deux solutions analytiques permettent d'exprimer le coefficient de portance sur une particule sphérique dans l'écoulement cisaillé simple ont été obtenues. Pour un fluide non visqueux remplissant la condition $S_r << 1$, Auton et al. (1988) a obtenu le résultat

$$f^L = \frac{2}{3}\pi\rho_1 R^3 \alpha U_z \tag{V.3}$$

Ce qui donne à un coefficient de portance $C_{L,Auton} = 0,5$. Tous les cas de simulation dans les chapitres précédents ont été faites en utilisant ce modèle. Mais la vapeur est un fluide visqueux et l'écoulement est loin d'être considéré comme non visqueux en particulier à proximité de la paroi où la couche limite joue un rôle important.
Pour les écoulements visqueux, Saffman (1965) a proposé le modèle suivant

$$f^L = 6.46\mu R^2 U_z \sqrt{\frac{\alpha}{\nu}} \tag{V.4}$$

ce qui donne un coefficient de portance

$$C_{L,Saff} = \frac{1.54}{R}\sqrt{\frac{\nu}{\alpha}}$$

Saffman (1965) a déduit cette expression analytique de la force de portance dans les hypothèses suivantes,

$$Re_p << 1$$

$$Re_s \left[= \frac{\alpha(2R)^2}{\nu} \right] << 1$$

où Re_s est le nombre de Reynolds de cisaillement défini en termes de vitesse de cisaillement.
Re_p est supposé beaucoup plus petit que Re_s en définissant la variable ξ

$$\xi \left[= \frac{Re_s^{\frac{1}{2}}}{Re_p} = \left(\frac{S_r}{Re_p} \right)^{\frac{1}{2}} \right] >> 1$$

Dans notre cas d'interet, Re_p n'est pas plus petit que l'unité et peut atteindre des valeurs élevées de l'ordre 100, et ξ est toujours plus petit que un. Ceci rend l'expression de Saffman pour le coefficient de portance incompatible.
Selon nos connaissances, il n'existe pas un modèle analytique pour la force de portance pour des particules lourdes (particules solides ou gouttelettes) dans le cas de nombres de Reynolds élevés. Mais récemment, plusieurs auteurs ont abordé ce problème en effectuant des DNS pour nombre de Reynolds modérés et élevés. Ainsi les nouveaux modèles proposés pour la fermeture de la force de portance dans ce cas, sont basés sur la corrélation des résultats DNS.
Komori and Kurose (1996) et Kurose and Komori (1999) ont effectué une simulation numérique directe 3D pour le champ d'écoulement autour d'une sphère rigide pour une gamme de nombres de Reynolds particulaire $1 < Re_p < 500$. Ils ont constaté que la direction de la force de portance sur une sphère rigide stationnaires à Re_p élevé est opposée à celle prédite par les théories des écoulements non-visqueux à faible Reynolds. Kurose and Komori (1999) a précisé que la force de portance sur une sphère rigide stationnaire, dans un écoulement cisaillé linéaire, agit en poussant la particule de la zone des faibles vitesses vers celles des vitesses élevées $Re_p < 60$, alors que il agit dans le sens opposé pour $Re_p > 60$. Plus tard, Sugioka and Komori (2006) a constaté que le comportement du coefficient de portance sur une goutte sphérique est similaire à celle sur une sphère rigide, et que la force de portance agissant sur une goutte sphérique change sa direction à un nombre de Reynolds $Re_p \simeq 50$ dans un écoulement de cisaillement linéaire.
Zeng et al. (2009) a effectué des calculs DNS pour une sphère rigide dans un écoulement de cisaillement linéaire proche d'une paroi pour comprendre l'effet de la paroi sur la force de portance. Dans les calculs de Zeng et al. (2009), le gamme de nombres de Reynolds est de 2 à 250 à distances de la paroi de $L = 0,505$ à $L = 4$. Ils ont noté que pour les distances de séparation plus grande que $L = 0,75$ C_L change son signe et devient négatif

pour certains Re_p . Cependant, pour $L < 0,75$, le coefficient de portance reste positif sur toute la gamme de Re_p considérée. Par conséquent, dans le zone proche de la paroi, le nombre de Reynolds critique $RE_{p,cr}$ pour laquelle $C_L = 0$, n'est pas constant et il dépend de la distance à la paroi. Les valeurs de $RE_{p,cr}$ pour différents L d'aprés Zeng et al. (2009) se trouvent dans la table V. On voit que pour $L = 0,75$, le nombre de Reynolds critique est proche de 200 et diminue à $RE_{p,cr} = 60$ à $L = 4$. Zeng et al. (2009) a aussi remarqué, que pour des distances plus grandes que $L = 4$, la valeur critique du nombre de Reynolds particulaire $RE_{p,cr} \simeq 60$ est comparable à la valeur trouvée par Kurose and Komori (1999). Dans le cas présent des gouttelettes, Sugioka and Komori (2006) a spécifié que $RE_{p,cr} \simeq 50$ pour les écoulements de cisaillement loin de la paroi.

L	$Re_{p,cr}$
0.75	198.19
1	125.5
2	74.70
4	59.11

Table V.1: La valeur de $Re_{p,cr}$ à laquelle C_L inverse son signe pour différentes distances à la paroi, une table fournie par Zeng et al. (2009)

Dans l'écoulement en tube considéré ici et pour le diamètre des gouttelettes considéré dans l'étude, la distance adimensionnelle de la paroi est comprise entre 0,5 et 20. Par conséquent, dans la zone proche de la paroi on doit prendre en compte la portance induite par la paroi.
Zeng et al. (2009) a présenté une corrélation numériques pour le coefficient de portance basée sur ses résultat de DNS. Cette corrélation est valable sur une gamme $1 < Re_p < 200$ et $L > 0,5$. Cette corrélation a la forme suivante:

$$C_L = C_{L,w} exp(-0.5\delta(Re_p/250)^{4/3})[exp(\alpha_L^{\beta_L}) - \lambda_L] \tag{V.5}$$

ou

$$\begin{aligned} \delta &= L - 1/2 \\ C_{L,w} &= \frac{3.663}{(Re_p^2 + 0.1173)^{0.22}} \\ \alpha_L(Re_p) &= -exp(-0.3 + 0.025Re_p) \\ \beta_L(Re_p) &= 0.8 + 0.01Re_p \\ \lambda_L(\delta, Re_p) &= (1 - exp(-\delta))(Re_p/250)^{5/2} \end{aligned} \tag{V.6}$$

La validité de cette corrélation est présentée sur la figure V.2, où la valeur du coefficient de portance à partir des résultats DNS et la corrélation de Zeng et al. (2009) sont tracées en termes de Re_p à plusieurs distances de la paroi.

La corrélation de Zeng reproduit les résultats de DNS pour la zone proche de la paroi ($L \in [0505; 2]$). Pour les distances loin de la paroi ($L = 4$) la corrélation donne des valeurs dans le même ordre de grandeur que celles obtenues par le DNS, mais ce résultat présente un défaut : le coefficient de portance change de signe avant $Re_p = 50$. Par conséquent, une courbe supplémentaire est présentée en considérant que $L = 10$. Dans ce cas, la figure (V.2,d) montre que si nous appliquons la formule de Zeng loin de la paroi $RE_{p,cr}$ devient très faible par rapport à 50. Ainsi, nous pouvons conclure que la corrélation de Zeng n'est pas valable quand la distance de la paroi augmente.

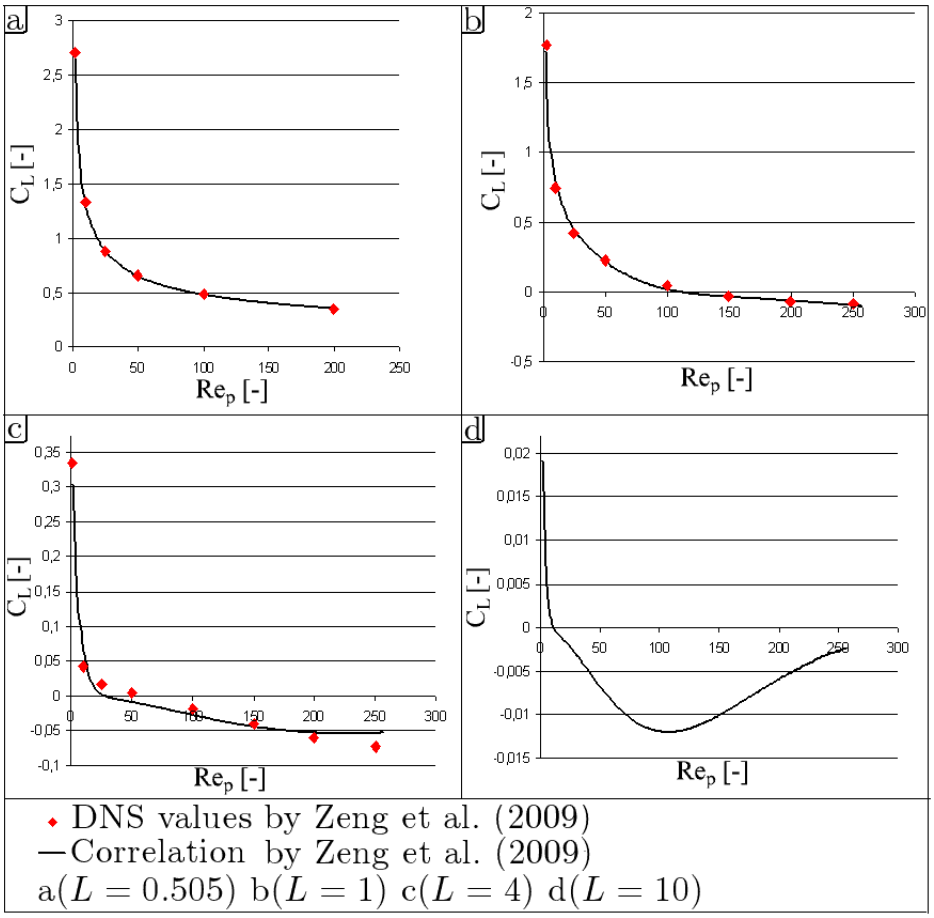

Figure V.2: Comparaison des valeurs DNS et la corrélation des Zeng et al. (2009) à plusieurs distances de la paroi

Par conséquent, la corrélation de Zeng et al. (2009) n'est pas valable pour tous les domaines de l'écoulement de notre étude. Selon nos connaissances, il n'existe pas de modèle pour le coefficient de portance pour le cas d'un écoulement de cisaillement loin de paroi. Dans ce chapitre, nous proposons

une corrélation qui correspond aux résultats de la DNS Sugioka and Komori (2006) qui sont valables pour les écoulements loin de la paroi. Cette corrélation s'écrit

$$\begin{aligned} C_L &= \left(15.5\frac{S_r}{Re_p^2}\exp^{-2Re_p^{-1.4}} + 0.12\right) \\ &+ \left(\frac{5}{Re_p} - 0.05S_r - 0.08\right)\left(\frac{\tanh(Re_p - 55) + 1}{2}\right) \end{aligned} \tag{V.7}$$

La figure V.3 présente la comparaison de la nouvelle corrélation avec les

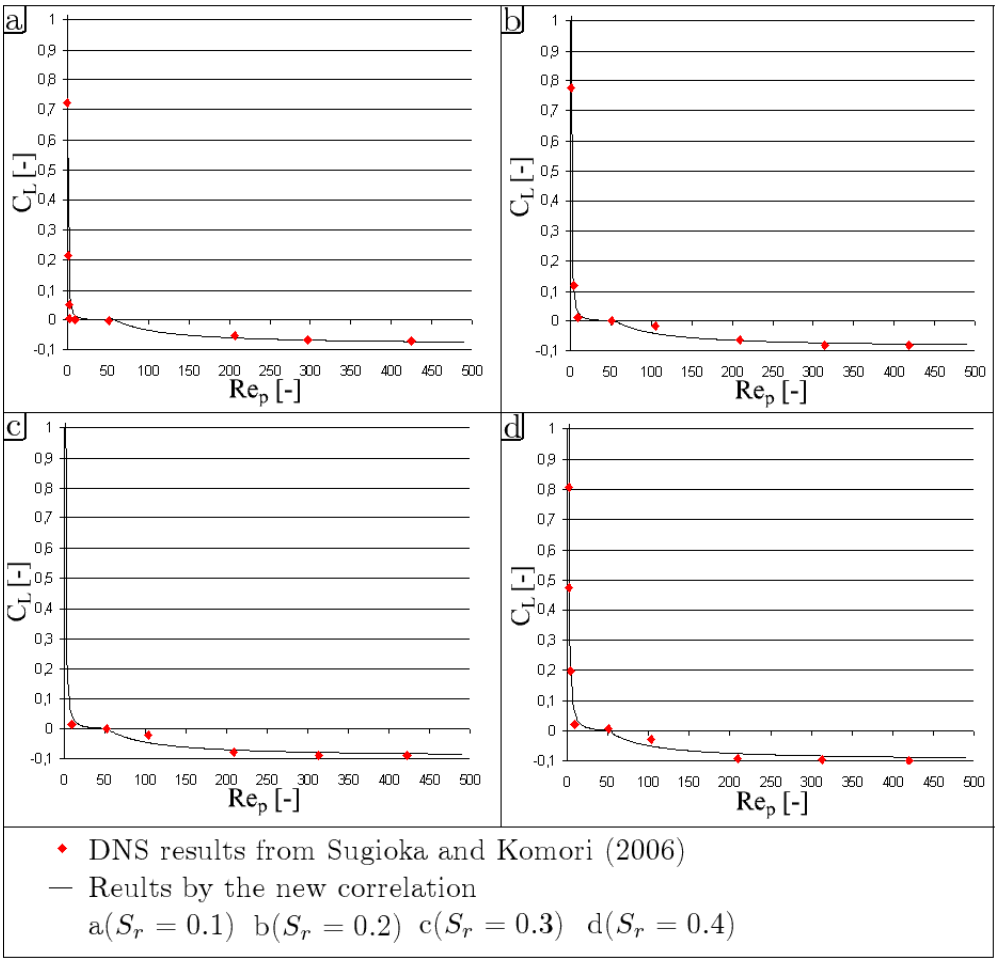

Figure V.3: Comparaison des valeurs DNS de Sugioka and Komori (2006) et la nouvelle corrélation des Zeng et al. (2009) à plusieurs taux de cisaillement

résultats de la DNS Sugioka and Komori (2006). Cette corrélation montre un accord favorable avec les résultats DNS et le respect de la caractéristique d'inverser le signe pour Re_p entre 50 et 60. Cette corrélation reste valide

dans la zone éloignée de la paroi. Pour une modélisation précise de la portance, nous proposons d'utiliser la corrélation de Zeng et al. (2009) dans la région proche-paroi et notre nouvelle corrélation pour la zone loin de la paroi.

V.1. Impact de la modélisation de la force de portance sur la distribution des gouttelettes

Après cette étude détaillée sur les différentes modélisations de la force de portance, l'impact de ces modélisations sur notre cas de étude est analysé dans cette section. Dans la figure V.4, les champs de la fraction volumique de vapeur sont présentés pour quatre cas de simulation avec des modèles différents de la portance. D'abord dans le cas (a) le modèle de Auton et al. (1988) est utilisé, ce modèle a été utilisé dans tous les chapitres précédents. La force de portance est ici surestimée ce qui pousse les gouttelettes de la paroi vers le centre. Dans le cas (b) le modèle de Saffman (1965) est utilisée, ici aussi tous les gouttelettes sont repoussées loin de la paroi et des zones de concentration se trouvent au centre. Dans le cas (c) le modèle de Zeng et al. (2009) est utilisé sur tout le domaine. Les gouttelettes n'approchent pas de la paroi du fait de la forte portance proche de la paroi. Mais les gouttelettes sont distribuées dans le reste du domaine et de manière homogène. Enfin, dans le cas (d) la nouvelle corrélation proposées dans l'équation (V.7)) et le modèle Zeng et al. (2009) proche de la paroi et des résultats similaires sont trouvés.

V.2. Conclusion

L'impact de la modélisation de la force de la portance sur la distribution des gouttelettes sur la section radiale de tube, montre que la modélisation de cette force est tres importante dans notre étude. Notre cas d'intérêt nécessite une bonne modélisation de la force de portance dans un domaine où le nombre de particules de Reynolds atteint des valeurs élevées et la gamme de vitesse de cisaillement adimensionnelle est comprise entre 0 et 1. La présente étude peut être divisée en deux domaines principaux, l'écoulement de cisaillement proche de paroi et loin de paroi. Les modèles analytiques de Auton et al. (1988) et Saffman (1965) surestiment la force de portance et ils ne correspondent pas aux valeurs des calculs DNS. L'analyse des différents résultats DNS nous montre que le coefficient de la force de portance est toujours positif et proportionnellement élevé en proche paroi. Loin de la paroi la force de portance inverse sa direction pour une valeur critique du nombre de Reynolds particulaire. Plusieurs solutions ont été proposées dans ce chapitre afin de tenir compte de ces phénomènes. Toutes les solutions proposées ont

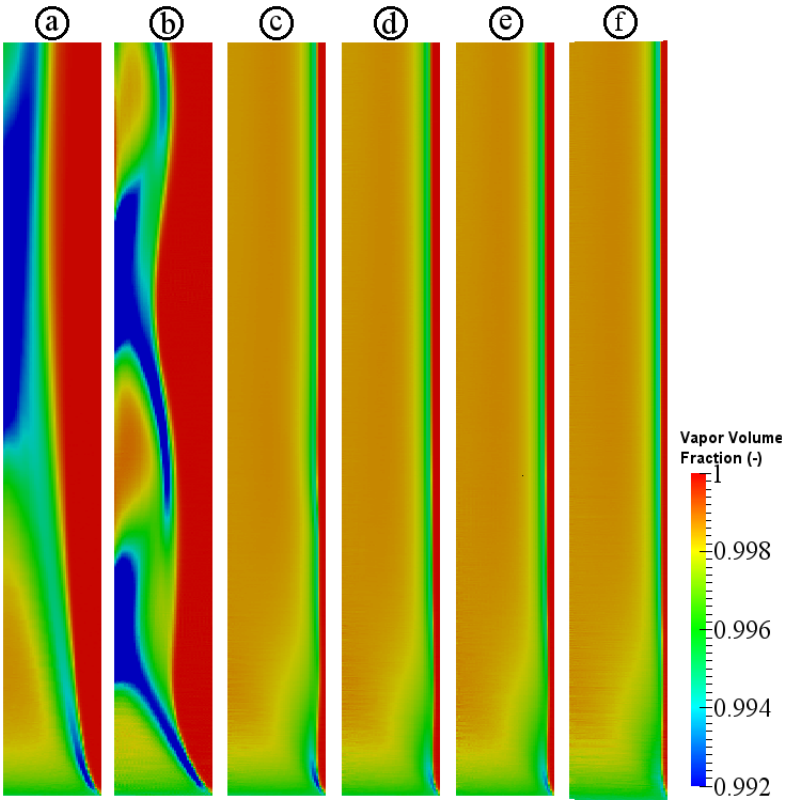

Figure V.4: L'impact des différentes modélisations de la portance sur la distribution spatiale des gouttelettes sur la section de tube: a) Modèle de Auton et al. (1988)- b) Modèle de Saffman (1965)- c) Modèle de Zeng et al. (2009)- d) La nouvelle corrélation proposées et le modèle Zeng et al. (2009)

donné un impact similaire sur la distribution des gouttelettes. Pour une modélisation précise de la force de portance, nous proposons d'utiliser la corrélation de Zeng et al. (2009) dans la région proche-paroi et la nouvelle corrélation proposée dans ce chapitre pour la zone loin de la paroi.

Chapter VI

Application sur le refroidissement du coeur accidenté d'un réacteur PWR

L'étude qui motive ce travail est l'estimation de la capacité de refroidissement de l'écoulement vapeur-gouttelettes dans un coeur accidenté d'un réacteur PWR. On a supposé que la distribution spatiale des gouttelettes est une caractéristique principale de l'écoulement et qui a un impact direct sur la capacité de refroidissement de l'écoulement. Il est temps de confirmer cette hypothèse et de vérifier si les modifications proposées sur la modélisation de la dynamique des gouttelettes modifient le taux de transfert de chaleur avec la paroi.
Comme on a montré dans les chapitres précédents, la modélisation de la turbulence et la force de portance ont un impact important sur la distribution spatiale des gouttelettes. Par ailleurs on a montré que les modèles de turbulence existants sous-estiment l'impact de la turbulence sur la distribution des gouttelettes, tandis que le modèle de la force de portance surestime l'impact de cette force sur les gouttelettes. Les résultats numériques dans ce cas montrent que les gouttelettes ont tendance à se concentrer dans le centre du tube, et que la zone proche paroi reste vide des gouttelette. Dans une tentative d'améliorer ces résultats, des modifications ont été proposées pour la modélisation de ces forces, ce qui a changé la distribution des gouttelettes. Dans ce chapitre, on va analyser les conséquences de ces modélisations sur la quantité de chaleur que l'écoulement absorbe de la paroi. Une nouvelle série de test a été effectuée en remplaçant la paroi adiabatique considérée dans tous les cas précédents par une paroi chaude à la température de $573K$.
Sur la figure I.2, nous avons précisé les différents mécanismes de transfert de chaleur se produisent ces dans ce type des écoulements, qui peuvent être résumés comme suit: la convection entre la vapeur et la paroi, la convection entre la vapeur et les gouttelettes, la conduction entre la gouttelette et la

paroi en cas de contact direct de la gouttelette sur la paroi, et le rayonnement de la paroi vers la vapeur et les gouttelettes. Ces deux derniers effets ne sont pas considérés dans le présent travail, mais ces effets dépendent aussi de la distribution spatiale des gouttelettes.
Quatre cas ont été réalisés pour montrer le rôle de chaque changement de la modélisation de la répartition des gouttelettes sur le taux de transfert de chaleur. Ces quatre cas sont faits avec le même maillage et conditions aux limites. Seuls les modèles de turbulence et le modèle de la force de portance seront modifiés d'un cas à l'autre. Nous allons définir les cinq cas et la problématique correspondante:

1. Le premier cas est un cas de base fait avec le modèle $k-\varepsilon$ pour la turbulence de la vapeur, le modèle Tchen-Hinze de la turbulence des gouttelettes, et le modèle de Auton et al. (1988) pour la force de portance.

2. Le deuxième cas est fait avec le modèle $R_{ij}-\varepsilon$ pour la turbulence de la vapeur, le modèle Q2Q12 pour la turbulence des gouttelettes, et le modèle de Auton et al. (1988) la force de portance. Ce cas est déjà fait pour le cas adiabatique et il vise ici à montrer l'importance du choix des modèles de turbulence, même sans aucune modification.

3. Le troisième cas est fait avec $R_{ij}-\varepsilon$ pour la turbulence de la vapeur, et le modèle Q2Q12 pour la turbulence des gouttelettes. Mais dans ce cas, nous avons remplacé le modèle de Auton et al. (1988) de la force de la portance par le modèle proposé. Ce test montre séparément l'impact de la surestimation de la force de portance sur le transfert de chaleur.

4. Le quatrième cas est fait avec le modèle $R_{ij}-\varepsilon$ pour la turbulence de la vapeur, le modèle modifié de Q2Q12 pour la turbulence des gouttelettes, et le nouveau modèle proposé pour la force de portance. Ce cas montre l'impact de tous les modèles proposés sur le transfert de chaleur.

Dans la suite, à des fins de simplicité, ces cas seront notés qcas 1, cas 2,.. .
Tout d'abord, la figure VI.1 montre les modifications dans la distribution des gouttelettes pour chaque cas. Ces cas sont déjà décrits dans les chapitres précédents dans le cas des parois adiabatique. Nous ne remarquons aucun effet particulier de la paroi chaude sur la structure dynamique de l'écoulement. Nous rappelons rapidement les différences entre les cas. Dans le cas 1, les gouttelettes sont concentrés au centre du tube et ne s'approche de la zone proche-paroi. Dans le cas 2, quand on remplace les modèles turbulents les gouttelettes sont un peu plus dispersées, mais elles restent au centre du tube. L'écoulement a la même structure que dans le cas 1, en raison de la surestimation de la force de portance qui repousse toutes les gouttelettes loin du mur dans les deux cas. C'est pourquoi en cas 3, quand le modèle de la force

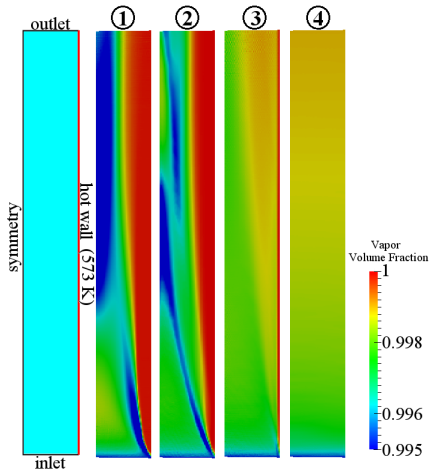

Figure VI.1: La répartition de la fraction du volume de la vapeur pour les quatre cas de modélisation

de portance Auton et al. (1988) est remplacé par le nouveau modèle de la force de portance, les gouttelettes deviennent distribuées presque sur toute la section du tube, mais elles n'approchent pas de la paroi (voir la ligne rouge près de la paroi). Dans le cas 4, quand la force portance et les modèles de turbulence sont modifiées, les gouttelettes sont réparties toute la section du tube.
La figure VI.2 montre le taux de transfert d'enthalpie de la paroi dans les quatre cas sous forme d'histogramme. L'écoulement extrait le maximum d'enthalpie quand les gouttelettes sont totalement dispersée (cas 4). De l'autre côté, le taux de transfert d'enthalpie extrait est minimum quand les gouttelettes sont concentrées dans le centre du tube (cas 1).
Dans cette analyse, on montre que chaque amélioration de la modélisation de la distribution des gouttelettes modifiée la quantité de chaleur extraite à la paroi. Le transfert de chaleur dans le cas 2 est plus important que le transfert de chaleur dans le cas 1 puisque les gouttelettes sont plus dispersées, même si elles restent dans le centre du tube. Dans le cas 3, la quantité de chaleur absorbée par la paroi augmente car on a retiré l'effet de la force de portance qui concentre les gouttelettes. Enfin dans le cas 4, les résultats sont comparables à ceux du cas 3. Mais il faut noter une remarque importante ici, que dans le cas 3 les gouttelettes ne touchent jamais la paroi, mais dans le cas 4 les gouttelettes peuvent être en contact direct avec la paroi. Par conséquent, dans le cas où on considère le modèle du transfert de chaleur entre la paroi et les gouttelettes en contact direct, le transfert de chaleur dans le cas 4 sera plus important que dans le cas de 3. Enfin, cette étude montre l'importance d'améliorer l'estimation de la distribution des gouttelettes sur l'estimation du refroidissement. Le taux de transfert de chaleur estimé avec les modèles

de turbulence et l'intégration des modifications dans le cas de 4 est de 118 % de plus que la valeur estimée dans le cas 1 fait avec les modèles de base.

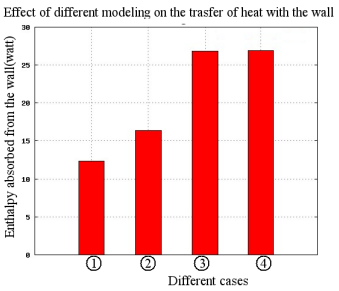

Figure VI.2: La quantité de chaleur absorbée par la paroi pour les quatre cas

Chapter VII

Conclusion

Notre travail vise à améliorer la compréhension des écoulements vapeur-gouttelettes turbulent non-isotherme en conduite. Plus précisément, dans le contexte de l'estimation du transfert de chaleur lors d'un accident APRP dans le coeur d'un REP, cette étude concerne l'adaptation du code Neptune-CFD pour les cas d'écoulement des gouttelettes dispersées. L'écoulement est considéré dilué et les gouttelettes sont considérées comme sphériques et non déformables. On introduit la méthodologie d'Euler-Euler utilisés par l'approche CFD. Ensuite, nous limitons notre étude à une caractéristique principale de l'écoulement qui est la distribution spatiale des gouttelettes en raison de son impact direct sur le transfert de chaleur entre la paroi et l'écoulement. Grace à une analyse physique et théorique, nous avons déterminé que les phénomènes principaux qui affectent la distribution des gouttelettes sont les forces entre les vapeurs et les gouttelettes et les turbulences des deux phases. L'analyse de cas test numérique à l'aide d'une étude bibliographique nous a aidé à préciser que les modèles principaux qui ont besoin de recherches supplémentaires pour être compatibles avec notre cas d'un écoulement des gouttelettes sont les modèles de la turbulence et le modèle de la force de portance.

Pour le modèle de la turbulence de la phase continue, nous avons montré que les deux modèles $k-\varepsilon$ et $R_{ij}-\varepsilon$ produisent le même type de structures d'écoulement avec quelques différences mineures. Pour un cas de géométrie simple comme le cas testé le modèle $k-\varepsilon$ peut être suffisant. Grâce à sa capacité à prendre en compte l'anisotropie de la vapeur l'utilisation du modèle $R_{ij}-\varepsilon$ devient nécessaire si des effets supplémentaires comme des géométries complexes sont ajoutées.

Pour le modèle de la turbulence de la phase dispersée, les deux modèles Tchen-Hinze et Q2Q12 sous-estiment la valeur de l'énergie cinétique turbulente des gouttelettes. Cela nous pousse à prolonger la recherche sur les

modèles de fermeture des différents termes en Q2Q12. De cette analyse, nous pouvons conclure que le terme du transfert interfacial de l'énergie turbulente est à l'origine de la sous-estimation faite par Q2Q12. Nous avons proposé une nouvelle fermeture de ce terme qui permet de prédire l'énergie cinétique turbulente dans le bon ordre de grandeur. Enfin, nous considérons que le modèle de Q2Q12 avec la fermeture proposée pour le transfert interfacial est la meilleure solution pour le moment reconnaissant que plus de recherches doivent être faites sur la fermeture du transfert interfacial turbulent en fonction notamment du ratio entre la taille de la particule et les échelles caractéristiques de la turbulence de la phase porteuse.

Pour la modélisation de la force de portance, nous avons montré que les modèles analytiques existants comme le modèle de Auton ou Saffman surestiment cette force dans le cas de l'écoulement de cisaillement des gouttelettes à haute nombre de Reynolds particulaire. L'analyse des résultats de DNS nous aide à comprendre le comportement de la force de portance dans ce type d'écoulement. Zeng a proposé une corrélation pour la force de portance valable pour la zone proche de la paroi. Selon notre connaissance, il y a aucun modèle de la force de portance pour des hautes valeurs du nombre de Reynolds particulaire dans la zone loin de la paroi. Donc nous avons proposé une corrélation basée sur les résultats DNS qui est valable pour la zone loin de la paroi. Enfin nous avons proposé la solution optimale est une combinaison entre le modèle de Zeng dans la zone proche-paroi et le nouveau modèle proposé pour la zone loin de la paroi.

Enfin nous avons étudié l'impact de toutes ces modélisations sur le transfert de chaleur avec la paroi. Nos résultats montrent que le taux de transfert de chaleur estimé après avoir choisi le bon modèle de turbulence et d'intégrer les modifications sur les modèles Q2Q12 et de la portance est de 118 % de plus que la valeur estimée dans le cas d'étude de base. Cela montre l'importance de notre étude pour le cas d'intérêt.

Bibliography

M Andreani and G Yadigaroglu. A 3-d eulerian-lagrangian model of dispersed flow film boiling including a mechanistic description of the droplet spectrum evolution i. the thermal-hydraulic model. *International Journal of Heat and Mass Transfer*, 1997.

T R Auton. The lift force on a spherical body in a rotational flow. *Journal of Fluid Mechanics*, 183:199–218, 1987.

T R Auton, J C R Hunts, and M Prud'Homme. The force exerted on a body in inviscid unsteady non-uniform rotational flow. *Journal of Fluid Mechanics*, 197:241–257, 1988.

J Chahed. *Forces interfaciales et turbulence dans les écoulements a bulles: modélisation et étude de cas de référence*. PhD thesis, Université des Sciences et Techniques de Tunis, 1999.

P Chassaing. *Turbulence en mécanique de fluides*, volume 40. Cépaduès, 1996.

C P Chen and P E Wood. A turbulence closure model for dilute gas particle flows. *The Canadian Journal of Chemical Engineering*, 63:349–360, 1985.

G Csanady. Turbulent diffusion of heavy particles in the atmosphere. *Journal of Atmospheric Sciences*, 20:201–208, 1963.

D S Dandy and H A Dwyer. A sphere in a shear flow at finite reynolds number: effect of shear on particle lift, drag, and heat transfer. *Journal of Fluid Mechanics*, 216:381–410, 1990.

J Delhaye, M Giot, and M Riethmuller. *Thermal-Hydraulics of Two-Phase Systems for Industrial Design and Nuclear Engineering*. Hemisphere Publishing Corp, New York, 1981.

J M Delhaye. Jump conditions and entropy sources in two-phase systems local instant formulations. *International Journal of Multiphase Flow*, 1: 395–409, 1974.

P Desjonqueres, G Gouesbe, A Berlemon, and A Picart. Dispersion of discrete particles by continuous turbulent motions - new results and discussions. *Physics of Fluids*, 29:2147–2151, 1986.

E Deutch. *Dispersion de particules dans une turbulence homogène isotrope stationnaire calculée par simulation numérique directe des grandes échelles.* PhD thesis, IMFT, 1992.

D A Drew. *Analytical modeling of multiphase flows. In R.T.LAHEY, editor, Boiling heat transfer.* Elsevier Science Publishers, 1992.

J K Eaton. Turbulence modification by particle in shear flows. *ASME FED Gas-Particle Flows*, ASME FED-228 Gas-Particle Flows, 1995.

J K Eaton and F R Fessler. Preferential concentration of particle by turbulence. *International Journal of Multiphase Flow*, 20:169?209, 1994.

S Elghobashi, T W Abou-arab, M Risk, and M Mostafa. Prediction of the particle-laden jet with two-equation turbulence model. *International Journal Multiphase Flow*, 10:697–710, 1984.

V Ferrand, R Bazile, J Borée, and G Charnay. Gas-droplets turbulent velocity correlations and two-phase interaction in axisymmetric jet laden with partly responsive droplets. *International Journal of Multiphase Flow*, 29: 195–217, 2003.

R Gatignol. The faxén formulae for a rigid particle in an unsteady non-uniform stokes flow. *Journal de Mécanique Théorie et Application*, 9(2): 143–160, 1983.

R A Gore and C T Crowe. Effect of particle size on modulating turbulent intensity. *Internation Journal of Multiphase Flow*, 15(2):279–285, 1989.

R. Groll, S Jakirlic, and C Tropea. Comparative study of euler/euler and euler/lagrange approaches simulating in a turbulent gas-liquid flow. *International journal for numerical methods in fluids*, 59:873–906, 2009.

K Hanjalic and D Laurence. Introduction to turbulence modeling. *Lecture series*, 02, 2002.

Y Hardalupas, A M Taylor, and J H Whitelaw. Velocity and particle-flux characteristics of turbulent particle-laden jets. *Proceedings of the Royal Society of London*, A426:31–78, 1989.

M Hendou. *Contribution à la modélisation des transferts simultanés lors de l'absorption de gaz traces par une pulvérisation.* PhD thesis, ENSIGC, 1992.

G Hestroni. Particle-turbulence interaction. *International Journal of Multiphase Flow*, 15:735–746, 1989.

G F Hewitt, J M Delhaye, N zuber Multiphase Sciences, and Technology, editors. *Two-fluid model for two-phase flow*. Hemisphere Publishing Corporation, 1990.

J Hinze. Introduction to turbulence modeling. *Mc Graw-Hill*, 2, 1975.

K Ikeda, Y Makino, and M Hoshi. Single-phase cfd applicability for estimating fluid hot-spot locations in a 55 fuel rod bundle. *Nuclear Engineering and Design*, 236:1149–1154, 2006.

M Ishii. *Thermo-fluid dynamic theory of two-phase flow*. Collection de la Direction des études et recherches d'Electricité de France. Eyrolles, Paris, 1975.

M Ishii and K Mishima. Two-fluid and hydrodynamic constitutive relations. *Nuclear Engineering and Design*, 82:107–126, 1984.

W P Jones and B E Launder. The prediction of laminarization with a two-equation model of turbulence. *International Journal of Heat and Mass Transfer*, 15:301–314, 1972.

P L Kirillov, V M Kashcheyev, and S Yuriev. A two dimensional mathematical model of the annular-dispersed and dispersed flows. *International Journal of Heat and Mass Transfer*, 30:791–800, 1987.

S Komori and R Kurose. The effects of shear and spin on particle lift and drag in shear flow at high reynolds numbers. *Advances in turbulence*, 4: 551–554, 1996.

J D Kulick, J R Fesseler, and J K Eaton. Particle response and turbulence modification in fully developed channel flow. *Journal of Fluid Mechanics*, 277:109–134, 1994.

R Kurose and S Komori. Drag and lift forces on a rotating sphere in a linear shear flow. *Fluid Mechanics*, 384:183–206, 1999.

R Kurose, R Misumi, and S Komori. Drag and lift forces acting on a spherical water bubble in a linear shear flow. *International Journal of Multiphase Flow*, 27:1247–1258, 2001.

C M Lee and Y D Choi. Comparison of thermo-hydraulic performances of large scale vortex flow (lsvf) and small scale vortex flow (ssvf) mixing vanes in 1717 nuclear rod bundle. *Nuclear Engineering and Design*, 237: 2322–2331, 2007.

D Lhuillier. Dynamics of interfaces and rheology of immiscible liquid-liquid mixture. *Comptes-Rendu de l'Académie des Sciences-Mécanique*, 331(2): 113–118, 2003.

D Lhuillier, C Morel, and J M Delhaye. Bilan d'aire interfaciale dans un melange diphasique: approche locale vs approche particulaire. *Comptes-Rendu de l'Académie des Sciences-Mécanique*, t.328 Série II b:143–149, 2000.

F Lucci, A Ferrante, and S Elghobashi. Modulation of isotropic turbulence particles of taylor length-scale. *Journal of Fluid Mechanics*, 650:5–55, 2010.

K Luo, M Klein, J Fan, and K Cen. Effects on particle dispersion by turbulent transition in a jet. *Physics Letters A*, 357:345–350, 2006.

A R Masri, R W Dibble, and R S Barlow. The structure of turbulent non-premixed flames revealed by raman-rayleigh-lif measurements. *Progress in Energy and Combustion Science*, 22:307–362, 1996.

M R Maxey and J J Riley. Equation of motion for a small rigid sphere in a nonuniform flow. *From the Transactions of the Cambridge Philosophical Society*, 26:883–889, 1983.

J P McLaughlin. Inertial migration of a small sphere in linear shear flows. *Journal of Fluid Mechanics*, 224:261–274, 1991.

J P McLaughlin. Inertial migration of a small sphere in a wall-bounded linear shear flows. *Journal of Fluid Mechanics*, 246:249–265, 1993.

J P McLaughlin and P Cherukat. The inertial lift on a rigid sphere in a linear shear flow feild near a flat wall. *Journal of Fluid Mechanics*, 263:1, 1994.

J P McLaughlin, Q Wang, K D Squires, and M Chen. On the role of the lift force in turbulence simulations of particle deposition. *International Journal of Multiphase Flow*, 23:749–763, 1997.

W K Melville and K N C Bray. A model of the two phase turbulent jet. *International Journal Heat and Mass Transfer*, 22:647–656, 1979.

R Mie. An approximate expression for the shear lift force on a spherical particle at finite reynolds number. *International Journal of Multiphase Flow*, 18:145–147, 1992.

R Mie. Shear lift force on a spherical bubbles at finite reynolds number. *International Journal of Heat fluid Flow*, 15:62–65, 1994.

S Mimouni, F Archambeau, M Boucker, J Laviéville, and C Morel. A second-order turbulence model based on a reynolds stress approach for two-phase flow-part i: adiabatic cases, , hindawi publishing corporation, 2008. *Science and Technology of Nuclear Installations*, article ID 792395, 2009.

A Mostafa and H Mongia. On the interaction of particles and turbulent flow. *International journal Heat and Mass Transfer*, 31:2063–2075, 1988.

M Rivero, J Magnaudet, and J Fabre. Quelques résultats nouveaux concernant les forces exercées sur une inclusion sphérique par un écoulement accéléré. *Comptes Rendus de l'Académie des Sciences. Série 2, Mécanique, Physique, Chimie, Sciences de l'univers, Sciences de la Terre ISSN 0764-4450 CODEN CRAMED*, 312:1499–1506, 1991.

P G Saffman. The lift on a small sphere in a slow shear flow. *Journal of Fluid Mechanics*, 224:385–400, 1965.

Y Sato, U Fukuichi, and K Hishida. Effect of inter-particle spacing on turbulence modulation by lagrangian piv. *International Journal of Multiphase Flow*, 21:554–561, 2000.

G Segré and A Silberberg. The lift force on a small sphere in a slow shear flow. *Journal of Fluid Mechanics*, 14:115–157, 1962.

O Simonin. Modélisation numérique des écoulements turbulents diphasique à inclusions disperées. *École de Printemps de Mécanique des fluides Numériques; Aussois*, 1991a.

O Simonin. Prediction of the dispersed phase turbulence in particle-laden jets. *American Society of Mechanical Engineers*, 121:197–206, 1991b.

O Simonin. Combustion and turbulence in two-phase flows. *von Karman Institute for Fluid Dynamis*, Lecture Series,1996-02, 1996.

O Simonin. Statistical and continuum modeling of turbulent reactive particulate flows. part 1: theoretical derivation of dispersed eulerian modeling from probability density function kinetic equation. theoretical and experimental modeling of particulate flows. *Theoretical and Experimental Modeling of Particulate Flows*, Lecture Series 2000-06, 2000.

O Simonin, E Deutsch, and J P Minier. Eulerian prediction of the fluid/particle correlated motion in turbulent two-phase flows. *Applied Scientific Research*, 51:275–283, 1993a.

O Simonin, E Deutsch, and J P Minier. Eulerian prediction of the fluid/particle correlated motion in turbulent two-phase flows. *Applied Scientific Research*, 51:275–283, 1993b.

M Sommerfeld, G Kohnen, and H Qui. Spray evaporation in turbulent flow: Numerical calculations and detailed experiments by phase-doppler anemometry. *Revues de l'Institut Francais de Petrole*, 48:677–695, 1993.

G G Stokes. On the effect of the internal friction on the motion of pendulums. *From the Transactions of the Cambridge Philosophical Society*, 9:8, 1850.

K Sugioka and S Komori. Drag and lift forces acting on a spherical water droplet in a homogeneous linear shear air flow. *Fluid Mechanics*, 570: 155–175, 2006.

S Sundaram and L R Collins. A numerical study of modulation of isotropic turbulence by suspended particles. *Journal of Fluid Mechanics*, 379:105–143, 1999.

C Tchen. *value and correlation problems connected with the motion of small particles suspended in turbulent fluid*. PhD thesis, Technische Hogeschool Delft, 1947.

A A Vinberg, L I Zaichick, and V A Pershukov. Computational model for turbulent gas-particle jet streams. *Journal of Engineering and Physics*, 61:554?563, 1991.

G Wallis. *One Dimensional Two-Phase Flow*. Mcgraw-Hill (Tx), 1969.

S W Webb and J C Chen. A numerical model for turbulent non-equilibrium dispersed flow heat transfer. *International Journal of Heat and Mass Transfer*, 25:325–335, 1982.

Y Wu, H Wang, Z Lui, and J Li. Experimental investigation on turbulence modification in a horizontal channel flow at relatively low mass loading. *Acta Mech Sinicia*, 22:99–108, 2006.

Y Xu and S Subramaniam. A multi scale model for dilute turbulent gas-particle flows based on the equilibration of energy concept. *Physics of Fluids*, 18:033301, 2006.

Y Xu and S Subramaniam. Consistent modeling of inter phase turbulent kinetic energy transfer in particle-laden turbulent flows. *Physics of Fluids*, 19:085101, 2007.

L P Yarin and G Hestroni. Turbulence intensity in dilute two phase flow. *International Journal of Multiphase Flow*, 20:27–44, 1993.

L Zeng, F Najjar, S Balchandar, and P Fischer. Forces on a finite-sized particle located close to a wall in a linear shear flow. *Physics of fluids*, 21: 033302, 2009.

L X Zhou. Advances in studies on two-phase turbulence in dispersed multiphase flows. *International Journal of Multiphase Flow*, 36:100–108, 2010.

L X Zhou and X Q Huang. Prediction of confined gas-particle jets by an energy equation model of particle turbulence. *Science in China English Addition*, 33:53–59, 1990.